Computational studies of zinc-seamed pyrogallol[4]arene nanocapsules and model systems

A Dissertation

Presented to

The Faculty of the Graduate School

University of Missouri

In Partial Fulfillment

Of the Requirements for the Degree

Doctor of Philosophy

by

Collin M. Mayhan

Dr. Carol A. Deakyne, Dissertation Supervisor

May 2014

The undersigned, appointed by the dean of the Graduate School, have examined the dissertation entitled

Computational studies of zinc-seamed pyrogallol[4]arene nanocapsules and model systems

presented by Collin M. Mayhan,

a candidate for the degree of doctor of philosophy of Chemistry,

and hereby certify that, in their opinion, it is worthy of acceptance.

Professor Carol A. Deakyne (Chair)

Professor Ioan Kosztin (Outside Member)

Professor John E. Adams (Member)

Professor C. Michael Greenlief (Member)

ACKNOWLEDGMENTS

The whole of process of graduate school from coursework and cumulative exams to teaching and research has been simplified by my family and research family. I defy someone to find a better mentor and advisor than Professor Carol Deakyne. She welcomed me into her research family as an undergraduate and, before I realized what was happening, I am writing an Acknowledgements section for my dissertation. Along the way, I had the opportunity to present at conferences around the country, publish several manuscripts, lecture in several courses, and work in a collaborative environment. (I debated several days on whether I should use the Oxford comma throughout this dissertation or not, but, out of respect for Carol, I have decided to use the Oxford comma.)

I have also had the privilege of working with Prof. John Adams. He has always provided guidance and alternative solutions, along with an ever plentiful chocolate bowl, when I would interrupt his office hours. His lectures covering "elementary" quantum mechanics finalized my decision to pursue a Ph.D.

I have been fortunate with my teaching assignments and had the pleasure to teach the physical chemistry lab four straight years. Before teaching, I was a student in this lab and had the good fortune of learning from and working for Prof. Michael Greenlief. The skills I acquired from teaching this lab have been invaluable.

Throughout my time at the University of Missouri I have come across four exceptional educators, all of whom are on my committee: Carol Deakyne, John Adams,

Michael Greenlief, and Ioan Kosztin. I had the privilege of hearing all four professors lecture and tell short stories of chemistry and physics. I found after every lecture that I had a false sense of understanding due to their polished lectures.

I'd also like to thank my fellow graduate students and post-docs: Amanda M. Drachnik, Dr. Andrew V. Mossine, Dr. Harshita K. Kumari, Dr. John V. Simpson, Dr. Huanani M. Thomas, and Dr. Jamin W. Perry. Without these individuals, many of my manuscripts and other endeavors would not have succeeded.

Mark and Ronda Mayhan, my parents, and Maggie Mayhan, my sister and baby-sitter extraordinaire, have been very supportive throughout my studies. Carey Bottom, my uncle and the other chemist in the family, has been a wonderful mentor as I prepare for the next journey of my life. Ron "Pops" and Betty "Goat" Johnston, my maternal grandparents, always made me smile when they would call to wish me a happy birthday or remind me of daylight savings time. Ken and Helena Mayhan, my paternal grandparents, have been supportive and enjoyed reading my journal articles. My Grandma Connie is missed and I know she would be proud of my accomplishments.

Lastly, I would like to thank Erin Mayhan, my wonderful wife, and Levi, our perfect son. Erin has been supportive throughout this whole process and I could not have completed this journey without her. Levi keeps everything in perspective and makes any hardship seem negligible. In the interest of maintaining your attention and due to the high cost of printing this document, I will leave it at that. Thank you all!

Table of Contents

LIST OF TABLES

LIST OF FIGURES

LIST OF EQUATIONS

ABSTRACT

Zinc-seamed pyrogallol[4]arene dimeric nanocapsules have been experimentally observed with a variety of *exo* ligands coordinating to the zinc and a variety of encapsulated guests. In an effort to gain additional insight into the properties of these dimers, electronic structure calculations were carried out on a number of model complexes and capsular assemblies.

Initial calculations focused on simple hydroxide-based and *Z*-ethene-1,2-diol-based mononuclear zinc model complexes representative of the zinc coordination sphere in the dimers. These calibration studies aided in the choice of an appropriate computational protocol to be implemented on the capsules themselves. The binding dissociation enthalpies of the ligands were evaluated, along with the effect of ligand choice on zinc coordination number. With the success of the *Z*-ethene-1,2-diol-based model complexes in reproducing the capsular zinc coordination environment, two sets of calculations exploring divergent ligands linking two of these model complexes were performed. The first set of calculations predicted the stability of a metal organic framework (MOF) comprising zinc-seamed pyrogallol[4]arene capsules linked by a 4,4'-bipyridyl ligand and aided in the choice of crystallization solvent in the subsequent synthesis of the MOF. The second set of calculations identified three additional divergent ligands as likely candidates for the construction of MOFs.

To gain further insight as to why pyrogallol forms macrocycles and the remaining trihydroxybenzene-based macrocycles remain unobserved, the proton affinity (PA) of these building blocks was examined. The preferred sites of protonation in the

trihydroxybenzenes were compared with those in the mono- and dihydroxybenzenes, as some of the latter hydroxybenzenes are also known to form macrocycles. A key factor with respect to formation of macrocycles appears to be the relative magnitudes of the PAs associated with the ring carbon-linking sites.

To better understand the capsular metric dimensions and encapsulation thermochemistry, studies on the zinc-seamed pyrogallol[4]arene nanocapsules themselves examined the effect of the *exo* ligands, R group, guest, and calculational level on these properties. In particular, the influence of these factors on the flexibility and robustness of the capsular framework, host-guest interactions, size limitations of a guest, and enhancement in guest basicity upon encapsulation was investigated. The presence of *exo* ligands has the largest effect on both geometric properties and encapsulation thermochemical values; however, the presence of a guest also has an effect on the capsular dimensions. The enhancement in basicity of an encapsulated guest, although dependent on the nature of the guest, is generally some 50 kJ/mol, a value consistent with those found for other host-guest assemblies. The computational results helped to rationalize the presence of observed guests and the absence of unobserved guests in the dimeric capsules and led to a proposed step in the unknown mechanism of formation of the capsules.

Chapter 1: Introduction

Supramolecular chemistry is the study of self-assembled entities formed from molecular building blocks.[1] Constructing molecular self-assemblies with desired host-guest interactions is one of the most challenging areas of supramolecular chemistry. Supramolecular host-guest systems rely on non-covalent interactions for stability, including hydrogen bonding, metal coordination, cation-π interactions, and π-π interactions. One host entity stabilized by these types of non-covalent interactions is a metal-seamed organic nanocapsule (MONC). One way to think about MONCs is to consider two, or more, bowls (macrocycles) combining together to form a sphere held together by hydrogen bonds and/or metal coordination sites. Not only are intracapsular interactions possible in these MONCs, but multiple MONCs can be linked together by a divergent ligand resulting in a metal-organic framework (MOF). MOFs typically enclose void volumes that can be occupied by guest molecules. The void space, in theory, allows guests to move and interact throughout the framework. MONCs, MOFs and other supramolecular nanoassemblies have been of interest for some time now due to possible applications in catalysis,[2] chemical separations,[3-10] gas storage,[11-14] and drug delivery.[15-17]

1.1 Calixarene family of macrocycles

Calixarene macrocycles are composed of phenolic units that are linked together by a –CHR moiety, where R denotes an alkyl or aryl group, and can form a chalice-shaped cavity. Calixarene macrocycles and their derivatives are represented by the notation calix[*n*]arene, where *n* = the number of phenolic units. Values of *n* = 4, 5, 6, and

8 have been observed depending on the calixarene family-based building block.[18] Examples of the common building blocks, phenol (hydroxybenzene, (A)), resorcinol (1,3-dihydroxybenzene, (B)), and pyrogallol (1,2,3-trihydroxybenzene, (C)), and macrocycles, calix[4]arene (A), resorcin[4]arene (B), and pyrogallol[4]arene (C), can be found in Fig. 1.1. As shown in the figure, the hydroxyls form the smaller lower rim of the calix[4]arene and the larger upper rim of the resorcine[4]arene and pyrogallol[4]arene. In each chalice-shaped macrocycle, the hydroxyl groups participate in a hydrogen-bonded network. The 8-membered hydrogen-bonded ring at the bottom of calix[4]arene limits its flexibility compared to that of the other two arenes. For this reason, resorcinol- and pyrogallol-based macrocycles can house a more sizeable guest or multiple smaller guests.

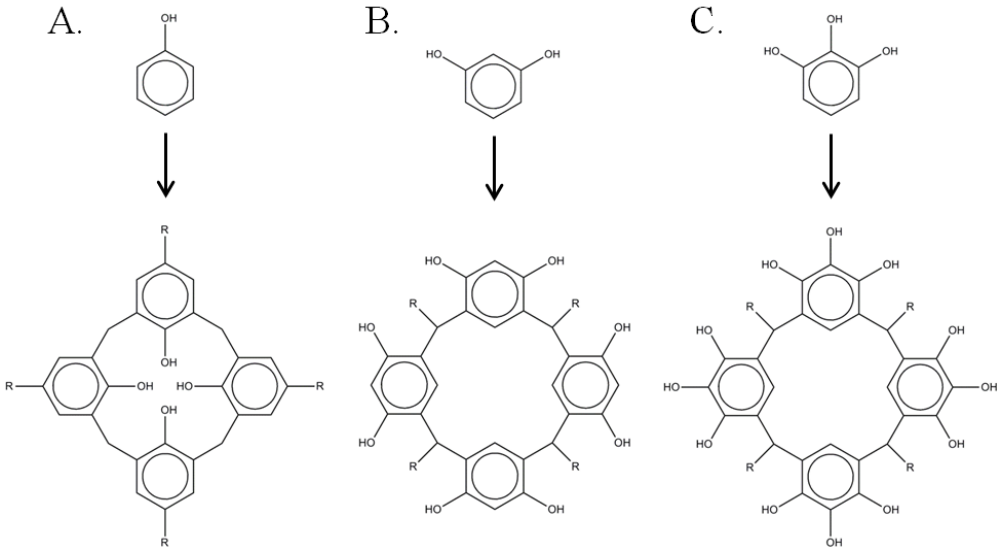

Figure 1.1 Calixarene family-based building blocks and the macrocycles formed from them. (A) top: phenol, bottom: calix[4]arene; (B) top: resorcinol, bottom: resorcin[4]arene; and (C) top: pyrogallol, bottom: pyrogallol[4]arene.

Observed solid-state arrangements for the calix[4]arenes, resorcin[4]arenes, and pyrogallol[4]arenes include bilayers, hydrogen-bonded capsules, and tubes.[19] Both

calixarenes and pyrogallolarenes have been shown to act as frustrated organic solids and to exhibit transient porosity.[20] Calixarenes are also of interest due to the single-crystal-to-single-crystal transformations that have been shown to occur upon absorption of small gas molecules.[19,21-23]

With the bulky *t*-butyl R groups (Fig 1.1 A), *p*-*t*-butylcalix[4]arene has the ability to sequester gases in the cavitand.[24-26] The entry of a gas molecule is thought to occur by a "gated" mechanism facilitated by the breathing movement of the *t*-butyl groups. A study by Adams et al.[27] utilized molecular dynamics (MD) simulations to investigate the stability of calixarene-guest complexes for calix[4]arenes with R = H, Me, or *t*-butyl (Fig. 1.1 A). The frequency at which the empty calix[4]arene hosts breathe is essentially equivalent regardless of the nature of the R group and/or the rotations of the methyl and *t*-butyl groups, an observation that supports the proposed gated mechanism for the absorption of gases. In the host/guest complexes, the guests typically align themselves to maximize their interaction with the negative charge density, primarily due to the aryl groups, of the calixarene cavity; guests can rotate but, with the exception of methane, maximizing interactions with adjacent aryl groups usually restricts their movement. The spherical shape of methane allows free rotational and translational movements.

For a methanol guest, the dynamical behavior of both the methanol and calixarene host is nearly identical for the gas-phase host-guest complex and the solvated complex, where the methanol guest was sequestered during the initial steps of the simulation.[27] The sequestered guest does interact with the bulk solvent by forming a hydrogen bond with a solvent molecule outside of the cavitand, but exchange was not observed on the timescale of the simulations.

Because the chalice shape of the cone conformer maximizes the potential for entrapment of a guest, only this conformation of calix[4]arene has been discussed thus far. However, the calixarene family of macrocycles can exist in a variety of conformations, the most common of which can be found in Fig. 1.2, depending on the arrangement of the aryl moieties. The relative stability of the structurally related pyrogallol[4]arene and resorcin[4]arene conformers, with various –CHR moieties, has been investigated by Thomas et al.[28] and Drachnik et al.[29] For both macrocycles, when R = H, the cone conformer is most stable, but, when R = phenyl, the chair conformer is most stable. The chair conformer, however, has been shown experimentally to convert to the cone conformer to form MONCs.[30] It should be noted that for all of the conformers of pyrogallol[4]arene and resorcin[4]arene, multiple stereoisomers exist that differ with respect to the axial or equatorial orientations of the R groups.

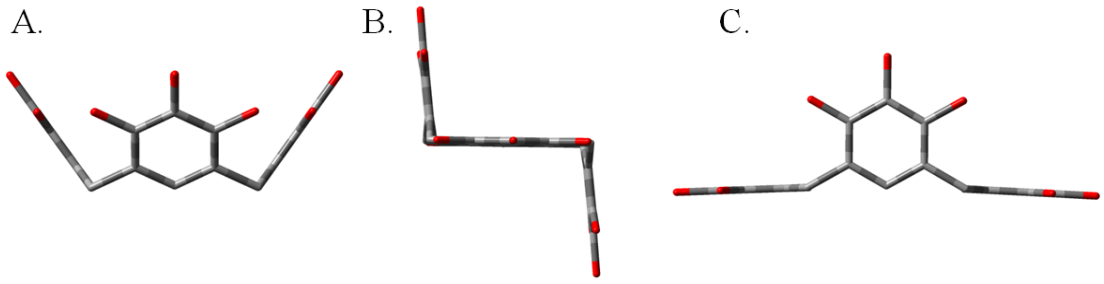

Figure 1.2 The most common conformers of the calixarene family of macrocycles, shown for pyrogallol[4]arene. Hydrogens and R groups have been removed for clarity for the cone (A), chair (B), and boat (C) conformers.

1.2 Metal-organic nanocapsules and frameworks

In addition to resorcin[4]arene- and pyrogallol[4]arene-based hydrogen-bonded capsules, the Atwood group has synthesized a number of MONCs composed of pyrogallol[4]arene macrocycles that are seamed together by Cu^{2+}, Zn^{2+}, Co^{2+}, Ni^{2+} or

Ga^{3+} metal centers.[31-35] The capsules have been constructed with R = alkyl or aryl groups on the –CHR linker moieties that connect the pyrogallols of each macrocycle. These solid-state MONCs generally have a spherical shape; the exception is the Ga^{3+}-seamed MONCs, which have a rugby-ball shape. In solution, both Ga and mixed Ga/Zn nanoassemblies rearrange to toroidal architectures.[36]

When considering the formation of the zinc-seamed pyrogallol[4]arene dimeric capsule, eight zincs seam the two chalice-shaped macrocycles together with concomitant deprotonation of 16 hydroxyls. The loss of two out of three protons on each pyrogallol yields two types of oxygen atoms in the capsule: one that is bridged via a hydrogen bond to an oxygen atom on an adjacent pyrogallol and one that is bridged between adjacent zinc centers. The resulting metal centers are 5-coordinate, where four of the coordination sites are occupied by oxygen atoms, two of each type, and the fifth coordination site is occupied by an equatorial ligand, typically from the reactant zinc complex. (The capsules are usually synthesized by a 4:1:14 ratio of zinc complex:macrocycle:pyridine.) However, facile substitution of this equatorial ligand has been observed in solution.[32] Single-crystal XRD analyses indicate that the zinc-seamed pyrogallol[4]arene dimeric capsules enclose one or more guests, but NMR and MALDI-TOF MS analyses suggest both empty and occupied dimers are stable.[37,38] The capsule is also stable without *exo* ligands, as they are stripped in the MALDI-TOF experiment. Furthermore, in this experiment either the capsule or the guest is protonated.[31]

In another study by the Atwood group, two distinct 1–D MOFs were constructed from preformed Cu^{2+} nanocapsules.[39] One MOF consists of direct linking where Cu^{2+} centers from adjacent capsules form a $[Cu–O]_2$ four-membered ring. The intercapsular

Cu–O bond length is approximately 0.30 Å longer than the intracapsular Cu–O bond length (1.97 Å). The other MOF consists of Cu^{2+}-seamed nanocapsules linked by 4,4'-bipyridyl (bpy) ligands. These results motivated our combined computational and experimental study of zinc-seamed pyrogallol[4]arene-based MOFs.[40] Not only did the computational results predict that bpy is a likely linking candidate, the geometric properties of the mononuclear zinc model complexes used to represent the dimers lie within the ranges observed experimentally for zinc-seamed MONCs.

1.3 Dissertation outline

Taking the zinc-seamed dimeric nanocapsule [Zn_8(*C*-propylpyrogallol[4]arene)$_2$(DMSO)$_8$⊂(3-methylpyridine)] as an example,[32] there are 151 heavy atoms and 286 total atoms. Due to the large number of atoms, high-level quantum chemical calculations are not practical. Before considering the nanocapsule in its entirety, therefore, we examined the properties of some of its components, specifically, the metal coordination sphere in the capsule and the aryl building block of the macrocyle. One function of this set of calculations was to develop a computational protocol for our study of the zinc-seamed dimers. Thus, a variety of density functional theory (DFT) and wavefunction theory (WFT) methods (e.g., PBE0, B3LYP, *w*B97X-D, MP2) and a variety of basis sets (e.g., LANL2DZ, cc-pVDZ, aug-cc-pVTZ, B2-PP[41]) were examined. The results of these method/basis set combinations were benchmarked against MP2/B2-PP or G4(MP2)[42] results.

To gain a better understanding of the coordination environment of the metal centers and their interaction with equatorial ligands, electronic structure calculations were

implemented to study the geometric and energetic properties of mononuclear and polynuclear zinc model complexes representative of the zinc-coordination sphere observed in the dimers. Initially, the monomeric Zn hydroxide complexes, $Zn(OH)_2X_2Y$ and $Zn(OH)_2X_2Y_2$, where X is water or methanol and Y is pyridine or ammonia, were studied.[43] These complexes were chosen because they are the simplest possible systems with the requisite Zn–O bonds and overall charge. However, the zinc centers in these hydroxide complexes have a coordination number of either three or four, which led to the investigation of a second type of model complex.[43,44] For the latter mononuclear metal complexes, the zinc atom was combined with two deprotonated (*Z*)-ethene-1,2-diol molecules and an *exo* Y ligand to form the models $Zn(C_2O_2H_3)_2Y$. Here, Y = NH_3, C_5H_5N, CH_3OH, $(CH_3)_2NCHO$, or $(CH_3)_2SO$. C_5H_5N, $(CH_3)_2NCHO$, and $(CH_3)_2SO$ have been observed as *exo* ligands for the zinc-seamed dimers.[44] The suitability of the $Zn(C_2O_2H_3)_2Y$ models was confirmed in several ways, one of which was to test whether building up polynuclear zinc complexes with 2, 4, 6, or 8 metal ions combined with $C_2O_2H_3^-$, $C_4O_3H_4^{2-}$, and NH_3 ligands leads to a closed ring. The $Zn(C_2O_2H_3)_2Y$ complexes were then used to determine the relative binding affinities of the Y ligands and to rationalize their absence or presence on the periphery of observed zinc dimers. In a subsequent study, $(Zn(C_2O_2H_3)_2)_{1,2}Y$ complexes, where Y is one of 16 divergent ligands, were used to identify possible linking ligands to construct dimer-based MOFs. This work is described in detail in Chs. 2, 3 and 5.

Self-assembled macrocycles are readily formed for the phenol, resorcinol and pyrogallol subunits, but have not yet been observed for other di- or tri-hydroxybenzenes. That the synthesis of the macrocycles is proposed to proceed by an electrophilic

substitution reaction mechanism suggests that proton affinity (PA) can be used to determine the likelihood for macrocyclic formation from phenolic-based building blocks. Although it has been established experimentally that hydroxybenzenes are protonated at carbon,[45-47] the magnitudes of the PA for the trihydroxybenzenes are still unknown. Bouchoux and coworkers[45] have reported the proton affinities of phenol and the dihydroxybenzenes. Therefore, electronic structure calculations were performed to evaluate the PAs of hydroxyquinol (1,2,4-trihydroxybenzene), phlorglucinol (1,3,5-trihydroxybenzene), and pyrogallol (1,2,3-trihydroxybenzene).[48,49] Once the PA associated with each possible protonation site was determined, the preferred –CHR linkage sites and likelihood of linkage were assessed. The results of the study on hydroxyquinol[48] are presented in Ch. 4.

The methods provided from the calibration studies of the zinc coordination spheres and the trihydroxybenzenes were then implemented to design and conduct a more focused investigation of the zinc-seamed pyrogallol[4]arene dimeric nanocapsules. In addition to establishing a computational protocol to study the dimers, a number of questions were addressed in this investigation. 1) Is an "empty" capsule, with and without *exo* ligands, stable? Is the capsular framework sufficiently flexible and robust to maintain its shape in the absence of a guest? 2) Does the presence of a guest and/or *exo* ligands alter the metric dimensions of the capsule? Is it necessary to consider the complete nanocapsular assembly to examine guest mobility and preferred orientation? 3) What are the guest size limitations with respect to encapsulation? Does guest contortion occur upon encapsulation? 4) Can we gain insight into the mechanism of formation of the capsular assembly? For example, is guest encapsulation thermodynamically favored or is the guest

kinetically trapped? 5) For a protonated assembly, is the capsule or the guest more likely to be protonated? Is proton transfer observed between the guest and host? 6) Does the basicity of a guest change upon encapsulation? Does the basicity change differ with the addition and placement of guest substituents? 7) Is there "communication" between the guest and *exo* ligands? That is, does the nature of the *exo* ligand influence guest encapsulation thermochemistry, basicity, and contortion? These questions are addressed in Chs. 6 and 7.

Chapter 2: Multiligand zinc(II) hydroxide complexes: $Zn(OH)_2X_2Y$ and $Zn(OH)_2X_2Y_2$; X = H_2O, CH_3OH and Y = NH_3, C_5H_5N

As one component of our computational study of zinc-seamed pyrogallol[4]arene nanocapsules, we are investigating small mononuclear and polynuclear zinc complexes. In this chapter the results of our quantum chemical calculations on $Zn(OH)_2X_2Y$ and $Zn(OH)_2X_{1,2}Y_2$ complexes, where X is water or methanol and Y is pyridine or ammonia, are described. Structures and energetics obtained with the LANL2DZ versus 6-311+G(d,p) versus B2(PP) basis sets and DFT versus MP2 methods are compared and contrasted. The effect of the hydroxide ligands on the preferred zinc coordination number and mode, inner- and outer-shell ligands, and hydrogen-bonding motifs is also examined. Trends in ligand binding energies are discussed. Of particular note is that the B3LYP/LANL2DZ calculations overemphasize the strength of both the conventional and unconventional hydrogen bonds. This work is published in *Comput. Theor. Chem*. 984 (2012) 19-35.[43]

2.1 Introduction

Supra- and supermolecular assemblies have received widespread interest in recent years as they may have practical applications as functional materials.[1,50-53] One group of such assemblies, metal-seamed pyrogallol[4]arene nanocapsules, has been synthesized by Atwood and coworkers.[31,32] The first capsule synthesized was [Zn_8(*C*-

propylpyrogallol[4]arene)$_2$(pyridine)$_8$⊂pyridine], with propyl R-groups, a pyridine guest and pyridine axial ligands (Fig. 2.1, pyridine guest and propyl R-groups removed for clarity). The zinc capsules are metal organic dimers coordinated by a ring of eight Zn (II) ions that have displaced 16 of the 24 hydroxy protons from the pyrogallol subunits of the pyrogallol[4]arenes. In the solid state and solution, each of the zinc centers has a distorted square pyramidal configuration and is ligated by four equatorial phenoxy groups, two from each cavitand, along with the axial ligand. One phenoxy group from each cavitand is bridged between neighboring zincs and the other is intramolecularly hydrogen bonded to a phenoxy group on the neighboring pyrogallol subunit, making the overall assembly neutral. In the gas phase, however, MALDI-TOF MS analysis has revealed that the dimers are stripped of their axial ligands.[30-32] These nanocapsules have now been made with a selection of metals, R-groups, guests, and axial ligands and may lead to applications such as molecular wires and molecule-based magnets.

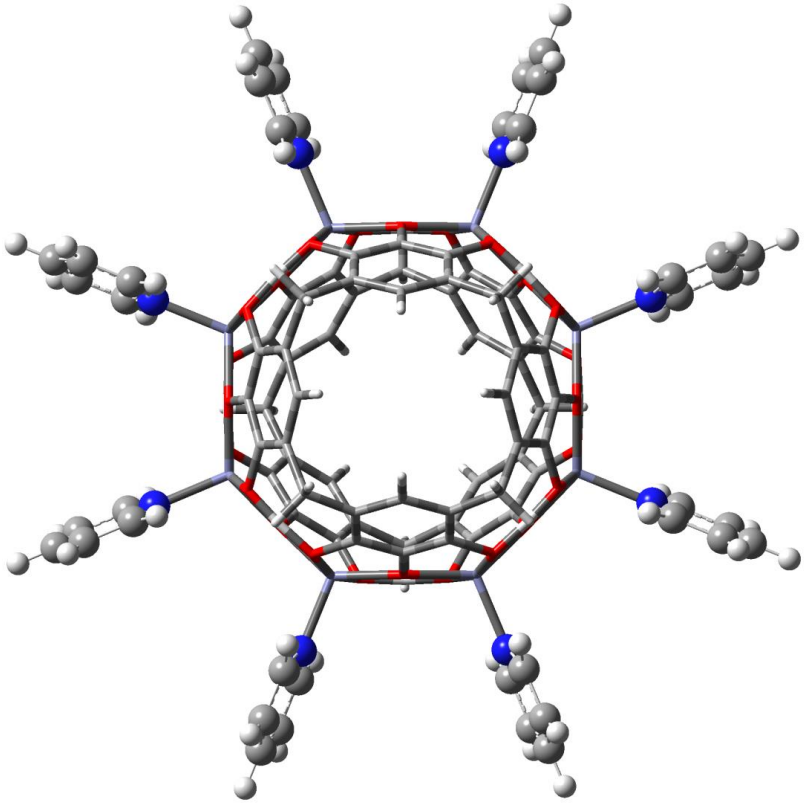

Figure 2.1[Zn_8(C-propylpyrogallol[4]arene)$_2$(pyridine)$_8 \subset$ pyridine] with pyridine guest and propyl R-groups removed for clarity.

We are interested in using quantum chemical techniques to examine the fundamental properties of the Zn-seamed pyrogallol[4]arene nanocapsules. In particular, the small interior volume of these dimers allows us to probe host-guest interactions and properties and behavior of a guest in "confined space". However, due to the size of the nanocapsules (120 atoms with R = H and no axial ligands), in addition to the nanocapsules themselves, we are investigating mononuclear and multinuclear zinc complexes representative of the metal environment in the capsules. For the initial studies reported in this chapter, we looked at the monomeric Zn hydroxide complexes, $Zn(OH)_2X_2Y$ and $Zn(OH)_2X_2Y_2$, the simplest systems representative of the metal-coordinating atoms and total charge of the pyrogallol[4]arene dimers. Here, X and Y are

combinations of H_2O, CH_3OH, NH_3, and C_5H_5N, but excluding the NH_3/C_5H_5N combination. Because of the application of the $[Zn(OH)_n(H_2O)_m]^{(2-n)}$ and $[Zn(OH)_n(H_2O)_m(NH_3)_3]^{(2-n)}$ complexes as biomimetics, as well as the relevance of the zincates to aqueous environments, previous computations on these two sets of complexes have been pursued.[54-59] Various combinations of n = 1 – 4 and m = 1 – 6 were considered; however, only the $Zn(OH)_2(H_2O)_2$ complex was examined in both our study and the earlier studies. The $[Zn(OH)_nX_{1,2}Y_{1,2}]^{(2-n)}$ complexes investigated in this work will thus provide additional information on the effect of nitrogen- versus oxygen-coordinating ligands on the structure of Zn(II) complexes.[60-63]

Synthetic and computational zinc-containing biomimetics have been advantageous in probing the structures and mechanisms of action of mononuclear and multinuclear zinc enzymes. For example, synthetic modeling of mononuclear zinc hydrolytic enzymes has helped to establish that the active nucleophile in the catalytic center is a terminal Zn-OH species.[62,64] As a second example, investigation of binuclear zinc model complexes that promote cleavage of phosphate diesters has shown the importance of synergistic effects between the charge on the catalyst and the dielectric constant of the medium.[65] Illustrative of the computational work in this area are the recent studies of biomimetic zinc hydroxide complexes to characterize the transition structures and intermediates in hydrolysis reactions of the mononuclear, binuclear, and trinuclear zinc enzymes carbonic anhydrase[66] and carboxypeptidase A,[67] glyoxylase II,[68] and nuclease-P1,[69] respectively. Other studies with more general implications for zinc metalloenzymes, and other zinc-containing species, have examined the factors that influence the coordination number and coordination mode of zinc,[60,70-74] the

deprotonation energy of a Zn-bound water molecule,[54,55,58,60] and the mechanisms of water-exchange reactions.[70] Conclusions from these studies that are relevant to our work include the following. 1) Significant lengthening and even breaking of Zn^{2+}-ligand bonds can occur as the Zn becomes less positive.[60,70-74] This effect has been termed the valence buffer effect.[75] 2) There is an indirect correlation between the proton affinities of the inner-shell ligands and the stabilities of the transition structure and resultant complex associated with outer-shell to inner-shell water exchange.[70]

With respect to our calculations on the capsules themselves, two of our goals in this study were to compare the coordination modes, geometric parameters, and thermochemical data obtained with the LANL2DZ, 6-311+G(d,p), and B2[41,76] basis sets and to confirm that NH_3 is a suitable substitute for C_5H_5N as an axial ligand. As in the above work,[60,70-74] we were also interested in exploring the effect of the hydroxide ligands, remaining oxygen versus nitrogen inner-shell ligands, and hydrogen-bonding interactions on the coordinative behavior of the zinc.

Benchmark computations on Zn^{2+} complexes have appeared in the literature,[41,55,76,77] but to our knowledge, only two studies have included double hydroxide species.[41,76] In these two studies, Amin and coworkers examined $Zn(OH)_2$, $Zn(OH)_2NH_3$ and $Zn(OH)_2(NH_3)_2$. Rayón and coworkers looked at Zn(II) –L complexes, where L includes OH^-, H_2O, NH_3, and CH_3OH,[77] and Frison and Ohanessian looked at $Zn–L_n$ complexes, where n = 3 – 5 and L = OH^-, H_2O, NH_3, and imidazole in various combinations.[55]

2.2 Computational details

2.2.1 Calculational methods

Both density functional theory (DFT) and wave function theory (WFT) have been used in recent studies of Zn complexes with four, five or six ligands.[41,55,68-70,76,78-84] In Frison and Ohanessian's[55] calibration study of Zn biomimetics, four basis sets were used ranging from the 6-31G* basis set for H, C, N, and O and Wachters'[85] [14s9p5d1f/9s5p3d1f] basis set for Zn to the aug-cc-pVTZ basis set for H, C, N, and O and Wachters' [15s11p6d3f1g/10s7p4d3f1g] basis set for Zn. The methods investigated range from semiempirical (PM3) to DFT (e.g. B3LYP) to post-Hartree-Fock (MP2 and CCSD(T)). Keeping in mind the size of the zinc-seamed pyrogallol[4]arene nanocapsules, we chose a set of calculational levels that meet or exceed those recommended by Frison and Ohanessian and are also consistent with the other studies in this area. Specifically, fully optimized geometries were obtained at the B3LYP/LANL2DZ and B3LYP/6-311+G(d,p) levels of theory; single-point energies (SPEs) were obtained at the B3LYP/6-311+G(d,p)//B3LYP/LANL2DZ, MP2/6-311+G(d,p)//B3LYP/LANL2DZ, and MP2/6-311+G(d,p)//B3LYP/6-311+G(d,p) levels of theory. The LANL2DZ basis set uses a non-relativistic electron core potential (ECP) for zinc, with 18 electrons in the core. To provide benchmark geometric and energetic data, as recommended by Amin and co-workers[41,76] geometries were optimized at the M05-2X/B2 level of theory,[86] with and without including scalar relativistic effects on Zn. To be consistent with the work of Amin et al.[41,76] the small-core Stuttgart/Dresden ECP (SDD) pseudopotential, which differs from the (MEFIT,*R*) pseudopotential[87] they used

by the addition of an f-term, was used in these calculations. The B2 basis set is [10s7p4d3f] for Zn[41] and 6-311+G(2df,2p) for the remaining atoms.[41,88] We designate calculations including the relativistic effective core potential for Zn as B2-PP; we designate calculations both with and without the effective core potential as B2(PP). MP2/B2-PP//M05-2X/B2-PP SPEs were computed, as were energies at the M05-2X/B2(PP) and MP2/6-311+G(d,p) level for all geometries. Normal-mode vibrational frequencies were evaluated to identify the nature of stationary points and to obtain thermal correction terms. All optimizations were done with tight threshold criteria, and all calculations used the int = ultrafine keyword in the Gaussian 09 suite of programs.[89]

2.2.2 Location of minima

Minima of the five-ligand reactant compounds $Zn(OH)_2X_2Y$, X = H_2O, CH_3OH and Y = NH_3, C_5H_5N, were located by arranging the ligands in all possible combinations from trigonal bipyramidal and square pyramidal starting geometries. A similar approach was taken for $Zn(OH)_2(H_2O)_2CH_3OH$. Tetrahedral and all *cis* and *trans* square planar starting arrangements were examined for the 4-coordinate product zinc complexes. Because our results for the 4- and 5-ligand $Zn(OH)_2X_2$, $Zn(OH)_2XY$, $Zn(OH)_2Y_2$, and $Zn(OH)_2X_2Y$ systems show that analogous H_2O/CH_3OH and NH_3/C_5H_5N complexes have analogous equilibrium structures, the H_2O- and NH_3-containing $Zn(OH)_2X_{1,2}Y_2$ minima were used as templates for the CH_3OH- and C_5H_5N-containing starting structures.

2.2.2.1 $Zn(OH)_2XY_2$ and $Zn(OH)_2X_2Y_2$ complexes

To identify the minima of the six-ligand zinc complex $Zn(OH)_2(H_2O)_2(NH_3)_2$, the ligands were first arranged in all possible combinations from octahedral starting

geometries. Given the relocation of water from the inner to the outer shell, square pyramidal starting geometries with all possible arrangements of an outer-shell H_2O were then examined. Finally, with only 4-coordinate zinc minima obtained from these optimizations, further starting structures with all remaining combinations and placements of outer-shell H_2O and NH_3 ligands were considered. Minima of the 5-ligand zinc complex $Zn(OH)_2(H_2O)(NH_3)_2$ were located as described in the previous section.

The specific set of H_2O/NH_3 templates used for the $Zn(OH)_2X_{1,2}Y_2$ systems containing CH_3OH/NH_3 and H_2O/C_5H_5N are the following: 1) the $[Zn(OH)_2(NH_3)_2](H_2O)_2$ global minimum and the two most stable local minima, 2) the most stable $[Zn(OH)_2(H_2O)(NH_3)](H_2O)(NH_3)$ and $[Zn(OH)_2(H_2O)_2](NH_3)_2$ local minima, 3) the $[Zn(OH)_2(NH_3)_2](H_2O)$ global and local minima, and 4) the $[Zn(OH)_2(H_2O)(NH_3)](NH_3)$ and $[Zn(OH)_2(NH_3)](H_2O)(NH_3)$ local minima (for the CH_3OH/NH_3 complexes only). The minima were selected with respect to the relevant B3LYP/6-311+G(d,p) global minimum. On the basis of the above structural and energetic results, only the structure for the CH_3OH/C_5H_5N system analogous to the optimal structure of the H_2O/C_5H_5N system was examined.

Again using the B3LYP/6-311+G(d,p) lowest energy structure as our reference structure, B3LYP/6-311+G(d,p)//B3LYP/LANL2DZ SPEs were determined for all B3LYP/LANL2DZ minima that are as stable as or more stable than the chosen structure. On the basis of our results for the $Zn(OH)_2X_2Y$ complexes and their fragment complexes, M05-2X/B2(PP) and MP2/6-311+G(d,p) SPEs were then calculated for all arrangements with B3LYP/6-311+G(d,p) energies within 10 kJ/mol of that of the reference structure. MP2/B2-PP//M05-2X/B2-PP SPEs were evaluated only for the global minima.

2.2.3 Binding energies

Bond strengths were compared by removal of ligands from both the inner and outer shells of the $Zn(OH)_2X_2Y_{1,2}$ and $Zn(OH)_2XY_2$ complexes (Eqs. 2.1 and 2.2). Structural changes resulting from removal of a hydroxide ligand were also examined (Eq. 2.3). The binding affinities were corrected for basis set superposition error (BSSE) using the counterpoise method[90] as implemented in Gaussian 09. Only the most stable reactant and product structures were used to compute binding affinities as determined by the MP2/6-311+G(d,p)//B3LYP/6-311+G(d,p) calculations.

$$Zn(OH)_2X_2Y_n \rightarrow Zn(OH)_2X_2Y_{n-1} + Y \quad \textbf{(2.1)}$$

$$Zn(OH)_2X_2Y_n \rightarrow Zn(OH)_2XY_n + X \quad \textbf{(2.2)}$$

$$Zn(OH)_2X_2Y \rightarrow Zn(OH)X_2Y^+ + OH^- \quad \textbf{(2.3)}$$

2.2.4 NBO and AIM analyses

An NBO analysis[91,92] of the Hartree-Fock molecular orbitals was performed to investigate the impact of hyperconjugative effects on the hydrogen-bonded networks and stabilities of the complexes. The second-order perturbation approach was employed to estimate the energies of the orbital interactions ($\Delta E^{(2)}$(donor$\rightarrow$acceptor)).[91] For all of the minima, the Lewis NBOs describe $\geq$ 97% of the total electron density. The presence of bond critical points was determined by AIM analysis,[93] and the bond critical point densities (ρ_b) were used as one means to assess bond strength.[94-96]

2.3 Results and analysis of results

2.3.1 Geometric structures: $Zn(OH)X_2Y^+$, $Zn(OH)_2X_2$, $Zn(OH)_2Y_2$, and $Zn(OH)_2X_{1,2}Y_{1,2}$; X = H_2O, CH_3OH and Y = NH_3, C_5H_5N

Five- and six-coordinate zinc complexes are common in both the solid state and solution.[62,97-103] However, such complexes with one or two hydroxide ligands tend to have the hydroxide(s) bridging two zinc centers, consistent with their propensity to bridge in the absence of sterically demanding ligands.[62,97,98,100,104] This observation combined with the preference for outer-shell water molecules in $[Zn(OH)(H_2O)_{4,5}]^+$,[58,59] $[Zn(OH)(NH_3)_3(H_2O)]^+$,[55] and $[Zn(OH)_2(H_2O)_4]$ [58] suggests that the preferred coordination numbers in the complexes of interest here will be four and five. However, despite starting with structures with all 4-, 5- or 6-ligands bound to the zinc, optimization resulted in only 3- or 4-coordinate zinc complexes.

Several minima were identified for each complex, but all ligands remained on the zinc for the global minima of only the $Zn(OH)X_2Y^+$, $Zn(OH)_2Y_2$, and $Zn(OH)_2(CH_3OH)(C_5H_5N)$ systems. The remaining global minima contain an outer-shell hydrogen-bonded H_2O or CH_3OH. To differentiate between the inner- and outer-shell ligands, notations of the form $[Zn(OH)_2X_2Y]$ and $[Zn(OH)_2XY]X$ will be utilized. Representative examples of the B3LYP/6-311+G(d,p) global minima located are depicted in Fig. 2.2. Illustrated in Figs. 2.3 and 2.4 are examples of the ligand arrangements found for the 3- and 4- coordinate local minima, respectively; arrangements similar to those depicted in Figs. 2.3 and 2.4 were found for all possible X, Y ligand pairs. The relative energies of the various isomeric forms of the complexes are collected in Tables 2.1-2.3.

Most of the complexes have C_1 symmetry. The exceptions are the $[Zn(OH)_2Y]X_2$ - systems, $[Zn(OH)_2(H_2O)_2]$ and the $[Zn(OH)_2Y_2]$ systems, and several of the $[Zn(OH)_2Y_2]X_2$ and $[Zn(OH)_2X_2]Y_2$ systems. The first set of systems has C_S symmetry. The latter sets have C_2 or C_{2V} symmetry. $[Zn(OH)_2(H_2O)_2]$ has C_2 symmetry as in the previous studies.[56-58] Tables 2.4 – 2.6 list geometric parameters for representative 4-, 5-, and 6-ligand global minima. The numbering scheme used in these tables is given in Fig. 2.5. The Cartesian coordinates of all global and most local minima (Table S2.1) and their total energies, enthalpies, and free energies (Table S2.2) are provided as supporting information. Some of the local minima differ by merely the orientation of the methyl hydrogens. Because the total energies of these minima vary by only 1-2 kJ/mol, the data for only the more stable of the two orientations has been included in Tables 2.1-2.3, S2.1, and S2.2. We note that the geometries of $[Zn(OH)_2(NH_3)_2](CH_3OH)$, $[Zn(OH)_2(CH_3OH)(C_5H_5N)]$, $[Zn(OH)_2(CH_3OH)](CH_3OH)(C_5H_5N)$, and $[Zn(OH)_2(H_2O)(C_5H_5N)](H_2O)(C_5H_5N)$ given in Table S2.1 are optimized with the regular convergence criteria in Gaussian 09,[89] and the thermochemical data reported in Tables 2.1-2.3 and S2.2 were evaluated with these geometries. All supplementary tables can be found at http://www.sciencedirect.com/science/article/pii/S2210271X12000187.

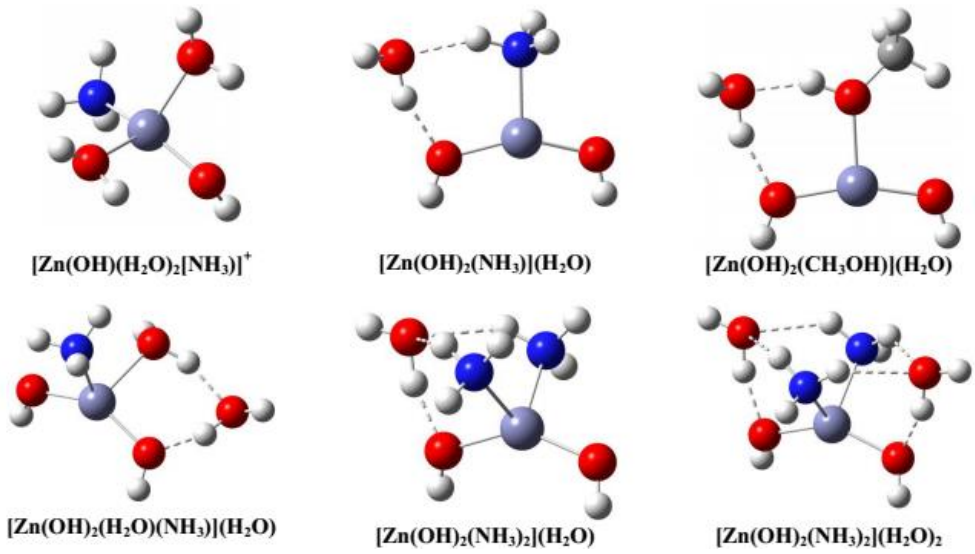

Figure 2.2 Representative examples of B3LYP/6-311+G(d,p) global minima. Color scheme: Zn: purple, O: red, N: blue, C: gray, H: white.

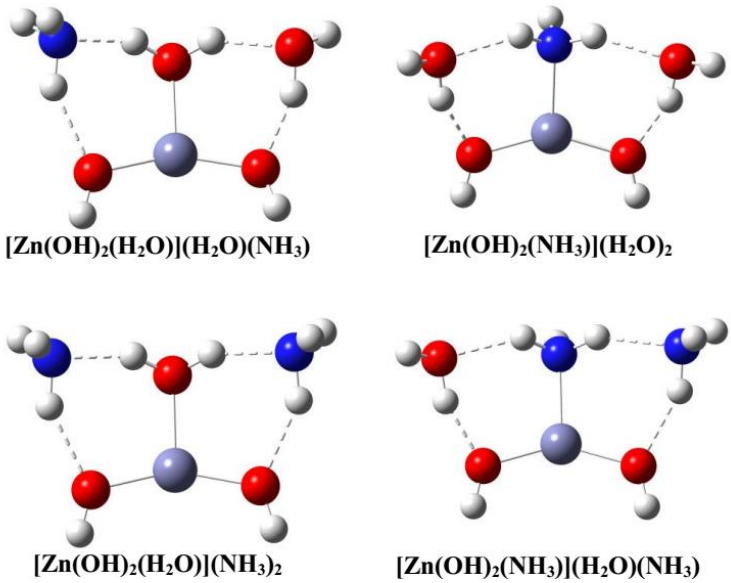

Figure 2.3 Representative examples of B3LYP/6-311+G(d,p) 3-coordinate local minima.

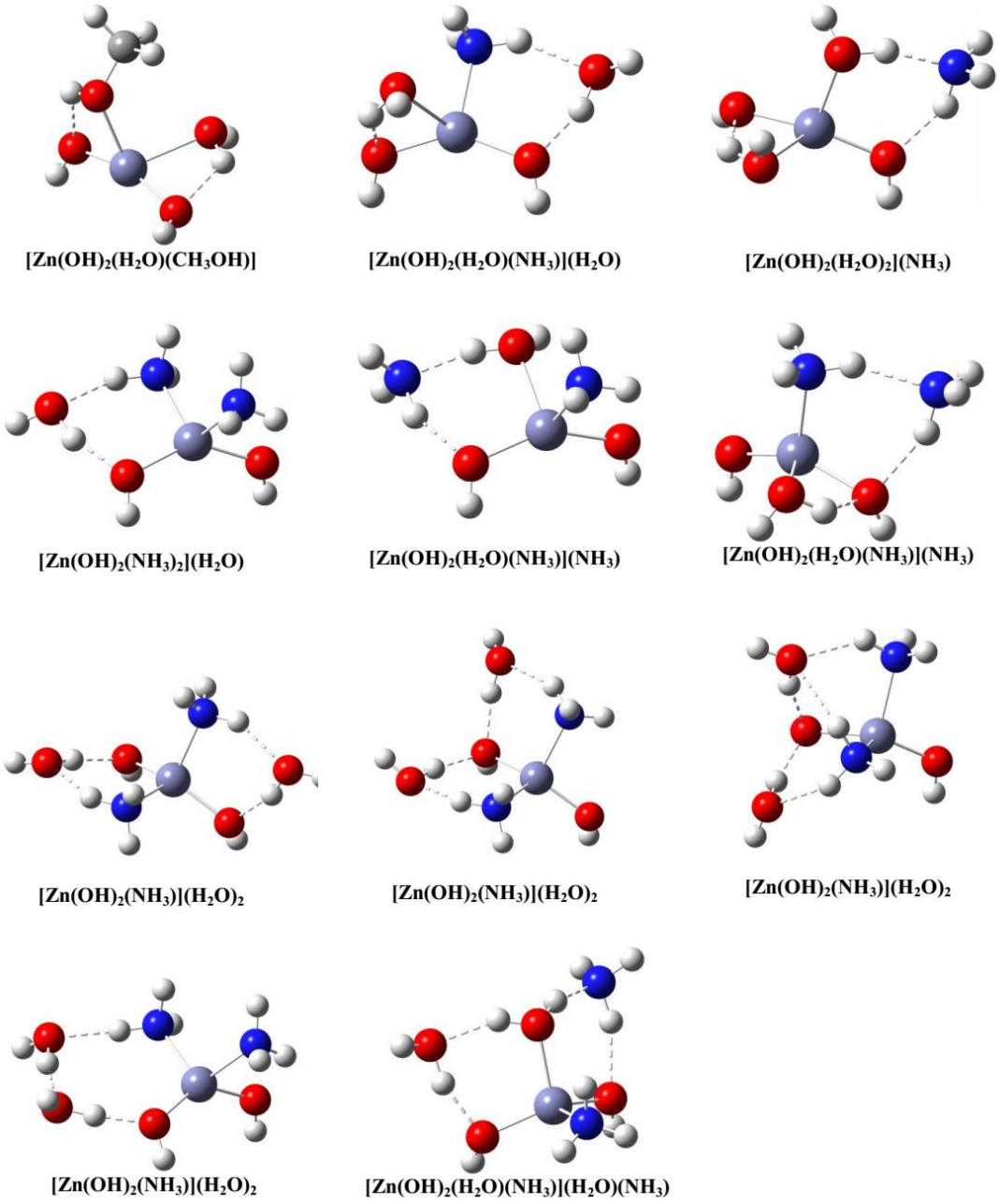

Figure 2.4 Representative examples of B3LYP/6-311+G(d,p) 4-coordinate local minima.

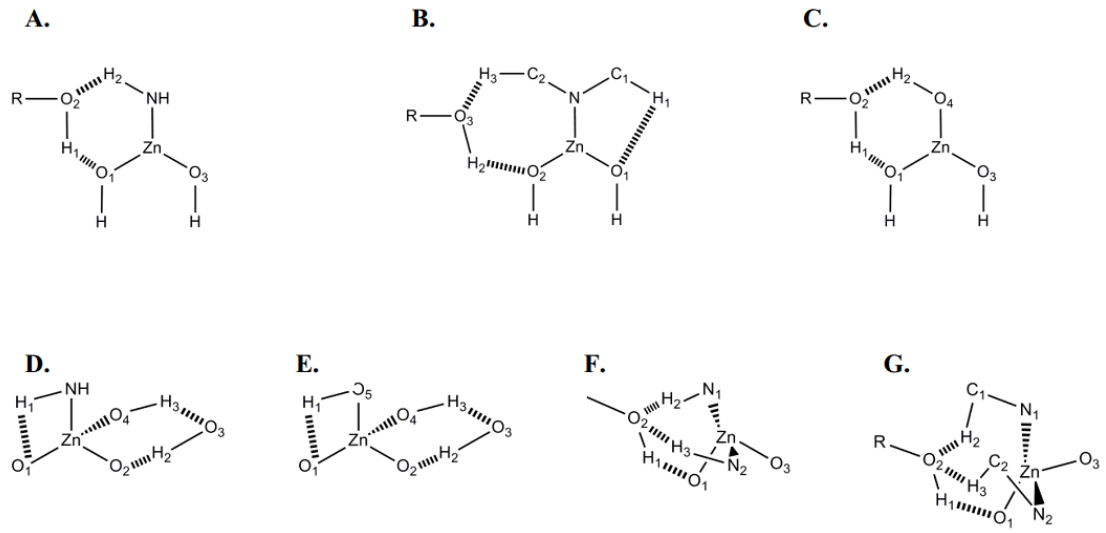

Figure 2.5 Representative numbering schematics for hydrogen-bonding interactions. (A) Representative hydrogen-bonding motif for 3-coordinate, 4-ligand complexes with Y = NH_3. (B) Representative hydrogen-bonding motif for 3-coordinate, 4-ligand complexes with Y = C_5H_5N. (C) Representative hydrogen-bonding motif for 3-coordinate, 4-ligand complexes with all O-binding species. (D) Representative hydrogen-bonding motif for 4-coordinate, 5-ligand complexes with Y = NH_3, C_5H_5N. (E) Representative hydrogen-bonding motif for 4-coordinate, 5-ligand complexes with O-binding species. (F) Representative hydrogen-bonding motif for 4-coordinate, 6-ligand complex global minima with Y = NH_3. (G) Representative hydrogen-bonding motif for 4-coordinate, 6-ligand complex global minima with Y = C_5H_5N.

Table 2.1 Relative enthalpies and free energies of 3- and 4-coordinate, 4-ligand complexes.

complex	ΔH_{298} (kJ/mol)[a]	ΔG_{298} (kJ/mol)[a]
$[Zn(OH)(H_2O)_2(NH_3)]^+$	0.0 (0.0)	0.0 (0.0)
	[0.0] {0.0}	[0.0] {0.0}
$[Zn(OH)(H_2O)(NH_3)](H_2O)^{+b}$	38.0 (36.7)	32.3 (32.2)
	[18.3] {29.6}	[16.3] {24.8}
$[Zn(OH)(H_2O)_2(C_5H_5N)]^+$	0.0 (0.0)	0.0 (0.0)
	[0.0] {0.0}	[0.0] {0.0}
$[Zn(OH)(H_2O)(C_5H_5N)](H_2O)^{+b}$	36.7 (35.9)	27.9 (24.5)
	[18.8] {30.1}	[9.3] {21.0}
$[Zn(OH)(H_2O)_2(CH_3OH)]^+$	0.0 (0.0)	0.0 (0.0)
	[0.0] {0.0}	[0.0] {0.0}
$[Zn(OH)_2(NH_3)](H_2O)^c$	0.0 (0.0)	0.0 (0.0)
	[0.0] {0.0}	[0.0] {0.0}
$[Zn(OH)_2(H_2O)(NH_3)]^d$	1.9 (3.0)	3.8 (4.5)
	[–] {6.0}	[–] {8.1}

$[Zn(OH)_2(C_5H_5N)](H_2O)^{c,e}$	0.0 (0.0) [0.0] {10.8}	0.0 (0.0) [0.0] {11.7}
$[Zn(OH)_2(H_2O)(C_5H_5N)]^{e,f}$	-7.4 (-6.2) [8.6] {0.0}	-3.7 (-2.3) [8.0] {0.0}
$[Zn(OH)_2(H_2O)](H_2O)^{g}$	0.0 (0.0) [0.0] {0.0}	0.0 (0.0) [0.0] {0.0}
$[Zn(OH)_2(H_2O)_2]$	15.3 (16.4) [30.2] {27.8}	13.4 (14.2) [26.0] {26.2}
$[Zn(OH)_2(CH_3OH)](H_2O)^{c,h}$	0.0 (0.0) [0.0] {0.0}	0.0 (0.0) [0.0] {0.0}
$[Zn(OH)_2(CH_3OH)](H_2O)^{i}$	4.8 (5.2) [3.8] {-2.6}	3.7 (3.9) [3.9] {-2.3}
$[Zn(OH)_2(H_2O)(CH_3OH)]^{e,f}$	13.8 (14.8) [28.1] {25.2}	12.6 (13.6) [25.1] {23.9}
$[Zn(OH)_2(H_2O)(CH_3OH)]^{f,j}$	16.7 (17.4) [32.1] {36.2}	14.1 (12.7) [27.7] {33.9}
$[Zn(OH)_2(CH_3OH)](CH_3OH)^{g}$	0.0 (0.0) [0.0] {0.0}	0.0 (0.0) [0.0] {0.0}
$[Zn(OH)_2(CH_3OH)_2]^{f}$	5.4 (6.3) [20.7] {22.2}	6.1 (8.1) [20.3] {23.3}
$[Zn(OH)_2(NH_3)](CH_3OH)^{c}$	0.0 (0.0) [0.0] {0.0}	0.0 (0.0) [0.0] {0.0}
$[Zn(OH)_2(CH_3OH)(NH_3)]^{d,f}$	-1.2 (-0.1) [–] {1.5}	1.6 (2.8) [–] {2.8}
$[Zn(OH)_2(CH_3OH)(C_5H_5N)]^{e,f}$	0.0 (0.0) [0.0] {0.0}	0.0 (0.0) [0.0] {0.0}
$[Zn(OH)_2(C_5H_5N)](CH_3OH)^{c}$	11.5 (10.3) [-6.7] {8.2}	5.6 (5.5) [-7.7] {8.0}
$[Zn(OH)_2(NH_3)_2]^{e}$	0.0 (0.0) [0.0] {0.0}	0.0 (0.0) [0.0] {0.0}
$[Zn(OH)_2(NH_3)](NH_3)^{k}$	16.1 (14.3) [-3.0] {12.4}	11.6 (9.7) [-4.0] {9.1}
$[Zn(OH)_2(C_5H_5N)_2]^{e}$	0.0 (0.0) [0.0] {0.0}	0.0 (0.0) [0.0] {0.0}
$[Zn(OH)_2(C_5H_5N)](C_5H_5N)^{k}$	54.7 (52.6) [32.5] {52.1}	44.0 (41.5) [23.3] {44.6}

[a] M05-2X/B2, M05-2X/B2-PP (in parentheses), B3LYP/6-311+G(d,p) (in square brackets), and B3LYP/LANL2DZ (in curly brackets) data. [b] X···X hydrogen bonding. [c] HO^-···X···Y hydrogen bonding. [d] No B3LYP/6-311+G(d,p) structure identified. [e] HO^-···Y hydrogen bonding. [f] HO^-···X hydrogen bonding. [g] HO^-···X···X hydrogen bonding. [h] For $Zn(OH)_2(H_2O)(CH_3OH)$, X = H_2O and Y = CH_3OH. [i] HO^-···Y···X hydrogen bonding. [j] HO^-···H-O (Y) hydrogen bonding. [k] HO^-···Y···Y hydrogen bonding.

Table 2.2 Relative enthalpies and free energies of 3- and 4-coordinate, 5-ligand complexes

complex	optimization level			
SPE[a]	M052X/B2[b]	M052X/B2-PP[b]	B3LYP/6311+G(d,p)[b]	B3LYP/LANL2DZ[b]
$[Zn(OH)_2(H_2O)(NH_3)](H_2O)$[c]	0.0 (0.0)	0.0 (0.0)	0.0 (0.0)	0.0 (0.0)
$[Zn(OH)_2(H_2O)(NH_3)](H_2O)$[d,e]				
B3LYP/LANL2DZ				18.7 (16.4)
B3LYP/6311+G(d,p)			4.3 (3.6)	5.2 (2.9)
M052X/B2	8.7 (7.0)	8.6 (7.7)	7.2 (6.5)	13.7 (16.4)
M052X/B2-PP	8.4 (6.7)	8.3 (7.4)	6.8 (6.1)	13.4 (11.2)
MP2/6-311+G(d,p)	6.4 (4.7)	6.4 (5.5)	6.2 (5.4)	5.7 (3.5)
$[Zn(OH)_2(NH_3)](H_2O)_2$[d]				
B3LYP/LANL2DZ				34.9 (28.8)
B3LYP/6311+G(d,p)			-3.8 (-6.3)	-7.3 (-13.3)
M052X/B2	13.4 (6.7)	13.3 (7.4)	10.5 (8.0)	15.3 (9.2)
M052X/B2-PP	11.8 (5.1)	11.7 (5.8)	8.9 (6.4)	13.0 (6.9)
MP2/6-311+G(d,p)	3.6 (-3.2)	3.5 (-2.4)	3.4 (0.9)	-1.4 (-7.4)
$[Zn(OH)_2(H_2O)_2](NH_3)$[e,f]				
B3LYP/LANL2DZ				10.3 (11.5)
B3LYP/6311+G(d,p)			23.7 (24.6)	31.7 (32.8)
M052X/B2	27.7(28.5)	27.8 (29.3)	26.5 (27.5)	40.1 (41.3)
M052X/B2-PP	27.3(28.1)	27.3 (28.9)	26.2 (27.2)	40.8 (42.0)
MP2/6-311+G(d,p)	29.7(30.5)	29.9 (31.5)	28.6 (29.5)	35.5 (36.7)
$[Zn(OH)_2(H_2O)](H_2O)(NH_3)$[c,f]				
B3LYP/LANL2DZ				23.2 (23.0)
B3LYP/6311+G(d,p)			4.6 (8.2)	3.6 (3.5)
M052X/B2	22.2(24.0)	22.1 (24.8)	20.6 (24.0)	26.1 (25.9)
M052X/B2-PP	20.6(22.5)	20.5 (23.2)	18.7 (22.4)	24.2 (24.1)
MP2/6-311+G(d,p)	14.7(16.6)	14.7 (17.4)	14.6 (18.3)	12.8 (12.6)
$[Zn(OH)_2(H_2O)(C_5H_5N)](H_2O)$[c,g]	0.0 (0.0)	0.0 (0.0)	0.0 (0.0)	0.0 (0.0)

$[Zn(OH)_2(H_2O)(C_5H_5N)](H_2O)^{d,e,g,h}$							
B3LYP/LANL2DZ						42.5	(40.5)
B3LYP/6311+G(d,p)				17.0	(16.0)	19.6	(17.7)
M052X/B2	20.9(17.7)	20.9	(19.0)	19.7	(18.7)	29.3	(27.4)
M052X/B2-PP	20.5(17.4)	20.7	(18.8)	19.4	(18.4)	29.2	(27.2)
MP2/6-311+G(d,p)	20.1(16.9)	19.2	(17.3)	19.0	(17.9)	19.7	(17.8)
$[Zn(OH)_2(C_5H_5N)](H_2O)_2^{d}$							
B3LYP/LANL2DZ						65.6	(58.3)
B3LYP/6311+G(d,p)				16.3	(10.7)	13.6	(6.4)
M052X/B2	36.1(26.0)	36.1	(27.1)	34.7	(29.1)	43.9	(36.6)
M052X/B2-PP	30.3(20.2)	34.5	(25.6)	33.2	(27.5)	41.9	(34.6)
MP2/6-311+G(d,p)	30.9(20.8)	27.8	(18.8)	27.4	(21.8)	23.8	(16.5)
$[Zn(OH)_2(H_2O)_2](C_5H_5N)^{e,f}$							
B3LYP/LANL2DZ						44.8	(43.2)
B3LYP/6311+G(d,p)				36.5	(33.1)	39.4	(37.8)
M052X/B2	44.6(43.3)	44.6	(43.8)	44.2	(40.8)	53.7	(52.1)
M052X/B2-PP	39.8(38.5)	44.0	(43.2)	43.4	(40.0)	53.8	(52.2)
MP2/6-311+G(d,p)	51.4(50.1)	48.1	(47.3)	46.6	(43.3)	47.4	(45.8)
$[Zn(OH)_2(H_2O)](H_2O)(C_5H_5N)^{c,f}$							
B3LYP/LANL2DZ						31.7	(30.8)
B3LYP/6311+G(d,p)				11.7	(12.1)	9.8	(8.9)
M052X/B2	33.9(33.0)	34.3	(32.8)	33.3	(33.7)	36.8	(35.9)
M052X/B2-PP	28.2(27.3)	32.5	(32.8)	31.6	(32.0)	35.1	(34.2)
MP2/6-311+G(d,p)	30.1(29.2)	26.8	(27.1)	27.1	(27.5)	23.5	(22.5)
$[Zn(OH)_2(H_2O)(CH_3OH)](H_2O)^{c,g,i}$	0.0 (0.0)	0.0	(0.0)	0.0	(0.0)	0.0	(0.0)

$[Zn(OH)_2(H_2O)(CH_3OH)](H_2O)$[d,e]								
B3LYP/LANL2DZ							3.8	(1.5)
B3LYP/6311+G(d,p)					1.5	(-0.7)	2.5	(0.3)
M052X/B2	1.5	(0.9)	1.3	(1.1)	0.8	(-1.5)	2.7	(0.4)
M052X/B2-PP	1.3	(0.8)	1.2	(1.0)	0.9	(-1.4)	2.8	(0.5)
MP2/6-311+G(d,p)	0.3	(-0.3)	0.3	(0.1)	-0.3	(-2.6)	1.1	(-1.2)
$[Zn(OH)_2(CH_3OH)](H_2O)_2$[d]								
B3LYP/LANL2DZ							36.5	(32.9)
B3LYP/6311+G(d,p)					3.4	(-1.4)	-1.9	(-5.5)
M052X/B2	21.6	(14.4)	21.5	(15.0)	19.1	(14.3)	16.6	(13.0)
M052X/B2-PP	20.3	(13.0)	20.1	(13.7)	17.7	(13.0)	14.6	(11.0)
MP2/6-311+G(d,p)	10.0	(2.7)	9.8	(3.4)	9.3	(4.6)	2.4	(-1.2)
$[Zn(OH)_2(H_2O)_2](CH_3OH)$[e,f]								
B3LYP/LANL2DZ							-0.5	(-1.4)
B3LYP/6311+G(d,p)					2.8	(1.4)	4.2	(3.4)
M052X/B2	4.0	(2.0)	4.1	(2.7)	4.2	(2.8)	3.7	(2.8)
M052X/B2-PP	3.9	(1.9)	4.0	(2.5)	4.0	(2.6)	3.8	(2.9)
MP2/6-311+G(d,p)	4.1	(2.1)	4.2	(2.8)	4.1	(2.7)	3.5	(2.7)
$[Zn(OH)_2(H_2O)(CH_3OH)](H_2O)$[c,g]								
B3LYP/LANL2DZ							12.8	(12.2)
B3LYP/6311+G(d,p)					5.8	(4.2)	3.1	(2.5)
M052X/B2	4.4	(4.2)	4.3	(4.6)	4.5	(3.0)	0.0	(-0.6)
M052X/B2-PP	3.9	(3.7)	3.9	(4.2)	4.2	(2.7)	-0.4	(-1.0)
MP2/6-311+G(d,p)	3.0	(2.8)	3.1	(3.5)	2.1	(0.6)	-1.1	(-1.7)

$[Zn(OH)_2(H_2O)](H_2O)(CH_3OH)^{c,f}$								
B3LYP/LANL2DZ							12.1	(8.7)
B3LYP/6311+G(d,p)					-13.1	(-12.9)	-17.4	(-20.8)
M052X/B2	3.6	(0.2)	3.4	(0.8)	1.4	(1.6)	3.1	(-0.3)
M052X/B2-PP	2.1	(-1.2)	2.0	(-0.6)	-0.2	(0.0)	0.8	(-2.6)
MP2/6-311+G(d,p)	-4.8	(-8.1)	-4.9	(-7.5)	-5.4	(-5.2)	-11.3	(-14.8)
$[Zn(OH)_2(CH_3OH)(NH_3)](CH_3OH)^{c}$	0.0	(0.0)	0.0	(0.0)	0.0	(0.0)	0.0	(0.0)
$[Zn(OH)_2(CH_3OH)(NH_3)](CH_3OH)^{d,e}$								
B3LYP/LANL2DZ							14.3	(13.0)
B3LYP/6311+G(d,p)					5.5	(4.6)	6.0	(4.7)
M052X/B2	11.1	(6.9)	10.9	(6.6)	9.6	(8.7)	14.2	(12.8)
M052X/B2-PP	10.8	(6.6)	10.6	(6.3)	9.3	(8.4)	14.0	(12.6)
MP2/6-311+G(d,p)	11.6	(7.4)	11.5	(7.2)	10.3	(9.4)	9.9	(8.6)
$[Zn(OH)_2(CH_3OH)(NH_3)](CH_3OH)^{d,e,h}$								
B3LYP/LANL2DZ							31.3	(27.7)
B3LYP/6311+G(d,p)					11.3	(10.1)	11.4	(7.8)
M052X/B2	15.2	(10.5)	15.1	(10.6)	14.3	(13.0)	20.2	(16.6)
M052X/B2-PP	14.7	(9.9)	14.6	(10.1)	13.9	(12.6)	19.6	(16.0)
MP2/6-311+G(d,p)	16.6	(11.8)	16.6	(12.1)	15.4	(14.1)	14.5	(10.9)
$[Zn(OH)_2(NH_3)](CH_3OH)_2^{d}$								
B3LYP/LANL2DZ							28.2	(23.0)
B3LYP/6311+G(d,p)					-1.0	(-6.7)	-2.1	(-7.3)
M052X/B2	19.3	(7.8)	19.2	(7.0)	15.9	(10.3)	19.2	(14.1)
M052X/B2-PP	17.7	(6.1)	17.5	(5.4)	14.2	(8.6)	17.2	(12.0)
MP2/6-311+G(d,p)	12.7	(1.1)	12.5	(0.4)	11.5	(5.9)	8.7	(3.5)

$[Zn(OH)_2(CH_3OH)_2](NH_3)^{e,f,h,j}$				
B3LYP/LANL2DZ				14.9 (16.2)
B3LYP/6311+G(d,p)			22.2 (24.8)	26.7 (27.9)
M052X/B2	24.7(27.7)	24.5 (26.9)	24.1 (26.7)	34.1 (35.3)
M052X/B2-PP	24.5(27.5)	24.3 (26.6)	23.9 (26.5)	34.5 (35.7)
MP2/6-311+G(d,p)	25.6(28.6)	25.5 (27.9)	25.4 (28.0)	30.6 (31.8)
$[Zn(OH)_2(CH_3OH)_2](NH_3)^{f,h,j}$				
B3LYP/LANL2DZ				32.6 (32.6)
B3LYP/6311+G(d,p)			31.4 (29.5)	33.1 (33.0)
M052X/B2	32.8(31.1)	32.7 (31.4)	32.0 (30.1)	37.8 (37.8)
M052X/B2-PP	32.6(30.9)	32.5 (31.1)	31.8 (29.8)	37.9 (37.8)
MP2/6-311+G(d,p)	34.6(32.8)	34.5 (33.2)	31.6 (29.6)	33.2 (33.1)
$[Zn(OH)_2(CH_3OH)](CH_3OH)(NH_3)^{f,k}$				
B3LYP/LANL2DZ				38.0 (36.6)
B3LYP/6311+G(d,p)			23.4 (18.7)	23.2 (21.9)
M052X/B2	45.2(37.4)	45.1 (37.0)	42.7 (38.0)	45.8 (44.4)
M052X/B2-PP	43.7(36.0)	43.6 (35.5)	41.2 (36.5)	44.4 (43.0)
MP2/6-311+G(d,p)	37.7(29.9)	37.6 (29.5)	37.0 (32.3)	35.4 (34.1)
$[Zn(OH)_2(CH_3OH)](CH_3OH)(NH_3)^{c,l}$				
B3LYP/LANL2DZ				57.0 (54.4)
B3LYP/6311+G(d,p)			35.0 (31.6)	37.3 (34.7)
M052X/B2	56.0(48.7)	56.0 (48.1)	54.2 (50.8)	57.2 (54.6)
M052X/B2-PP	54.4(47.1)	54.3 (46.5)	52.6 (49.1)	55.8 (53.3)
MP2/6-311+G(d,p)	47.9(40.6)	47.9 (40.0)	47.6 (44.2)	49.4 (46.9)
$[Zn(OH)_2(CH_3OH)(C_5H_5N)](CH_3OH)^{c,e,g}$	0.0 (0.0)	0.0 (0.0)	0.0 (0.0)	0.0 (0.0)

$[Zn(OH)_2(CH_3OH)(C_5H_5N)](CH_3OH)$[d,e,g,h]				
B3LYP/LANL2DZ				36.9 (34.8)
B3LYP/6311+G(d,p)			18.3 (15.9)	20.7 (18.7)
M052X/B2	21.3(20.5)	21.2 (20.7)	21.9 (19.6)	29.4 (27.3)
M052X/B2-PP	20.9(20.2)	20.8 (20.4)	21.7 (19.4)	29.3 (27.2)
MP2/6-311+G(d,p)	21.0(20.3)	21.0 (20.6)	22.9 (20.6)	24.9 (22.9)
$[Zn(OH)_2(C_5H_5N)](CH_3OH)_2$[d]				
B3LYP/LANL2DZ				56.9 (47.8)
B3LYP/6311+G(d,p)			20.0 (11.9)	19.4 (10.4)
M052X/B2	43.7(30.0)	43.5 (30.3)	40.9 (32.8)	47.7 (38.6)
M052X/B2-PP	42.0(28.3)	41.8 (28.6)	39.3 (31.1)	45.8 (36.8)
MP2/6-311+G(d,p)	38.6(25.0)	38.7 (25.4)	37.1 (28.9)	35.9 (26.8)
$[Zn(OH)_2(CH_3OH)_2](C_5H_5N)$[f,h,j]				
B3LYP/LANL2DZ				61.2 (60.6)
B3LYP/6311+G(d,p)			45.0 (41.9)	45.7 (45.1)
M052X/B2	49.2(47.8)	49.3 (48.2)	49.5 (46.4)	53.5 (52.9)
M052X/B2-PP	48.4(46.9)	48.4 (47.3)	48.6 (45.6)	53.2 (52.6)
MP2/6-311+G(d,p)	47.8(46.3)	47.9 (46.9)	47.8 (44.8)	48.4 (47.8)
$[Zn(OH)_2(CH_3OH)](CH_3OH)(C_5H_5N)$[f,k]				
B3LYP/LANL2DZ				60.6 (56.7)
B3LYP/6311+G(d,p)			36.0 (27.3)	35.6 (31.6)
M052X/B2	61.3(47.9)	61.2 (43.7)	59.2 (50.4)	62.2 (58.2)
M052X/B2-PP	59.7(46.3)	59.5 (42.0)	57.4 (48.6)	60.7 (56.7)
MP2/6-311+G(d,p)	55.6(42.2)	55.5 (38.0)	54.3 (45.6)	52.3 (48.4)

$[Zn(OH)_2(CH_3OH)](CH_3OH)(C_5H_5N)$[c,l]								
B3LYP/LANL2DZ							71.8	(63.9)
B3LYP/6311+G(d,p)					48.3	(37.9)	49.6	(41.7)
M052X/B2	73.2	(59.6)	73.3	(59.8)	71.8	(61.4)	73.5	(65.6)
M052X/B2-PP	71.3	(57.8)	71.3	(57.8)	69.8	(59.4)	72.0	(64.1)
MP2/6-311+G(d,p)	67.4	(53.8)	67.5	(54.0)	66.4	(56.0)	65.8	(57.9)
$[Zn(OH)_2(NH_3)_2]H_2O$[d,m]	0.0	(0.0)	0.0	(0.0)	0.0	(0.0)	0.0	(0.0)
$[Zn(OH)_2(NH_3)_2]H_2O$[d]								
B3LYP/LANL2DZ							3.1	(1.2)
B3LYP/6311+G(d,p)					2.5	(-0.7)	2.9	(1.0)
M052X/B2	9.0	(-0.2)	8.3	(3.2)	8.3	(5.1)	-10.4	(-12.3)
M052X/B2-PP	9.2	(0.1)	8.6	(3.5)	8.6	(5.4)	-11.3	(-13.2)
MP2/6-311+G(d,p)	5.4	(-3.8)	4.7	(-0.4)	5.8	(2.6)	6.0	(4.1)
$[Zn(OH)_2(NH_3)](H_2O)(NH_3)$[d,n]	–	(–)	–	(–)	10.6	(7.3)	34.1	(29.8)
$[Zn(OH)_2(H_2O)(NH_3)](NH_3)$[g]	–	(–)	–	(–)	13.7	(10.8)	-5.9	(5.0)
$[Zn(OH)_2(H_2O)(NH_3)](NH_3)$[e,n]	–	(–)	–	(–)	26.5	(22.2)	37.0	(34.4)
$[Zn(OH)_2(H_2O)](NH_3)_2$[g]	–	(–)	–	(–)	13.4	(13.9)	13.4	(15.1)
$[Zn(OH)_2(C_5H_5N)_2]H_2O$[d,m]	0.0	(0.0)	0.0	(0.0)	0.0	(0.0)	0.0	(0.0)
$[Zn(OH)_2(C_5H_5N)_2]H_2O$[e]	–	(–)	–	(–)	–	(–)	38.4	(35.4)
$[Zn(OH)_2(NH_3)_2]CH_3OH$[d,m]	0.0	(0.0)	0.0	(0.0)	0.0	(0.0)	0.0	(0.0)
$[Zn(OH)_2(NH_3)_2]CH_3OH$[d]								
B3LYP/LANL2DZ							2.6	(0.3)
B3LYP/6311+G(d,p)					2.4	(-2.6)	2.6	(0.3)
M052X/B2	7.7	(1.2)	–	(–)	7.7	(2.7)	11.7	(9.5)
M052X/B2-PP	7.9	(1.5)	7.8	(0.7)	8.1	(3.1)	12.0	(9.7)
MP2/6-311+G(d,p)	4.7	(-1.7)	4.5	(-2.6)	5.8	(0.8)	7.2	(4.9)

$[Zn(OH)_2(CH_3OH)(NH_3)](NH_3)$[g]	–	(–)	–	(–)	12.0	(11.1)		0.4	(0.9)	
$[Zn(OH)_2(NH_3)](CH_3OH)(NH_3)$[d,n]	–	(–)	–	(–)	10.2	(6.3)		30.8	(32.7)	

[a]Level at which the SPE is calculated. [b]Relative ΔH_{298} and ΔG_{298} (in parentheses) data. Dash indicates calculation not performed or no minima was obtained. [c]$HO^-\cdots X\cdots X$ hydrogen bonding. [d]$HO^-\cdots X\cdots Y$ hydrogen bonding. [e]$HO^-\cdots X$ hydrogen bonding. [f]$HO^-\cdots Y\cdots X$ hydrogen bonding. [g]$HO^-\cdots Y$ hydrogen bonding. [h]Hydrogen bonding to same HO^-. [i]For the $Zn(OH)_2(H_2O)_2(CH_3OH)$ complexes, X = H_2O and Y = CH_3OH. [j]$HO^-\cdots X$ (H-C) hydrogen bonding. [k]$HO^-\cdots X\cdots X$ (H-C) hydrogen bonding. [l]$HO^-\cdots Y\cdots X$ (H-C) hydrogen bonding. [m]X ligand hydrogen bonded to two Y ligands. [n]$HO^-\cdots Y\cdots Y$ hydrogen bonding.

Table 2.3 Relative enthalpies and free energies of 4-coordinate, 6-ligand complexes.

complex	ΔH (kJ/mol)[a]	ΔG (kJ/mol)[a]
$[Zn(OH)_2(NH_3)_2](H_2O)_2$[b,c]	0.0 (0.0)	0.0 (0.0)
	[0.0] {0.0}	[0.0] {0.0}
$[Zn(OH)_2(NH_3)_2](H_2O)_2$[b]	–[d] (–)[d]	– (–)
	[2.2]{-17.8}	[-7.4]{-11.5}
$[Zn(OH)_2(NH_3)_2](H_2O)_2$[b,e]	[12.8]{20.3}	[4.8] {17.5}
$[Zn(OH)_2(NH_3)_2](H_2O)_2$[b,c,e]	[15.7]{25.2}	[11.6]{25.2}
$[Zn(OH)_2(NH_3)_2](H_2O)_2$[f]	[17.1]{22.7}	[15.1]{20.1}
$[Zn(OH)_2(H_2O)(NH_3)](H_2O)(NH_3)$[b,g]	26.2 (26.3)	27.2 (27.4)
	[13.6]{-14.0}	[9.6]{-11.4}
$[Zn(OH)_2(H_2O)(NH_3)](H_2O)(NH_3)$[g,h]	23.4 (23.5)	24.3 (24.5)
	[14.2] {2.0}	[8.9] {2.1}
$[Zn(OH)_2(H_2O)(NH_3)](H_2O)(NH_3)$[h,i]	[18.5] {-3.5}	[15.0] {-0.6}
$[Zn(OH)_2(H_2O)(NH_3)](H_2O)(NH_3)$[b,e,g]	[23.1] {13.4}	[17.1]{13.6}
$[Zn(OH)_2(H_2O)(NH_3)](H_2O)(NH_3)$[e,h,i]	[29.0]{20.6}	[23.8]{21.2}
$[Zn(OH)_2(H_2O)(NH_3)](H_2O)(NH_3)$[b,i,j]	[39.7]{40.5}	[32.3]{40.0}
$[Zn(OH)_2(H_2O)_2](NH_3)_2$[g]	50.0 (50.3)	51.1 (51.7)
	[36.1]{-17.8}	[33.6]{-11.5}
$[Zn(OH)_2(H_2O)_2](NH_3)_2$[e,g]	[41.7]{26.5}	[37.6]{31.2}
$[Zn(OH)_2(H_2O)_2](NH_3)_2$[g,j]	[46.3]{18.9}	[40.1]{21.3}
$[Zn(OH)_2(C_5H_5N)_2](H_2O)_2$[b,c]	0.0 (0.0)	0.0 (0.0)
	[0.0] {0.0}	[0.0] {0.0}
$[Zn(OH)_2(C_5H_5N)_2](H_2O)_2$[b,e,h]	[12.9]{25.7}	[18.9]{27.9}
$[Zn(OH)_2(H_2O)(C_5H_5N)](H_2O)(C_5H_5N)$[b,g]	[22.4] {–}[d]	[25.3] {–}
$[Zn(OH)_2(H_2O)(C_5H_5N)](H_2O)(C_5H_5N)$[g,h]	19.9 (20.1)	17.4 (17.6)
	[7.7] {-8.0}	[11.5] {-9.9}
$[Zn(OH)_2(H_2O)_2](C_5H_5N)_2$[g]	66.9 (66.8)	64.8 (64.8)
	[47.0]{27.2}	[48.6]{20.3}
$[Zn(OH)_2(NH_3)_2](CH_3OH)_2$[b,c]	0.0 (0.0)	0.0 (0.0)
	[0.0] {0.0}	[0.0] {0.0}
$[Zn(OH)_2(NH_3)_2](CH_3OH)_2$[b]	[0.1] {-3.6}	-7.8 {-9.1}
$[Zn(OH)_2(NH_3)_2](CH_3OH)_2$[b,e]	[11.8]{20.9}	0.9 {13.3}
$[Zn(OH)_2(CH_3OH)(NH_3)](CH_3OH)(NH_3)$[b,g]	21.3 (21.5)	22.4 (22.7)
	[11.5] {-6.4}	6.0 {-8.9}
$[Zn(OH)_2(CH_3OH)_2](NH_3)_2$[g]	40.4 (40.6)	41.5 (41.9)
	[31.0] {-4.0}	26.8 {-5.4}

[a]M05-2X/B2, M05-2X/B2-PP (in parentheses), B3LYP/6-311+G(d,p) (in square brackets), and B3LYP/LANL2DZ (in curly brackets) data. [b]$HO^-\cdots X\cdots Y$ hydrogen bonding. [c]X ligand hydrogen bonded to two Y ligands. [d]Complex geometry optimized to a different minima. [e]Outer-shell ligands hydrogen bonded to same OH^-. [f]$HO^-\cdots X\cdots X\cdots Y$ hydrogen bonding. [g]$HO^-\cdots Y\cdots X$ hydrogen bonding. [h]$HO^-\cdots X\cdots X$ hydrogen bonding. [i]$HO^-\cdots Y\cdots Y$ hydrogen bonding. [j]$HO^-\cdots X$ hydrogen bonding.

Table 2.4 Bond lengths, ρ_b values and bond angles of 3-coordinate, 4-ligand global minima.

complex	bond length (Å)[a]	ρ_b[a,b]	bond angles (°)[a]
$[Zn(OH)_2(NH_3)](H_2O)$	$Zn–O_1$: 1.852 (1.845)	0.112 (0.114)	$O_1–Zn–O_3$: 151.4 (152.1)
	[1.863]{1.903}	[0.106] {0.089}	[152.8]{144.7}
	$Zn–O_3$: 1.824 (1.817)	0.121 (0.123)	$O_1–Zn–N$: 102.4 (102.2)
	[1.831]{1.844}	[0.116] {0.103}	[100.6]{101.6}
	Zn–N: 2.098 (2.098)	0.071 (0.071)	$O_3–Zn–N$: 106.3 (105.7)
	[2.118]{2.098}	[0.068] {0.067}	[106.6]{113.7}
	$O_1\cdots H_1$: 1.718 (1.723)	0.040 (0.040)	$O_1\cdots H_1–O_2$: 159.2 (159.3)
	[1.708]{1.504}	[0.043] {0.075}	[157.8]{157.6}
	$H_1–O_2$: 0.983 (0.983)	0.337 (0.338)	$H_1–O_2\cdots H_2$: 90.6 (90.3)
	[0.990]{1.036}	[0.329] {0.263}	[91.3] {96.9}
	$O_2\cdots H_2$: 1.943 (1.947)	0.025 (0.024)	$O_2\cdots H_2–N$: 150.2 (150.2)
	[1.915]{1.673}	[0.027] {0.049}	[151.3]{154.7}
	$H_2–N$: 1.020 (1.020)	0.337 (0.337)	
	[1.029]{1.055}	[0.323] {0.278}	
$[Zn(OH)_2(C_5H_5N)](CH_3OH)$	$Zn–O_1$: 1.845 (1.839)	0.114 (0.116)	$O_1–Zn–O_3$: 149.8 (150.4)
	[1.855]{1.884}	[0.109] {0.094}	[149.8]{145.6}
	$Zn–O_3$: 1.835 (1.828)	0.118 (0.120)	$O_1–Zn–N$: 110.3 (109.7)
	[1.845]{1.861}	[0.112] {0.099}	[111.2]{114.5}
	Zn–N: 2.074 (2.073)	0.075 (0.075)	$O_3–Zn–N$: 99.9 (99.9)
	[2.098]{2.085}	[0.071] {0.068}	[99.0] {99.8}
	$O_1\cdots H_1$: 1.736 (1.740)	0.039 (0.039)	$O_1\cdots H_1–O_2$: 169.7 (169.7)
	[1.722]{1.559}	[0.042] {0.067}	[167.7]{168.1}
	$H_1–O_2$: 0.978 (0.977)	0.347 (0.348)	$H_1–O_2\cdots H_2$: 81.0 (80.0)
	[0.985]{1.021}	[0.338] {0.282}	[85.6] {95.8}
	$O_2\cdots H_2$: 2.167 (2.178)	0.016 (0.016)	$O_2\cdots H_2–C_1$: 172.4 (173.0)
	[2.132]{1.974}	[0.018] {0.026}	[170.3]{163.3}

	H_2–C_1: 1.081 (1.080) [1.087]{1.093}	0.304 (0.305) [0.290] {0.270}	O_3···H_3–C_2: 123.5 (123.2) [123.7]{125.5}
	O_3···H_3: 2.285 (2.287) [2.281]{2.241}	0.014 (0.014) [0.014] {0.015}	
	H_3–C_2: 1.080 (1.080) [1.085]{1.088}	0.304 (0.304) [0.290] {0.272}	
$[Zn(OH)_2(H_2O)](H_2O)$	Zn–O_1: 1.848 (1.839) [1.852]{1.916}	0.113 (0.113) [0.108] {0.087}	O_1–Zn–O_3: 158.7 (159.9) [161.7]{147.6}
	Zn–O_3: 1.811 (1.804) [1.815]{1.835}	0.125 (0.127) [0.121] {0.105}	O_1–Zn–O_4: 95.8 (95.8) [94.3] {94.6}
	Zn–O_4: 2.055 (2.061) [2.102]{1.996}	0.066 (0.065) [0.058] {0.070}	O_3–Zn–O_4: 105.3 (104.2) [104.0]{117.8}
	O_1···H_1: 1.688 (1.700) [1.701]{1.417}	0.044 (0.043) [0.044] {0.093}	O_1···H_1–O_2: 156.5 (156.5) [155.5]{156.4}
	H_1–O_2: 0.989 (0.988) [0.993]{1.068}	0.330 (0.332) [0.326] {0.238}	H_1–O_2···H_2: 90.7 (90.5) [91.7] {97.0}
	O_2···H_2: 1.670 (1.683) [1.694]{1.409}	0.048 (0.046) [0.045] {0.094}	O_2···H_2–O_4: 156.7 (156.3) [154.7]{154.7}
	H_2–O_4: 0.991 (0.989) [0.994]{1.066}	0.325 (0.328) [0.323] {0.237}	
$[Zn(OH)_2(CH_3OH)](H_2O)$	Zn–O_1: 1.845 (1.838) [1.852]{1.909}	0.114 (0.116) [0.110] {0.088}	O_1–Zn–O_3: 159.7 (160.4) [161.8]{150.1}
	Zn–O_3: 1.816 (1.808) [1.819]{1.837}	0.124 (0.126) [0.120] {0.105}	O_1–Zn–O_4: 97.7 (97.5) [95.8] {95.8}
	Zn–O_4: 2.035 (2.038) [2.076]{1.998}	0.069 (0.069) [0.062] {0.070}	O_3–Zn–O_4: 102.4 (102.0) [102.4]{114.1}
	O_1···H_1: 1.709 (1.715) [1.707]{1.455}	0.042 (0.041) [0.043] {0.085}	O_1···H_1–O_2: 157.6 (157.5) [156.5]{156.7}

	H_1–O_2:	0.987 (0.986) [0.992]{1.055}	0.334 (0.335) [0.327] {0.249}	H_1–O_2···H_2: 90.9 (90.6) [91.6] {96.8}
	O_2···H_2:	1.723 (1.735) [1.730]{1.473}	0.041 (0.041) [0.042] {0.081}	O_2···H_2–O_4: 153.3 (153.4) [152.8]{153.5}
	H_2–O_4:	0.982 (0.981) [0.988]{1.044}	0.339 (0.340) [0.331] {0.257}	
$[Zn(OH)_2(CH_3OH)](CH_3OH)$	Zn–O_1:	1.850 (1.841) [1.853]{1.909}	0.112 (0.115) [0.109] {0.088}	O_1–Zn–O_3: 149.8 (151.7) [150.8]{136.9}
	Zn–O_3:	1.815 (1.808) [1.819]{1.835}	0.124 (0.126) [0.120] {0.105}	O_1–Zn–O_4: 95.4 (95.5) [94.0] {94.6}
	Zn–O_4:	2.053 (2.061) [2.111]{2.016}	0.067 (0.066) [0.058] {0.067}	O_3–Zn–O_4: 114.7 (112.6) [115.1]{128.6}
	O_1···H_1:	1.669 (1.685) [1.687]{1.439}	0.047 (0.045) [0.046] {0.089}	O_1···H_1–O_2: 155.7 (155.6) [154.8]{156.6}
	H_1–O_2:	0.989 (0.987) [0.992]{1.061}	0.333 (0.336) [0.330] {0.248}	H_1–O_2···H_2: 89.9 (89.8) [91.6] {95.2}
	O_2···H_2:	1.606 (1.624) [1.654]{1.431}	0.058 (0.055) [0.051] {0.091}	O_2···H_2–O_4: 161.7 (161.3) [152.8]{157.6}
	H_2–O_4:	1.000 (0.997) [0.998]{1.064}	0.318 (0.322) [0.321] {0.244}	

[a]M05-2X/B2, M05-2X/B2-PP (in parentheses), B3LYP/6-311+G(d,p) (in square brackets), and B3LYP/LANL2DZ (in curly brackets) data. See Fig. 2.5 for numbering. [b]Same atoms as corresponding bond length.

Table 2.5 Bond lengths, ρ_b values and bond angles of $[Zn(OH)_2XY]X$ global minima.

complex	bond length (Å)[a]	ρ_b[a,b]	bond angle (°)[a]
$[Zn(OH)_2(H_2O)(NH_3)](H_2O)$	$Zn–O_1$: 1.862 (1.855)	0.109 (0.111)	$O_1–Zn–O_2$: 143.1 (144.1)
	[1.869] {1.899}	[0.105] {0.090}	[145.1] {133.2}
	$Zn–O_2$: 1.894 (1.886)	0.101 (0.103)	$O_1–Zn–O_4$: 105.5 (104.2)
	[1.903] {1.962}	[0.097] {0.078}	[107.0] {121.3}
	$Zn–O_4$: 2.133 (2.140)	0.056 (0.055)	$O_1–Zn–N$: 92.9 (93.6)
	[2.200] {2.049}	[0.048] {0.062}	[93.1] {83.1}
	Zn–N: 2.130 (2.128)	0.065 (0.065)	$O_2–Zn–O_4$: 97.3 (97.5)
	[2.153] {2.160}	[0.061] {0.057}	[95.6] {93.4}
	$O_1{\cdots}H_1$: 2.526 (2.551)	– (–)	$O_2–Zn–N$: 114.7 (114.1)
	[2.601] {2.073}	[–] {0.021}	[113.2] {117.4}
	$O_2{\cdots}H_2$: 1.564 (1.578)	0.064 (0.061)	$O_4–Zn–N$: 92.9 (92.0)
	[1.622] {1.341}	[0.055] {0.113}	[91.2] {107.8}
	$H_2–O_3$: 1.012 (1.009)	0.304 (0.308)	$O_2{\cdots}H_2–O_3$: 163.4 (163.4)
	[1.006] {1.105}	[0.312]{0.215}	[160.7] {158.8}
	$O_3{\cdots}H_3$: 1.652 (1.668)	0.050 (0.048)	$H_2–O_3{\cdots}H_3$: 89.8 (89.7)
	[1.691] {1.391}	[0.046]{0.100}	[91.3] {95.9}
	$H_3–O_4$: 0.995 (0.992)	0.323 (0.326)	$O_3{\cdots}H_3–O_4$: 159.2 (158.7)
	[0.995] {1.076}	[0.323] {0.232}	[157.8] {157.5}
			$O_1{\cdots}H_1–N$: 101.3 (100.4)
			[98.2] {116.8}
$[Zn(OH)_2(CH_3OH)(C_5H_5N)](CH_3OH)$	$Zn–O_1$: 1.864 (1.858)	–[c] (–)[c]	$O_1–Zn–O_2$: 146.0 (146.5)
	[1.874] {1.894}	[–][c] {0.092}	[146.8] {136.3}
	$Zn–O_2$: 1.902 (1.895)	– (–)	$O_1–Zn–O_4$: 105.0 (104.8)
	[1.911] {1.960}	[–] {0.078}	[105.6] {119.3}
	$Zn–O_4$: 2.099 (2.102)	– (–)	$O_1–Zn–N$: 99.5 (99.7)
	[2.152] {2.058}	[–] {0.060}	[98.0] {94.7}

		Zn–N: 2.105 (2.103)	– (–)	O_2–Zn–O_4: 95.0 (94.9)	
		[2.140] {2.144}	[–] {0.059}	[94.0] {91.2}	
		O_1···H_1: 2.401 (2.405)	– (–)	O_2–Zn–N: 104.5 (104.3)	
		[2.370] {2.171}	[–] {0.018}	[105.5] {107.9}	
		O_2···H_2: 1.596 (1.603)	– (–)	O_4–Zn–N: 98.5 (97.9)	
		[1.635] {1.396}	[–] {0.099}	[98.4] {104.5}	
		H_2–O_3: 1.001 (1.000)	– (–)	O_2···H_2–O_3: 162.3 (162.2)	
		[1.000] {1.079}	[–] {0.236}	[160.0] {159.8}	
		O_3···H_3: 1.691 (1.698)	– (–)	H_2–O_3···H_3: 87.2 (87.0)	
		[1.721] {1.476}	[–] {0.082}	[89.6] {92.5}	
		H_3–O_4: 0.988 (0.987)	– (–)	O_3···H_3–O_4: 159.9 (159.9)	
		[0.989] {1.048}	[–] {0.256}	[156.7] {156.9}	
				O_1···H_1–C: 122.0 (121.7)	
				[122.7] {126.3}	
38	$[Zn(OH)_2(H_2O)(CH_3OH)](H_2O)$	Zn–O_1: 1.867 (1.859)	0.108 (0.108)	O_1–Zn–O_2: 149.9 (151.2)	
		[1.876] {1.921}	[0.104] {0.085}	[152.3] {135.9}	
		Zn–O_2: 1.870 (1.860)	0.107 (0.107)	O_1–Zn–O_4: 103.4 (102.0)	
		[1.875] {1.938}	[0.104]{0.082}	[104.7] {120.3}	
		Zn–O_4: 2.102 (2.107)	0.060 (0.060)	O_1–Zn–O_5: 81.3 (81.7)	
		[2.144] {2.024}	[0.054]{0.066}	[78.4] {72.6}	
		Zn–O_5: 2.142 (2.144)	0.054 (0.054)	O_2–Zn–O_4: 96.8 (96.9)	
		[2.207] {2.124}	[0.047]{0.051}	[94.9] {93.5}	
		O_1···H_1: 2.007 (2.023)	[–] (–)	O_2–Zn–O_5: 119.2 (118.4)	
		[1.957] {1.627}	[0.028]{0.056}	[118.6] {122.3}	
		O_2···H_2: 1.612 (1.628)	0.055 (0.055)	O_4–Zn–O_5: 95.3 (94.8)	
		[1.651] {1.365}	[0.050]{0.106}	[97.6] {112.5}	
		H_2–O_3: 1.001 (0.998)	0.316 (0.317)	O_2···H_2–O_3: 159.7 (159.5)	
		[1.000] {1.092}	[0.319]{0.223}	[157.1] {157.5}	

$O_3{\cdots}H_3$: 1.657 (1.673)	0.049 (0.049)	$H_2–O_3{\cdots}H_3$: 90.2 (90.1)	
[1.685] {1.391}	[0.047]{0.099}	[91.4] {96.0}	
$H_3–O_4$: 0.994 (0.992)	0.323 (0.323)	$O_3{\cdots}H_3–O_4$: 159.4 (159.0)	
[0.996] {1.076}	[0.322] {0.232}	[158.0] {156.9}	
		$O_1{\cdots}H_1–O_5$: 119.0 (118.4)	
		[120.6] {128.3}	

[a]M05-2X/B2, M05-2X/B2-PP (in parentheses), B3LYP/6-311+G(d,p) (in square brackets), and B3LYP/LANL2DZ (in curly brackets) data. See Fig. 2.5 for numbering. [b]Same atoms as corresponding bond length. [c]AIM analysis found duplicate critical points.

Table 2.6 Bond lengths, ρ_b values and bond angles of $[Zn(OH)_2Y_2]X_2$ global minima.

complex	bond length (Å)[a]	ρ_b[a,b]	bond angles (°)[a]
$[Zn(OH)_2(NH_3)_2](H_2O)_2$	$Zn–O_1$: 1.898 (1.892)	0.100 (0.101)	$O_1–Zn–O_3$: 141.2 (141.2)
	[1.909] {1.929}	[0.095] {0.083}	[143.7] {144.1}
	$Zn–N_1$: 2.131 (2.129)	0.066 (0.066)	$O_1–Zn–N_1$: 107.5 (107.5)
	[2.156] {2.141}	[0.062] {0.061}	[106.2] (102.5)
	$O_1{\cdots}H_1$: 1.645 (1.647)	0.051 (0.051)	$O_1–Zn–N_2$: 99.2 (99.1)
	[1.675] {1.500}	[0.048] {0.076}	[98.9] {102.5}
	$H_1–O_2$: 0.998 (0.998)	0.319 (0.320)	$N_1–Zn–N_2$: 92.6 (92.5)
	[1.000] {1.045}	[0.319] {0.258}	[91.7] {91.0}
	$O_2{\cdots}H_2$: 2.204 (2.213)	0.015 (0.015)	$O_1{\cdots}H_1–O_2$: 161.4 (161.5)
	[2.245] {2.078}	[0.014] {0.021}	[158.9] {158.9}
	$H_2–N_1$: 1.013 (1.014)	0.344 (0.344)	$H_1–O_2{\cdots}H_2$: 92.1 (88.0)
	[1.020] {1.029}	[0.331] {0.301}	[92.3] {93.3}
	$O_2{\cdots}H_3$: 2.216 (2.202)	– (–)	$O_2{\cdots}H_2–N_1$: 132.3 (134.3)
	[2.259] {2.078}	[0.014] {0.021}	[132.8] {138.0}

	H_3–N_2:	1.014	(1.013)	0.343	(0.343)	H_1–O_2···H_3:	88.3	(91.9)
		[1.020]	{1.029}	[0.331]	{0.301}		[89.1]	{93.3}
						O_2···H_3–N_2:	134.1	(132.4)
							[133.7]	{138.0}
$[Zn(OH)_2(C_5H_5N)_2](CH_3OH)_2$	Zn–O_1:	1.897	(1.891)	0.100	(0.101)	O_1–Zn–O_3:	133.8	(134.1)
		[1.911]	{1.933}	[0.095]	{–}[c]		[132.2]	{124.3}
	Zn–N_1:	2.109	(2.107)	0.069	(0.069)	O_1–Zn–N_1:	107.4	(107.3)
		[2.142]	{2.132}	[0.064]	{–}		[108.4]	{107.9}
	O_1···H_1:	1.628	(1.631)	0.053	(0.053)	O_1–Zn–N_2:	102.4	(102.4)
		[1.647]	{1.478}	[0.051]	{–}		[102.3]	{107.9}
	H_1–O_2:	0.992	(0.991)	0.330	(0.331)	N_1–Zn–N_2:	98.2	(98.0)
		[0.995]	{1.041}	[0.327]	{–}		[98.7]	{97.7}
	O_2···H_2:	2.301	(2.303)	0.012	(0.012)	O_1···H_1–O_2:	169.9	(169.9)
		[2.256]	{2.216}	[0.014]	{–}		[166.9]	{165.9}
	H_2–C_1:	1.080	(1.080)	0.304	(0.304)	H_1–O_2···H_2:	74.3	(74.0)
		[1.086]	{1.089}	[0.290]	{–}		[80.9]	{82.1}
	O_2···H_3:	2.404	(2.405)	0.011	(0.011)	O_2···H_2–C_1:	163.9	(164.1)
		[2.568]	{2.216}	[0.007]	{–}		[168.0]	{158.4}
	H_3–C_2:	1.080	(1.080)	0.304	(0.304)	H_1–O_2···H_3:	68.6	(68.4)
		[1.084]	{1.089}	[0.290]	{–}		[66.6]	{82.1}
						O_2···H_3–C_2:	153.9	(153.8)
							[148.4]	{158.4}

[a]M05-2X/B2, M05-2X/B2-PP (in parentheses), B3LYP/6-311+G(d,p) (in square brackets), and B3LYP/LANL2DZ (in curly brackets) data. See Fig. 2.5 for numbering. [b]Same atoms as corresponding bond length. [c]AIM analysis found duplicate critical points.

2.3.1.1 Zn coordination number and coordination mode

That the zinc is 3- or 4-coordinate in the optimal structures of the $Zn(OH)_2XY_2$ and $Zn(OH)_2X_2Y_{1,2}$ complexes is another manifestation of the valence buffer effect (Fig. 2.2 and Tables 2.1-2.3).[60,70-74] A more unexpected result is that no local minima with a five-coordinate zinc was located, even for complexes with 6-ligands. Binding of two hydroxides to the zinc stabilizes low-coordination zinc environments and, in general, the H_2O and CH_3OH ligands are more favorable in the outer shell. Calculations carried out by Zhu and Pan[58] indicate that the global minimum of $Zn(OH)_2(H_2O)_4$ is $[Zn(OH)_2(H_2O)_3](H_2O)$ (B3LYP functional and 6-311++G(3df) (Zn) or 6-311++G(d,p) (O and H) basis set). Apparently, the interaction of the coordinating ligands with the second-shell water molecule decreases electron donation to the zinc sufficiently to stabilize the higher metal coordination number in this system. Similarly, Smith et al.[56] have reported that addition of outer-shell water molecules helps to stabilize tetracoordination of the metal in $[[Zn(OH)_4](H_2O)_2]^{2-}$. A second demonstration of the valence buffer effect in this work is that the preferred metal coordination number is four for the cationic $Zn(OH)X_2Y^+$ complexes but is three for the neutral $Zn(OH)_2X_2$ complexes (Fig. 2.2 and Table 2.1). The former result agrees with those of previous computations on related systems ($Zn(OH)X_3^+$, X = H_2O,[56-58] NH_3, and $C_3H_4N_2$ [55]) at similar levels of theory; the latter result does not. In the earlier studies of $Zn(OH)_2(H_2O)_2$, three-coordinate zinc complexes either were not located[56,58] or were of higher energy.[57]

For all of the species with a coordination number of four, repulsion between the OH^- ligands leads to distortion from a tetrahedrally coordinated zinc(II) ion. Such a

distortion was also reported by Smith et al. for $[Zn(OH)_2(H_2O)_2]$.[56] In all 3-coordinate systems the zinc and its three coordinated atoms lie essentially in a plane (Figs. 2.1 and 2.2 and Tables 2.1 and 2.2). These results are in accord with those from X-ray diffraction studies that have demonstrated that the zinc centers in a variety of three-coordinate complexes adopt a trigonal planar geometry.[105-114] Also, other computational studies have shown, for example, that $[[Zn(OH)_3](H_2O)]^-$ [56] and [Zn(1,10-phenanthroline)(OH)]$^+$ [115] are three-coordinate planar zinc(II) complexes. As mentioned above, however, to our knowledge no one has reported the trigonal planar $[Zn(OH)_2(H_2O)](H_2O)$ complex as the global minimum of $Zn(OH)_2(H_2O)_2$. Only Tiraboschi et al.[57] have reported a local minimum with a related structure. In their optimal structure, one of the water molecules is a double proton donor, forming hydrogen bonds with the two hydroxides ($HO^-\cdots HOH\cdots OH^-$). The water molecule is still loosely bound to the zinc, however, because the Zn-O bond distance is only elongated by about 0.15 – 0.2 Å. In our optimal structure, the outer-shell water molecule is both a proton and an electron donor, forming a cooperative hydrogen-bonding network with one of the hydroxides and the other water molecule ($HO^-\cdots H_2O\cdots HOH$, Fig. 2.1). In fact, the $HO^-\cdots X\cdots X(Y)$ hydrogen-bonding motif is found in all of the 3-coordinate, 4- and 5-ligand complexes (Fig. 2.2). When we searched for the $HO^-\cdots HOH\cdots OH^-$ motif, invariably the starting structure rearranged to a minimum with a different hydrogen-bonding motif.

2.3.1.1.1 M05-2X versus B3LYP minima

There is excellent agreement between the minima located at the M05-2X/B2, M05-2X/B2-PP, B3LYP/6-311+G(d,p), and B3LYP/LANL2DZ levels of theory (Tables

2.1-2.3 and S2.1-2.2). With just a few exceptions, the same set of isomers is found at all levels of theory (Tables 2.1-2.3 and S2.1-2.2). The B3LYP/LANL2DZ results diverge more from the other three sets of results with respect to the magnitudes of and trends in the relative energies of the various isomers. Similar results for B3LYP/6-311+G(d,p) versus B3LYP/LANL2DZ have been reported by Peschke et al. and Pavlov et al. for zinc-acetone and zinc-water complexes, respectively.[116,117] There is some variation in the global minima of the 4-ligand $Zn(OH)_2XY$ metal complexes; otherwise, the global minimum is the same for all four levels of calculation (Table 2.1 and S2.2).

2.3.1.1.2 Effect of geometry on single-point energies

2.3.1.1.2.1 B3LYP/6-311+G(d,p), M05-2X/B2, and M05-2X/B2-PP geometries

At a given level of theory (MP2/6-311+G(d,p) or M05-2X/B2(PP)), the relative isomer enthalpies and free energies are nearly independent of whether the B3LYP/6-311+G(d,p), M05-2X/B2 or M05-2X/B2-PP equilibrium geometry is utilized. The deviations usually range from 0 – 3 kJ/mol. For example, the difference between the highest and lowest values among the MP2/6-311+G(d,p)//M05-2X/B2, MP2/6-311+G(d,p)//M05-2X/B2-PP, and MP2/6-311+G(d,p)//B3LYP/6-311+G(d,p) relative enthalpies for $[Zn(OH)_2(H_2O)_2](NH_3)$ is 1.1 kJ/mol. On the basis of these results, the next section will compare SPEs only for the B3LYP-optimized geometries.

2.3.1.1.2.2 B3LYP/6-311+G(d,p) versus B3LYP/LANL2DZ geometries

Computation of MP2/6-311+G(d,p) SPEs from the B3LYP/6-311+G(d,p) and B3LYP/LANL2DZ geometries yields good agreement in relative enthalpies and free energies, even though the relative enthalpies of some analogous B3LYP/LANL2DZ and

B3LYP/6-311+G(d,p) structures differ by as much as 50 kJ/mol (Tables 2.2, 2.3 and S2.2). With two exceptions, the trends are now the same. The two exceptions are $[Zn(OH)_2(NH_3)_2](H_2O)_2$ and $[Zn(OH)_2(NH_3)_2](CH_3OH)_2$, for which the C_2 (C_{2v}) isomers are nearly equal in stability at all levels of theory (Tables 2.3 and S2.2). In fact, the MP2 relative enthalpy values now agree within 7 kJ/mol for the two sets of geometries. A similar agreement is observed when the B3LYP/6-311+G(d,p) and B3LYP/6-311+G(d,p)//B3LYP/LANL2DZ values are compared, whereas the M05-2X/B2(PP) data for these two geometries generally vary by a larger amount.

2.3.1.1.3 Variations of single-point energies for a given geometry

For any given equilibrium structure, the M05-2X/B2 and M05-2X/B2-PP relative thermochemical values indicate that calculating only the latter SPEs is sufficient. There are often significant deviations between the B3LYP/6-311+G(d,p) and M05-2X/B2(PP) data, however. In general, the local minima are more competitive with respect to the global minimum for the B3LYP/6-311+G(d,p) calculations. For example, for $[Zn(OH)_2(H_2O)](H_2O)(NH_3)$ the B3LYP/6-311+G(d,p) relative enthalpy is 4.6 kJ/mol, whereas the M05-2X/B2//B3LYP/6-311+G(d,p) and M05-2X/B2-PP//B3LYP/6-311+G(d,p) relative enthalpies are 20.6 and 18.7 kJ/mol, respectively (Table 2.2).

When comparing the MP2 and DFT relative thermochemistry for a complex containing no more than one NH_3 or C_5H_5N, the global minima are either the same or the difference in energy among the most stable isomers is negligible (Tables 2.2 and S2.2). As reported by Cooper et al. for the $[Zn(H_2O)_n]^{2+}$ complexes,[84,118] the trends in relative enthalpies and free energies among all the isomers, however, are not the same for the

DFT and MP2 calculations. (See for example $[Zn(OH)_2(H_2O)(NH_3)]H_2O$ and $[Zn(OH)_2(NH_3)](H_2O)_2$ (Tables 2.2 and S2.2).) Nevertheless, the isomers that are not competitive with the DFT methods are also not competitive with the WFT method, although improving the electron correlation sometimes stabilizes and sometimes destabilizes the non-competitive isomers. Thus, the results suggest that calculating SPEs is not necessary for isomers with B3LYP/6-311+G(d,p) relative thermochemical values greater than 10-15 kJ/mol. This approach was followed for the remaining complexes (Tables 2.1-2.3 and S2.2). For the rest of this section, the MP2/6-311+G(d,p)//B3LYP/6-311+G(d,p) thermochemical values are used.

2.3.1.1.4 Global versus local minima

The 4-coordinate, 5-ligand Zn(II) complexes $[Zn(OH)_2XY]X$ have two stable isomers with X in the outer shell, but the global minimum has $HO^{-}\cdots X\cdots X$ rather than $HO^{-}\cdots X\cdots Y$ hydrogen bonding (Fig. 2.2). In contrast the 4-coordinate, 6-ligand global minima $[Zn(OH)_2Y_2]X_2$ contain the latter type of hydrogen bonding. Isomers of a third type $[Zn(OH)_2(X)_2]Y_{1,2}$, with an outer-shell dually hydrogen-bonded NH_3 or C_5H_5N ligand, are less stable by 5 – 50 kJ/mol. There are also mixed combinations of outer-shell ligands $[Zn(OH)_2XY]XY$ observed for the 4-coordinate, 6-ligand systems; these complexes are higher in enthalpy by approximately 15 – 40 kJ/mol (Table 2.3). Doubly bridged $HO^{-}\cdots H_2O\cdots HOH\cdots OH^{-}$ arrangements were examined but are not stable. These results are consistent with the experimental result that the solvent CH_3OH does not replace C_5H_5N in the zinc axial position of the metal-seamed nanocapsules.[30-32] Overall, the trends in relative enthalpy are similar for the various sets of 5- and 6-ligand

complexes as the corresponding inner-/outer-shell ligands and hydrogen-bonding motifs change (Tables 2.2 and 2.3).

The 3-coordinate, 5-ligand $[Zn(OH)_2Y]X_2$ complexes are more stable than the $[Zn(OH)_2X]XY$ systems. These complexes have the same hydrogen bonding motifs as described above. With respect to the 3-coordinate versus 4-coordinate, 5-ligand systems ($[Zn(OH)_2Y]X_2$ versus $[Zn(OH)_2XY]X$), complexes with one outer-shell water are similar in energy to those with two outer-shell waters. Changing Y from NH_3 to C_5H_5N or changing X from H_2O to CH_3OH makes the 3-coordinate systems less competitive with respect to the 4-coordinate systems.

Both 3- and 4-coordinate, 5-ligand species were observed for the $Zn(OH)_2XY_2$ complexes. The $[Zn(OH)_2Y_2]X$ global minima mirror the $[Zn(OH)_2Y_2]X_2$ global minima with one X ligand removed. Additional minima of the form $[Zn(OH)_2XY]Y$, $[Zn(OH)_2Y]XY$, and $[Zn(OH)_2X]Y_2$ were identified. The hydrogen-bonding motifs and trends in energetics are similar to those discussed for the 4-coordinate, 5- and 6-ligand species $Zn(OH)_2X_2Y_{1,2}$ (Tables 2.2 and 2.3).

Compared to the 3-coordinate, 4-ligand metal systems $[Zn(OH)_2X]X$, minima of the form $[Zn(OH)_2X_2]$ are approximately 20-30 kJ/mol less stable (Table 2.1). The reversed stability order for the nitrogen based complexes has the $[Zn(OH)_2Y]Y$ arrangements up to 50 kJ/mol higher in energy than the $[Zn(OH)_2Y_2]$ arrangements. For $Zn(OH)_2XY$, both 3- and 4-coordinate global minima are found, depending on both the nature of X and Y and the level of calculation. The 4-coordinate, single-hydroxide complexes $[Zn(OH)(X)_2Y]^+$ are approximately 20 kJ/mol more stable than the $[Zn(OH)XY]X^+$ complexes (Table 2.1). This preference is consistent with the observation

that three-coordinate zinc cationic complexes are even less common than their neutral and anionic counterparts.[119]

2.3.1.2 Geometric parameters

The general trends observed for the geometric parameters (Tables 2.4-2.6) are similar to those reported previously for Zn complexes[60,70-74] and can be attributed primarily to the repulsion between the hydroxide ligands and/or the valence buffer effect.[75] See Fig. 2.5 for the numbering schemes used in the tables. Although the following trends, observed at M05-2X/B2(PP), B3LYP/6-311+G(d,p), and B3LYP/LANL2DZ levels of theory, are based on data from the global minima, similar trends were obtained for the local minima. First, the HO^-–Zn–OH^- bond angles range from ca. 130-160°. Concomitantly, HO^-–Zn–O(H)R angles are as small as 70°. Second, the range for the N–Zn–N bond angles is 90-100° and that for the N–Zn–O bond angles is 80-120°. Third, Zn–N bond lengths (2.07 – 2.16 Å) generally lie between the Zn–OH^- (1.82 – 1.96 Å) and the Zn–O(H)R (2.05 – 2.20 Å) bond lengths. These geometric parameters are in reasonable agreement with those for the [Zn_8(*C*-propylpyrogallol[4]arene)$_2$(pyridine)$_8$⊂pyridine] nanocapsule. In the capsule, the O–Zn–O bond angles range from 80-165°, the N–Zn–O angles range from 90-125°, and the Zn–N and Zn–O bonds are about equal in length at 2.03-2.07 Å [31]. Fourth, replacing a hydroxide ligand with X or removing an X or Y ligand from the inner shell shortens the bond lengths to Zn by as much as 0.2 Å. For the OH^- replacement, the distortion from tetrahedral coordination of the metal center is also reduced. Fifth, hydrogen bonds are

considerably more linear when an outer-shell ligand is a proton donor than when it is a proton acceptor (Tables 2.4-2.6).

As found by Amin and coworkers,[41,76] including the relativistic ECP on the zinc causes small changes in the geometries of the complexes. With respect to the B2 geometries, the B2-PP Zn-OH^- bond lengths are shorter by up to 0.01 Å, the Zn-O(H)R bond lengths are longer by up to 0.01 Å, the O···H bond lengths are longer by up to 0.02 Å and the Zn-N bond lengths are essentially unchanged. The two sets of bond angles differ by no more than 2 to 3º.

The M05-2X/B2(PP) zinc-ligand bonds are shorter than those obtained with B3LYP/6-311+G(d,p). The largest differences are observed for the Zn-O(H)R bonds (0.04-0.07 Å) and the smallest differences are observed for the Zn–OH^- bonds (0.01-0.02 Å). The O···H bonds both shorten and lengthen, usually by 0.04-0.08 Å. The bond angles typically agree to within 3º but can vary by as much as 9º when comparing hydrogen bonds with an outer-shell oxygen ligand acting as an electron donor.

Although no five-coordinate Zn complexes were located, three of the four-coordinate complexes, $[Zn(OH)_2(H_2O)_2]$, $[Zn(OH)_2(H_2O)(CH_3OH)]$, and $[Zn(OH)_2(CH_3OH)_2]$, do reproduce the Zn coordination sphere in the gas-phase pyrogallol[4]arene nanocapsules. However, as noted above, the inner-shell hydrogen bonding and repulsion between the hydroxides lead to ZnO_4 moieties in the complexes that are more asymmetric than those in the capsules.[31] Nevertheless, the B3LYP/6-311+G(d,p) equilibrium structure obtained for $[Zn(OH)_2(H_2O)_2]$ is the same within 0.01 Å and 1° as that obtained by Smith et al.[56] with a larger basis set. Assessing the sensitivity of the molecular geometries of these three complexes to the choice of

LANL2DZ versus 6-311+G(d,p) basis set, perhaps the most noticeable disparity between the two groups of data is the overemphasized hydrogen bonding observed for the former basis set compared to the latter. On average for the smaller basis set, the O–H bond lengths are 0.046 Å longer, the H···O bond lengths are 0.33 Å shorter, and the O–H···O bond angles are 7° larger. The differences in hydrogen bonding also affect the Zn-ligand bond lengths and, correspondingly, the Zn–OH^- bond lengths are 0.045-0.055 Å longer and the Zn–O(H)R bond lengths are 0.10 – 0.20 Å shorter at the B3LYP/LANL2DZ level of theory than at the B3LYP/6-311+G(d,p) level. Overemphasized hydrogen bonding results in similar trends when the B3LYP/LANL2DZ and M05-2X/B2(PP) equilibrium structures are compared. These data are representative of that found for the other complexes studied in this work, although the discrepancies in the outer-shell hydrogen bond parameters are smaller, on average, than those for the inner-shell hydrogen bonds. Overemphasized hydrogen bonding was also obtained with the smallest basis set considered by Frison and Ohanessian in their study of the 4- and 5-ligand cations $ZnX_{1,2}Y_3^{q+}$, where X = OH^-, H_2O; Y = NH_3, imidazole; and q = 1, 2.[55]

The especially exaggerated importance of N–H···O and inner-shell O–H···O hydrogen bonding at the B3LYP/LANL2DZ level of calculation helps to rationalize the divergence in relative isomer energies noted above between this level of theory and the other levels of theory. In fact, in some cases the strengths of these interactions are sufficiently different that bond critical points and ring points are found for the B3LYP/LANL2DZ optimized structures but not for the corresponding B3LYP/6-311+G(d,p) and M05-2X/B2(PP) structures. Likewise, $n_0 \rightarrow \sigma^*$(H-Z) hyperconjugation effects are minimal or non-existent at the higher levels of calculation (Table 2.7). For all

types of hydrogen bonding found at the four levels of theory, the ρ_b values for the three higher level computations are greater by as much as 0.1 for Z–H bonds and are typically half the value obtained from the B3LYP/LANL2DZ computations for H···O bonds. Finally, examining related O–H···O hydrogen bonds shows that ρ_b and $\Delta E^{(2)}$ correlate directly with $R_{O\cdots H}$ and indirectly with r_{H-O} (Tables 2.4-2.6).

Table 2.7 $\Delta E^{(2)}$ for global minima.

complex *atom₁–atom₂*	$\Delta E^{(2)}(n_0 \rightarrow \sigma^*(H\text{-}Z))$ (kJ/mol)	
$[Zn(OH)_2(NH_3)](H_2O)$		
$O_1\cdots H_1$	81	(80)
	[72]	{237}
$O_2\cdots H_2$	33	(33)
	[36]	{113}
$[Zn(OH)_2(C_5H_5N)](CH_3OH)$		
$O_1\cdots H_1$	79	(78)
	[72]	{178}
$O_2\cdots H_2$	18	(18)
	[21]	{39}
$O_3\cdots H_3$	5	(5)
	[5]	{[120]}
$[Zn(OH)_2(H_2O)](H_2O)$		
$O_1\cdots H_1$	96	(90)
	[76]	{76}
$O_2\cdots H_2$	113	(106)
	[89]	{325}
$[Zn(OH)_2(CH_3OH)](H_2O)$		
$O_1\cdots H_1$	87	(84)
	[73]	{277}
$O_2\cdots H_2$	90	(88)
	[80]	{259}
$[Zn(OH)_2(CH_3OH)](CH_3OH)$		
$O_1\cdots H_1$	106	(98)
	[81]	{299}
$O_2\cdots H_2$	151	(140)
	[110]	{306}

$[Zn(OH)_2(H_2O)(NH_3)](H_2O)$		
$O_1\cdots H_1$	–	(–)
	[–]	{17}
$O_2\cdots H_2$	182	(172)
	[121]	{427}
$O_3\cdots H_3$	121	(113)
	[88]	{351}
$[Zn(OH)_2(CH_3OH)(C_5H_5N)](CH_3OH)$		
$O_1\cdots H_1$	4	(4)
	[4]	{12}
$O_2\cdots H_2$	159	(153)
	[110]	{–}[b]
$O_3\cdots H_3$	108	(105)
	[84]	{–}
$[Zn(OH)_2(H_2O)(CH_3OH)](H_2O)$		
$O_1\cdots H_1$	17	(17)
	[21	]{126}
$O_2\cdots H_2$	138	(137)
	[92]	{389}
$O_3\cdots H_3$	120	(120)
	[92]	{351}
$[Zn(OH)_2(NH_3)_2](H_2O)_2$		
$O_1\cdots H_1$	121	(120)
	[93]	{236}
$O_2\cdots H_2$	10	(7)
	[8]	{28}
$O_2\cdots H_3$	10	(7)
	[8]	{28}
$[Zn(OH)_2(C_5H_5N)_2](CH_3OH)_2$		
$O_1\cdots H_1$	139	(134)
	[106]	{–}[b]
$O_2\cdots H_2$	10	(10)
	[13]	{16}
$O_2\cdots H_3$	7	(7)
	[3]	{16}

[a]M05-2X/B2, M05-2X/B2-PP (in parenthesis), B3LYP/6-311+G(d,p) (in square brackets), and B3LYP/LANL2DZ (in curly brackets) data. See Fig. 2.5 for numbering.[b] NBO analysis split the complex into too many fragments.

Better agreement in geometric parameters is obtained when comparing H_2O versus CH_3OH and NH_3 versus C_5H_5N at the same level of theory; comparable B3LYP/6-311+G(d,p) and M05-2X/B2(PP) bond lengths differ by 0.000 – 0.025 Å, whereas the

B3LYP/LANL2DZ bond lengths differ by 0.001 – 0.055 Å. The latter differences are larger due to the distortions caused by the overemphasized outer-shell hydrogen bonding. The corresponding ligand-Zn-ligand and hydrogen-bond angles vary from 1 – 22°. Excellent agreement between analogous ρ_b values is observed; for example, the H_2O/CH_3OH values and the NH_3/C_5H_5N values are within 0.01 at the three higher levels of theory (Tables 2.4-2.6). Thus, structurally NH_3 is a reasonable substitute for pyridine, with only slight variations in the orientation of the Y ligand due to the different steric interactions and hydrogen-bonding motifs of the ligands. Also, similar types of isomers were located for analogous complexes containing the two ligands, and any differences in relative isomer energies are consistent with the differences in hydrogen-bonding motifs. As one would expect H_2O is also a reasonable model for CH_3OH, for the same reasons cited for NH_3 and C_5H_5N (Tables 2.1-2.3).

2.3.2 $Zn(OH)_2(H_2O)_2CH_3OH$

In a further attempt to identify a 4-coordinate complex that reproduces the zinc environment observed in the capsule, the 5-ligand system $Zn(OH)_2(H_2O)_2(CH_3OH)$ containing the two least basic ligands was examined.[120] Even with this ligand choice, the global minimum is the 3-coordinate $[Zn(OH)_2(H_2O)](H_2O)(CH_3OH)$ (Table 2.2). This global minimum contains hydrogen bonding motifs similar to those for the XY ligand pairs, and the preference for this arrangement can be rationalized by the relative coordination strengths of outer- versus inner-shell H_2O/CH_3OH ligands. As with $Zn(OH)_2(H_2O)_2(CH_3OH)$, the global minimum for $Zn(OH)_2(H_2O)(CH_3OH)$ is 3-

coordinate with a preferential outer-shell H_2O ligand. The other trends described in the above section also apply to the $Zn(OH)_2(H_2O)_{1,2}(CH_3OH)$ complexes.

It should be noted that for $Zn(OH)_2(H_2O)_2(CH_3OH)$, the complex denoted with 0.0 kJ/mol for the relative enthalpy and free energy was used to investigate ligand binding affinities even though other isomers are more stable (Table 2.2). This choice allows CH_3OH to be studied as an inner-shell ligand and H_2O to be studied as an outer-shell ligand in a complex structure analogous to the global minima found for the $[Zn(OH)_2XY]X$ complexes. The analogous systems are used to understand the axial ligand observed for the capsule.[31,32]

2.3.3 Bond dissociation thermochemistry

Table 2.8 presents $\Delta_{rx}H_{298}$ and $\Delta_{rx}G_{298}$ values for dissociation of both inner- and outer-shell ligands (eqs 2.1 and 2.2) from the $Zn(OH)_2X_2Y$, $Zn(OH)_2XY_2$, and $Zn(OH)_2X_2Y_2$ complexes. Only the results at the M05-2X/B2-PP, MP2/6-311+G(d,p)//M05-2X/B2-PP, and MP2/B2-PP//M05-2X/B2-PP levels of theory are included in the table. The results for the global minima at all levels of theory considered can be found in Table S2.3. Both the BSSE corrected and uncorrected thermochemical data are given in the two tables. The correction is minimal for the M05-2X calculations and is generally within 5 kJ/mol (Table S2.3). For the B3LYP calculations the larger 6-311+G(d,p) basis set typically has a correction within approximately 7 kJ/mol, while that of the smaller LANL2DZ basis set is larger at up to 20 kJ/mol (Table S2.3). The correction for the MP2/6-311+G(d,p) calculations can be as large as 30 kJ/mol, and the MP2/B2-PP correction is at least 10 kJ/mol smaller (Table 2.8). In general, better

agreement is observed among the levels of theory for the uncorrected values, but the trends remain the same.

The B3LYP/LANL2DZ binding affinities are consistently too large by as much as 40 kJ/mol. Similar results were obtained by Pavlov et al. in their study of $[M(H_2O)_n]^{2+}$ ions, M = Be, Mg, Ca, or Zn and n = 1-7 and 12.[117] The bond dissociation enthalpies support the geometric findings that the B3LYP/LANL2DZ method overemphasizes hydrogen bonding in these complexes. Despite the dissimilarities in geometry, reasonable agreement among the ligand binding energies is obtained at the remaining levels of theory examined, especially with respect to trends (Table S2.3). The agreement is much better, however, when M05-2X/B2(PP) and MP2/6-311+G(d,p) binding enthalpies (and relative isomer enthalpies) are obtained with the B3LYP/6-311+G(d,p) and M05-2X/B2(PP) geometries. This latter result is encouraging because the B3LYP/6-311+G(d,p) optimizations converge more quickly than the M05-2X/B2-PP optimizations for the $Zn(OH)_2X_{1,2}Y_{1,2}$ complexes.

Comparing MP2/B2-PP//M05-2X/B2-PP and M05-2X/B2-PP ligand binding enthalpies, the $\Delta_{rx}H_{298}$(MP2 – DFT) values are similar for dissociation of both outer-shell X and inner-shell Y ligands. Most frequently, the improved treatment of electron correlation decreases $\Delta_{rx}H_{298}$ for both the uncorrected and BSSE corrected data. Comparing MP2/B2-PP//M05-2X/B2-PP and MP2/6-311+G(d,p)//M05-2X/B2-PP uncorrected ligand binding enthalpies, increasing the size of the basis set again decreases the binding enthalpy. The trend is sometimes reversed for the corrected binding affinities because of the larger correction for the smaller basis set. Again, the magnitude of the change in binding affinity is similar for the X and Y ligands (Table 2.8).

Table 2.8 Ligand binding affinities for $[Zn(OH)_2XY]X$, $[Zn(OH)_2Y_2]X$, and $[Zn(OH)_2Y_2]X_2$ global minima.

complex	binding affinities[a]		
ligand	M05-2X/B2-PP[b]	MP2/6-311+G(d,p)[c]	MP2/B2-PP[d]
$[Zn(OH)_2(H_2O)(NH_3)](H_2O)$			
NH_3	**74.6 (36.3)**	**53.9 (15.5)**	**55.2 (16.9)**
	77.3 (39.0)	72.9 (34.6)	64.2 (25.8)
H_2O	**63.3 (19.8)**	**38.4 (-5.2)**	**39.7 (-3.8)**
	67.0 (23.4)	58.0 (14.4)	51.3 (7.8)
$[Zn(OH)_2(H_2O)(C_5H_5N)](H_2O)$			
C_5H_5N	**82.3 (41.1)**	**61.6 (20.4)**	**66.5 (25.2)**
	86.2 (45.0)	84.9 (43.6)	79.7 (38.5)
H_2O	**68.6 (26.3)**	**49.6 (7.3)**	**47.6 (5.3)**
	72.2 (29.9)	68.3 (26.0)	58.6 (16.3)
$[Zn(OH)_2(H_2O)(CH_3OH)](H_2O)$			
CH_3OH	**59.8 (16.9)**	**38.1 (-4.8)**	**39.9 (-3.0)**
	63.9 (21.0)	58.1 (15.2)	51.8 (8.9)
H_2O	**52.0 (11.9)**	**29.2 (-10.8)**	**30.4 (-9.7)**
	55.4 (15.4)	47.7 (7.6)	41.2 (1.2)
$[Zn(OH)_2(CH_3OH)(NH_3)](CH_3OH)$			
NH_3	**77.1 (35.1)**	**57.8 (15.8)**	**59.6 (17.6)**
	79.8 (37.8)	77.5 (35.5)	68.7 (26.7)
CH_3OH	**70.0 (21.5)**	**49.7 (1.1)**	**49.7 (1.2)**
	73.8 (25.3)	70.5 (21.9)	62.1 (13.5)
$[Zn(OH)_2(CH_3OH)(C_5H_5N)](CH_3OH)$			
C_5H_5N	**85.5 (39.9)**	**66.4 (20.8)**	**71.6 (26.0)**
	89.6 (43.9)	90.9 (45.2)	85.3 (39.6)
CH_3OH	**76.5 (28.7)**	**61.3 (13.4)**	**58.5 (10.7)**
	80.3 (32.5)	81.4 (33.5)	70.7 (22.9)

$[Zn(OH)_2(NH_3)_2](H_2O)$			
NH_3	**70.6 (25.6)**	**46.5 (1.5)**	**49.2 (4.2)**
	73.6 (28.6)	66.6 (21.6)	59.2 (14.2)
H_2O	**69.7 (27.3)**	**55.0 (12.7)**	**59.4 (17.1)**
	73.2 (30.9)	73.0 (30.6)	70.7 (28.4)
$[Zn(OH)_2(C_5H_5N)_2](H_2O)$			
C_5H_5N	**81.2 (32.3)**	**66.1 (17.3)**	**68.9 (20.1)**
	85.8 (36.9)	94.7 (45.9)	84.7 (35.9)
H_2O	**52.6 (12.8)**	**43.4 (3.6)**	**46.7 (6.9)**
	56.1 (16.3)	61.3 (21.6)	57.5 (17.7)
$[Zn(OH)_2(NH_3)_2](CH_3OH)$			
NH_3	**70.1 (23.5)**	**47.1 (0.4)**	**49.8 (3.1)**
	73.2 (26.5)	67.4 (20.7)	60.0 (13.3)
CH_3OH	**69.9 (25.7)**	**57.5 (13.3)**	**62.5 (18.4)**
	73.7 (29.6)	75.6 (31.4)	74.4 (30.3)
$[Zn(OH)_2(NH_3)_2](H_2O)_2$			
NH_3	**74.7 (26.6)**	**56.2 (8.1)**	**64.5 (16.4)**
	78.1 (30.0)	77.9 (29.8)	76.0 (28.0)
H_2O	**68.2 (21.6)**	**53.8 (7.2)**	**57.9 (11.4)**
	71.4 (24.8)	70.3 (23.7)	68.2 (21.6)
$[Zn(OH)_2(C_5H_5N)_2](H_2O)_2$			
C_5H_5N	**57.9 (14.7)**	**48.5 (5.2)**	**59.2 (15.9)**
	62.8 (19.6)	79.7 (36.5)	76.1 (32.9)
H_2O	**46.3 (9.5)**	**37.3 (0.5)**	**40.5 (3.8)**
	49.3 (12.6)	53.4 (16.7)	50.1 (13.3)

$[Zn(OH)_2(NH_3)_2](CH_3OH)_2$			
NH_3	**67.9 (20.2)**	**47.5 (-0.3)**	**57.4 (9.7)**
	71.5 (23.7)	69.4 (21.6)	69.3 (21.5)
CH_3OH	**68.6 (19.0)**	**55.7 (6.1)**	**60.6 (11.0)**
	72.1 (22.5)	72.4 (22.9)	71.4 (21.8)
$[Zn(OH)_2(C_5H_5N)_2](CH_3OH)_2$			
C_5H_5N	**50.8 (11.9)**	**40.1 (1.3)**	**52.0 (13.2)**
	55.7 (16.9)	71.6 (32.8)	69.2 (30.3)

[a] $\Delta_{rx}H_{298}$ and $\Delta_{rx}G_{298}$ (in parentheses) data. BSSE corrected values are bolded. [b] M05-2X/B2-PP values. [c] MP2/6-311+G(d,p)//M05-2X/B2-PP values. [d] MP2/B2-PP//M05-2X/B2-PP values.

2.3.3.1 $[Zn(OH)_2XY]X$ and $[Zn(OH)_2Y_2]X$

For the remainder of section 2.3.3, the MP2/B2-PP//M05-2X/B2-PP thermodynamic data will be used. The $\Delta_{rx}G_{298}$ values for dissociation of the N-based inner-shell ligands in $[Zn(OH)_2(ROH)(NH_3)]ROH$ and $[Zn(OH)_2(ROH)(C_5H_5N)]ROH$ indicate that the complex is more stable than the separated ligand system, whereas the dissociation of the inner-shell CH_3OH ligand in $[Zn(OH)_2(H_2O)(CH_3OH)](H_2O)$ has significantly less positive $\Delta_{rx}G_{298}$ values and correspondingly significantly smaller $\Delta_{rx}H_{298}$ values (Table 2.8). C_5H_5N is more strongly bound than NH_3 by about 12 – 16 kJ/mol; these results combined with the geometric findings support the use of NH_3 as a model for C_5H_5N. That the binding affinity of NH_3 in $[Zn(OH)_2X(NH_3)]X$ is higher (65-70 kJ/mol) than its benchmark value in $[Zn(OH)_2(NH_3)_2]$ (37 kJ/mol) is consistent with the stronger binding affinity of NH_3 than H_2O or CH_3OH with Zn.[76]

The difference in H_2O and CH_3OH binding enthalpies is approximately 10 kJ/mol, regardless of whether Y = NH_3 or C_5H_5N. The reaction free energies more strongly favor retention of X in the outer shell when Y = C_5H_5N than when Y = NH_3. Again, all of these thermodynamic results are consistent with the experimental result that CH_3OH solvent molecules do not replace the axial pyridines in the zinc-seamed nanocapsules.[31,32]

Interestingly, the X ligands of the $[Zn(OH)_2Y_2]X$ systems are now more tightly bound than NH_3 by at least 10 kJ/mol, whereas the C_5H_5N ligands remain bound more tightly by nearly 20 kJ/mol regardless of the X ligand. The magnitude of the binding affinity for an X ligand is dependent on the XY pairing. In contrast, the NH_3 binding affinity is independent of the X ligand.

2.3.3.2 $[Zn(OH)_2Y_2]X_2$

For a given X the $\Delta_{rx}H_{298}$ values are nearly equivalent when NH_3 is used to model C_5H_5N; likewise, for a given Y the $\Delta_{rx}H_{298}$ values are nearly equivalent when H_2O is used to model CH_3OH (Table 2.8). These relative Y-ligand binding enthalpies are reversed by approximately 15 kJ/mol compared with the results for the $[Zn(OH)_2XY]X$ systems. One reason for this reversal is the greater steric repulsion between the two C_5H_5N's than between the two NH_3's, manifested in a canting of the C_5H_5N's with respect to each other that is not observed for the NH_3's (Table 2.6). Secondly, this canting causes unequal $X\cdots H\text{-}C_5H_4N$ bond lengths when an outer-shell X ligand is hydrogen bonded to both inner-shell C_5H_5N's. Although one of the hydrogen bonds to the C_5H_5N is about equivalent in strength to that to the NH_3, the other is about half the strength (Tables 2.6 and 2.7). Thirdly, according to the AIM analysis, $Y\text{-}H^{\cdots}OH^-$ bond critical points were located for C_5H_5N but not for NH_3 in the $[Zn(OH)_2XY]X$ global minima.

2.4 Summary

We have investigated the structures and energetics of $Zn(OH)X_2Y^+$, $Zn(OH)_2X_2$, $Zn(OH)_2Y_2$, and $Zn(OH)_2X_{1,2}Y_{1,2}$, as the simplest possible mononuclear zinc complexes with metal-ligand bonds analogous to those in the zinc-seamed pyrogallol[4]arene nanocapsules.[31,32] The complexes exhibit unusual zinc coordination numbers and conventional and unconventional inner- and outer-shell hydrogen-bonding networks. One of the most important results of this work is that although the hydrogen-bonding motifs are similar at the B3LYP/LANL2DZ, B3LYP/6-311+G(d,p), M05-2X/B2, and M05-2X/B2-PP levels of theory, the strength of both the conventional and unconventional

hydrogen bonds is overemphasized at the lowest level of theory. Nevertheless, generally the same minima are obtained at all four levels of calculation. The presence of the two small, anionic hydroxides in the $Zn(OH)_2X_{1,2}Y_{1,2}$ systems leads to 4-coordinate distorted tetrahedral and atypical 3-coordinate, planar Zn(II) ions. The latter results, which are demonstrations of the valence buffer effect,[75] further our understanding of the coordinative behavior of zinc. The preference for nitrogen ligands in the inner-shell of these complexes yields a zinc coordination sphere related to that of many zinc enzymes.[62] SPEs evaluated with B3LYP/6-311+G(d,p) and M05-2X/B2(PP) equilibrium structures exhibit essentially identical binding affinities and relative isomer enthalpies. Binding affinities were benchmarked against MP2/B2-PP//M05-2X/B2-PP data. The trend in inner-shell ligand binding affinities is $C_5H_5N > NH_3 > CH_3OH$, for the $[Zn(OH)_2XY]X$ systems.

Although larger, the ranges observed for the optimized Zn–N and Zn–O bond lengths and O–Zn–O(N) bond angles for the $Zn(OH)_2X_{1,2}Y_{1,2}$ complexes encompass those observed for $[Zn_8(C\text{-propylpyrogallol[4]arene})_2(pyridine)_8 \subset pyridine]$. The relative binding affinities of the C_5H_5N and CH_3OH ligands elucidate why substitution of a methanol solvent molecule for a pyridine axial ligand is not observed experimentally for the zinc-seamed pyrogallol[4]arene nanocapsules. Furthermore, NH_3 is a suitable model for C_5H_5N as the axial ligand of the nanocapsules. Finally, we will continue to assess the reliability of the LANL2DZ basis set in our study of larger zinc complexes, $Zn(C_2H_3O_2)_2Y_{1,2}$ and $Zn(C_6H_5O_3)_2$, and the capsules themselves, as overemphasized hydrogen bonding is less relevant to those species.

Chapter 3: Mononuclear and polynuclear 5-coordinate zinc(II) model complexes: A calibration study

To further our understanding of the properties of zinc-seamed pyrogallol[4]arene nanocapsules, we have investigated the energetic and geometric properties of the model complexes $Zn(C_2O_2H_3)_2Y$, Y = NH_3, C_5H_5N, CH_3OH, $(CH_3)_2NCHO$, or $(CH_3)_2SO$, with a zinc coordination sphere representative of that in the capsules. The effect of the choice of density functional, basis set, and zinc pseudopotential on the equilibrium structures and Y ligand bond dissociation enthalpies (BDEs) has been assessed. Among the ways in which the suitability of these models has been confirmed was by construction of polynuclear zinc complexes having 2, 4, 6, or 8 metal ions combined with $C_2O_2H_3$, $C_4O_3H_4^{2-}$, and NH_3 ligands, which indeed show that a closed ring is formed. The natural curvature of these complexes suggests that pentacoordination of Zn may be a key factor in seaming the pre-existing cone-shaped pyrogallol[4]arenes to form dimer capsules. This work is published in *Struct. Chem.* 24 (2013) 2089-2099.[44]

3.1 Introduction

Self-assembling molecular capsules have received attention for some time now. Of particular interest to our group are metal-seamed capsules (e.g., Cu, Ni, Co, Ga, and Zn),[50,121-124] specifically the zinc-seamed pyrogallol[4]arene dimeric capsules (Fig. 3.1).[31,32] Neighboring pyrogallol (1,2,3-trihydroxybenzene) subunits of the pyrogallol[4]arene macrocycles used to construct the dimer are linked together via –CHR moieties, where the R group is typically an alkyl or aryl group instead of H. The eight Zn(II) ions that seam the two macrocycles fit within an equatorial belt, and

intramolecular phenoxy–O···H···O–phenoxy hydrogen-bonded networks lie above and below this belt. Each zinc is coordinated to two oxygens from each arene, one oxygen that is bridged between two metal centers and one that is involved in the hydrogen-bonded network. In the condensed phases, the zinc ions are also coordinated to a fifth, external ligand and are in distorted square pyramidal environments (Fig. 3.1). The dimeric metal-seamed pyrogallol[4]arene-based nanocapsules, which have a small internal volume of ca. 145 Å^3,[31,32] are fundamentally of interest with respect to the "communication" between host and guest and electron exchange and transfer both within individual capsules and between connected capsules. More generally, however, pyrogallol[4]arene-based nanoassemblies are of interest with respect to their diversity of architectures,[39,50,125-127] their magnetic behavior,[34,128-130] and their possible gas sorption properties.[20,40]

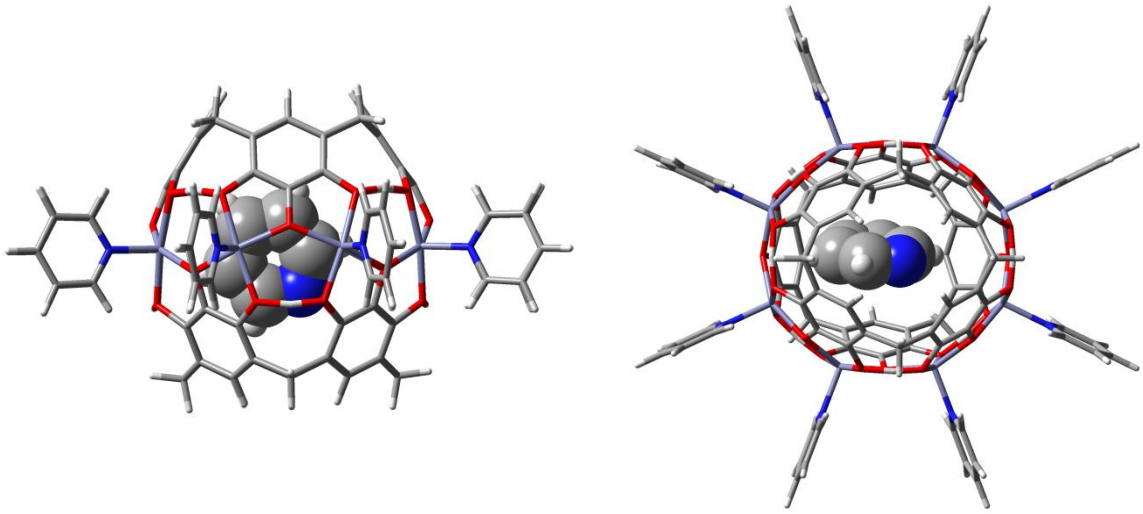

Figure 3.1 Side (left) and top (right) views of Zn_8(C-propylpyrogallol[4]arene)$_2$(pyridine)$_8$⊂pyridine. The pyridine guest is shown in space-filled form, and the host complex is shown in tubular form. Propyl R-groups are removed for clarity. Color scheme: Zn: purple, O: red, N: blue, C: gray, H: white.

Due to the size of the metal-containing systems found in supramolecular chemistry and biochemistry, small model molecular assemblies have been used to probe the intermolecular forces implicated in molecular recognition and the factors controlling the assembly process with respect to the metal centers.[34,131-134] A number of density functional theory (DFT) studies have been performed on zinc-containing model complexes,[41,43,55,72,76,135-138] but many of these studies involve 4-coordinate zinc. In fact, in a previous study we investigated the simplest complex that could contain the correct number of Zn–O and Zn–N bonds to reproduce the Zn coordination geometry in the pyrogallol[4]arene-based dimeric capsules:[43] two hydroxide ligands and two water or methanol ligands were used to model the Zn–O bonds. However, the anionic hydroxide ligands led to only 3- or 4-coordinate zinc species even though as many as six possible ligands were present. In each case, the non-ligated molecules formed an outer-shell hydrogen-bonded network that bridged the ligated molecules.

In order to better model the 5-coordinate zinc in the capsules, determine an appropriate level of theory to use with the capsules themselves, and evaluate the effectiveness of these models for tethered multi-capsule systems, we assess a ligand that better mimics the pyrogallol[4]arene portion of the capsule in this work. Specifically, in these complexes a zinc(II) ion interacts with two deprotonated (Z)-ethene-1,2-diol bidentate ligands ($C_2O_2H_3^-$) and an equatorial ligand Y chosen to include external ligands observed experimentally for the capsules (Fig. 3.2). That is, Y is NH_3, C_5H_5N, CH_3OH, $(CH_3)_2NCHO$, or $(CH_3)_2SO$. We note that although this model complex was explicitly designed for our investigation of the Zn-seamed pyrogallol[4]arene dimeric capsules, the results of this work may also be relevant to the investigation of other metal organic

frameworks, e.g. MOF-2 and MOF-5,[135,139-141] and enzymatic systems, e.g. hydrolases,[72,142,143] in which the Zn centers adopt similar coordination environments.

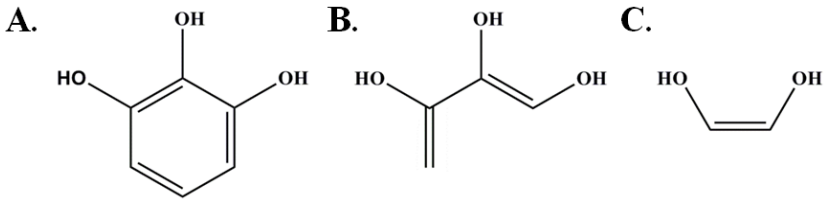

Figure 3.2 Schematic representations of pyrogallol (A), (*Z*)-1,2,3-trihydroxy-1,3-butadiene (B), and (*Z*)-ethene-1,2-diol (C).

The work reported herein focuses mainly on the geometric parameters of the mononuclear zinc complexes $Zn(C_2O_2H_3)_2Y$, including zinc bond lengths and bond angles, and the energetics of the complexes, including bond dissociation enthalpies of the Y ligands. The influence of the choice of basis set, DFT method, and zinc pseudopotential on these properties was examined. These choices will become crucial in our study of the capsules, considering the smallest metal-seamed dimeric capsule contains eight zinc atoms and a total of 120 atoms when R-groups (replaced by hydrogens), equatorial ligands and encapsulated guests are removed. In a second component of the study, we further tested the validity of the mononuclear zinc model systems by systematically building up an eight-zinc model system with the requisite number of deprotonated (Z)-ethene-1,2-diol, 1,2,3-trihydroxy-*cis*-1,3-butadiene, and NH_3 ligands to satisfy the metal binding and charge and to form the O···H···O hydrogen-bonding networks above and below the metal centers (Fig. 3.2).

3.2 Computational details

All calculations in this study were performed with the Gaussian09 suite of programs,[89] and the results were visualized with GaussView5.[144] Several DFT hybrid functionals, B3LYP,[145,146] M05-2X,[86] PBE0,[147,148] and the long-range corrected ωB97X-D,[149] as well as the pure functional M06-L,[150] were employed in the calibration study of $Zn(C_2O_2H_3)_2Y$, Y = NH_3, C_5H_5N, CH_3OH, $(CH_3)_2NCHO$, or $(CH_3)_2SO$. With the exception of NH_3, the Y ligands were chosen from the solvents used to synthesize the metal-seamed pyrogallol[4]arene nanocapsules. Although all of these solvents are possible external metal ligands, not all of them have been observed.[32,33] We considered replacing the methyl groups with hydrogen atoms to simplify the Y ligands, but the simplified ligands sometimes led to non-physical transfer of a hydrogen atom.

Fully optimized geometries (tight threshold criteria and int = ultrafine keyword) and normal-mode vibrational frequencies (for verification that stationary points are minima and generation of thermal correction terms) were computed. Single-point energies (SPEs) were calculated with both DFT and wave function theory (WFT) using the M05-2X, M06-L, PBE0, and ωB97X-D DFT methods and the MP2 WFT method. For the geometric optimizations and SPEs, a variety of double- and triple-zeta basis sets were used, with and without a small-core (SDD) or a large-core (LANL2DZ) pseudopotential on the zinc. Both Pople and correlation consistent basis sets were investigated. A complete list of the calculational levels surveyed can be found in Table S3.1. All supplementary tables can be found at http://link.springer.com/article/10.1007%2Fs11224-013-0346-6.

In order to reproduce the metal environment found in the zinc-seamed pyrogallol[4]arene capsules,[31,32] addition of ligand Y to only a vacant zinc coordination site was considered. Although all of the resultant 5-coordinate zinc complexes $Zn(C_2O_2H_3)_2Y$ have a similar connectivity, where applicable, minima were located by orienting methyl groups of non-linear Y ligands over the O^-, over the OH, between the O^- and OH of a given $C_2O_2H_3^-$ ligand, and between the O^- and OH of separate $C_2O_2H_3^-$ ligands. Initial B3LYP/LANL2DZ optimization and frequency calculations were used to determine the most stable orientation for a given Y ligand before further optimizations were performed. All relative enthalpies are within 5 kJ/mol irrespective of the Y ligand orientation; thus, the orientation adopted will not affect the overall trends in binding affinity of the various ligands.

A geometric and energetic calibration study at all calculational levels implemented in this work has been carried out for only $Zn(C_2O_2H_3)_2(C_5H_5N)$ and $Zn(C_2O_2H_3)_2(CH_3OH)$, two complexes representative of the zinc coordination environment found in the pyrogallol[4]arene-based nanocapsules. Also, the difference in the bond dissociation enthalpies (BDEs) of these two complexes allow us to examine the effect of the calibration parameters for ligands that are bound at the extremes, CH_3OH at the weaker end and C_5H_5N at the higher end, of ligand binding affinity. On the basis of these results, optimization and frequency calculations for the remaining complexes were performed at the following levels: B3LYP/B2-PP, M05-2X/B2-PP, M05-2X/MBS1, M05-2X/SDD(All), M06-L/B2-PP, M06–L/MBS1, M06-L/SDD(All), PBE0/B2-PP, PBE0/MBS1, PBE0/LANL2DZ, PBE0/SDD(All) ωB97X-D/B2-PP, ωB97X-D/MBS1, and ωB97X-D/SDD(All). The notation B2-PP refers to the B2 basis set[41] and SDD

pseudopotential on the zinc and the 6-311+G(2df,2p) basis set on all other atoms; the notation MBS1 refers to the same basis set and pseudopotential on the zinc and the 6-31G(d) basis set on all other atoms. For all complexes, SPEs were evaluated with the M05-2X, M06-L, PBE0, ωB97X-D, and MP2 methods and the aug-cc-pVTZ-PP and B2-PP basis sets. Equilibrium structures were benchmarked against the M05-2X/B2-PP optimized geometries,[41,43,76] and BDEs were benchmarked against the MP2/aug-cc-pVTZ-PP//M05-2X/B2-PP values. Cartesian XYZ coordinates for selected optimized geometries can be found in Table S3.2.

To replicate the Zn–O–Zn motif in the pyrogallol[4]arene based nanocapsules, a 1,2,3-trihydroxy ligand must be introduced into model complexes with more than one zinc center. Thus, the polynuclear zinc models were constructed by combining 2, 4, 6, or 8 metal atoms with a sufficient number of $C_2O_2H_3^-$ and deprotonated 1,2,3-trihydroxy-*cis*-1,3-butadiene ($C_4O_3H_4^{2-}$) ligands to complete the Zn–O coordination sphere and the O···H···O hydrogen-bonded networks above and below the metal centers. The coordination mode of both the $C_2O_2H_3^-$ and $C_4O_3H_4^{2-}$ ligands is bidentate, with the central oxygen of the latter ligand bridged between adjacent zinc centers. One or two equatorial NH_3 ligands were attached to make the zincs 5- or 6-coordinate. NH_3 was chosen as the additional ligand because we have shown previously[43] that it can be reliably substituted for the external pyridine ligands observed for the pyrogallol[4]arene nanocapsules.[31,32] As our aim in performing these calculations is to determine whether a closed capsule will form on addition of metal atoms, the four polynuclear Zn structures were optimized only at the B3LYP/LANL2DZ level of theory, as was the butadiene. The normal-mode vibrational frequency calculations confirmed that minima were obtained.

3.3 Results and analysis of results

3.3.1 Mononuclear Zn models: calibration study of $Zn(C_2O_2H_3)_2Y$, Y = C_5H_5N or CH_3OH

3.3.1.1 Geometric properties

With one exception (the 4-coordinate $Zn(C_2O_2H_3)_2(CH_3OH)$ B3LYP/B2-SDD(Zn):D95V(C,O,H) optimized structure) 5-coordinate minima were identified for all complexes examined. These results are consistent with those obtained by Brown et al. in their computational study of the inhibition of zinc hydrolases by hydroxamic acid.[72] They found that addition of water to zinc hydroxamates, which form 5-membered rings with the zinc, preferentially leads to binding at a fifth zinc coordination site, whereas addition of water to zinc acetates, which form 4-membered rings with the zinc, preferentially leads to insertion into a Zn–O bond.

A complete list of bond lengths and bond angles for $Zn(C_2O_2H_3)_2(CH_3OH)$ and $Zn(C_2O_2H_3)_2(C_5H_5N)$ (Fig. 3.3) can be found in Table S3.3; representative geometries can be found in Table 3.1. Because each of the model ligands has one O–H, one O^-, and no bridging hydrogen, unlike what is found in the zinc capsule, the range and average of the Zn–O bond lengths are reported. As in our previous study involving zinc, geometries of the zinc coordination sphere are minimally affected by using an effective core potential compared to an all-electron model;[43] thus, several pseudopotentials have been examined for the $Zn(C_2O_2H_3)_2Y$ models in order to save computational time. A related, general result is that inclusion of relativistic effects in all-electron calculations has little effect on the geometry of the model complexes. The results for only the representative

geometries collected in Table 3.1 are analyzed in the remainder of this section, although most trends hold for the remaining calculational levels.

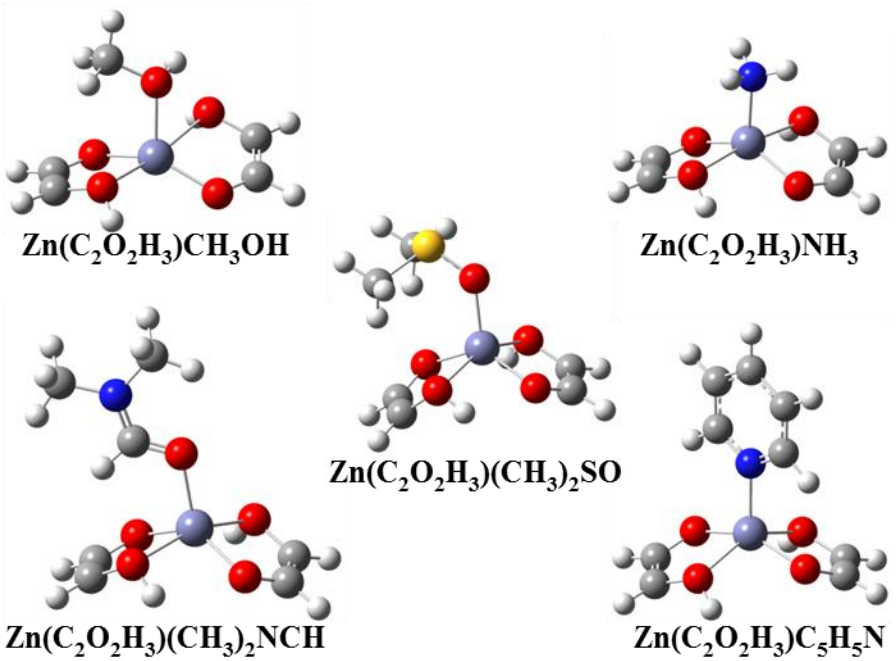

Figure 3.3 M05-2X/B2-PP minima of $Zn(C_2O_2H_3)_2Y$ complexes. Color scheme: S: yellow.

Table 3.1 Representative geometric properties of $Zn(C_2O_2H_3)_2Y$, Y = C_5H_5N or CH_3OH.

complex	bond length (Å)		bond angle range (°)	
level of theory	$Zn–O_{avg}$ (range)	Zn–Y	O–Zn–O	O–Zn–Y
$Zn(C_2O_2H_3)_2(C_5H_5N)$				
M05-2X/B2-PP	2.068 (1.924– 2.213)	2.068	82.7–160.9	99.5–108.0
M05-2X/MBS1	2.062 (1.924– 2.201)	2.061	83.6–155.5	102.3–109.3
ωB97X-D/B2-PP	2.095 (1.907– 2.284)	2.062	81.6–165.7	97.1–107.9
ωB97X-D/MBS1	2.084 (1.910– 2.259)	2.061	82.7–160.4	99.8–108.1
PBE0/B2-PP	2.084 (1.912– 2.257)	2.062	82.1–157.7	101.2–108.0
PBE0/MBS1	2.076 (1.917– 2.235)	2.051	83.1–150.0	105.0–109.9
PBE0/LANL2DZ	2.073 (1.983– 2.164)	2.085	81.0–150.6	104.7–107.6
PBE0/SDD	2.069 (1.945– 2.192)	2.026	82.2–147.7	106.2–108.8
PBE0/SDDAll	2.068 (1.954– 2.182)	2.032	81.6–147.2	106.4–108.8
M06-L/B2-PP	2.097 (1.916– 2.277)	2.085	82.1–174.6	92.7–108.4
M06-L/MBS1	2.090 (1.921– 2.259)	2.089	83.2–174.8	92.6–109.6
B3LYP/B2-PP	2.111 (1.919– 2.303)	2.089	81.3–158.3	100.8–107.8
B3LYP/MBS1	2.097 (1.921– 2.273)	2.078	82.5–152.4	103.8–109.1
B3LYP/cc-pVDZ-PP	2.094 (1.931– 2.257)	2.086	82.3–151.6	104.2–107.9
B3LYP/LANL2DZ: 6-31G(d)	2.101 (1.975– 2.227)	2.137	82.3–146.9	106.6–108.7
B3LYP/LANL2DZ	2.088 (1.992– 2.185)	2.104	80.9–150.3	104.8–107.1
B3LYP/LANL2TZ:6-31G(d)	2.105 (1.977– 2.233)	2.141	82.2–148.7	105.6–108.3
$Zn(C_2O_2H_3)_2(CH_3OH)$				
M05-2X/B2-PP	2.056 (1.892– 2.242)	2.100	83.2–175.5	82.9–114.9
M05-2X/MBS1	2.052 (1.889– 2.247)	2.091	83.9–174.2	80.8–116.2
ωB97X-D/B2-PP	2.084 (1.871– 2.350)	2.135	81.3–170.5	78.2–111.0
ωB97X-D/MBS1	2.080 (1.871– 2.357)	2.124	81.9–170.1	75.7–112.2
PBE0/B2-PP	2.076 (1.874– 2.332)	2.135	81.6–172.7	78.0–110.8
PBE0/MBS1	2.074 (1.874– 2.347)	2.123	82.1–173.8	75.3–112.2
PBE0/LANL2DZ	2.069 (1.953– 2.204)	2.058	82.1–177.7	81.9–112.4
PBE0/SDD	2.079 (1.894– 2.359)	2.059	80.9–174.4	73.9–112.3

PBE0/SDDAll	2.080 (1.903– 2.354)	2.048	80.2–173.4	72.8–111.0
M06-L/B2-PP	2.084 (1.878– 2.342)	2.171	81.8–166.9	76.0–107.3
M06-L/MBS1	2.081 (1.884– 2.330)	2.158	82.9–167.9	75.8–109.2
B3LYP/B2-PP	2.107 (1.879– 2.411)	2.160	80.1–172.2	76.1–109.3
B3LYP/MBS1	2.104 (1.878– 2.430)	2.145	80.6–174.8	73.4–110.9
B3LYP/cc-pVDZ-PP	2.108 (1.885– 2.448)	2.133	79.9–174.8	72.2–111.2
B3LYP/LANL2DZ: 6-31G(d)	2.088 (1.945– 2.251)	2.145	82.6–177.9	81.1–117.2
B3LYP/LANL2DZ	2.084 (1.963– 2.225)	2.072	82.0–177.7	82.0–112.7
B3LYP/LANL2TZ:6-31G(d)	2.100 (1.945– 2.301)	2.154	81.9–178.3	77.3–115.6

Characteristically, the choice of the DFT functional has the greatest effect on the $Zn–O_{avg}$ bond lengths, with the length increasing in the order M05-2X < PBE0 < ωB97X-D < M06-L < B3LYP. In contrast, the Zn–ligand bond length tends to fluctuate more with the method, but has a similar trend to that of the $Zn–O_{avg}$ bond length (Table 3.1). The pseudopotential and basis set have a noticeably smaller effect on the average Zn–O bond lengths and exhibit no clear trend with respect to the predicted Zn–Y bond length.

When comparing the $Zn–O_{avg}$ bond lengths, we find that the PBE0/LANL2DZ, PBE0/MBS1, and M05-2X/MBS1 optimized geometries match the M05-2X/B2-PP geometry most closely (Table 3.1). There is greater variance found among the levels when comparing the Zn–Y bond lengths; for example, the PBE0/LANL2DZ $Zn–C_5H_5N$ bond length deviates by 0.02 Å and the $Zn–CH_3OH$ bond length deviates by 0.04 Å compared with the M05-2X/B2-PP values. The greater discrepancies in the LANL2DZ equilibrium structures for $Zn(C_2O_2H_3)_2Y$ are most likely due to the overemphasized O···H–Y hydrogen-bonding between the ligands observed for this basis set.[43] However, this overemphasis will not be an issue for the capsule, with its less flexible framework and involvement of the oxygen atoms in internal O···H···O hydrogen bonds.

As one assessment of the models, the Zn–O and Zn–Y bond lengths and the O–Zn–O and O–Zn–Y bond angles are compared to experimental values. For the [Zn_8(*C*-propylpyrogallol[4]arene)$_2$(pyridine)$_8$⊂pyridine] and [Zn_8(C-propylpyrogallol[4]arene)$_2$(DMSO)$_8$⊂(3-methylpyridine)] capsules,[31,32] the Zn–N and Zn–O bond lengths range from 2.03 – 2.08 Å, the O–Zn–O bond angles range from 80 – 165° and the O–Zn–Y bond angles range from 90 – 125°.[31,32] The O–Zn–O and O–Zn–N bond angles are within the range of the experimental values for both the

$Zn(C_2O_2H_3)_2(C_5H_5N)$ and $Zn(C_2O_2H_3)_2(CH_3OH)$ model systems at all levels of theory considered. For the $Zn(C_2O_2H_3)_2(C_5H_5N)$ complex, the $Zn–O_{avg}$ and the Zn–N bond lengths fall within the range of the experimental values for only the M05-2X, PBE0, and ωB97X-D optimized structures; the B3LYP and M06–L bond lengths are 0.02 – 0.07 Å too long. For the $Zn(C_2O_2H_3)_2(CH_3OH)$ complex, only the M05-2X and PBE0 $Zn–O_{avg}$ bond lengths and the B3LYP/LANL2DZ and PBE0/LANL2DZ $Zn–CH_3OH$ bond lengths are within the experimental range; the remaining $Zn–O_{avg}$ and $Zn–CH_3OH$ bond lengths are 0.01 – 0.03 Å and 0.02 – 0.1 Å too long, respectively.

3.3.1.2 Energetic properties

In order to obtain more accurate thermochemical data, particularly BDEs, a series of DFT and WFT single-point energy calculations were performed. M05-2X, M06-L, PBE0, ωB97X-D, and MP2 SPEs were calculated with a variety of basis sets (Table S3.1), and the thermochemical data from the aug-cc-pVTZ-PP and B2-PP calculations (Table 3.2) are analyzed in this section. All of the trends reported in the remainder of this chapter for the enthalpy changes associated with the dissociation reactions also hold for the free energy changes, a result indicating that entropy effects can be (essentially) ignored in differentiating among the computational procedures.

Excellent agreement in BDEs is observed for a given method regardless of the choice of optimized geometry or the choice of aug-cc-pVTZ-PP or B2-PP basis set. That is, for any method the aug-cc-pVTZ-PP and B2-PP BDEs differ at most by 5 kJ/mol for the set of geometries. Also, it should be noted that the BDEs using the aug-cc-pVDZ-PP basis set were found to be at most 10 kJ/mol greater than those for the aug-cc-pVTZ-PP

basis set for a given method and follow the same trends. The M05-2X BDEs reproduce the MP2 BDEs best, but the ωB97X-D and M06-L BDEs only vary by 5 – 15 kJ/mol from the MP2 BDEs and thus will be assessed for the remaining Y ligands.

Table 3.2 Y ligand binding affinities for $Zn(C_2O_2H_3)_2Y$ minima.[a]

complex	aug-cc-pVTZ-PP		B2-PP	
method	ΔH_{298} (kJ/mol)	ΔG_{298} (kJ/mol)	ΔH_{298} (kJ/mol)	ΔG_{298}(kJ/mol)
$Zn(C_2O_2H_3)_2(C_5H_5N)$				
MP2	95.4 [94.9]	53.4 [53.0]	96.6 [96.3]	54.7 [54.4]
	(93.0) {95.9}	(51.3) {51.4}	(94.2) {96.8}	(52.5) {52.3}
M05-2X	91.5 [91.6]	49.5 [49.8]	94.8 [94.9]	52.8 [53.0]
	(90.2) {92.2}	(48.5) {47.7}	(93.4) {95.3}	(51.6) {50.8}
ωB97X-D	85.7 [85.9]	43.8 [44.1]	88.9 [89.1]	46.9 [47.2]
	(82.6) {87.1}	(40.9) {42.6}	(86.0) {90.1}	(44.2) {45.6}
M06-L	79.5 [80.2]	37.1 [38.3]	80.5 [81.4]	38.1 [39.5]
	(76.7) {82.4}	(34.9) {37.9}	(77.5) {83.0}	(35.8) {38.5}
PBE0	69.3 [69.4]	27.3 [27.6]	73.4 [73.5]	31.4 [31.6]
	(67.8) {71.9}	(26.0) {27.4}	(72.2) {75.8}	(30.4) {31.3}
$Zn(C_2O_2H_3)_2(CH_3OH)$				
MP2	56.6 [55.5]	12.1 [11.2]	57.6 [56.4]	13.0 [12.1]
	(55.3) {54.1}	(13.5) {12.7}	(56.3) {55.2}	(14.5) {13.9}
M05-2X	62.2 [60.5]	17.6 [16.2]	65.4 [63.7]	20.9 [19.4]
	(60.6) {59.2}	(18.8) {17.8}	(63.6) {61.8}	(21.8) {20.4}
ωB97X-D	49.2 [49.5]	4.7 [5.2]	52.6 [52.9]	8.1 [8.6]
	(49.3) {48.0}	(7.5) {6.7}	(52.6) {50.9}	(10.8) {9.6}
M06-L	51.8 [50.1]	7.3 [5.8]	53.9 [51.9]	9.4 [7.6]
	(50.2) {47.3}	(8.4) {6.0}	(51.9) {48.5}	(10.0) {7.2}
PBE0	35.7 [35.6]	-8.9 [-8.7]	39.5 [39.4]	-5.0 [-4.9]
	(36.3) {36.9}	(-5.6) {-4.4}	(39.9) {40.2}	(-1.9) {-1.2}
$Zn(C_2O_2H_3)_2(NH_3)$				
MP2	76.3 [75.4]	44.0 [42.8]	77.4 [76.7]	45.1 [44.1]
	(74.9) {90.8}	(43.4) {55.0}	(76.2) {90.9}	(44.6) {55.1}
M05-2X	82.4 [82.1]	50.1 [49.4]	85.3 [85.0]	53.1 [52.3]

	(81.6)	{93.3}	(50.0)	{57.5}	(84.5)	{95.9}	(52.9)	{60.1}
ωB97X-D	72.5	[72.2]	40.3	[39.6]	74.8	[74.5]	42.5	[41.9]
	(70.1)	{85.6}	(38.5)	{49.8}	(72.6)	{87.0}	(41.0)	{51.2}
M06-L	70.5	[68.9]	38.2	[36.3]	71.7	[70.3]	39.4	[37.7]
	(66.8)	{86.9}	(35.2)	{51.1}	(68.0)	{87.1}	(36.4)	{51.4}
PBE0	64.7	[64.2]	32.4	[31.6]	67.6	[67.1]	35.3	[34.5]
	(62.8)	{78.6}	(31.2)	{42.8}	(65.9)	{80.9}	(34.4)	{45.1}
$Zn(C_2O_2H_3)_2((CH_3)_2SO)$								
MP2	97.3	[96.6]	49.4	[45.8]	96.5	[95.4]	48.5	[44.6]
	(96.1)	{114.7}	(44.6)	{62.1}	(94.8)	{116.7}	(43.4)	{64.2}
M05-2X	105.4	[104.9]	57.4	[54.1]	106.7	[105.8]	58.7	[55.0]
	(103.9)	{117.8}	(52.5)	{65.2}	(104.8)	{121.7}	(53.4)	{69.2}
ωB97X-D	86.8	[86.2]	38.8	[35.4]	89.6	[88.9]	41.6	[38.1]
	(84.9)	{103.9}	(33.5)	{51.4}	(87.7)	{108.6}	(36.2)	{56.0}
M06-L	85.2	[83.3]	37.2	[32.5]	85.6	[83.4]	37.6	[32.6]
	(82.3)	{103.8}	(30.8)	{51.3}	(82.5)	{105.3}	(31.0)	{52.8}
PBE0	67.1	[66.8]	19.1	[16.0]	70.3	[69.9]	22.4	[19.1]
	(66.0)	{85.1}	(14.5)	{32.6}	(69.3)	{90.3}	(17.9)	{37.8}
$Zn(C_2O_2H_3)_2((CH_3)_2NCHO)$								
MP2	73.1	[68.1]	27.4	[26.6]	73.2	[68.8]	27.5	[27.3]
	(66.8)	{71.2}	(23.8)	{25.8}	(67.4)	{72.2}	(24.4)	{26.9}
M05-2X	81.5	[76.8]	35.8	[35.3]	83.4	[78.5]	37.7	[37.0]
	(75.7)	{79.0}	(32.7)	{33.7}	(77.4)	{81.3}	(34.5)	{35.9}
ωB97X-D	63.2	[61.0]	17.5	[19.5]	66.1	[64.0]	20.4	[22.5]
	(58.2)	{64.5}	(15.2)	{19.2}	(61.4)	{67.7}	(18.4)	{22.3}
M06-L	60.0	[55.5]	14.3	[14.0]	61.1	[56.7]	15.4	[15.2]
	(52.9)	{60.2}	(10.0)	{14.8}	(54.0)	{61.2}	(11.1)	{15.8}
PBE0	51.0	[49.7]	5.3	[8.2]	54.5	[53.0]	8.8	[11.6]

	(47.6)	{53.5}	(4.6)	{8.1}	(51.2)	{57.2}	(8.3)	{11.8}

[a]M05-2X/B2-PP, ωB97X-D/MBS1 (in square brackets), PBE0/MBS1 (parentheses) and PBE0/LANL2DZ (in curly brackets) optimized-geometry data.

3.3.2 Mononuclear Zn models: $Zn(C_2O_2H_3)_2Y$, Y = NH_3, $(CH_3)_2SO$, or $(CH_3)_2NCHO$

3.3.2.1 Geometric properties

Equilibrium structures were obtained for $Zn(C_2O_2H_3)_2Y$, Y = NH_3, $(CH_3)_2SO$ and $(CH_3)_2NCHO$, at the 19 levels of calculation described in the Computational details section and are listed in Table S3.3. On the basis of the results for $Zn(C_2O_2H_3)_2C_5H_5N$ and $Zn(C_2O_2H_3)_2CH_3OH$, a more limited set of method and basis set combinations was examined for the complexes with Y = NH_3, $(CH_3)_2SO$, and $(CH_3)_2NCHO$ (Table S3.2). The effects of the choice of DFT functional and basis set observed for the geometric parameters of the latter three complexes are similar to the effects observed for the former two complexes. Consequently, an even more limited set of geometric parameters, namely those obtained from the M05-2X/B2-PP, ωB97X-D/MBS1 PBE0/B2-PP, PBE0/MBS1, PBE0/LANL2DZ, PBE0/SDDAll, and B3LYP/LANL2DZ minimizations are included in Table 3.3 and will be discussed in the rest of this section. The results for the MBS1 basis set were tabulated because the geometric parameters evaluated with this basis, for a given method and Y ligand, are essentially identical to those evaluated with the larger B2-PP basis set. The results for the LANL2DZ and SDDAll basis sets were tabulated because of the computational efficiency of these bases.

Table 3.3 Representative geometric properties of $Zn(C_2O_2H_3)_2Y$, Y = NH_3, $(CH_3)_2SO$, and $(CH_3)_2NCHO$.

complex	bond length (Å)		bond angle range (°)	
level of theory	$Zn–O_{avg}$ (range)	Zn–Y	O–Zn–O	O–Zn–Y
$Zn(C_2O_2H_3)_2(NH_3)$				
M05-2X/B2-PP	2.064(1.915–2.215)	2.103	83.3–171.1	94.0–111.6
ωB97X-D/MBS1	2.081(1.903–2.266)	2.087	83.1–169.9	93.9–111.5
PBE0/B2-PP	2.081(1.904–2.265)	2.094	82.5–171.6	92.5–110.3
PBE0/ MBS1	2.070(1.910–2.237)	2.075	83.6–161.4	97.2–112.7
PBE0/LANL2DZ	2.073(1.966–2.193)	2.118	81.8–162.8	93.9–111.3
PBE0/SDDAll	2.067(1.940–2.205)	2.061	82.0–162.3	95.9–112.1
B3LYP/LANL2DZ	2.088(1.975–2.212)	2.136	81.7–163.5	94.3–110.9
$Zn(C_2O_2H_3)_2((CH_3)_2SO)$				
M05-2X/B2-PP	2.080(1.917–2.253)	1.990	81.3–154.0	102.4–120.7
ωB97X-D/MBS1	2.096(1.907–2.311)	1.987	80.9–148.2	104.0–121.6
PBE0/B2-PP	2.091(1.904–2.295)	2.008	80.9–153.5	103.2–118.0
PBE0/ MBS1	2.092(1.911–2.294)	1.987	79.6–144.5	105.5–122.4
PBE0/LANL2DZ	2.103(1.980–2.270)	2.004	75.6–142.0	103.9–123.9
PBE0/SDDAll	2.100(1.952–2.317)	1.971	74.3–141.3	108.5–123.1
B3LYP/LANL2DZ	2.116(1.988–2.281)	2.019	76.9–143.0	104.2–122.6
$Zn(C_2O_2H_3)_2((CH_3)_2NCHO)$				
M05-2X/B2-PP	2.072(1.913–2.263)	2.021	81.5–161.2	92.1–123.3
ωB97X-D/MBS1	2.086(1.898–2.345)	2.033	82.1–160.9	93.3–113.6
PBE0/B2-PP	2.080(1.894–2.260)	2.046	81.8–161.2	97.5–118.8
PBE0/ MBS1	2.078(1.904–2.311)	2.027	80.8–154.4	95.2–114.5
PBE0/LANL2DZ	2.083(1.958–2.263)	2.037	81.8–161.2	97.5–118.8
PBE0/SDDAll	2.080(1.922–2.317)	2.014	77.7–155.0	91.6–113.8
B3LYP/LANL2DZ	2.097(1.967–2.284)	2.050	81.2–158.2	91.5–114.5

Again, the $Zn–O_{avg}$ bond length is shortest for the M05-2X/B2-PP optimized geometry, longest for the B3LYP/LANL2DZ geometry and within this range for the PBE0 and ωB97X-D geometries, while there is no clear trend for the Zn–Y bond length (Tables 3.1 and 3.3). Compared with the M05-2X/B2-PP optimized parameters, the $Zn–O_{avg}$ and Zn–Y bond lengths vary by as much as 0.04 Å and 0.05 Å, respectively. Although the $Zn–O_{avg}$ bond lengths are similar in magnitude regardless of the computational level, the difference $(Zn–O_{max}) – (Zn–O_{min})$ is about an order of magnitude greater when this quantity is compared across the levels. The difference is as large as 0.49 Å ($Zn(C_2O_2H_3)_2CH_3OH$, *ω*B97X-D/MBS1) and as small as 0.18 Å ($Zn(C_2O_2H_3)_2C_5H_5N$, PBE0/LANL2DZ) (Table 3.1). The majority of the $Zn–O_{min}$ and $Zn–O_{max}$ bond lengths deviate by approximately 0.25 – 0.35 Å (Tables 3.1 and 3.3). That the $(Zn–O_{max}) – (Zn–O_{min})$ values observed computationally are larger than those observed experimentally for the pyrogallol[4]arene-based capsules (0.05 Å)[31,32] can again be attributed to the $C_2O_2H_3^-\cdots H–Y$ hydrogen bonds exhibited by some of the Y ligands. For a given Y, the ranges of O–Zn–O and O–Zn–Y bond angles are consistent for the six levels of theory considered, differing by at most 10°. With few exceptions, regardless of the Y ligand or computational level, the O–Zn–O and O–Zn–Y bond angles fall within the range observed experimentally[31,32] (Tables 3.1 and 3.3).

3.3.2.2 Energetic properties

Higher-level SPEs were computed for all 19 equilibrium structures obtained for each Y ligand, yielding 274 BDEs (Tables S3.1 and S3.2). Due to the consistent magnitudes of the BDEs, the data reported in Table 3.2 has been limited to 40 values, our

best results for a given geometry and method. The tabulated calculational levels at which the geometries were optimized are M05-2X/B2-PP, ωB97X-D/MBS1, PBE0/MBS1, and PBE0/LANL2DZ. These procedures range from the most to the least computationally demanding of those considered. The tabulated methods at which SPEs were evaluated are MP2, M05-2X, M06-L, PBE0, and ωB97X-D; the basis sets are aug-cc-pVTZ-PP and B2-PP (Table 3.2).

Despite the variations in the optimized structures, in general the BDEs for $(CH_3)_2NCHO$, $(CH_3)_2SO$, and NH_3 vary by no more than 6 kJ/mol for a given SPE method/basis set, and thus are consistent with the variations observed for the C_5H_5N and CH_3OH ligands (Tables 3.2 and S3.1). The exceptions occur for the BDEs of $(CH_3)_2SO$ and NH_3 computed with the PBE0/LANL2DZ equilibrium structures, which overemphasize hydrogen bonding, for which the BDEs vary by approximately 8 – 18 kJ/mol. We note that the largest discrepancies in the BDEs computed for a given Y ligand with a given SPE method/basis set occur when the geometries are optimized with the SDDAll basis set (Table S3.1). There is no significant difference in the thermochemical data computed with the aug-cc-pVTZ-PP and B2-PP basis sets (Tables 3.2 and S3.1). Regardless of the Y ligand, the magnitudes of the BDEs vary according to the following trend: M05-2X ≥ MP2 > ωB97X-D ≥ M06-L > PBE0; at each step, the BDE diminishes by approximately 5 – 10 kJ/mol. Although there is some variance in the relative BDEs among the different calculational levels, the trends in the BDEs across the Y ligands are consistent with the trend $(CH_3)_2SO \geq C_5H_5N > NH_3 \approx (CH_3)_2NCHO > CH_3OH$ (Tables 3.2 and S3.1). Overall, M05-2X/B2-PP SPEs for any of the optimized geometries yield reliable trends in the BDEs.

3.3.3 Polynuclear zinc models: building the capsule

To further support the replacement of deprotonated pyrogallol ($C_6O_3H_4^{2-}$) by $C_2O_2H_3^-$ and $C_4O_3H_4^{2-}$ as the capsule backbone, we first verified that 1,2,3-trihydroxy-*cis*-1,3-butadiene is a minimum at the B3LYP/LANL2DZ level of theory (Fig. 3.2). Although (*Z*)-1,3-butadiene itself is a transition structure at this level of theory, the internal hydrogen bonding interactions in the (*Z*) isomer of the trihydroxybutadiene stabilize this isomer, and in fact it is now the global minimum. In lieu of analyzing individual Zn–O/Zn–Y bond lengths and O–Zn–O/O–Zn–Y bond angles, we then compared the average τ5 values for the Zn atoms in the complexes $Zn_2(C_6O_3H_4)(C_2O_2H_3)_2(NH_3)_2$, $Zn_2(C_4O_3H_4)(C_2O_2H_3)_2(NH_3)_2$, and $Zn(C_2O_2H_3)_2(NH_3)$ (Figs. 3.4 and 3.5). The τ5 value is a simple index that provides a quantitative measure of the square pyramidal (τ5 = 0) versus trigonal bipyramidal (τ5 = 1) character of the coordination geometry of a pentacoordinate metal center.[151] For these complexes τ5 is defined as: $\tau = |\angle(\text{O–Zn–O}) - \angle(\text{HO–Zn–OH})|/60$. The average τ5 values obtained for $Zn_2(C_6O_3H_4)(C_2O_2H_3)_2(NH_3)_2$, $Zn_2(C_4O_3H_4)(C_2O_2H_3)_2(NH_3)_2$, and $Zn(C_2O_2H_3)_2(NH_3)$ are 0.42, 0.35 and 0.41, respectively. Thus, all three complexes have a distorted square pyramidal arrangement of the ligands around the zincs, with the distortion of the $Zn_2(C_4O_3H_4)(C_2O_2H_3)_2(NH_3)_2$ complex slightly less than that of the other two complexes. This difference in geometry most likely results from the greater flexibility of $C_4O_3H_4^{2-}$ compared with $C_6O_3H_4^{2-}$ and from the difference in the hydrogen bonding in the two complexes. In both cases, the $C_2O_2H_3^-$ proton that is not involved in the O–H···O hydrogen bond between the two $C_2O_2H_3^-$ moieties is transferred from the $C_2O_2H_3^-$ to the

$C_4O_3H_4^{2-}$ or $C_6O_3H_4^{2-}$, forming a second O–H···O hydrogen bond (Fig. 3.4). However, a third O–H···O hydrogen bond, between the C3 hydroxyl group and a $C_2O_2H_3^-$ oxygen atom, is present only in the pyrogallol complex.

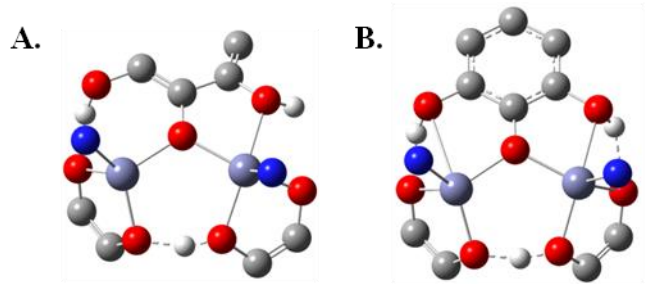

Figure 3.4 $Zn_2(C_4O_3H_4)(C_2O_2H_3)_2(NH_3)_2$ (A) and $Zn_2(C_6O_3H_4)(C_2O_2H_3)_2(NH_3)_2$ (B). The O–H···O hydrogen bonds are shown as dashed lines. Hydrogens on carbon and nitrogen are removed for clarity.

As $C_4O_3H_4^{2-}$ and $C_2O_2H_3^-$ were found to be viable substitutions for $C_6O_3H_4^{2-}$, a capsule was built up from the requisite number of $C_4O_3H_4^{2-}$ and $C_2O_2H_3^-$ anions with 2, 4, 6, or 8 Zn(II) cations and NH_3 molecules (Fig. 3.5). Upon optimization, each of the pentacoordinate Zn models curves naturally to form a portion of a capsule, with the 4-Zn model forming a half capsule and the 8-Zn model forming a closed ring. Despite the absence of methylene linkers, the empty $Zn_8(C_4O_3H_4)_8(NH_3)_8$ model has Zn-Zn and Zn-O distances similar to those found in the crystal structure of [Zn_8(*C*-propylpyrogallol[4]arene)$_2$(pyridine)$_8$⊂pyridine],[31] yielding a diameter for the model that is only ca. 0.2 Å larger than that of the capsule. That is, the difference in flexibility and hydrogen-bonding motifs noted above diminishes as the trihydroxy species participate in the O···H···O hydrogen-bonding networks. The average τ5 value is 0.40 ± 0.04 for $Zn_8(C_4O_3H_4)_8(NH_3)_8$ and 0.42 ± 0.03 for [Zn_8(*C*-propylpyrogallol[4] arene)$_2$(pyridine)$_8$ ⊂pyridine].[32] (Notice that the τ5 value of 0.41 for $Zn(C_2O_2H_3)_2(NH_3)$ is in good

agreement with these values.) The main difference between the model and the capsule is the size of the axial portals, which are much larger for the model (Fig. 3.5).

Even though the progression of multinuclear Zn models is not representative of the actual dimer synthesis in solution (the pyrogallol[4]arene monomers are preformed), the models do give useful information about the formation process. In contrast to the natural curvature of the 5-coordinate polynuclear zinc models, when the zinc is made 6-coordinate, each model flattens out. These results suggest that pentacoordination of Zn permits the metal to take advantage of the pre-existing curvature of the pyrogallol[4]arene monomers.

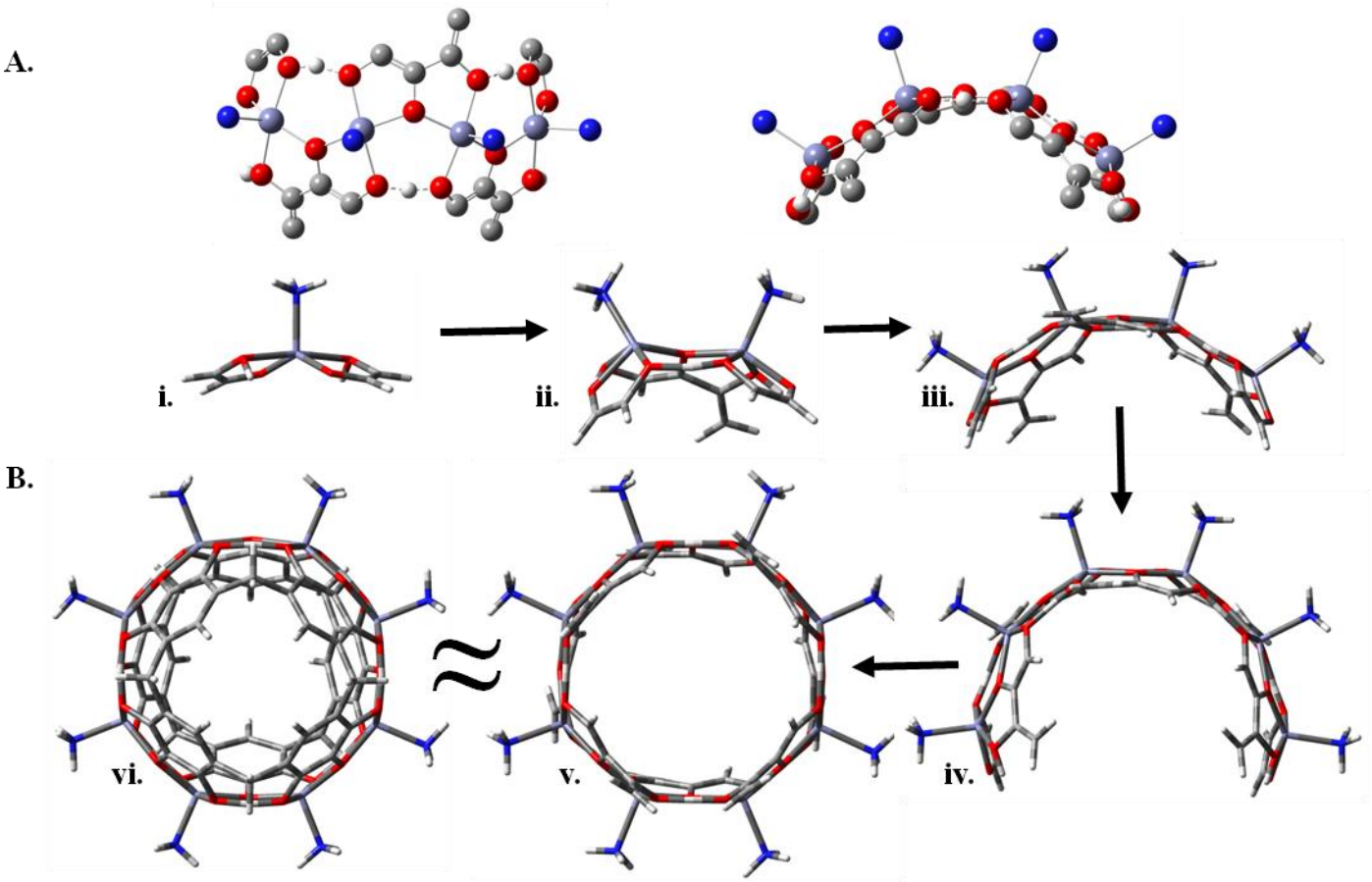

Figure 3.5 (A) Side (left) and top (right) views of the 4-Zn model shown in ball and stick form. Hydrogens are removed from the N–H and C–H bonds for clarity. (B) Tubular perspective of the systematic building of a model capsule with 1-, 2-, 4-, 6-, and 8-Zn complexes.

3.4 Summary

In order to determine an appropriate protocol for studying zinc-seamed pyrogallol[4]arene dimeric nanocapules and multi-zinc models, we assessed a wide range of DFT methods and basis sets with respect to the equilibrium structures and bond dissociation enthalpies of $Zn(C_2O_2H_3)_2Y$ complexes, where Y = C_5H_5N, CH_3OH, NH_3, $(CH_3)_2SO$, or $(CH_3)_2NCHO$. Support for the use of the $Zn(C_2O_2H_3)_2Y$ mononuclear model complex to represent the zinc coordination environment in the nanocapsules was demonstrated in two ways. First, in the systematic build up of an 8-Zn model, each complex in the progression curves naturally to form a section of a capsule, and the 8-Zn model forms a ring. Second, the $\tau 5$ value of the Zn in the mononuclear complex is essentially identical to the average $\tau 5$ value for the zincs in both the $Zn_8(C_4O_3H_4)_8(NH_3)_8$ model system and the [Zn_8(*C*-propylpyrogallol[4] arene)$_2$(pyridine)$_8 \subset$pyridine] dimer.

Geometries of the $Zn(C_2O_2H_3)_2Y$ complexes were benchmarked against M05-2X/B2-PP equilibrium structures; BDEs were benchmarked against MP2/aug-cc-pVTZ-PP//M05-2X/B2-PP values. Because the same atom connectivity and similar trends in geometry were observed for all Y ligands at any level of theory, M05-2X/B2-PP energies combined with PBE0/MSB1 (and perhaps even PBE0/LANL2DZ) equilibrium structures can be used to predict reliable BDEs for the external ligands of mononuclear or polynuclear zinc model complexes, individual dimers, and tethered model complexes or dimers. The recommended procedure may also be applied to Y ligand BDEs of MOFs and enzymatic systems with similar zinc coordination environments. However, we recognize that host-guest assemblies exhibit interactions not present in the mononuclear

zinc complexes that could affect guest orientation and other properties of the assembly. Consequently, due to the good agreement between the ωB97X-D/MBS1, PBE0/MBS1, PBE0/LANL2DZ, and B3LYP/LANL2DZ optimized geometries and the benchmark geometry, and their lower computational cost, these levels of theory will be assessed further to evaluate their performance in describing the dimeric pyrogallol[4]arene-based nanoassemblies. For similar reasons, SPEs will be computed at the M05-2X/B2-PP, ωB97X-D/B2-PP, and M06-L/B2-PP levels of theory.

Chapter 4: Proton affinity and gas-phase basicity of hydroxyquinol: A computational study

Hydroxyquinol (1,2,4-trihydroxybenzene) exhibits a variety of activities of interest to the biomedical and organic chemist. In the particular, hydroxyquinol has numerous possible inequivalent sites for protonation and reaction with other electrophiles. High-level DFT and conventional ab initio quantum chemical calculations, diverse isodesmic proton transfer reactions, and qualitative understanding, of both intramolcular hydrogen bonding and carbocation stability, are used to explain the energy and geometry changes, and the location (which carbon or oxygen) associated with the still unmeasured proton affinity and gas-phase basicity of this species. Application is made to the synthesis of still unknown calixarene-related macrocycles. This work is published in *J. Chem. Thermo.* DOI: 10.1016/j.jct.2013.12.015.[48]

4.1 Introduction

The proton affinity (PA) and gas-phase basicity (GB) of a molecule are useful thermochemical data to someone trying to understand the molecule's reactivity, as many chemical and biochemical reaction pathways are initiated by or involve a proton transfer. PAs and GBs have therefore been the focus of a number of reviews[152-162] and have also been of interest to our group for some time.[163-173] The protonation of benzene, polysubstituted benzenes and other aromatics has been the focus of a number of research articles.[174-179] Of particular interest to this work is the protonation of trihydroxybenzenes. Although the protonation of phenol has been studied extensively both experimentally and

theoretically,[45,47,162,180-182] there have been fewer studies involving the protonation of di- and trihydroxybenzenes.[45-47] In this work, we evaluate the PA and GB of hydroxyquinol, more properly named 1,2,4-trihydroxybenzene or 1,2,4-benzenetriol.

Hydroxyquinol has several roles in biological systems. The most prevalent pathways in which hydroxyquinol plays a role involve microbial degradation, where hydroxyquinol is formed by either resorcinol or chloro-substituted di- or trihydroxybenzenes and subsequently forms maleylacetate or 2,4-dihydroxymuconic semialdehyde.[183,184] Hydroxyquinol and chlorohydroxyquinol are also substrates for hydroxyquinol-1,2-dioxygenases of the 2,4,6-trichlorophenol-degrading strains in the bacterium *Cupriavidus necator*.[184]

Although the preferred site of protonation has been determined experimentally for the trihydroxybenzenes,[46] no PAs or GBs were reported in this study. In fact, to our knowledge, the PAs and GBs of these species have not been determined experimentally or computationally. However, the neutral trihydroxybenzenes have been investigated with respect to (1) the hydrogen-bonding interactions between water and 1,3,5-trihydroxybenzene,[185] (2) the interactions between 1,3,5-trihydroxybenzene dimers,[186] (3) the relative stabilities of the di- and trihydroxybenzenes,[187] (4) the interconversion between 1,2,3- and 1,3,5-trihydroxybenzene (pyrogallol and phloroglucinol, respectively) through anaerobic degradation,[188] and (5) the enthalpies of formation of pyrogallol, phloroglucinol and hydroxyquinol.[189]

A complementary theoretical and experimental study by Bouchoux et al. determined the proton affinity of both mono- and dihydroxybenzenes and good agreement between the calculations and experiment was observed.[45] The most stable

protonation site in all cases is a carbon that is *para* and/or *ortho* to a hydroxy group, while protonation of an oxygen is less favored. In general, formation of intramolecular hydrogen bonds and protonation at a *para* position is favored, whereas in the case of hydroquinone, 1,4-dihydroxybenzene, only protonation at an *ortho* position is observed. Their calculations show that protonation of an oxygen atom is approximately 60 – 70 kJ/mol less stable than protonation at the most favored carbon site. This result supports the finding by Defrees et al. that the PA of the oxygen in phenol is 55 – 85 kJ/mol smaller than that of a site on the ring.[180] In the earlier experimental studies by Olah and Mo, superacids were used to elucidate the preferred protonation sites for mono-, di- and trihydroxybenzenes, via both ^{1}H and ^{13}C NMR.[46,47] The most favorable carbon-protonated species calculated by Bouchoux and coworkers[45] agree with the carbon-protonated species identified by Olah and Mo.

In previous theoretical investigations of the protonation of substituted aromatic systems,[45,152,156,158-160,175-181,187,190-193] the calculational methods ranged from HF and DFT to MP2 to QCISD and CCSD(T), and these methods were combined with a variety of double- and triple-zeta basis sets. In fact, gas-phase acidities and basicities evaluated with DFT methods and a valence triple-zeta basis set augmented with polarization functions on the heavy atoms, e.g., B3LYP/6-311+G(d,p), have been found to be within chemical accuracy for the series of acids and bases investigated by Burk and coworkers.[194] In this study, we have also employed a variety of methods and basis sets. Specifically, geometries have been optimized with the DFT hybrid functionals B3LYP [145,146] and ωB97X-D,[149] which includes empirical dispersion, and the LANL2DZ and aug-cc-pVTZ basis sets. PAs have been obtained with the MP2, M05-2X,[86] and ωB97X-D methods in

conjunction with the aug-cc-pVTZ basis set and with the G4(MP2) method.[42] The lower-level B3LYP/LANL2DZ and ωB97X-D/LANL2DZ optimizations have been included in the study because of our interest in extending the PA and GB calculations to supramolecular host-guest complexes for which a hydroxybenzene comprises the framework of the constituent macrocycles or acts as a guest.[34,125,126,128,195] Previous studies have revealed host-guest complexes of hydroxyquinol (guest) with pyridinyl macrocycles.[196] Given the presence of the hydroxyl groups, introduction of hydroxyquinol into existing macrocycles or metal-seamed/hydrogen-bonded capsules as a possible gate or an exo-guest for metal coordination is possible.[197] In this study of a possible building block for supramolecular host-guest complexes, in addition to determining the PA of hydroxyquinol and the preferred site of protonation, we also (1) determine the difference in PA for oxygen and carbon protonations, (2) examine the effect of loss or enhancement of intramolecular hydrogen bonding on the magnitude of the PA, and (3) gain insight into the cyclization of hydroxybenzenes to form macrocycles.

4.2 Computational details

All calculations were carried out using the Gaussian09 suite of programs[89] and the results were visualized with Gaussview5.[144] The geometries of hydroxyquinol and protonated hydroxyquinol were optimized completely at the B3LYP/LANL2DZ, ωB97X-D/LANL2DZ, and ωB97X-D/aug-cc-pVTZ levels of theory with the int = ultrafine and opt = tight keywords. For the rest of this chapter, the aug-cc-pVTZ basis set will be abbreviated aVTZ. Minima were confirmed and thermochemical corrections were

obtained via normal-mode vibrational frequency analyses. Single-point energies (SPEs) were evaluated at the MP2/aVTZ, M05-2X/aVTZ, and ωB97X-D/aVTZ calculational levels, where applicable. The thermochemical data obtained at the two lower calculational levels have been benchmarked against the MP2/aVTZ//ωB97X-D/aVTZ data. Because the Gn(MP2) methods have been shown to provide reliable PAs for hydroxybenzenes,[45] PAs and GBs for selected systems have also been evaluated with G4(MP2) theory.[42]

In order to locate all stable minima and unique protonation sites for hydroxyquinol, starting geometries with all possible arrangements of the hydroxyl hydrogen atoms, both in and out of the plane, for the neutral molecule were optimized at the B3LYP/LANL2DZ level of theory. The equilibrium geometries located were subsequently reoptimized at the ωB97X-D/LANL2DZ and ωB97X-D/aVTZ levels of theory. All possible protonation sites were examined for the six stable neutral conformations identified, and protons were oriented both in and out of the plane for protonated O–H sites. The same protocol for optimizations was carried out as was described above for the neutral species. Cartesian coordinates for all neutral and protonated complexes optimized at the ωB97X-D/aVTZ level of theory can be found in Table S4.1, and complete energetic results for all optimization and SPE calculations can be found in Table S4.2. All supplementary tables can be found at http://www.sciencedirect.com/science/article/pii/S0021961413004801.

PAs at 298K can be determined by equations 4.1 and 4.2 or, written more simply, as $-\Delta_{rx4.3}H_{298}$ for reaction 4.3. The GB is given by $-\Delta_{rx4.3}G_{298}$. Recall that $E_T(H^+) = 0$ and that $E_T(B^{n-1})$ and $E_T(HB^n)$ are the total energies of the base (B) and its protonated form

(BH^+). Also, the changes for the reaction in the translational, rotational and vibrational energy differences between 298 K and 0 K are denoted by E_x, where x = t, r and v, respectively. The change in the zero-point vibrational energies of the reactants and products is given by ΔZPE and ΔpV is the change in the *pV* work term. PAs can also be predicted by the proton-transfer reaction given in equation 4.4, using the experimental PA value for base B_2.[158,159,162] Reaction 4.4 is isodesmic when both bases are protonated on carbon or when both bases are protonated on oxygen.

$$PA = \Delta E^0 + \Delta E_t^{298} + \Delta E_r^{298} + \Delta E_v^{298} + \Delta pV \quad \textbf{(4.1)}$$

$$\Delta E^0 = [E_T(B^{n-1}) + E_T(H^+) - E_T(HB^n) + \Delta ZPE \quad \textbf{(4.2)}$$

$$B + H^+ \rightarrow BH^+ \quad \textbf{(4.3)}$$

$$B_1H^+ + B_2 \rightarrow B_1 + B_2H^+ \quad \textbf{(4.4)}$$

4.3 Results and analysis of results

4.3.1 Neutral species

Of the six equilibrium structures located for neutral hydroxyquinol, all of which are planar and have C_S symmetry, the four most stable isomers A-D exhibit O–H···O intramolecular hydrogen bonding and have relative enthalpies within 4 kJ/mol (Tables 4.1 and S4.3). In contrast, the remaining two isomers E and F exhibit no hydrogen bonding, have lone pairs facing each other on the 1- and 2-oxygens, and are sensibly 15 – 20 kJ/mol less stable at the MP2/aVTZ//ωB97X-D/aVTZ level of calculation (Fig. 4.1). In fact, the relative enthalpies and free energies at a given calculational level (e.g., MP2/aVTZ//B3LYP/LANL2DZ, MP2/aVTZ//ωB97X-D/LANL2DZ, and MP2/aVTZ//ωB97X-D/aVTZ) vary by less than 1 kJ/mol and for a given geometry (e.g., MP2/aVTZ//B3LYP/LANL2DZ, M05-2X/aVTZ//B3LYP/LANL2DZ, and ωB97X-

D/aVTZ//B3LYP/LANL2DZ) vary by less than 2 kJ/mol (Tables 4.1 and S4.3). In a previous study of hydroxyquinol, Mammino and Kabanda located structures B and D-F;[187] they reported relative energies, calculated at the MP2/6-31++G(d,p) level of theory, that are within 3 kJ/mol of our MP2/aVTZ//ωB97X-D/aVTZ values.

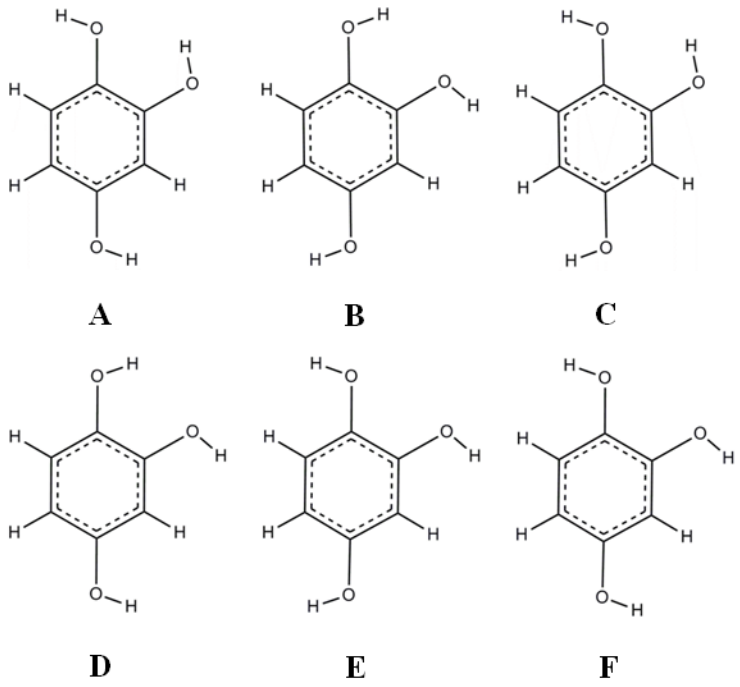

Figure 4.1 Schematic representation of the 6 neutral and planar hydroxyquinol minima located.

Table 4.1 Relative enthalpies and free energies of hydroxyquinol.

complex	ΔH (kJ/mol)[a]	ΔG (kJ/mol)[a]
A	0.0	0.0
B	0.2	0.8
C	0.4	0.5
D	3.7	3.8
E	16.4	16.8
F	18.8	18.9

[a]MP2/aVTZ//ωB97X-D/aVTZ data.

The ωB97X-D/aVTZ optimized geometry of neutral hydroxyquinol A has nearly equal C–C bond lengths, with $(C–C)_{avg}$ = 1.387 ± 0.005 Å, and C–C–C angles, with ∠(C–

C–C)$_{avg}$ = 120.0 ± 0.5°. This limited disruption in the aromatic ring by an OH group was also observed by Bouchoux et al. in their study of the protonation of phenol and dihydroxy-substituted benzenes.[45] There is a slightly larger range of C–O bond lengths and C–O–H bond angles observed, with (C–O)$_{avg}$ = 1.363 ± 0.010 Å and ∠(C–O–H)$_{avg}$ = 109.4 ± 1.0°. Isomer A has an $O_1\cdots H_2–O_2$ hydrogen bond that has an $O_1\cdots H_2$ distance of 2.143 Å and $O_1\cdots H_2–O_2$ angle of 113.5° (which are within the accepted criteria of $R_{O\cdots H}$ < 2.5 Å and ∠O···H–O > 90.0°[198-200]). Similar geometric properties were found for the remaining five conformers, and the same trends apply at the lower levels of theory, but the bonds are slightly elongated.

4.3.2 Protonated species

The notation A:C_1 will be used to denote that compound A (Fig. 4.1) has been protonated at carbon C_1 (Fig. 4.2). PAs and GBs for all calculations can be found in Table S4.4. The cationic compounds have C_1 symmetry when the *ipso* carbons (C_1, C_2 or C_4) are protonated or C_S symmetry when the oxygen atoms (with a few exceptions) or remaining carbon atoms are protonated. All species with a protonated oxygen retained a distorted tetrahedral form about the oxygen, with an $H–O–H^+$ bond angle within a few degrees of 109°. When an oxygen is protonated and all atoms are in the plane, the resulting systems are transition structures.

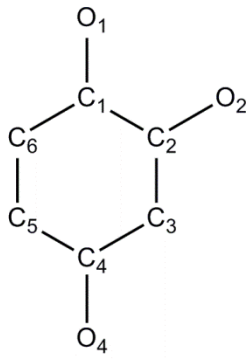

Figure 4.2 Numbering schematic for protonated hydroxyquinol.

In the following, the geometric parameters of protonated and neutral hydroxyquinol A are compared. Very little change in the C–C_{avg} bond length is observed when an oxygen is protonated. As a CH moiety is transformed into a CH_2 moiety and the hybridization nominally changes from sp^2 to sp^3, protonation at carbon leads to more distorted C–C bonds, with the largest distortions found for the *ipso* carbons (e.g., for A:C_1 $(C–C)_{avg}$ = 1.423 ± 0.069 Å). The increase in the C–O bond length is as much as 0.121 Å when an oxygen or an *ipso* carbon is protonated (e.g., for A:O_4 $(C–O)_{avg}$ = 1.387 ± 0.084 Å) as C–O conjugation is removed. A smaller range of C–O bond lengths are observed when an *ortho* carbon is protonated (e.g., for A:C_6 $(C–O)_{avg}$ = 1.328 ± 0.015 Å). Another significant structural rearrangement is the shortening of the C–O bond of a carbon adjacent to a protonated *ipso* carbon (e.g., for A:C_2, the C_1–O_1 bond length shortens 0.078 Å). In contrast, protonation of hydroxyquinol causes minimal changes in the C–C–C and the C–O–H bond angles. In the protonated species, the $O_1 \cdots H_2$ hydrogen bond lengths range from 1.865 – 2.500 Å and the $O_1 \cdots H_2$–O_2 hydrogen bond angles range from 90.3 – 113.8°. As with the neutral species, although the average bond lengths

and angles are slightly larger, similar trends are observed with the smaller LANL2DZ basis set.

The most favorable carbon-protonated species is A:C_5 with a MP2/aVTZ//ωB97X-D/aVTZ PA of 838.7 kJ/mol, and the most favorable oxygen-protonated species is B:O_1 with a PA of 757.3 kJ/mol (Table 4.2). Olah and Mo also found that protonation at C_5 is preferred in their solution phase studies.[46] It should be noted that protonation at C_1, C_3, C_5, and C_6 leads to larger PAs than protonation at any oxygen. The approximately 80 kJ/mol difference in the PAs of the carbon and oxygen sites is similar to the differences seen by both Bouchoux and coworkers and Defrees and coworkers for phenol and the dihydroxybenzenes.[45,180] All of the carbon protonation sites are *meta* to an OH substituent and/or on an *ipso* carbon. Protonation at C_5 is preferred because that site is also *para* to the C_2 hydroxyl substituent and *ortho* to the C_4 substituent, consistent with the activating and *ortho*, *para*-orienting influence of OH groups in electrophilic aromatic substitution reactions. Despite disrupting the ring aromaticity, protonation at a carbon is favored over protonation at an oxygen because the resulting delocalized carbocation is stabilized by electron donation from the hydroxyl groups, whereas no such stabilizing electron donation occurs from the ring to a protonated oxygen. (From the experimental literature[162] we find the PA and GB of the unsaturated crotonaldehyde, $CH_3CH{=}CHCHO$ are ca. 40 kJ/mol higher than these corresponding quantities for the saturated butyraldehyde, $CH_3CH_2CH_2CHO$ and n-butanol, $CH_3CH_2CH_2CH_2OH$, a finding consistent with the greater delocalization of the positive charge.) For the A conformer of hydroxyquinol, A:C_5 has the shortest $O_1\cdots H_2$ hydrogen bond at 2.032 Å, whereas A:C_2, the least stable of the protonated A species, has

an O_1–to–H_2 distance (2.550 Å) outside the accepted hydrogen bond range. In general, protonation of an oxygen or an *ipso* carbon is as much as 130 kJ/mol less favorable than protonation of the remaining carbons. Similar trends are observed at all levels of calculation, including at the G4(MP2) level although the trends were checked only for the A conformers (Tables S4.2 and S4.4). More specifically, the G4(MP2) PAs of carbon protonated sites are enhanced 20 – 30 kJ/mol in comparison to the MP2/aVTZ//ωB97X-D/aVTZ data, whereas the PAs of oxygen protonated sites are enhanced by only 5 – 15 kJ/mol.

Table 4.2 PAs and GBs of hydroxyquinol.[a]

H^+	neutral species					
site	A	B	C	D	E	F
C_1	791.1 (758.1)	777.2 (745.4)	788.4 (755.5)	775.3 (743.4)	–[b] (–)	–[b] (–)
C_2	719.4 (688.1)	730.3 (699.0)	712.0 (681.4)	737.2 (704.8)	706.0 (677.4)	721.8 (691.2)
C_3	800.4 (770.5)	795.8 (764.3)	808.3 (778.1)	784.9 (753.7)	785.0 (754.1)	774.3 (743.8)
C_4	725.5 (694.6)	743.7 (713.4)	725.5 (694.6)	743.1 (712.9)	721.8 (691.5)	721.8 (691.2)
C_5	838.7 (806.0)	817.5 (785.2)	833.5 (800.9)	818.3 (786.0)	813.2 (780.7)	814.9 (782.4)
C_6	760.6 (730.1)	780.0 (749.0)	765.3 (734.0)	770.3 (740.6)	758.9 (727.8)	750.4 (720.4)
O_1	717.4 (686.4)	757.3 (725.4)	716.5 (685.6)	753.8 (722.4)	738.4 (708.4)	736.2 (706.1)
O_2	749.0 (718.4)	712.5 (683.3)	754.3 (723.6)	704.7 (675.3)	–[b] (–)	–[b] (–)
O_4	752.1 (721.2)	745.5 (714.5)	751.4 (720.8)	742.7 (711.8)	730.3 (699.5)	728.6 (697.7)

[a]MP2/aVTZ//ωB97X-D/aVTZ data. PA and GB (in parentheses) data (in kJ/mol). [b]Optimized geometry rearranged to a previously identified minima.

For a given carbon protonation site (e.g., A:C_1 and B:C_1) or the protonation of O_4, there is at most a 25 kJ/mol variance in the proton affinity among the six conformers; larger variations in PA are found for the protonation of O_1 and O_2 and are due to the resulting orientations of the hydrogens, some of which disrupt the $O_1 \cdots H_2$ or $O_2 \cdots H_1$ hydrogen bonds in conformers A – D. The PA associated with the O_4 protonation site is used as a reference value in the discussion below because O_4 does not participate in intramolecular hydrogen bonding. When the protonated oxygen is the proton donor in the hydrogen bond of the neutral conformer, the PA is at best minimally enhanced compared with the protonation of O_4 (2 – 10 kJ/mol). When the protonated oxygen is the electron donor in the hydrogen bond of the neutral conformer, the PA is significantly diminished (up to 40 kJ/mol). This minimal enhancement in PA can be explained, at least partially, by the rotation of the hydrogen-bonded proton out of the plane. When no intramolecular hydrogen bonding is observed, conformers E and F, the PA associated with protonation at O_4 drops 15 – 20 kJ/mol.

For protonation at any carbon, the PA is essentially independent of the geometry used in the SPE calculation; the magnitude of the PA varies by 3 – 6 kJ/mol. For protonation at oxygen, if the structures optimized at the three different calculational levels have equivalent point groups, the PA has a 5 – 10 kJ/mol variance, but if non-equivalent point groups are observed, the PAs vary by as much as 30 kJ/mol. The enhanced PAs associated with the protonated oxygens are most likely due to the overemphasized hydrogen bonding that is sometimes found with the LANL2DZ basis set.[43,44] Regardless of the optimized geometry, the magnitude of the PA increases as follows: MP2/aVTZ < M05-2X/aVTZ < ωB97X-D/aVTZ (Table S4.4). However, the

deviation in PA across equivalent equilibrium structures decreases as follows: MP2/aVTZ > ωB97X-D/aVTZ ≥ M05-2X/aVTZ.

4.3.3 Comparison with mono- and dihydroxybenzenes

Addition of one hydroxyl group to benzene increases the PA from 750.4 kJ/mol to 820.5 kJ/mol.[45,162] Bouchoux et al. found the following trend in the PA of phenol with respect to the position of the protonation site relative to the hydroxyl substituent: *para* (0) > *ortho* (12 and 17) > oxygen (64) > *meta* (69 and 73) > *ipso* (128). The relative PAs are given in kJ/mol and were calculated at the MP2/6-31G(d) level of theory.[45] The change in PA is not consistent upon addition of a second hydroxyl group, a result which also can be rationalized on the basis of the *ortho/para* orienting influence of the OH group(s) as well as the possible intramolecular O···H–O hydrogen bonding.[45] With its internal hydrogen bond and protonation at a ring site that is *meta*, *para* to the hydroxyl group substituents, catechol (1,2-dihydroxybenzene) has a PA ($PA_{catechol}$ = 822.9 kJ/mol) that is essentially equivalent to that of phenol. The absence of an internal hydrogen bond combined with carbon protonation that is *ortho*, *meta* to the hydroxyl substituents leads to a decrease of about 15 kJ/mol in the PA of hydroquinone (1,4-dihydroxybenzene, $PA_{hydroquinone}$ = 808.4 kJ/mol) compared to that of phenol. In contrast, even without stabilization provided by intramolecular hydrogen bonding, protonation at a ring site that is *ortho*, *para* to the substituents increases the PA of resorcinol (1,3-dihydroxybenzene, $PA_{resorcinol}$ = 856.4 kJ/mol) by about 30 kJ/mol. This enhancement in PA arises from effective donation of electron density into the ring by two oxygen atoms in resorcinol as compared with one oxygen atom in phenol, catechol and hydroquinone.[45]

The position of the hydroxyl substituents in hydroxyquinol can be considered a combination of the positions of the substituents in all three dihydroxybenzenes. Given the above results for phenol and the dihydroxybenzenes, one would predict protonation site C_5 of conformer A, B, C, or D to be most stable and protonation site C_4 of conformer E or F to be least stable, which is precisely what was found (Tables 4.2 and 4.3).

Table 4.3 Substitution site of carbons.

protonation site[a]	substitution site
C_5	*ortho*, *meta*, *para*
C_3	*ortho*, *ortho*, *meta*
C_1	*ipso*, *ortho*, *para*
C_6	*ortho*, *meta*, *meta*
C_4	*ipso*, *meta*, *para*
C_2	*ipso*, *ortho*, *para*

[a]Complexes are listed from highest to lowest PA for conformer A.

Bouchoux et al. found PAs calculated at the MP2/6-311+G(3df,2p)//MP2/6-31G(d) level of theory to underestimate the experimental PAs of hydroxybenzenes by approximately 30 – 35 kJ/mol, whereas B3LYP/6-311+G(3df,2p)//B3LYP/6-31G(d) and G2(MP2,SVP) PAs were found to be within 15 kJ/mol of the experimental values.[45] In an effort to obtain a PA for hydroxyquinol that is as accurate as possible, isodesmic reactions involving a carbon-protonated reference base (benzene, phenol, or a dihydroxybenzene) were considered (Table 4.4).[45,162] In the isodesmic reaction given in equation 4.4, where B_1 is hydroxyquinol and B_2 is the reference base, $PA_{iso}(\text{hydroxyquinol}) = PA_{calc}(B_1) + PA_{exp}(B_2) - PA_{calc}(B_2)$. To obtain $PA_{calc}(B_2)$, the most stable species identified by Bouchoux and coworkers for the reference bases[45] were re-optimized at the ωB97X-D/aVTZ level of theory, and SPEs were evaluated at the

M05-2X/aVTZ and MP2/aVTZ levels. G4(MP2) calculations were also performed for each reference base. Averaging the MP2/aVTZ//ωB97X-D/aVTZ PA_{iso}(hydroxyquinol) for all five B_2 reference bases leads to an average PA_{iso}(hydroxyquinol) = 868.0 ± 2.0 kJ/mol, again some 30 kJ/mol greater than the MP2/aVTZ//ωB97X-D/aVTZ PA calculated with equation 4.3. Likewise, averaging the G4(MP2) PA_{iso}(hydroxyquinol) for all five B_2 reference bases leads to an average PA_{iso}(hydroxyquinol) = 868.0 ± 1.2 kJ/mol, which is only 6 kJ/mol greater than the G4(MP2) PA (861.9 kJ/mol) calculated with equation 4.3 (Tables 4.4 and S4.2). In fact, equivalent PA_{iso}(hydroxyquinol) averages are found regardless of whether G4(MP2), MP2/aVTZ, M05-2X/aVTZ or ωB97X-D/aVTZ SPEs are employed in equation 4.4 (Table S4.5). Interestingly, the average of the M05-2X/aVTZ and ωB97X-D/aVTZ PAs calculated with equation 4.3 are within 5 kJ/mol of the experimental PA of benzene, phenol and the three dihydroxybenzenes (Tables S4.2 and S4.5).[45,162] As expected, averaging the M05-2X/aVTZ and ωB97X-D/aVTZ PAs for hydroxyquinol (873 kJ/mol) leads to a PA that is essentially equivalent to the results from the isodesmic reactions (Tables S4.2 and S4.4).

Table 4.4 Calculated PA for hydroxyquinol using isodesmic reactions.[a]

B_2	$PA_{exp}(B_2)$	$PA_{calc}(B_2)$	PA_{iso}(hydroxyquinol)
benzene	750.4	744.6 (723.8)	867.7 (865.3)
phenol	817.3	811.5 (787.1)	867.7 (868.9)
catechol	822.9	818.4 (794.4)	866.3 (867.2)
resorcinol	856.4	849.7 (827.1)	868.5 (868.0)
hydroquinone	808.4	800.7 (776.4)	869.5 (870.7)

[a]All PAs in kJ/mol. Experimental values from references 46 and 166. All calculated values from G4(MP2) and MP2/aVTZ//ωB97X-D/aVTZ (in parentheses) data. $PA_{calc}[B_2]$ calculated using reaction 4.3 and PA_{iso}[hydroxyquinol] calculated using reaction 4.4.

4.3.4 Preferred CHR linkage site in hydroxybenzene-based macrocycles

For some time now, our group has been investigating the structures and energetics of macrocycles constructed from hydroxybenzene building blocks and the hydrogen-bonded or metal-seamed host-guest complexes constructed from those macrocycles.[34,49,125,126,128,195] In the most common macrocycles built from resorcinol and pyrogallol, the resorcin[4]arenes and pyrogallol[4]arenes, respectively, the four hydroxybenzene subunits are linked together through a CHR group (Fig. 4.3). For a given subunit, linker groups add to carbon sites that lie 1,3 to each other on the ring, and each of these carbon sites is *ortho* to a hydroxyl substituent. The macrocycles are synthesized via an acid-catalyzed reaction between a hydroxybenzene moiety and an aldehyde, and the synthesis has been suggested to proceed by an electrophilic aromatic substitution reaction in which the electrophile is an acetal.[195] The carbon sites at which the substitutions occur are consistent with the two equivalent carbons that have been shown to have the highest preference for a proton in resorcinol and pyrogallol.[45-47] Linking the aryl groups at these carbon sites places the hydroxyl groups at the upper rim of the macrocycle, where they can form a network of intramolecular hydrogen bonds within and/or between the aryl subunits to stabilize the cone conformer of the macrocycle. In contrast, the equivalent, preferred protonation/linking sites in phenol that are *ortho* to the hydroxyl group place this group at the lower rim of the calix[4]arene macrocycle, with the four hydroxyls in close enough contact to form a hydrogen-bonded ring. Placing the hydroxyl group at the upper rim of the phenol-based macrocycle would require connecting the subunits at the 1,3-carbons that are *meta* to the OH, which is not only less preferred but also likely to decrease the strength of the O–H···O interactions. Extending

this analysis to catechol, hydroquinone, and hydroxyquinol suggests that synthesizing similarly linked macrocycles from these dihydroxy- and trihydroxybenzenes is less favorable. If the linkage occurs through carbons that lie 1,3 with respect to each other on the aryl ring, the relevant carbons are *ortho, meta* or *meta, para* relative to the hydroxyl groups in catchol and hydroquinone, as opposed to the *ortho, para* orientation of the relevant carbons in resorcinol. Furthermore, the two linkage sites in catchol are not equally preferred with respect to gas-phase protonation. The latter observation is also true for hydroxyquinol, where the CHR addition sites are *ortho, ortho, meta* and *ortho, meta, para* relative to the hydroxyl groups. Substitution at the former site may also be disfavored by steric constraints, as that carbon is located between two of the hydroxyl groups.

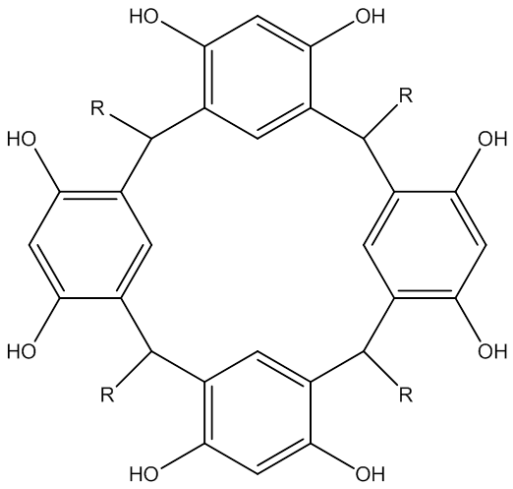

Figure 4.3 Schematic of resorcin[4]arene macrocycle.

4.4 Summary

Our results suggest that hydroxyquinol is a carbon base, as is observed for phenol and the three dihydroxybenzenes.[45] Hydroxyquinol is preferentially protonated at carbon

C_5, supporting the findings of Olah and Mo,[46] with a PA of 868.0 ± 1.2 kJ/mol, determined by a series of isodesmic reactions. When the protonation site is oriented *ortho*/*para* to the hydroxyl substituents, the ring carbocation is stabilized due to donation of electrons from the hydroxyl groups. The MP2/aVTZ//ωB97X-D/aVTZ calculated PA (838.7 kJ/mol) is 30 kJ/mol smaller than the corrected PA, whereas the G4(MP2) calculated PA (861.9 kJ/mol) is only 6 kJ/mol smaller. Similar trends in calculated PAs were observed by Bouchoux et al., and the use of benzene as the reference base in their isodesmic reactions led to PAs for phenol and the three dihydroxybenzenes that are within 5 kJ/mol of the experimental PAs.[45] When an intramolecular O–H···O hydrogen bond is present, hydroxyquinol, neutral or protonated, is stabilized by approximately 20 kJ/mol. Addition of a hydroxyl group leads to a higher PA compared with phenol and the dihydroxybenzenes. That is, the proton affinity (basicity) increases as follows: hydroquinone < phenol ≤ catechol < resorcinol < hydroxyquinol. The preferred gas-phase protonation site in phenol, resorcinol (and pyrogallol) helps to rationalize (1) the site at which the CHR linker moieties add to the ring in the construction of the macrocycles formed from these hydroxybenzenes and (2) the placement of the OH groups at the lower rim of calix[4]arene but at the upper rim of resorcin[4]arene.

For a given conformer, the protonation of the most favorable oxygen site results in a PA that is at least 60 kJ/mol smaller than that of the most stable carbon protonation site. Protonating an electron-donating oxygen can disrupt the intramolecular hydrogen bonding and thus further diminish the PA of an oxygen protonation site, whereas protonating an oxygen proton donor can slightly enhance the PA.

Chapter 5: Screening for tethering ligands: Models of zinc-seamed pyrogallol[4]arene nanocapsules

Metal-organic frameworks (MOFs) are a class of porous materials with a wide variety of applications, including molecular adsorption and separation. Recently, the first MOF based on the zinc-seamed pyrogallol[4]arene nanocapsule as a secondary building unit was reported. The zinc-seamed nanocapsules are linked together with 4,4'-bipyridine, which is a divergent ligand commonly used in the synthesis of MOFs. In an effort to identify other likely candidates for nanocapsular linking, this work presents electronic structure calculations performed to determine the energetic and geometric properties of $(Zn(C_2O_2H_3)_2)_{1,2}Y$ model complexes, which have been shown previously to reliably model the zinc coordination sphere found in the nanocapsules. Here, Y represents one of sixteen divergent ligands with N, S, or O electron-donating atoms. Of these, 1,3,5-trimethylimidazole-2,4,6-triethylbenzene, 1,4-bis(imidazol-1-ylmethyl)benzene, and 1,3-bis(imidazol-1-ylmethyl)benzene are suggested as most suitable for further experimental study. This work has been submitted to *Chemistry– A European Journal*.[201]

5.1 Introduction

Metal-organic frameworks (MOFs) are a fascinating class of porous materials characterized by a tunable, rigid matrix that makes them attractive for applications such as molecular adsorption, separations, and catalytic transformations, among others.[202] These materials are typically made from two components: metal "nodes" and divergent organic linkers, the latter yielding a "net" through coordinative bonding. Although the

"node" component is typically a monoatomic metal cation, polymetallic clusters likewise have been used to generate novel framework-type materials.[203-206] Such materials offer several benefits over those constructed from the simpler cationic building blocks.[205-207] For example, the larger size of the clusters helps prevent structural intercalation. Furthermore, the discrete positioning of cations within a polymetallic cluster limits the number of possible arrangements of the node and linkers. This restriction allows a more accurate prediction of the geometry of a node/linker combination and thus of the resultant MOF.

Recently, the Atwood group reported that coordination polymers can be formed using pyrogallol[4]arene-based metal organic nanocapsules (MONCs) as secondary building units. Pyrogallol[4]arenes (PgCs) are calixarene-like macrocyclic molecules that are used primarily as supramolecular building blocks (SBBs) in materials constructed through non-covalent means.[127,208-220] However, with an upper rim consisting of twelve phenolic hydroxyl groups, these macrocycles can also function as coordinative building blocks in the construction of more complex superstructures. Common structural motifs of PgC-based entities include the hexameric $(PgC)_6M_{24}$ and dimeric $(PgC)_2M_8$ metal-organic nanocapsules (MONCs) formed with transition metal cations[30-34,125,126,221] and the infinite layered networks formed with alkali cations,[222,223] among others.[130,224] The cage-like coordination complexes formed from transition metal cations are very similar in size and shape to their non-covalently seamed complementary supramolecules[225] and feature two distinct coordination patterns: eight distinct trimetal clusters in the hexamer and an "octametal belt" in the dimer (Fig. 5.1). The coordination number of the metal cations is

also different in the two motifs, with tetra- or hexa-coordinate sites seen in the hexamer and penta-coordinate sites typically seen in the dimer.

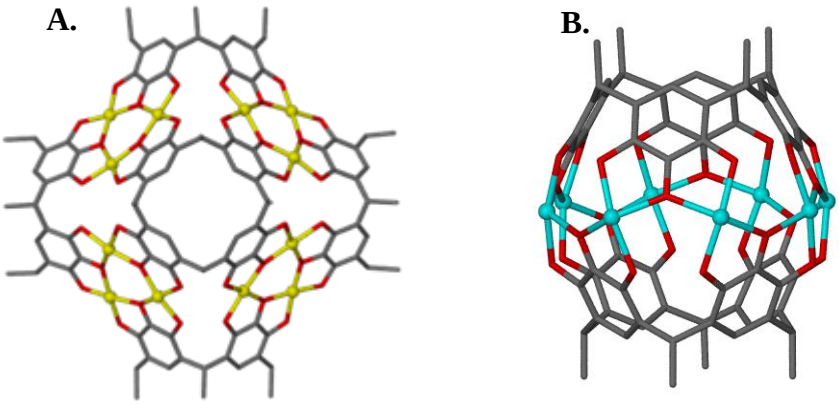

Figure 5.1 Perspective drawings of hexameric (A) and dimeric (B) MONCs.

As the metal cations are located on the exterior wall of the capsule, most are capped by one or two peripheral ligands to complete the coordination sphere (Fig. 5.2). Generally, these ligands are solvents of crystallization (acetone, dimethyl sulfoxide) or reagents added during synthesis (pyridine). Previous work has shown that the peripheral ligands can be readily exchanged for others without affecting the structural integrity of the capsule.[32] This result suggested that the MONC could be post-synthetically modified by exchanging pre-existing ligands with those of a greater functionality.

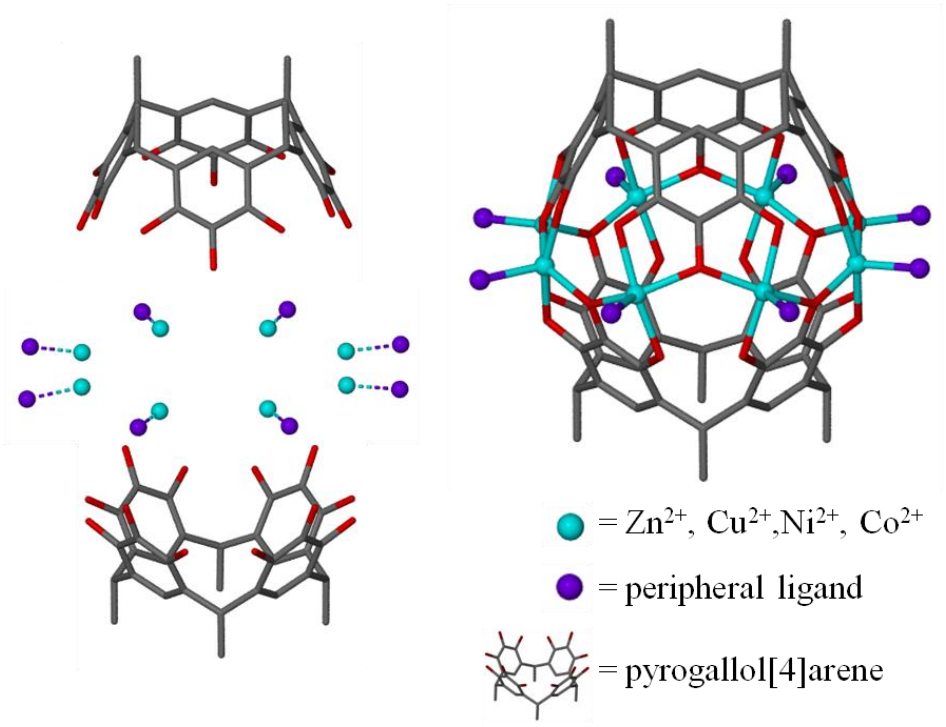

Figure 5.2 Components of a zinc-seamed dimeric MONC. Zn^{2+} cations (turquoise) coordinatively seam two macrocyclic hemispheres via an "octametal belt." Each Zn^{2+} center also coordinates to an additional peripheral ligand (violet).

Coordination polymers derived from both copper-seamed and zinc-seamed pyrogallol[4]arene-based nancapsules have now been observed, all of which were formed using ligand exchange methodologies.[39,40] Two different 1-D "chain-like" polymers were observed using the Cu^{2+} dimer.[39] The first utilizes 4,4'-bipyridyl (bpy) as an equatorial linking ligand to replace pre-existing DMSO ligands, while the second features "direct" linking, wherein pyridine ligands are replaced with direct coordination of Cu^{2+} centers to hydroxyls on adjacent MONCs.

Given the similarity in the structure of the copper- and zinc-seamed dimeric MONCs, the zinc dimer was similarly investigated in a joint experimental and computational study by our groups.[40] In the computational segment of this study,

quantum chemical calculations were performed to investigate the geometric and energetic properties of model systems comprising zinc, deprotonated (*Z*)-ethene-1,2-diol, and bpy. Combined with a peripheral ligand Y, where Y is pyridine, methanol, dimethylsulfoxide, etc., complexes built from zinc and deprotonated (*Z*)-ethene-1,2-diol, $Zn(C_2O_2H_3)_2Y$, reproduced the crystallographic coordination environment and other geometric properties of the zinc metal centers in the pyrogallol[4]arene dimeric nanocapsules.[44] To explore the suitability of bpy as a ligand for Zn^{2+} dimers, two model systems were examined, one in which the bpy is bound to a single zinc complex, $Zn(C_2O_2H_3)_2$bpy, and one in which the bpy is tethered between two zinc complexes, $(Zn(C_2O_2H_3)_2)_2$bpy. Given the minimal drop-off (<4 kJ/mol) in the Zn-bpy binding energy (~90 kJ/mol) observed when the second zinc moiety is also bound to bpy, construction of a MOF from zinc-seamed pyrogallol[4]arene building blocks appeared feasible and thus was pursued experimentally. The 2-D bpy-linked MOF that was synthesized was isolated in the solid state as single crystals, and its structure was determined using X-ray diffraction. In addition to six penta-coordinate zinc centers, this MOF contained two hexa-coordinate zinc centers, leading to zinc-coordination spheres that differ significantly from those in the non-linked Zn^{2+} analog. A representation of two zinc-seamed MONCs linked with a bpy ligand is shown in Fig. 5.3.

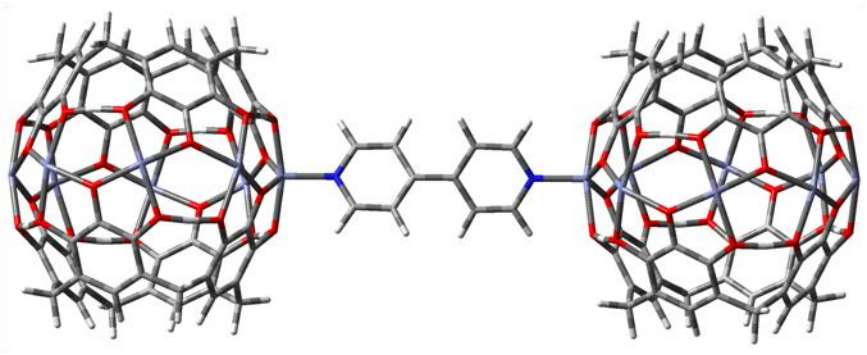

Figure 5.3 Zinc-seamed pyrogallol[4]arene nanocapsules linked by bpy. Equatorial ligands, alkyl chains and guests have been removed for clarity. Note the octametal belt and the O–Zn–O–Zn and O···H···O networks in the MONCs. Color scheme: Zn: purple, O: red, N: blue, C: gray, H: white.

The calculational data were also used initially to determine the ligands with bond dissociation enthalpies (BDEs) lower than that of bpy. It was assumed that use of such ligands would be advantageous, as they could be readily exchanged for other, stronger-binding linking ligands. However, it was experimentally determined that ligands with higher BDEs relative to the linker are actually preferable to those with lower BDEs, in that their presence slows the ligand exchange process, thereby slowing the growth of the MOF and promoting the growth of well-formed crystals instead of powder.

To further explore the notion of ligand exchange and to gain more insight into the metal-coordination sphere found in PgC-based MONCs, we have extended our electronic structure calculations on the $(Zn(C_2O_2H_3)_2)_{1,2}Y$ model complexes to include additional divergent ligands (Y). The ligands chosen for the current study are primarily cyclic systems with N, O or S electron donor atoms (Fig. 5.4). Ligands containing (1) primary amines, tertiary amines, or a mixture of the two; (2) ketones, hydroxyls, or their sulfur analogs; or (3) carboxylic acids have been investigated. Both geometric and energetic

data have been evaluated for the complexes with the primary goal of assessing whether or not the ligands could function as effective linkers.

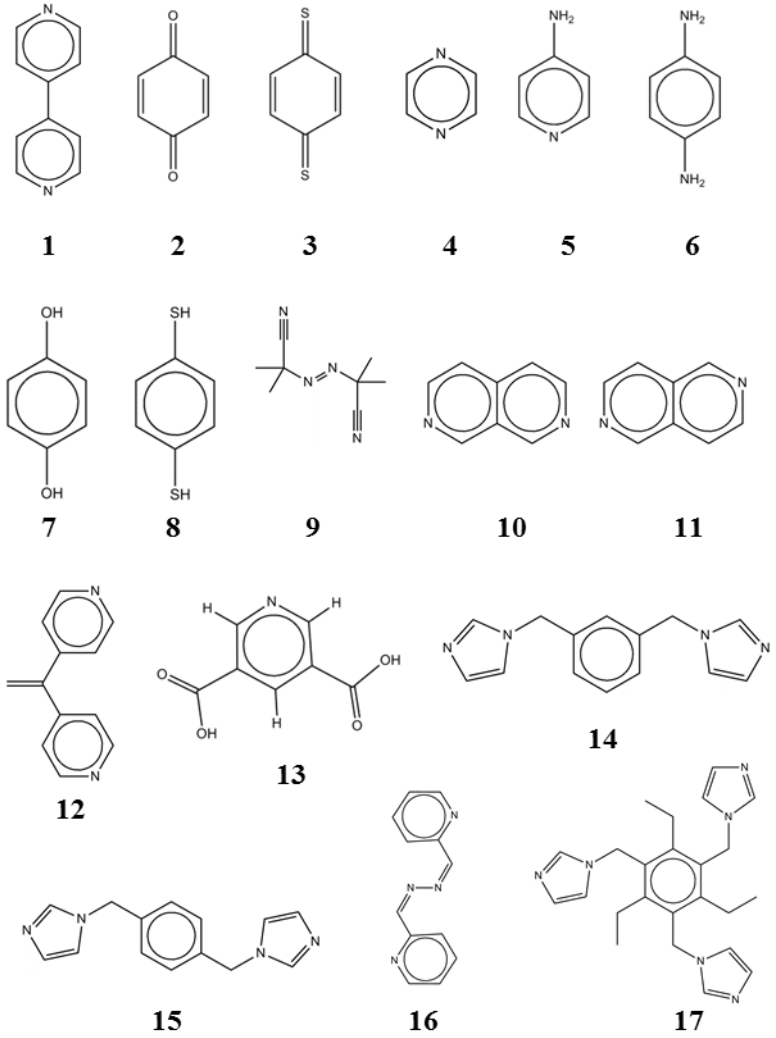

Figure 5.4 Schematic representations of Y ligands.

5.2 Computational details

All calculations were performed with the Gaussian09 suite of programs[89] and visualized with GaussView5.[144] Following the approach from our earlier work,[40,44] deprotonated *Z*-ethene-1,2-diol molecules were used to model the pyrogallol[4]arene framework that makes up the zinc coordination sphere in zinc-seamed pyrogallol[4]arene

nanocapsules.[44] Model complexes of the form $Zn(C_2O_2H_3)_2Y$ (abbreviated ZE_2Y) and $(Zn(C_2O_2H_3)_2)_2Y$ (abbreviated $(ZE_2)_2Y$), where Y is a divergent ligand (Fig. 5.4), have been fully optimized with tight threshold criteria and the int = ultrafine keyword. (We note that the $(ZE_2)_2$**15** complex was optimized using loose criteria due to convergence issues.) Common names for the ligands used in this study can be found in Table S5.1. Normal-mode vibrational frequencies were calculated to verify minima (no imaginary frequencies) and to obtain thermal correction terms.

The unsubstituted complex comprising zinc and deprotonated *Z*-ethene-1,2-diol, $Zn(C_2O_2H_3)_2$, has a distorted tetrahedral coordinative geometry (C_2 symmetry). When the Y ligands were added, they were oriented to provide a starting structure with a square pyramidal geometry. They were also positioned so that only Y–H···O hydrogen bonding interactions were allowed between Y and $C_2O_2H_3^-$ because we have previously shown that the Y–H···O and Y–H···OH interaction strengths vary by no more than 5 kJ/mol.[44] In addition, tetra-coordinate complexes with outer-shell hydrogen bonding motifs were not considered in this study as such motifs are not observed experimentally. The geometries of the tethered complexes $(ZE_2)_2Y$ were constrained to at least C_2 symmetry, when possible.

In our earlier work on ZE_2Y complexes, where Y was a nondivergent ligand, we performed a calibration study investigating the effect of the method, density functional theory (DFT) versus MP2, and basis set, double- versus triple-zeta and small- versus large-core pseudopotential, on the geometric and energetic properties of the complexes. On the basis of those results, the LANL2DZ basis set and two mixed basis sets were used in this study. The larger mixed basis set, B2-PP, uses the B2 basis set by Amin et al.[41]

and SDD pseudopotential on the zinc atom and the 6-311+G(2df,2p) basis set on all other atoms; the smaller mixed basis set, MBS1, uses the same basis set and pseudopotential on the zinc atom and the 6-31G(d) basis set on all other atoms. The calculational levels prescribed for optimizations,[44] ωB97X-D/MBS1, PBE0/MBS1, PBE0/LANL2DZ, and B3LYP/LANL2DZ, have been applied to zinc models linked by 4,4'-bipyridyl (bpy, **1**), *p*-benzoquinone (**2**) and its sulfur analog 2,5-cyclohexadiene-1,4-dithione (**3**), that is, to $(ZE_2)_{1,2}$(**1** – **3**). These complexes exhibit Zn–N, Zn–O, and Zn–S binding, respectively, as well as C–H···O hydrogen bonding. Ligands **1** – **3** were used as sample systems to confirm that the prescribed levels are reliable for tethered zinc complexes and Zn–S coordination. The equilibrium structures obtained for the sample systems have been benchmarked against M05-2X/B2-PP equilibrium structures. M05-2X/B2-PP and MP2/B2-PP single-point energies (SPEs) were computed to evaluate binding dissociation enthalpies (BDEs) and free energies (BDFs) for the sample $(ZE_2)_{1,2}Y$ complexes (eqs. 5.1 and 5.2). The M05-2X/B2-PP data have been benchmarked against the MP2/B2-PP data.

$$ZE_2Y \rightarrow ZE_2 + Y \qquad \textbf{(5.1)}$$

$$(ZE_2)_2Y \rightarrow ZE_2Y + ZE_2 \qquad \textbf{(5.2)}$$

On the basis of the results for ligands **1** – **3**, only PBE0/LANL2DZ optimizations and M05-2X/B2-PP//PBE0/LANL2DZ SPE calculations were performed for all remaining ligands that were screened. In the case where a ligand has multiple conformations, only the global minimum structure of the isolated ligand was used to form the $(ZE_2)_{1,2}Y$ complexes, and all possible binding sites of the ligand were considered for ligands **9** and **13** – **17**.

5.3 Results and analysis of results

The geometric properties of interest with respect to the zinc-coordination sphere of the $(ZE_2)_{1,2}Y$ complexes include the Zn–O and Zn–Y bond lengths, intercomplex closest-contact distances, O–Zn–O and O–Zn–Y bond angles, and τ5 values. τ5 values are used to measure the distortion of a 5-coordinate metal complex from trigonal bipyramidal (τ5 =1) to square pyramidal (τ5 = 0) arrangements.[151] Their use is an efficient way to compare computational and experimental data and, for the zinc-seamed capsules or other supramolecular systems, to determine the extent of distortion caused by an encapsulated guest or strongly bound equatorial ligand. In this manuscript, the τ5 value is calculated by the difference between the *trans* (H)O–Zn–O(H) bond angles found in the zinc model; that is, $\tau5 = |\angle(O–Zn–O) – \angle(HO–Zn–OH)|/60$ (Fig. 5.3).

Fig. 5.5 depicts the reaction described in eq.5.2, showing the ZE_2, ZE_2**1,** and $(ZE_2)_2$**1** complexes as an example. Similar equilibrium geometries were obtained for the model systems irrespective of the calculational level used to perform the optimizations (Table 5.1). The ZE_2**1**, ZE_2**4**, and $(ZE_2)_2Y$ complexes, where Y ≠ **5**, **13**, **14**, and **17**, have at least C_2 symmetry. The remaining ZE_2Y and $(ZE_2)_2Y$ complexes have C_1 symmetry. $(ZE_2)_3$**17** has C_3 symmetry. XYZ coordinates (Table S5.1) and complete geometric and energetic properties are provided as supplementary information (Table S5.2).

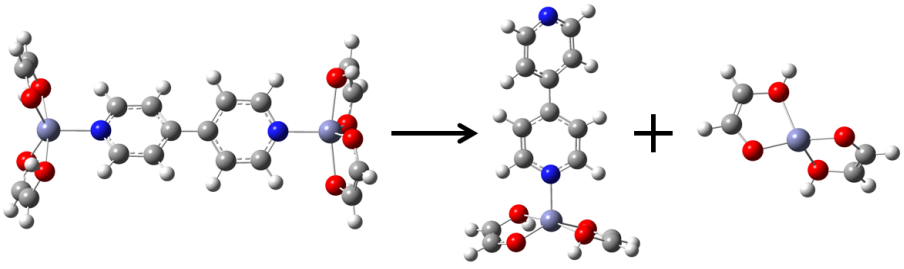

Figure 5.5 Dissociation of $(ZE_2)_2$**1** to ZE_2**1** and ZE_2.

Table 5.1 Geometric properties for $(ZE_2)_{1,2}$(**1** – **3**).

complex		bond length (Å)		bond angle range (°)		
level of theory	X	Zn–O_{avg} (range)	Zn–Y	O(H)–Zn–O(H)	O–Zn–ligand	τ5
$(ZE_2)_X$**1**						
M05-2X/B2-PP	1	2.069(1.919–2.219)	2.074	82.8– 171.5	94.2–110.4	0.54
	2	2.068(1.916–2.219)	2.082	82.8– 173.2	93.4–109.6	0.54
ωB97X-D/MBS1	1	2.083(1.908–2.258)	2.065	82.7– 161.8	99.1–107.6	0.28
	2	2.081(1.906–2.257)	2.075	82.7– 163.7	98.2–106.7	0.28
PBE0/MBS1	1	2.075(1.916–2.234)	2.055	83.1– 151.3	104.4–109.2	0.16
	2	2.073(1.912–2.233)	2.069	83.1– 154.2	102.9–107.5	0.15
PBE0/LANL2DZ	1	2.072(1.983–2.161)	2.087	81.0– 152.7	103.7–107.9	0.14
	2	2.070(1.983–2.157)	2.092	80.9– 154.8	102.6–108.1	0.18
B3LYP/LANL2DZ	1	2.087(1.992–2.182)	2.106	80.9– 152.1	102.9–107.5	0.11
	2	2.085(1.992–2.179)	2.112	80.8– 154.2	102.9–107.5	0.15
$(ZE_2)_X$**2**						
M05-2X/B2-PP	1	2.052(1.897–2.221)	2.099	83.5– 172.5	88.9–109.3	0.50
	2	2.050(1.893–2.223)	2.118	83.5– 174.3	87.4–108.0	0.49
ωB97X-D/MBS1	1	2.064(1.880–2.257)	2.128	83.5– 174.5	89.1–109.7	0.53
	2	2.062(1.875–2.265)	2.152	83.6– 176.0	86.5–108.0	0.51
PBE0/MBS1	1	2.057(1.889–2.218)	2.113	83.6– 166.7	94.9–111.5	0.43
	2	2.054(1.884–2.217)	2.139	83.6– 170.6	93.1–110.4	0.45
PBE0/LANL2DZ	1	2.061(1.951–2.169)	2.100	81.5– 155.8	96.6–114.4	0.20
	2	2.062(1.959–2.163)	2.076	81.3– 154.2	99.7–114.7	0.19
B3LYP/LANL2DZ	1	2.076(1.966–2.185)	2.097	81.3– 155.3	98.9–114.1	0.20
	2	2.080(1.976–2.183)	2.062	80.8– 152.5	102.0–114.6	0.19
$(ZE_2)_X$**3**						
M05-2X/B2-PP	1	2.058(1.910–2.214)	2.480	83.4– 165.5	94.3–115.5	0.44
	2	2.054(1.905–2.217)	2.508	83.5– 170.0	90.6–114.6	0.45
ωB97X-D/MBS1	1	2.074(1.899–2.244)	2.450	82.8– 161.4	99.0–115.0	0.43
	2	2.069(1.891–2.236)	2.490	83.0– 167.0	96.4–113.1	0.46

PBE0/MBS1	1	2.087(1.888–2.330)	2.418	80.1– 169.4	78.9–125.3	0.48
	2	2.091(1.892–2.334)	2.397	79.9– 166.7	80.4–126.2	0.48
PBE0/LANL2DZ	1	2.060(1.963–2.164)	2.571	80.5– 150.9	101.6–108.3	0.09
	2	2.064(1.971–2.168)	2.537	80.0– 149.2	102.2–110.2	0.11
B3LYP/LANL2DZ	1	2.076(1.976–2.185)	2.594	80.2– 149.5	103.3–108.7	0.08
	2	2.082(1.985–2.188)	2.558	79.8– 147.3	104.9–110.7	0.09

5.3.1 $(ZE_2)_{1,2}$(1-3)

5.3.1.1 Geometric properties

At a given level of theory, the addition of a second zinc model has little effect on the $Zn–O_{avg}$ bond length (Table 5.1, Fig. 5.5). With few exceptions, the difference in the range of the Zn–O bond lengths varies most for those complexes optimized with the small-core pseudopotential; the difference is at least 0.1 Å larger than that obtained with the large-core pseudopotential. The change in the Zn–Y bond length from ZE_2Y to $(ZE_2)_2Y$ depends on the ligand; the length uniformly increases for the $(ZE_2)_{1,2}$**1** complexes, whereas the change is more dependent on the calculational level for the $(ZE_2)_{1,2}$**2**(**3**) complexes.

The O–Zn–OH bond angles vary much less with respect to calculational level (within 10°) than the *trans* O–Zn–O or HO–Zn–OH bond angles (up to 20°, Table S5.2). The larger variance observed for the *trans* (H)O–Zn–O(H) bond angles explains the disagreement observed in the τ5 values among the different levels. A discrepancy of 6° in the *trans* bond angles changes the τ5 value by 0.1. Complexes optimized with a small-core pseudopotential tend to have τ5 values that fall within the 0.37 – 0.45 range observed experimentally;[31,32,40] complexes optimized with a large-core pseudopotential do not. The difference in the τ5 values for the $(ZE_2)_{1,2}$**1** complexes versus the $(ZE_2)_{1,2}$**2**(**3**) complexes is primarily due to the tilting of the Y ligand in the latter complexes, which maximizes the hydrogen bonding interaction between the ligand and the zinc model (Table 5.1).

5.3.1.2 Energetic properties

For a given equilibrium structure, the BDEs calculated from the M05-2X/B2-PP and MP2/B2-PP SPEs are essentially equivalent (Table 5.2 and Fig. 5.5). Given this excellent agreement and the comparative computational efficiency of the M05-2X/B2-PP SPE calculations, only those SPEs were computed for the remaining ligands. In general, upon addition of the second ZE_2, there is minimal drop-off in the BDE (up to 4 kJ/mol), but larger BDE drop-offs (up to 12 kJ/mol) do occur for the $(ZE_2)_{1,2}$**2**(**3**) structures optimized with the LANL2DZ basis set. The latter result is likely due to the overemphasized hydrogen-bonding interactions sometimes observed with the LANL2DZ basis set.[43,44] The BDFs have the same trends as the BDEs; however, the $(ZE_2)_2$**2**(**3**) structures optimized with the LANL2DZ basis set have negative BDFs, which indicate that the dissociated complexes are favored.

Table 5.2 BDEs and BDFs for $ZE_2Y \rightarrow ZE_2 + Y$ (1) and $(ZE_2)_2Y \rightarrow ZE_2Y + ZE_2$ (2) reactions.

ligand	reaction	ΔH^a	ΔG^a
optimization level			
1			
M05-2X/B2-PP[b]	1	95.7 (93.2)	55.6 (53.9)
	2	92.3 (89.9)	49.5 (47.2)
ωB97X-D/MBS1	1	94.9 (92.9)	54.5 (52.6)
	2	92.3 (90.2)	49.9 (47.7)
PBE0/MBS1	1	93.0 (91.7)	53.5 (52.2)
	2	90.6 (89.6)	46.9 (46.0)
PBE0/LANL2DZ	1	94.9 (93.1)	52.1 (50.3)
	2	90.4 (89.0)	44.2 (42.8)
B3LYP/LANL2DZ	1	95.0 (93.3)	52.3 (50.6)
	2	91.1 (89.4)	44.8 (43.1)
2			
M05-2X/B2-PP	1	54.6 (57.8)	13.4 (16.6)
	2	52.7 (54.7)	7.5 (9.4)
ωB97X-D/MBS1	1	54.1 (57.3)	14.2 (17.4)
	2	52.4 (54.3)	6.6 (8.4)
PBE0/MBS1	1	52.9 (56.9)	14.4 (18.5)
	2	51.7 (54.2)	9.9 (12.4)
PBE0/LANL2DZ	1	53.5 (57.7)	12.0 (16.2)
	2	43.4 (46.0)	–2.5 (0.1)
B3LYP/LANL2DZ	1	52.5 (56.3)	11.5 (15.3)
	2	35.0 (36.8)	–10.5 (–8.7)
3			
M05-2X/B2-PP	1	57.8 (55.4)	18.0 (15.6)
	2	54.5 (51.3)	12.2 (8.9)
ωB97X-D/MBS1	1	56.6 (54.3)	18.7 (16.4)
	2	53.2 (50.6)	8.0 (5.4)
PBE0/MBS1	1	56.9 (48.1)	14.1 (5.3)
	2	57.5 (50.4)	12.3 (5.2)
PBE0/LANL2DZ	1	50.3 (46.8)	10.6 (7.2)
	2	38.6 (34.9)	–6.4(–10.1)
B3LYP/LANL2DZ	1	46.6 (43.6)	7.2 (4.2)
	2	34.1 (31.1)	–9.3(–12.4)

[a]SPE data for the dissociation reactions at the MP2/B2-PP and M05-2X/B2-PP (in parentheses) levels of theory. Data in kJ/mol. [b]This data was previously reported in reference 40.

The BDEs for $(ZE_2)_{1,2}$**1** (90 – 95 kJ/mol) are nearly double those for $(ZE_2)_{1,2}$**2**(**3**) (35 – 58 kJ/mol). As shown previously,[40] the affinity **1** exhibits for the ZE_2 models makes it an ideal candidate against which to compare energetic and geometric properties for the ligands screened in this study. It should also be noted that the calculated BDEs for $(ZE_2)_{1,2}$**1** fall within the range calculated for a variety of experimentally observed capsular *exo* ligands (80 – 120 kJ/mol).[31,32,44] The cited range is from the M05-2X/B2-PP//PBE0/LANL2DZ BDEs for ZE_2Y, where Y includes DMF (81.3 kJ/mol), pyridine (95.3 kJ/mol) and DMSO (121.7 kJ/mol).

5.3.1.3 Comparison to zinc-seamed pyrogallol[4]arene nanocapsules, Zn-MOFs and other systems

The $Zn–O_{avg}$ bond lengths for the $(ZE_2)_{1,2}$(**1** – **3)** complexes all fall within the range of the experimentally observed Zn–O bond lengths of 2.01– 2.11 Å obtained from crystal structures of several zinc dimers.[31,32] On the other hand, the range of the Zn–O bond lengths for the mononuclear zinc model complexes is just outside of the experimentally observed range. The model complexes lack the O–Zn–O–Zn and O···H···O bridges found in the capsules and are therefore more flexible (Figs. 5.3 and 5.5). The Zn–Y bond lengths and O–Zn–O(Y) bond angles lie within the experimentally observed ranges.

Another measure by which to compare linked systems is the inter-capsular distance. This distance is typically measured by determining the centroid-centroid length between linked capsules, but in this work, because the model complexes lack a definite center, the inter-capsular distance has been defined as the closest-contact point between

the MONCs or model complexes. The closest-contact point in the MONCs and $(ZE_2)_{1,2}$**1**(**4**) complexes is the Zn–Zn distance, but for the remaining complexes, where ZE_2 is not aligned along the primary axis of the ligand, the closest contact is typically the distance between O atoms. In fact, for the latter complexes, the closest-contact distance is typically 2 Å shorter than the Zn–Zn distance.

The solid-state results for the 2-D bpy-linked MOF show that there are two distinct Zn–Zn inter-capsular distances for the 5-coordinate zincs; the zinc atoms adjacent to a 6-coordinate zinc have an inter-capsular distance of 11.288 Å (Zn–Zn(A)) and the zinc atoms adjacent to two Zn–Zn(A) zincs have an inter-capsular distance of 11.171 Å (Zn–Zn(B), Fig. 5.6).[40] Even though there are some variations in the inter-capsular distances for the $(ZE_2)_2$**1** complexes among the calculational levels, all of the calculated distances are in good agreement with the experimental values. For example, the PBE0/LANL2DZ Zn–Zn distance is 11.271 Å and the M05-2X/B2-PP Zn–Zn distance is 11.159 Å. Given the reliability of the PBE0/LANL2DZ level of theory in reproducing the M05-2X/B2-PP benchmark inter-capsular distance and other geometric and energetic properties, all of the remaining ligands discussed in this text were screened at the M05-2X/B2-PP//PBE0/LANL2DZ level.

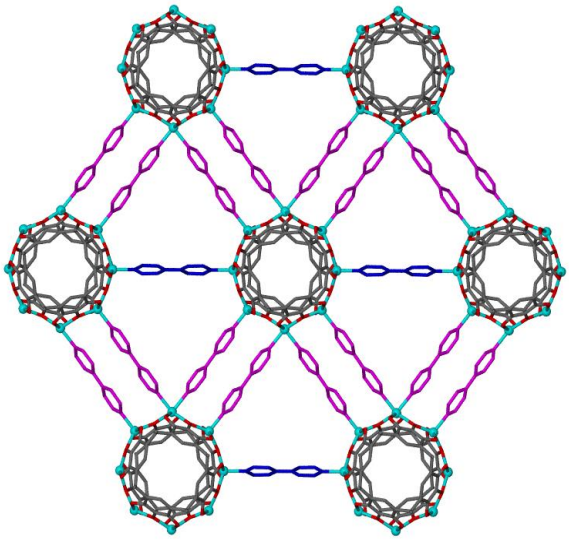

Figure 5.6 Two distinct coordinative modes are seen in bpy molecules present within the previously reported MOF.[40] Bpy of type A (rose) link penta-coordinate Zn^{2+} centers to hexa-coordinate centers, whereas bpy of type B (blue) link solely penta-coordinate Zn^{2+} centers.

In addition to appearing in the pyrogallol[4]arene capsules, the 5-coordinate zinc environments considered in these calculations incorporate metal centers similar to those found in MOF-2,[141,226] MOF-5,[227] MOF-74,[228] zinc hydrolases,[142,143] and other zinc-biomimetic complexes.[54-59,229] For example, the Zn–O bond lengths and O–Zn–O bond angles of our $(ZE_2)_{1,2}Y$ model complexes match those found experimentally for MOF-2 and its analogs.[141,226] Model complexes have also been used in other computational studies of MOFs. Hou et al. implemented several DFT methods in conjunction with double- and triple-zeta basis sets to study the adsorption mechanism of several gases using a model complex for MOF-74.[228]

5.3.2 $(ZE_2)_{1,2}$(4 – 17)

Ligands **1** and **17**, or similar analogs, have been shown experimentally to form linked systems;[230-234] thus, we used properties of their model complexes to guide the

screening process. Ligand **13** has also been shown to form MOFs, but the metals are connected via inter-ligand hydrogen bonding.[235] Both geometric and energetic criteria were used to screen the ligands: (1) the inter-capsular distance must be ≥ 10.5 Å, (2) the BDE must be ≥ 80 kJ/mol, and (3) there must be minimal drop-off in the BDE from ZE_2Y to $(ZE_2)_2Y$ (less than 5 kJ/mol). The closest-contact distance criterion of 10.5 Å is based on the shorter of the $(ZE_2)_2$**1** and $(ZE_2)_{2,3}$**17** inter-capsular distances. The 80 kJ/mol BDE threshold criterion derives from the weakest calculated ZE_2Y interaction strength among the known capsule *exo* ligands.[44] Choosing ligands with BDEs above this threshold should therefore enhance the possibility of ligand exchange.[40] Requiring that there be a maximum drop-off of 5 kJ/mol stems from the calculational results for $(ZE_2)_{1,2}$**1**.[40] This criterion favors the formation of bi-complex linking over simple uni-complex coordination.

5.3.2.1 Geometric properties

The geometric trends found for $(ZE_2)_{1,2}$(**4** – **17**) are similar to those for $(ZE_2)_{1,2}$(**1** – **3**) (Table S5.3); that is, little change in the geometric properties following the addition of a second zinc model is observed. Although there is a lengthening of the Zn–Y bond as the electron donor changes from a tertiary amine to a primary amine, from a ketone to a hydroxyl, or from a sulfoxide to a sulfhydryl, the effect is generally small (Tables 5.l and S5.3). The largest bond lengthening is about 0.1 Å. The $(ZE_2)_{1,2}$**13** complexes have a non-physical transfer of a hydrogen from **13** to ZE_2, which leads to an O–Zn–Y angle that is outside the experimentally observed range. The preferred binding sites for ligand **9** are the terminal N atoms, and for ligand **16** they are the ring N atoms. For ligand **13**, the

preferred coordinating atoms are the carbonyl O atoms, a situation which differs from that in *trans*-[$Re_6(\mu_3\text{-}Se)_8(PEt_3)_4$(3,5-pyridinedicarboxylic acid)$_2$], with its softer Re metals, for which the carboxyl group participates in the inter-ligand hydrogen bonding.[235] The most stable structures of selected, representative complexes are shown in Fig. 5.7, and the geometric and energetic properties discussed below are compared for the most stable structures.

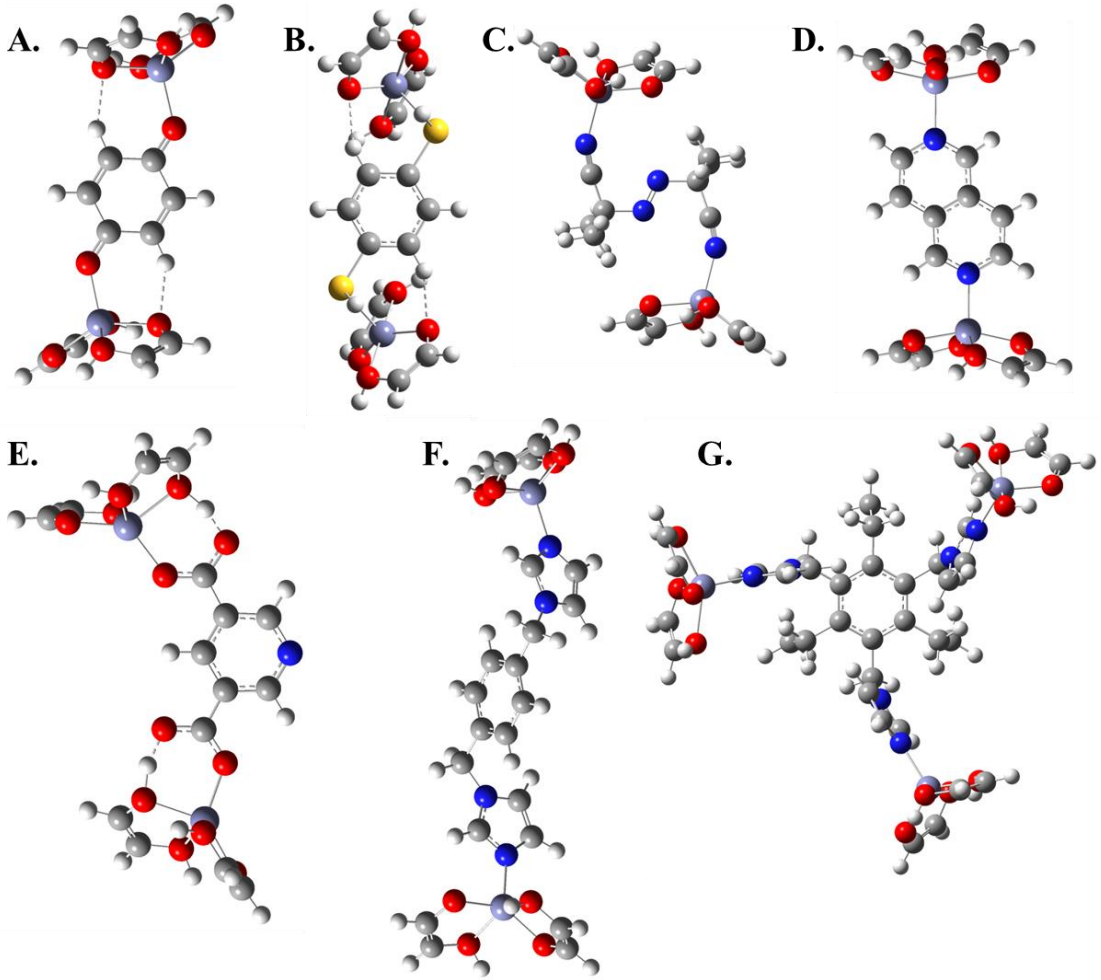

Figure 5.7 Equilibrium structures for selected complexes. Top row: $(ZE_2)_2$**2** (A), $(ZE_2)_2$**8** (B), $(ZE_2)_2$**9** (C) and $(ZE_2)_2$**11** (D). Bottom row: $(ZE_2)_2$**13** (E), $(ZE_2)_2$**15** (F) and $(ZE_2)_3$**17** (G). Color scheme: S: yellow.

Although the calculated bond lengths and bond angles generally lie within the ranges observed for the solid-state structures, the calculated τ5 values do not agree with experiment ($0.37 \leq \tau5 \leq 0.45$).[31,32,40] As noted previously,[40] however, the discrepancy in calculated and experimental τ5 values is due to the greater flexibility of the model complexes compared with the capsules. In general, the zinc coordination spheres in the model complexes show very little distortion from either trigonal bipyramidal or square pyramidal character. The PBE0/LANL2DZ equilibrium structures for which the zinc coordination environment has the largest percentage of trigonal bipyramidal character are those with ligands containing primary amine, hydroxyl, sulfhydryl, or cyano groups. That is, the $(ZE_2)_{1,2}$(**6**, **8**, **9**) complexes have values in the range $0.31 < \tau5 < 0.53$, showing mixed character, and $(ZE_2)_{1,2}$**7** has a value of $\tau5 = 0.97$, showing nearly pure trigonal bipyramidal character (Table S5.3). The remaining $(ZE_2)_{1,2}$Y complexes approach square pyramidal character.

The closest-contact distance between zinc models is of interest due to possible steric constraints imposed by the ligands on adjacent zinc centers. Contact distances range from 5.87 – 14.69 Å for the ligands investigated, but the majority of the linked complexes have contact distances between 7 – 10 Å. The shortest inter-capsular distance is observed for $(ZE_2)_2$**8** (O–O inter-capsular distance = 5.867 Å), consistent with the tendency of S and other third row atoms to form angles closer to 90°. The inter-capsular distance of 6.987 Å found for $(ZE_2)_2$**4** may explain why, despite our efforts, a 2-D pyrazine-linked MOF has not been experimentally observed to date. Although the preference for binding through the carbonyl O for ligand **13** may be an artifact of the use of the model, the closest-contact distance for the N-bound structure is too short to meet

our criterion, a result which may help to rationalize the formation of the inter-ligand hydrogen bonded *trans*-[$Re_6(\mu_3\text{-}Se)_8(PEt_3)_4$(3,5-pyridinedicarboxylic acid)$_2$] complex.[235] Ligands that have the largest inter-capsular distances are **14**, **15**, and **17** (contact distance $\geq$ 10.92 Å). From a geometric perspective, the latter three ligands appear to be prime candidates for further experimental study.

5.3.2.2 Energetic properties

Although ligands **4** – **9** do not meet the closest-contact distance criterion, the BDEs have nevertheless been evaluated to determine whether longer ligands with these types of electron-donating atoms should be examined. The magnitudes of the ZE_2(**4** – **6**) BDEs are all above the 80 kJ/mol target, but the drop-off is 10 kJ/mol for the tertiary amines and at least 15 kJ/mol for the primary amines (Table 5.3). It is possible that the drop-off for $(ZE_2)_{1,2}$**4** would be closer to the 5 kJ/mol criterion if $(ZE_2)_2$**4** were not constrained to D_2 symmetry; however, the BDEs lie just above the proposed threshold value. Although the sulfur-containing complexes tend to have stronger BDEs than their oxygen-containing analogs, ligands **2**, **3**, **7**, and **8** are non-competitive with respect to most of the other ligands. Overall, none of the complexes ZE_2(**7 – 9**) and $(ZE_2)_2$(**4 – 9**) meet the proposed threshold for the first BDE criterion.

Table 5.3 Binding dissociation enthalpies and free energies for $ZE_2Y \rightarrow ZE_2 + Y$ (1) and $(ZE_2)_2Y \rightarrow ZE_2Y + ZE_2$ (2).

ligand	reaction	ΔH^a	ΔG^a
4	1	82.9	40.3
	2	72.9	26.9
5	1	106.4	61.5
	2	56.6	15.7
6	1	89.0	44.9
	2	75.6	31.4
7	1	40.8	0.4
	2	40.4	–4.2
8	1	56.1	10.5
	2	47.3	0.1
9	1	61.0	16.5
	2	63.7	14.1
10	1	91.1	48.1
	2	84.4	38.3
11	1	89.8	46.7
	2	83.8	39.3
12	1	94.5	51.6
	2	91.4	46.0
13	1	113.1	62.0
	2	114.0	62.4
14	1	105.3	60.1
	2	100.4	55.0
15	1	104.9	60.0
	2	103.4	56.2
16	1	91.8	44.4
	2	91.3	41.0
17	1	105.7	62.1
	2	104.6	59.5
	3	103.8	56.4

[a]M05-2X/B2-PP//PBE0/LANL2DZ data in kJ/mol. Notation for ligands can be found in Fig. 5.4.

Most of the $(ZE_2)_{1,2}$(**10** – **17**) complexes meet both BDE criteria (Table 5.3). In fact, there is actually an increase in the BDE for $(ZE_2)_{1.2}$ **9** and $(ZE_2)_{1,2}$**13**. However, $(ZE_2)_{1,2}$**13** has the non-physical transfer of a hydrogen to the ZE_2 model and, when bound

through the N atom, the complex is less stable by 30 kJ/mol, resulting in a BDE near the cut-off of 80 kJ/mol. It should also be noted that, to date, no *exo* ligands have been bound to the zinc-seamed pyrogallol[4]arene capsules through a carboxyl group. The zinc-inner N atom interactions for ligands **9** and **16** are even less favorable as these interactions are up to 60 kJ/mol weaker than those with the terminal N atoms. In sum, the calculations suggest that ligands that bind through a tertiary amine are the most promising linking candidates.

Of particular interest are the tripodal ligand **17**, which shows a total of a 2 kJ/mol drop-off in BDE from the removal of the first (105.7 kJ/mol) to the third zinc model (103.8 kJ/mol), and the diimidazole ligands **14** and **15**, which show less than a 5 kJ/mol drop-off in BDEs and binding strengths of ~100 kJ/mol. Novel two-dimensional linked arrangements could be formed with these ligands, given the *meta* versus *para* positioning of the imidazole groups in **14** and **15** and the possibility of linking three capsules with **17**.

5.4 Summary

To gain further insight into the linkage of zinc-seamed pyrogallol[4]arene dimeric capsules, $Zn(C_2O_2H_3)_{1,2}Y$ model systems have been studied to determine the geometric and energetic properties of possible tethered systems. An earlier complementary study of experiment and theory showed that the zinc dimers can be linked with a bpy ligand.[40] Given the previous success in using quantum chemical results to guide the experimental studies,[40] we have examined the effectiveness of 16 additional divergent Y ligands for tethering. The ligands chosen exhibit Zn–N, Zn–O, and Zn–S bonding. Reliable BDEs are obtained regardless of the level of theory used for the optimizations as long as higher

level SPEs are performed. That is, BDEs calculated at the M05-2X/B2-PP//PBE0/LANL2DZ level of theory match those calculated at the MP2/aug-cc-pVTZ//M05-2X/B2-PP level. The geometric properties of the $(ZE_2)_{1,2}Y$ models are within the ranges seen experimentally for the dimeric nanocapsules. Also, minimal changes to the zinc coordination sphere (ZE_2Y) are observed following the addition of the second ZE_2 model ($(ZE_2)_2Y$).

The likelihood that a molecule will function as a linking *exo* ligand for zinc-seamed dimeric nanocapsules was screened with a combination of geometric and energetic criteria. Specifically, the thresholds for the closest-contact distance, BDE magnitude and BDE drop-off on formation of the $(ZE_2)_2Y$ complex are 10.5 Å, 80 kJ/mol, and 5 kJ/mol, respectively. Although we recognize that the mononuclear zinc models do not account for all of the interactions exhibited by the polynuclear zinc dimers, on the basis of these criteria, ligands **14**, **15**, and **17** are prime candidates to link zinc-seamed dimers.

Chapter 6: Zinc-seamed pyrogallol[4]arene nanocapsules: A systematic exploration of capsular dimensions and interactions

Quantum chemical calculations were performed on zinc-seamed pyrogallol[4]arene dimeric nanocapsules to elucidate the effects of the *exo* ligands, R group, guest, and calculational level on the metric dimensions of the capsule and encapsulation thermochemistry of the guest. The *exo* ligands examined are C_5H_5N, NH_3, and $(CH_3)_2SO$; the R groups examined are –H and $–CH_2CH_2CH_3$; the guests examined are C_6H_6 and $C_5H_5NH^+$. A number of density functionals, with and without empirical dispersion corrections, and basis sets, double- or triple-zeta with small- or large-core pseudopotentials, were assessed. In this work, the presence of *exo* ligands has been found to have the predominate effect on the capsular dimensions and the encapsulation thermochemistry.

6.1 Introduction

Supramolecular chemistry has been of practical interest for some time due to applications in areas of gas storage, gas separation, and drug delivery.[2-17] A variety of molecular assemblies have been investigated, including nanocapsules,[50,121,126,197,236-243] nanotubes,[212,244-247] bilayers,[248,249] helicates,[250] rotaxanes,[251] metal organic frameworks (MOFs),[40,252] hemicarcerands,[253] and dendrimers.[254] Of these, nanocapsules have been of particular interest due to the presence of enclosed cavities which make them suitable for the above applications. Hydrogen-bonded and metal-seamed organic nanocapsules have been synthesized with an assortment of macrocycles, metals, and ligands. The upper rim functionality of pyrogallol[4]arenes and resorcin[4]arenes has prompted their use as

supramolecular building blocks. Capsules composed of these macrocycles range in radius from 7 to 18 Å with interior volumes that range from 250 to 3000 $Å^3$.[255]

The Atwood group has synthesized and characterized a number of resorcin[4]arene and pyrogallol[4]arene-based MONCs. Resorcin[4]arene, cyclized 1,3-dihydroxybenzene macrocycles, have been reported to form hydrogen-bonded dimers and hexamers.[256,257] The only metal-seamed complexes synthesized thus far contain Zr or Ag, but the macrocycles do not form discrete capsular entities.[258] More recently, Atwood and coworkers have accomplished encapsulation of Co and Mn complexes within extended hydrogen-bonded resorcin[4]arene dimers.[256] On the other hand, the presence of the central hydroxyl on the upper rim of pyrogallol[4]arenes, makes them preferable candidates for metal complexation. Specifically, pyrogallol[4]arenes have been shown to complex Cu^{2+}, Zn^{2+}, Co^{2+}, Ni^{2+}, and Ga^{3+} metal centers to form discrete nanocapsular entities.[31-35] Power et al. were the first to observe zinc-seamed pyrogallol[4]arene dimeric nanocapsules, namely Zn_8(*C*-propylpyrogallol[4]arene)$_2$(pyridine)$_8$⊂pyridine (ZnPgC_3Py⊂Py) and ZnPgC_3DMSO⊂3-MePy (Fig. 6.1). The notation PgC_X is used to denote a pyrogallol[4]arene, with X = alkyl chain length and Py = pyridine. Several key results, which have driven both past and present studies, were obtained from single-crystal XRD, NMR and MALDI-TOF MS analyses of PgC_Xs.[31,32] (1) Both empty and occupied capsules appear to be stable in the solid and solution phases. This observation has also been verified by gas-phase electronic structure calculations and molecular dynamics (MD) simulations and by solution-phase MD simulations.[38] (2) The stability of the capsule is unaffected by the presence or absence of *exo* ligands. (3) *Exo* ligands can be readily substituted. (4) Frequently either the capsule or the guest is protonated.

Moving beyond characterizing individual nanocapsules, Mossine et al. have exploited the facile substitution of *exo* ligands to construct a 2-dimensional metal-organic framework (MOF), wherein zinc-seamed dimeric capsules are linked.[40] Regardless of whether the zinc centers are 5-coordinate or 5- and 6-coordinate (2D MOF), the capsular framework remains intact.

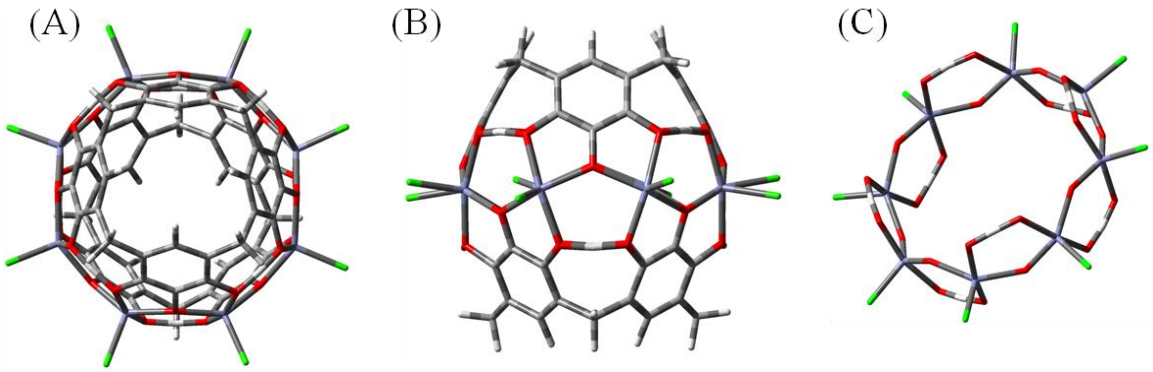

Figure 6.1 Top (A) and side (B) views of the representative $ZnPgC_0Y$ assembly, where Y = an *exo* ligand. Guests, propyl groups, and non-zinc binding ligand atoms have been removed for clarity. (C) Representation of the central belt of $ZnPgC_0$ with *exo* ligands to emphasize the Zn coordination environment. C and non-bridging H atoms have been removed for clarity. Color scheme: Zn: purple, O: red, H: white, Y: green.

In one component of our calculational studies on zinc-seamed pyrogallol[4]arene nanocapsular systems, we have been investigating the geometric and energetic properties of elementary units of the nanocapsules. The focus of these studies, thus far, has been the aryl building blocks of the macrocycles and the coordination sphere of the metal centers.[40,43,44,48,201] Possible trihydroxybenzene building blocks were investigated to determine the likelihood that macrocycles other than phenol-based, resorcinol-based, or pyrogallol-based macrocycles will form. The calculations show that the hydroxybenzene building blocks known to form macrocycles (e.g., pyrogallol and pyrogallol[4]arene, respectively) have –CHR linkage sites with nearly equivalent (within ≈ 5 kJ/mol) proton

affinities (PAs).[45,49] Thus, the calculations suggest that hydroxybenzenes such as 1,2,4-trihydroxybenzene, for example, with its ≥ 20 kJ/mol drop-off in the PAs of the linkage sites and possible steric constraints, are not likely candidates to form a macrocycle.[48]

In subsequent work, two mononuclear zinc model complexes have been used to reproduce the zinc coordination sphere in the dimeric nanocapsules. The simpler hydroxide-based models[43] (e.g., $Zn(OH)_2(H_2O)_2Y_{1,2}$) and the more representative deprotonated *Z*-ethene-1,2-diol-based models[40,44,201] ($(Zn(C_2O_2H_3)_2)_{1,2}Y$, where Y = an *exo* ligand) both have geometric properties similar to those found experimentally for the nanocapsules. That is, the Zn–O and Zn–Y bond lengths and O–Zn–O and O–Zn–Y bond angles are within the ranges observed for the solid-state nanocapsular structures.[31,32] However, the equilibrium structures for the hydroxide complexes have 4-coordinate zinc centers despite the presence of five or six ligands. Even with the lower zinc coordination numbers, however, the zinc hydroxide complexes still reproduce the binding dissociation enthalpies of the *exo* Y ligands found for the more represenative $Zn(C_2O_2H_3)_2Y$ complexes. The calculational studies on $(Zn(C_2O_2H_3)_2)_{1,2}Y$ helped direct experimental studies in crystallization solvent choice and predicted that 4,4'-bipyridyl would be a likely candidate to link multiple zinc-seamed MONCs together to form a MOF, a prediction that was subsequently confirmed.[40]

In the second component of our calculational studies on zinc-seamed pyrogallol[4]arene nanocapsular systems, we have been investigating the geometric and energetic properties of the capsules themselves. In the work reported herein, we investigated the effect of the *exo* ligand, R group, guest, and calculational level on the metric dimensions of the zinc-seamed dimers first observed by Power et al.[31,32] One

function of the model calculations was to narrow the range of calculational levels assessed for the capsules, with the recommended method and basis set combinations being tested for the simplest capsule investigated, i.e. no *exo* ligands, no guest, and R = H ($ZnPgC_0$). The combinations were further reduced to investigate the capsular dimensions of $ZnPgC_3$, $ZnPgC_0$(NH_3, Py, and DMSO), $ZnPgC_3NH_3$, $ZnPgC_0$⊂(Ph–H and PyH^+), and $ZnPgC_0NH_3$⊂(Ph–H and PyH^+) with respect to those of $ZnPgC_0$. The guests are represented as follows: benzene = Ph–H and protonated pyridine = PyH^+. DMSO and Py are experimentally observed *exo* ligands, whereas NH_3 has been shown to be a reasonable small model (40 fewer heavy atoms in the ligated dimer) for Py.[43,44] The particular geometric parameters investigated are capsule diameter, capsule length, τ5 values, and capsular interior void volume. Encapsulation energies of PyH^+, an experimentally observed guest,[31] and Ph–H, a guest that will primarily exhibit dispersion-driven host-guest interactions, were studied. Other goals of the calculations are the following. (1) Confirm the stability of empty and occupied capsules with and without *exo* ligands. (2) Confirm that the calculated dimer geometric properties are within experimental ranges. (3) Determine the effect of *exo* ligands on encapsulation energetics ($ZnPgC_0$⊂(Ph–H and PyH^+) versus $ZnPgC_0NH_3$⊂(Ph–H and PyH^+)). (4) Determine efficient levels of theory for geometry optimizations and single-point energy calculations. The results of this work have enabled us to identify an appropriate calculational protocol and $ZnPgC_X$-based dimer with which we can obtain reliable results in our studies of host-guest interactions, guest mobility, guest basicity enhancement, guest size limitations, and guest-ligand communication in the zinc-seamed pyrogallol[4]arene nanocapsules.

6.2 Computational details

The effect of the M05-2X, M06-L, PBE0, ωB97X-D, and B3LYP density functionals in conjunction with a variety of basis sets, double zeta or triple zeta with either a small-core or a large-core pseudopotential, on the geometric properties of the zinc-seamed pyrogallol[4]arene capsules was evaluated. The Gaussian09 suite of programs[89] was implemented for all calculations and the results were visualized with GaussView5.[144] The keyword int = ultrafine and normal convergence criteria were used. Complete optimizations were performed for all nanoassemblies investigated, and partial optimizations were also performed for $ZnPgC_0 \subset$Ph–H. The partial optimizations were carried out to determine if a two-step optimization process would decrease the overall CPU time for minimization. In order to identify the nature of stationary points, normal-mode vibrational analyses were performed.

Following the procedure set out in our previous investigations,[40,44] we optimized the structure of $ZnPgC_0$, the empty, stripped capsule, at the benchmark level of theory, M05-2X/B2-PP and the suggested levels of theory, PBE0/LANL2DZ, B3LYP/LANL2DZ, PBE0/MBS1, and ωB97X-D/MBS1. B2-PP stands for the B2 basis set[41] and SDD pseudopotential (PP) on the zinc with the 6-311+G(2df,2p) basis set on all remaining atoms; SDD refers to the fully relativistic, small-core MDF10 PP.[259] MBS1 denotes the B2-PP basis set on zinc and the 6-31G(d) basis set on all other atoms. The LANL2DZ basis set has a non-relativistic, large-core PP for Zn. Please note that the nature of the stationary point could not be determined for the capsule optimized at the M05-2X/B2-PP level of theory due to insufficient available computational resources. Also, $ZnPgC_0$ structures with point groups of D_{4d}, C_2, and C_1 were attempted for the

optimizations with the MBS1 basis set, but the resulting structures had D_4d symmetry and were all saddle points on the potential energy surface. For all other optimizations, the point group was only lowered if higher symmetry resulted in saddle points. Due to these findings for the MBS1 calculations, we chose to extend our calibration study to additional calculational levels. Specifically, we tested the PBE0/SDD(All), M05-2X/LANL2DZ, M06-L/LANL2DZ, and ωB97X-D/LANL2DZ levels.

In an effort to identify a less expensive computational level than the M05-2X/B2-PP level of theory prescribed by our earlier calibrations,[43,44] single-point energies (SPEs) were also evaluated at the M05-2X/SDD(All), M05-2X/VDZ-PP, M06-L/VDZ-PP, ωB97X-D/VDZ-PP, M05-2X-D3/VDZ-PP, and APFD/VDZ-PP levels of theory. The VDZ-PP basis set[260] and MDF10 PP for zinc[259] were retrieved from the EMSL basis set library.[261,262] Encapsulation energies were computed via eqs. 6.1 and 6.2.

$$ZnPgC_0 + guest \rightarrow ZnPgC_0 \subset guest \quad \textbf{(6.1)}$$

$$ZnPgC_0(ligand) + guest \rightarrow ZnPgC_0(ligand) \subset guest \quad \textbf{(6.2)}$$

6.3 Results and analysis of results

In this work, the diameter of the capsule is determined by taking the distance between two zincs that are directly opposite each other (i.e., for zincs numbered Zn_1 – Zn_8, the distance is taken between, e.g., Zn_1 and Zn_5, Zn_2 and Zn_6). The length of the capsule is defined as the distance between the two centroids of the carbons at the apex of the aryl rings that form the rim of each hemisphere of the capsule and was calculated using Mercury CSD 2.0.[263] The centroids were based on the aryl carbons because the linker carbons are prone to distortion. The τ5 value is an index that measures the amount of distortion in a five-coordinate species from a square pyramidal geometry (τ5 = 0) to a

trigonal bipyramidal geometry ($\tau5 = 1$).[151] $\tau5$ is calculated from the difference in the *trans* angles around the atom of interest; that is, from Fig. 6.1, $\tau5 = |\angle(HO–Zn–OH) – \angle(O–Zn–O)|/60$. The internal volume of the empty capsules, guest removed where applicable, was obtained using the MSRoll interface in X-Seed with a probe radius of 1.25 Å.[264,265]

6.3.1 $ZnPgC_0$ and $ZnPgC_3$

Regardless of the calculational level, the calculated diameter is at least 0.26 Å too small compared to the 9.89 Å diameter experimentally observed for $ZnPgC_3$DMSO⊂3-MePy[31] (Table 6.1, Fig. 6.2), but all of the capsules have a stable framework in agreement with MALDI-TOF analyses.[31,32] The structures optimized with a small-core pseudopotential, including the M05-2X/B2-PP geometry, have diameters that differ the most (0.45 Å too small) from the experimental values. That the diameter is underestimated suggests that the *exo* ligands and/or guest may have an effect on the capsular metric dimensions.

Table 6.1 Geometric properties of $ZnPgC_0$.

method/basis set	diameter (Å)	length (Å)	τ5	volume (Å^3)
experimental[a]	9.984 ± 0.022	8.774	0.41 ± 0.02	141
experimental[b]	9.893 ± 0.047	8.834	0.42 ± 0.03	143
M05-2X/B2-PP[c]	9.347	8.790	0.37	157
M05-2X/LANL2DZ	9.572	8.936	0.41	162
M06-L/LANL2DZ	9.632	8.932	0.38	165
ωB97X-D/LANL2DZ	9.573	8.964	0.40	164
B3LYP/LANL2DZ	9.630	9.016	0.39	171
PBE0/LANL2DZ	9.582	8.962	0.39	165
PBE0/SDD	9.446	8.948	0.40	164
PBE0/SDDAll	9.439	8.932	0.39	164

[a]Data of $ZnPgC_3Py{\subset}Py$.[31] [b]Data of $ZnPgC_3DMSO{\subset}3\text{-}MePy$.[32] [c]Vibrational frequencies not computed.

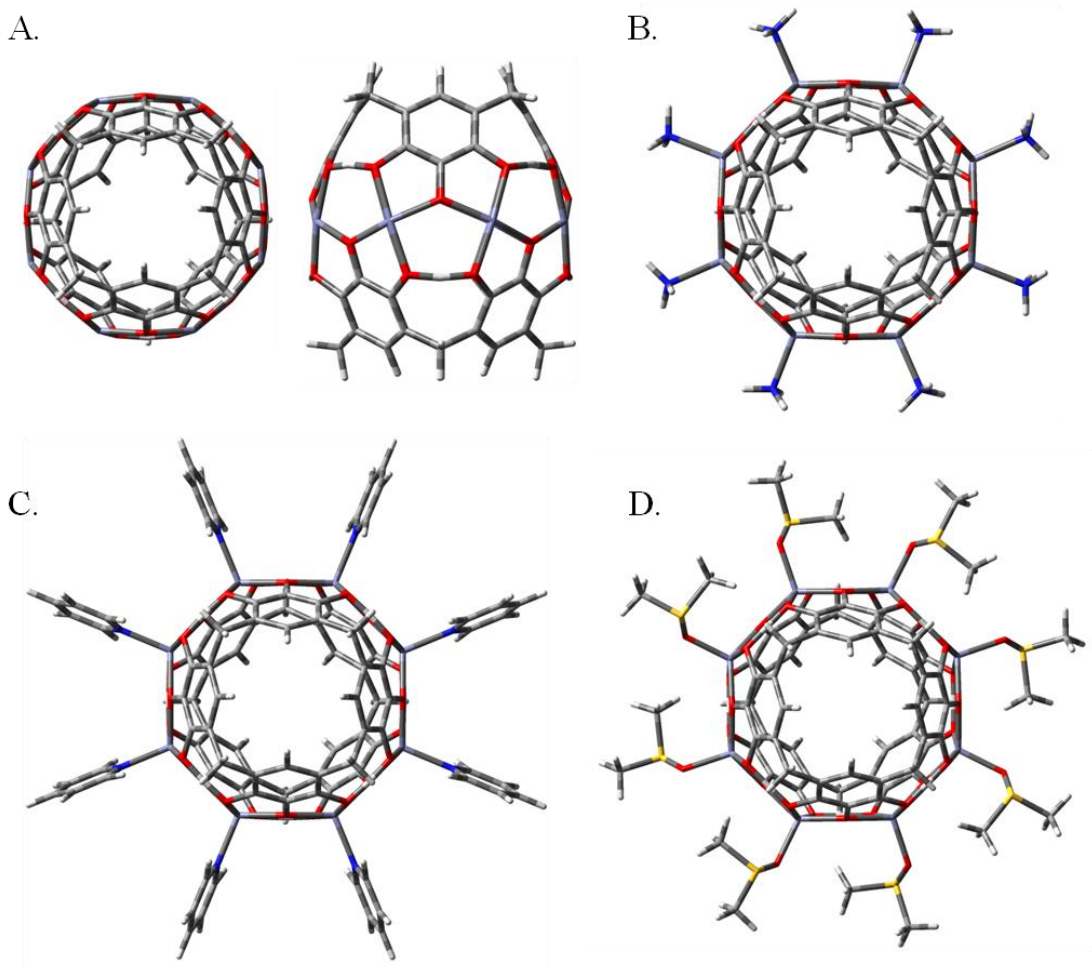

Figure 6.2 Top (left) and side (right) views of $ZnPgC_0$ (A). Top views of $ZnPgC_0NH_3$ (B), $ZnPgC_0Py$ (C), and $ZnPgC_0DMSO$ (D). PBE0/LANL2DZ equilibrium structures shown for all complexes.

There are no clear trends in the capsule length, τ5 value, or capsule volume among the calculational levels. Although by definition τ5 is a way to classify 5-coordinate species, $ZnPgC_0$, which lacks a fifth ligand coordinated to the zinc, has the basic framework observed for the 5-coordinate systems and a τ5 value was evaluated. All τ5 values are within 0.04 of the experimental $\tau5_{avg}$ value (Table 6.1). At any level of theory, the volume of $ZnPgC_0$ is at least 14 $Å^3$ greater than the experimentally observed volumes.[31,32,40]

The initial geometry of $ZnPgC_3$ was constrained to D_{4d} symmetry, but the resulting PBE0/LANL2DZ optimized structure is a saddle point. The equilibrium structure reported herein for $ZnPgC_3$ has C_1 symmetry and represents one possible minimum; minimal changes in the capsular metric dimensions are observed for different orientations of the Pr groups. Upon replacing R = H ($ZnPgC_0$) with R = Pr ($ZnPgC_3$), decreases of 0.01 Å are observed for capsule $diameter_{avg}$ and length (9.569 and 8.951 Å, respectively) and an increase of 0.01 in $\tau5_{avg}$ (0.40) are observed. No change in the volume is observed.

Given the similarity of the calculated geometric properties to the experimental data and the computational efficiency of the LANL2DZ calculations, the M06-L/LANL2DZ, B3LYP/LANL2DZ, and PBE0/LANL2DZ levels of theory were used for the $ZnPgC_0$(NH_3, Py, DMSO) and $ZnPgC_0\subset$(Ph–H and PyH^+) systems. The ωB97X-D/LANL2DZ calculational level was also investigated further due its inclusion of empirical dispersion corrections.

6.3.2 $ZnPgC_0Py$, $ZnPgC_0NH_3$, $ZnPgC_0DMSO$, and $ZnPgC_3NH_3$

The point groups for the ligated capsules are S_8 for $ZnPgC_0NH_3$ and $ZnPgC_0DMSO$ and D_{4d} for $ZnPgC_0Py$ (Fig. 6.2). The DMSO ligands in $ZnPgC_0DMSO$ were all initially oriented with the methyl groups of the DMSO ligands directed uniformly along the equator of the capsule, but the resulting equilibrium structure has the methyl groups oriented axially. The methyl groups of adjacent DMSO ligands are oriented over different hemispheres of the capsule, resulting in a capsule with S_8 symmetry.

Regardless of the *exo* ligand, the capsule diameter increased by at least 0.20 Å in comparison to that of $ZnPgC_0$ at all levels of theory investigated. In fact, addition of at least one of the *exo* ligands results in a capsule diameter that is within the experimental range of 9.86 – 10.00 Å (Table 6.2). The changes in diameter are as follows and are observed at all calculational levels: $ZnPgC_0Py < ZnPgC_0NH_3 < ZnPgC_0DMSO$. The diameter increases 0.20 – 0.25 Å for $ZnPgC_0Py$, 0.25 – 0.28 Å for $ZnPgC_0NH_3$ and 0.34 – 0.37 Å for $ZnPgC_0DMSO$. The largest increase in diameter and the largest diameters are found for the B3LYP/LANL2DZ optimizations.

Lesser deviations are observed for the capsule lengths, τ5 values, and capsule volumes between $ZnPgC_0$ and $ZnPgC_0$(Py, NH_3, and DMSO). The capsule lengthens most upon addition of *exo* Py ligands (≈ 0.06 Å), whereas limited lengthening is observed for NH_3 ligands (≤ 0.02 Å) and DMSO ligands (≈ 0.0 Å). The changes in τ5 values follow the same trend as that for capsule length. The addition of Py ligands resulted in τ5 values that have more mixed character (τ5 ≈ 0.45) and agree well with experimental values. Minimal changes in the capsule volume are observed (differ by no more than 3 $Å^3$), and the change is largest for $ZnPgC_0NH_3$. All of the $Zn–L_{avg}$ bond lengths are overestimated by the calculations.

Table 6.2 Geometric properties of $ZnPgC_0Py$, $ZnPgC_0NH3$, and $ZnPgC_0DMSO$

method/basis set	ligand	$diameter_{avg}$ (Å)	length (Å)	$\tau5_{avg}$	V ($Å^3$)	$Zn–L_{avg}$ (Å)
experimental[a]	Py	9.984 ± 0.022	8.774	0.41 ± 0.02	141	2.048 ± 0.022
experimental[b]	DMSO	9.893 ± 0.047	8.834	0.42 ± 0.03	143	1.995 ± 0.016
B3LYP/LANL2DZ	Py	9.880	9.072	0.44	169	2.126
B3LYP/LANL2DZ	NH_3	9.906	9.033	0.37	172	2.152
B3LYP/LANL2DZ	DMSO	9.999	9.020	0.40	169	2.070
PBE0/LANL2DZ	Py	9.817	9.020	0.44	163	2.104
PBE0/LANL2DZ	NH_3	9.847	8.981	0.37	167	2.133
PBE0/LANL2DZ	DMSO	9.941	8.964	0.40	164	2.053
M06-L/LANL2DZ	Py	9.834	8.998	0.43	165	2.104
M06-L/LANL2DZ	NH_3	9.875	8.956	0.36	167	2.141
M06-L/LANL2DZ	DMSO	9.976	8.926	0.36	166	2.060
ωB97X-D/LANL2DZ	Py	9.778	9.032	0.46	162	2.099
ωB97X-D/LANL2DZ	NH_3	9.822	8.981	0.38	165	2.138
ωB97X-D/LANL2DZ	DMSO	9.917	8.958	0.39	164	2.052

[a]Data of $ZnPgC_3Py⊂Py$.[31] [b]Data of $ZnPgC_3DMSO⊂3$-MePy.[32]

On the basis of results for $ZnPgC_3$, only C_1 symmetry was considered for $ZnPgC_3NH_3$. As with $ZnPgC_3$ versus $ZnPgC_0$, the same 0.01 Å decrease in capsule $diameter_{avg}$ and length (9.836 and 8.968 Å, respectively) and 0.01 increase in $\tau5_{avg}$ (0.38) are observed for $ZnPgC_3NH_3$ versus $ZnPgC_0NH_3$. The capsular volume decreases by 2 $Å^3$. The Pr groups add substantial calculational time (24 additional heavy atoms) and have a negligible effect on the capsular dimensions. All future calculations will use only the $ZnPgC_0$ (R = H) framework.

Because optimization of $ZnPgC_0$(Py, NH_3, and DMSO) at the ωB97X-D/LANL2DZ level of theory results in capsule diameters and lengths that deviate the most with respect to experimental results, only B3LYP/LANL2DZ, M06-L/LANL2DZ, and PBE0/LANL2DZ optimizations were performed for all remaining host-guest complexes. SPEs were evaluated with the ωB97X-D functional to assess the effect of an empirical dispersion correction on energetics.

6.3.3 $ZnPgC_0$⊂Ph–H

In order to determine an appropriate calculational level to account for host-guest interactions where dispersion could have an impact, we have looked at the properties of $ZnPgC_0$⊂Ph–H. In addition to full optimizations, partial optimizations where the coordinates of $ZnPgC_0$ are frozen and only the Ph–H is optimized were performed. Unexpectedly, the latter optimization took no less CPU time than the former, indicating that a two-step optimization process is not advantageous for these systems. The Ph–H is aligned along the vertical axis of the capsule (Fig. 6.3), for both the full and partial optimizations, regardless of whether Ph–H was initially oriented in an equatorial position.

The PBE0 and B3LYP optimized structures have C_{2v} symmetry, while the M06-L has C_1 symmetry. The $diameter_{avg}$ decreases upon encapsulation of Ph–H with respect to that of $ZnPgC_0$ (Table 6.3). This decrease is most likely due to two reasons. (1) The Zn atoms perpendicular to the Ph–H move inward slightly, perhaps to maximize Zn^{2+}–Ph–H interactions. (2) The Zn atoms in the plane of the Ph–H pull away slightly to accommodate the guest and also to form an $O_{capsule}\cdots H–C_{Ph–H}$ hydrogen bond. For the PBE0/LANL2DZ structure, $O_{capsule}\cdots H_{Ph–H}$ = 2.37 Å and $\angle(O_{capsule}\cdots H–C_{Ph–H})$ = 157.3°. These data fall within the accepted criteria for hydrogen bonding of $R_{O\cdots H}$ < 2.50 Å and $\angle(O\cdots H–C) > 90.0°$.[198-200] Although there is a decrease in the capsule $diameter_{avg}$, the change is an order of magnitude smaller than the increase in $diameter_{avg}$ following addition of *exo* ligands. Minimal increases are observed for capsule length, τ5, and capsule volume.

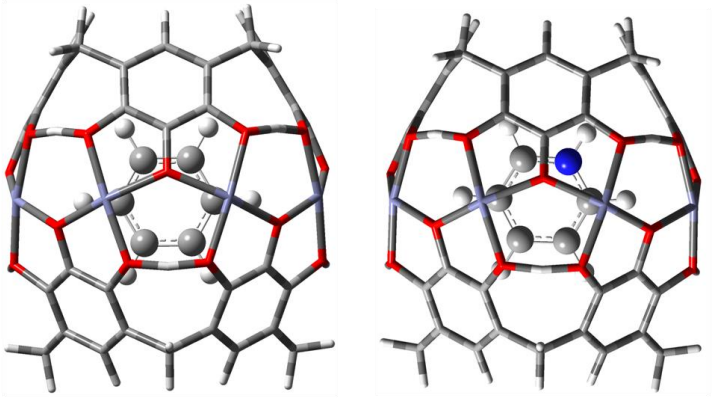

Figure 6.3 Optimized structures of $ZnPgC_0$⊂Ph–H (A) and $ZnPgC_0$⊂PyH^+ (B).

Table 6.3. Geometric properties of $ZnPgC_0 \subset Ph–H$.

method/basis set	$diameter_{avg}$ (Å)	length (Å)	$\tau5_{avg}$ [b]	V (Å^3)
PBE0/LANL2DZ	9.569 ±0.109 (9.582)	8.965 (8.962)	0.37 (0.39)	167 (165)
B3LYP/LANL2DZ	9.622 ±0.105 (9.630)	9.018 (9.016)	0.37 (0.39)	173 (171)
M06-L/LANL2DZ	9.595 ±0.093 (9.632)	8.935 (8.932)	0.36 (0.38)	166 (165)

[a]Data of fully optimized structure and partial optimizations (in parenthesis, $ZnPgC_0$ data has been repeated for the reader's convenience). [b]τ5 values have less than 0.005 standard deviation.

Due to the size of the host-guest systems of interest, a computationally efficient level of theory that yields reliable encapsulation thermochemistry must be determined. Our previous studies have shown that reliable binding dissociation enthalpies (BDEs) are obtained at the M05-2X/B2-PP level. That is, the M05-2X/B2-PP BDEs reproduce both the trends and magnitudes of the BDEs calculated at the MP2/B2-PP and MP2/aug-cc-pVTZ levels of theory.[40,43,44] However, accounting for dispersion effects is likely essential to properly characterize interactions in these host-guest systems. Thus, in addition to evaluating M05-2X/B2-PP encapsulation thermochemical data, the effect on the thermochemistry of smaller basis sets and methods with and without dispersion corrections was explored.

Another manifestation of the comparatively minor changes in capsular dimensions caused by guest encapsulation is that $\Delta\Delta_{encap}E_{298}$ at a given level of theory is within 10 kJ/mol, for both the PBE0/LANL2DZ and B3LYP/LANL2DZ fully and partially optimized structures (Table 6.4, e.g. entry 3). However, the M06-L/LANL2DZ $\Delta_{encap}E_{298}$ values vary up to nearly 25 kJ/mol; this greater difference is due to the larger deviation in the fully optimized structure of $ZnPgC_0 \subset Ph–H$ in comparison with that of $ZnPgC_0$.

Table 6.4. Encapsulation energies for $ZnPgC_0 \subset Ph–H$.[a]

method/basis set (opt, *SPE*)	ΔE[b]	ΔH	ΔG
PBE0/LANL2DZ			
M05-2X/B2-PP	–106.6	–101.8	–61.1
M05-2X/VDZ-PP	–112.7 (–105.4)	–108.0	–67.3
M05-2X/SDD	–101.3 (–97.9)	–96.5	–55.8
M05-2X/SDDAll	–107.6 (–103.2)	–102.8	–62.2
M06-L/VDZ-PP	–149.7 (–139.6)	–145.0	–104.3
ωB97X-D/VDZ-PP	–172.6 (–164.1)	–167.8	–127.2
M05-2X-D3/VDZ-PP	–156.8	–152.1	–111.4
APFD/VDZ-PP			
B3LYP/LANL2DZ			
M05-2X/B2-PP	–102.2	–96.2	–55.7
M05-2X/VDZ-PP	–108.4 (–98.4)	–102.4	–61.8
M05-2X/SDD	–97.2 (–92.9)	–91.2	–50.6
M05-2X/SDDAll	–104.2 (–99.1)	–98.1	–57.6
M06-L/VDZ-PP	–144.3 (–134.0)	–138.2	–97.7
ωB97X-D/VDZ-PP	–166.4 (–155.0)	–160.4	–119.9
M06-L/LANL2DZ			
M05-2X/B2-PP	–113.6	–109.9	–75.0
M05-2X/VDZ-PP	–119.8 (–97.7)	–116.1	–81.1
M05-2X/SDD	–103.8 (–93.3)	–100.1	–65.1
M05-2X/SDDAll	–109.7 (–97.5)	–105.9	–71.0
M06-L/VDZ-PP	–156.4 (–135.2)	–152.7	–117.7
ωB97X-D/VDZ-PP	–180.0 (–156.0)	–176.3	–141.4

[a]All data in kJ/mol. [b]Data for full optimizations and partial optimizations (in parenthesis).

When comparing method/basis set effects for a given geometry, the differences in $\Delta_{encap}E_{298}$, $\Delta_{encap}H_{298}$, and $\Delta_{encap}G_{298}$ (e.g., $\Delta\Delta H = \Delta H_{M05\text{-}2X/B2\text{-}PP//PBE0/LANL2DZ} - \Delta H_{M05\text{-}2X/VDZ\text{-}PP//PBE0/LANL2DZ}$) are essentially equivalent, regardless of the geometry chosen. At a given calculational level (e.g., M05-2X/VDZ-PP//PBE0/LANL2DZ versus M05-2X/VDZ-PP//B3LYP/LANL2DZ versus M05-2X/VDZ-PP//M06-L/LANL2DZ), the relative thermochemical values vary by no more than 20 kJ/mol. The M05-2X/SDD, M05-2X/SDDAll, and M05-2X/VDZ-PP SPEs all have encapsulation energies that are within 10 kJ/mol of the earlier benchmark level of theory, M05-2X/B2-PP. Moreover, the

M06-L/VDZ-PP and ωB97X-D/VDZ-PP SPEs yield encapsulation enthalpies and free energies that are 40 kJ/mol and 65 kJ/mol, respectively, more stable than those determined at the M05-2X/B2-PP level. The latter increase in stability appears to result from the inclusion of dispersion effects, as the M05-2X-D3/VDZ-PP//PBE0/LANL2DZ ($\Delta_{encap}H_{298}$ = –152.1 kJ/mol and $\Delta_{encap}G_{298}$ = –111.4 kJ/mol) and APFD/VDZ-PP//PBE0/LANL2DZ ($\Delta_{encap}H_{298}$ = –175.0 kJ/mol and $\Delta_{encap}G_{298}$ = –134.4 kJ/mol) thermochemical values are more negative by some 50 kJ/mol.

6.3.4 $ZnPgC_0 \subset PyH^+$

Whereas forming $ZnPgC_0 \subset$Ph–H leads to a decrease in the $diameter_{avg}$ of the dimer, forming $ZnPgC_0 \subset PyH^+$ leads to an increase in the $diameter_{avg}$, by at least 0.14 Å (Fig. 6.3 and Table 6.5). This increase in $diameter_{avg}$ ($ZnPgC_0 \subset PyH^+$ versus $ZnPgC_0$) is 0.05 – 0.20 Å smaller than the increase caused by the addition of an *exo* ligand (e.g., $ZnPgC_0NH_3$ versus $ZnPgC_0$). Regardless of the level of theory employed for optimization, the length and volume of $ZnPgC_0 \subset PyH^+$ with respect to those of $ZnPgC_0$ decrease by at least 0.04 Å and 2 $Å^3$, respectively. Consistent with the $ZnPgC_0$(NH_3, Py, and DMSO) and $ZnPgC_0 \subset$Ph–H assemblies, the $\tau 5_{avg}$ values of $ZnPgC_0 \subset PyH^+$ are similar to those of $ZnPgC_0$ and are within the experimentally observed range of values.[31,32,40]

Table 6.5. Geometric and energetic properties of $ZnPgC_0 \subset PyH^+$.

	optimization level		
properties	PBE0/LANL2DZ	B3LYP/LANL2DZ	M06-L/LANL2DZ
$diameter_{avg}$ (Å)	9.729± 0.095	9.781± 0.091	9.768± 0.087
length (Å)	8.922	8.977	8.886
$\tau 5_{avg}$	0.39± 0.01	0.39± 0.01	0.38± 0.00
V ($Å^3$)	163	168	161
ΔH (ΔG)[a]			
M05-2X/B2-PP	–178.9 (–136.7)	–173.2 (–131.1)	–187.6 (–151.3)
M05-2X/VDZ-PP	–179.6 (–137.4)	–174.0 (–131.9)	–188.3 (–152.0)
M05-2X/SDD	–156.6 (–114.5)	–150.8 (–108.6)	–160.6 (–124.3)
M05-2X/SDDAll	–160.3 (–118.2)	–155.2 (–113.1)	–163.4 (–127.1)
M06-L/VDZ-PP	–200.7 (–158.5)	–193.8 (–151.7)	–209.2 (–172.9)
ωB97X-D/VDZ-PP	–231.5 (–189.4)	–224.6 (–182.5)	–240.7 (–204.5)
M05-2X-D3/VDZ-PP	–227.2 (–185.0)	– (–)	– (–)
APFD/VDZ-PP	–254.0 (–211.8)	– (–)	– (–)

[a]All calculational levels refer to level of theory for SPE. Energy data in kJ/mol.

Regardless of the level of theory used for the SPE calculation, the $ZnPgC_0 \subset PyH^+$ encapsulation enthalpies evaluated using the PBE0/LANL2DZ and B3LYP/LANL2DZ equilibrium structures typically agree to within 5 kJ/mol. However, enthalpies based on the M06-L/LANL2DZ equilibrium structure vary up to 15 kJ/mol with respect to those based on the B3LYP/LANL2DZ structure. For a given geometry, the M05-2X/VDZ-PP encapsulation thermochemical values reproduce the M05-2X/B2-PP results, whereas the M05-2X/SDD and M05-2X/SDDAll data are underestimated by 20 kJ/mol and 25 kJ/mol, respectively. As with $ZnPgC_0 \subset$Ph–H, the M06-L/VDZ-PP and ωB97X-D/VDZ-PP encapsulation thermochemical data are overestimated with respect to the M05-2X/B2-PP results by 20 and 50 kJ/mol respectively. Likewise, the M05-2X-D3/VDZ-PP and APFD/VDZ-PP encapsulation enthalpies are more negative by up to 75 kJ/mol (Table 6.5). Because the encapsulation thermochemical data evaluated at the M05-2X/VDZ-PP level of theory are within 10 kJ/mol of the M05-2X/B2-PP data for $ZnPgC_0 \subset PyH^+$ and

$ZnPgC_0$⊂Ph–H, M05-2X/VDZ-PP results will be used as a lower limit in gauging thermochemical data for larger systems such as $ZnPgC_0NH_3$⊂PyH^+.

6.3.5 $ZnPgC_0NH_3$⊂Ph–H and $ZnPgC_0NH_3$⊂PyH^+

Direct comparison of the PBE0/LANL2DZ optimized structure of $ZnPgC_0NH_3$⊂PyH^+ to the experimentally observed structure of $ZnPgC_3Py$⊂Py shows a negligible disparity in $diameter_{avg}$ for the two capsules ($diameter_{avg}$ of $ZnPgC_0NH_3$⊂PyH^+ = 9.988 Å and of $ZnPgC_3Py$⊂Py = 9.984 Å, Table 6.6). The B3LYP/LANL2DZ $diameter_{avg}$ is at the upper limit of the experimentally observed ranges. The $ZnPgC_3Py$⊂Py notation was used in the original article,[31] but there is now NMR and solid-state evidence that suggests the Py guest is actually protonated.[266] This result is consistent with the excellent agreement in the metric dimensions observed between the calculated $ZnPgC_0NH_3$⊂PyH^+ structure and the experimentally observed $ZnPgC_3Py$⊂PyH^+ structure.) Although shorter, the average capsule diameters of the $ZnPgC_0NH_3$⊂Ph–H capsules are also within the experimental ranges (Tables 6.1 and 6.6). As with the previous nanoassemblies, $ZnPgC_0$, $ZnPgC_0NH_3$, and $ZnPgC_0$⊂(Ph–H and PyH^+), the capsule length and V_{empty} are overestimated. The $\tau5_{avg}$ values are at the lower limit of the experimentally observed range ($0.37 \leq \tau5 \leq 0.45$).[31,32] Due to the larger capsule diameters and lengths found from the B3LYP/LANL2DZ optimizations, only PBE0/LANL2DZ optimizations will be performed in future studies on zinc-seamed pyrogallol[4]arene nanocapsules.

Table 6.6 Geometric properties of $ZnPgC_0NH_3{\subset}Ph–H$ and $ZnPgC_0NH_3{\subset}PyH^+$.

complex	diameter$_{avg}$ (Å)	length (Å)	$\tau5_{avg}$	V_{empty} (Å^3)
method/basis set				
$ZnPgC_0NH_3{\subset}Ph–H$				
PBE0/LANL2DZ	9.844 ± 0.092	8.982	0.35± 0.01	169
B3LYP/LANL2DZ	9.906 ± 0.088	9.034	0.35± 0.01	175
$ZnPgC_0NH_3{\subset}PyH^+$				
PBE0/LANL2DZ	9.988 ± 0.069	8.932	0.37± 0.02	164
B3LYP/LANL2DZ	10.052 ± 0.062	8.984	0.36± 0.01	169

Larger increases in capsule diameter$_{avg}$ (up to 0.46 Å) are observed for $ZnPgC_0NH_3{\subset}$(Ph–H and PyH^+) with respect to $ZnPgC_0$ (Table 6.6). Capsule length decreases of about 0.03 Å are observed for $ZnPgC_0NH_3{\subset}PyH^+$, and increases of about 0.02 Å are observed for $ZnPgC_0NH_3{\subset}Ph–H$, with respect to $ZnPgC_0$. The $\tau5_{avg}$ value decreases in all cases by 0.02 – 0.04, while the V_{empty} value fluctuates by at most 4 Å^3 for $ZnPgC_0NH_3{\subset}$(Ph–H and PyH^+) compared to $ZnPgC_0$. In fact, the changes in capsule length and diameter$_{avg}$ and in $\tau5_{avg}$ for $ZnPgC_0NH_3{\subset}$(Ph–H and PyH^+) are nearly additive (within 0.01 Å and 0.01, respectively) when compared to the increases for *exo* ligand addition ($ZnPgC_0NH_3$) and guest addition ($ZnPgC_0{\subset}$(Ph–H and PyH^+)) individually to $ZnPgC_0$.

The effect of addition of *exo* NH_3 ligands on the enthalpies and free energies of encapsulation is dependent on the guest. For $ZnPgC_0NH_3{\subset}Ph–H$ versus $ZnPgC_0{\subset}Ph–H$, both $\Delta_{encap}H_{298}$ and $\Delta_{encap}G_{298}$ become more positive by 10 kJ/mol and up to 5 kJ/mol, respectively (Table 6.7). Because this destabilization is small, encapsulation of Ph–H is still favorable overall. For $ZnPgC_0NH_3{\subset}PyH^+$ versus $ZnPgC_0{\subset}PyH^+$, both $\Delta_{encap}H_{298}$ and $\Delta_{encap}G_{298}$ become more negative by up to 200 kJ/mol. One possible explanation for this

greatly increased stability is an enhanced electrostatic interaction between the PyH^+ guest and the $ZnPgC_0$ framework upon addition of the *exo* NH_3 ligands. For $ZnPgC_0 \subset PyH^+$, the Mulliken charge on $ZnPgC_0$ is 0.105, making the charge on the PyH^+ 0.895, indicating minimal transfer of electron density from $ZnPgC_0$ to PyH^+. For $ZnPgC_0NH_3$, the net charge on the *exo* NH_3 ligands is 0.984, making that on $ZnPgC_0$ –0.984. Consequently, the presence of the *exo* NH_3 ligands results in a transformation of $ZnPgC_0$ from neutral or slightly positive to negative. For $ZnPgC_0NH_3 \subset PyH^+$, the charge on PyH^+ is 0.921 and the net charge on the *exo* NH_3 ligands is 1.131, resulting in a charge of –1.052 on $ZnPgC_0$. That is, for $ZnPgC_0NH_3 \subset PyH^+$, the PyH^+ guest retains its nearly +1 charge, whereas the *exo* NH_3 ligands take on a +1 charge from donating one electron to $ZnPgC_0$, creating a strong, attractive electrostatic host-guest interaction. As a comparison, for $ZnPgC_0NH_3 \subset$ Ph–H, although the *exo* NH_3 ligands do transfer about one electron to $ZnPgC_0$, the charge on the Ph–H is merely 0.078.

The trends described above are independent of the level of calculation used to obtain SPEs; furthermore, $\Delta_{encap}H_{298}$ and $\Delta_{encap}G_{298}$ obtained from SPEs calculated at a given level of theory but evaluated for the two different geometries vary by no more than 8 kJ/mol. The similar energetics obtained using the B3LYP and PBE0 equilibrium structures further supports our conclusion that PBE0/LANL2DZ optimizations are sufficient for future studies.

Table 6.7 Energetic properties of $ZnPgC_0NH_3$⊂Ph–H and $ZnPgC_0NH_3$⊂PyH^+.

complex *method/basis set* (SPE)	ΔH (kJ/mol)[a]	ΔG (kJ/mol)[a]
$ZnPgC_0NH_3$⊂Ph–H		
M05-2X/VDZ-PP	–102.7 (–97.6)	–63.6 (–58.9)
M05-2X/SDD	–92.2 (–87.3)	–53.1 (–48.6)
M05-2X/SDDAll	–97.5 (–93.2)	–58.4 (–54.6)
M06-L/VDZ-PP	–138.6 (–133.0)	–99.4 (–94.3)
ωB97X-D/VDZ-PP	–162.4 (–155.6)	–123.3 (–116.9)
$ZnPgC_0NH_3$⊂PyH^+		
M05-2X/VDZ-PP	–364.8 (–358.4)	–332.0 (–325.4)
M05-2X/SDD	–326.1 (–319.9)	–293.4 (–286.9)
M05-2X/SDDAll	–334.6 (–328.7)	–301.8 (–295.7)
M06-L/VDZ-PP	–388.1 (–381.6)	–355.4 (–348.6)
ωB97X-D/VDZ-PP	–421.0 (–413.4)	–388.2 (–380.4)

[a]Data from PBE0/LANL2DZ and B3LYP/LANL2DZ (in parenthesis) equilibrium structure.

The structures and energetics of the host-guest complexes are clearly dependent on both the presence of the *exo* ligands and the nature of the guest. Inclusion of *exo* ligands will be important when investigating most of the properties of interest for the nanoassemblies. Because the M05-2X/VDZ-PP thermochemical data agrees best with the M05-2X/B2-PP results for $ZnPgC_0$⊂(Ph–H and PyH^+) and tends to be underestimated compared to M06-L and ωB97X-D data, M05-2X/VDZ-PP SPEs will be evaluated to determine a lower limit for encapsulation thermodynamic data.

6.4 Summary

In an effort to better understand the properties of zinc-seamed pyrogallol[4]arene dimeric nanocapsules, we have investigated whether the presence of *exo* ligands and guest molecules changes the geometric and energetic properties of these nanocapsules. The robust framework of the equilibrium structures located for $ZnPgC_0$ and $ZnPgC_0$(NH_3,

Py, and DMSO) at all levels of theory considered confirms the stability of an empty capsule, as suggested by previous experimental studies.[31,32,38] Agreement between the computationally and experimentally observed geometric parameters was achieved only for the ligated capsules. The presence of *exo* ligands in $ZnPgC_0$(NH_3, Py, and DMSO) led to the largest increase in capsule $diameter_{avg}$ (up to nearly 0.4 Å) in comparison to that of $ZnPgC_0$, whereas smaller changes (up to 0.15 Å) were observed upon encapsulation of a guest. Lesser ligand and guest effects were found for capsule lengths, τ5 values, and capsular volumes. Also, minimal effects on capsule geometry were found for the $ZnPgC_3$-based assemblies, and thus only $ZnPgC_0$-based assemblies will be used for future studies. Interestingly, the changes to these geometric properties are additive. In the absence of *exo* NH_3 ligands, the encapsulation thermodynamic data for both PyH^+ ($\Delta_{encap}G_{298}$ = –130 kJ/mol) and Ph–H ($\Delta_{encap}G_{298}$ = –50 kJ/mol) indicate that encapsulation of these guests is favorable. Upon addition of *exo* NH_3 ligands, there is nearly 200 kJ/mol stabilization of $\Delta_{encap}H_{298}$ and $\Delta_{encap}G_{298}$ for $ZnPgC_0NH_3{\subset}PyH^+$ versus $ZnPgC_0{\subset}PyH^+$, whereas there is a 10 kJ/mol destabilization of $\Delta_{encap}H_{298}$ and $\Delta_{encap}G_{298}$ for $ZnPgC_0NH_3{\subset}$Ph–H versus $ZnPgC_0{\subset}$Ph–H. The huge increase for the former encapsulation is due to the transfer of electron density (about 1e overall) from the *exo* NH_3 ligands to $ZnPgC_0$, which enhances the attractive electrostatic host-guest interaction.

From our systematic comparison of the effects of *exo* ligands, guests, and alkyl chain length on capsular properties, we recommend the PBE0/LANL2DZ level of theory for obtaining equilibrium structures and normal-mode vibrational frequencies for the zinc-seamed dimers. The PBE0/LANL2DZ optimized structure of $ZnPgC_0NH_3{\subset}PyH^+$

and experimentally observed structure of $ZnPgC_3Py{\subset}Py$ have essentially the same average capsule diameter. Also, smaller discrepancies were observed in capsule length, $\tau 5_{avg}$, and V_{empty}, with respect to the experimental values at this level of calculation. A calculational protocol in which, e.g., $ZnPgC_0{\subset}PyH^+$, is first optimized before adding the *exo* ligands saves computational time overall. Upon addition of *exo* ligands, alternate orientations of the guests, including equatorial orientations, can be considered. The M05-2X/VDZ-PP//PBE0/LANL2DZ thermochemical data for $ZnPgC_0{\subset}$guest nanoassemblies can be used for an initial screening to determine if guest encapsulation is thermodynamically favorable because the addition of *exo* ligands will most likely make encapsulation more favorable.

Chapter 7: The effects of guest encapsulation on the host and guest properties of zinc-seamed pyrogallol[4]arene dimeric nanoassemblies

The effects on the geometric and energetic properties of zinc-seamed pyrogallol[4]arene dimeric nanoassemblies caused by encapsulation of a neutral or protonated pyridine-based, imidazole-based, or solvent guest were investigated. The size limitations of the capsule have been explored with respect to the flexibility and position of pyridine alkyl-substituents of increasing size and the possibility of enclosing multiple guests. The proton affinities and gas-phase basicities of isolated versus encapsulated guests have been evaluated and are compared to the proton affinity of the capsule. Encapsulation and relative isomer thermochemical data are also presented. The calculational results are correlated with experimental observations.

7.1 Introduction

With applications to catalysis,[2] chemical separations,[3-10] gas storage,[11-14] and drug delivery,[15-17] supramolecular self-assembled systems have been of interest for some time. The Atwood group has focused on the study of calixarenes and pyrogallolarenes, which have been shown to absorb gases selectively.[19,21-23,267] The group has synthesized metal-seamed organic nanocapsules (MONCs), specifically, pyrogallol[4]arene-based nanocapsules with Cu^{2+}, Zn^{2+}, Co^{2+}, Ni^{2+}, or Ga^{3+} metal centers.[31-35] Either dimeric or hexameric capsules were formed, with a variety of *exo* ligands and encapsulated guests.

The choice of metal center and the corresponding coordination sphere impact capsular shape, capsular dimensions, and guest entrapment.

In an effort to better understand the properties of the MONCs, we are studying zinc-seamed pyrogallol[4]arene dimeric nanocapsules via quantum chemical calculations. The first of these studies focused mainly on the capsules originally identified by Power et al.,[31,32] [Zn_8(*C*-propylpyrogallol[4]arene)$_2$(pyridine)$_8$⊂pyridine] ($ZnPgC_3Py$⊂Py, Py = pyridine) and $ZnPgC_3$DMSO⊂3-MePy (Ch. 6). The results of that work showed that there is a minimal effect on capsular dimensions when R = propyl ($ZnPgC_3$) is replaced with R = H ($ZnPgC_0$); thus, capsules with R = H were investigated in the current work. Also, the effects of an *exo* ligand and a guest are additive with respect to capsular dimensions, and the thermochemical data for the unligated host-guest system, $ZnPgC_0$⊂guest, tends to provide a lower limit for encapsulation thermochemistry.

Several key findings have come from follow-up experimental studies on the zinc-seamed dimers. ^{1}H NMR analysis has shown that some guests are protonated[266] and that proton exchange is observed between D_2O solvent and a PyH^+ or $MePyH^+$ guest, but not an $EtPyH^+$ guest.[268] Guest protonation is supported by the electronic structure calculations on $ZnPgC_0NH_3$⊂PyH^+, for which the experimentally observed capsule $diameter_{avg}$[31] is reproduced only when the guest is protonated (Ch. 6). MALDI-TOF MS analyses have also confirmed the stability of a protonated host-guest nanoassembly,[30,37] but in this case it is unclear whether the proton is on the capsule or the guest. In addition, these analyses have shown that the capsule can be stripped of its *exo* ligands, may be unoccupied, and may contain multiple guests. The entrapment of CH_3OH and CH_3CN

molecules, in varying combinations, is thought to occur when the capsule is built from the chair conformation of the pyrogallol[4]arene (Fig. 1.2).

When the cone form of pyrogallol[4]arene is used to synthesize the zinc-seamed dimer, the guest typically originates from the Zn–ligand reactant complex (within reasonable steric constraints).[31,32] However, when the chair form of the pyrogallol[4]arene is used to synthesize the zinc-seamed dimer, the time required for the chair → cone conformational flip is thought to allow the more abundant solvent molecules to sweep out any possible guests from the original reactant complex.[37] These observations raise the question of whether the product host-guest assembly from the first dimer synthesis above is thermodynamically stable. That is, is the guest merely kinetically trapped by the "instantaneous" seaming of the dimers?

In an effort to gain additional insight into the above experimental results and associated questions, we performed electronic structure calculations on $ZnPgC_0 \subset (CH_3OH)_{1,2}(H^+)$, $ZnPgC_0 \subset (CH_3CN)_{1,2}(H^+)$, $ZnPgC_0 \subset Py(H^+)$, $ZnPgC_0 \subset MePy(H^+)$, $ZnPgC_0 \subset EtPy(H^+)$, $ZnPgC_0 \subset PrPy(H^+)$, $ZnPgC_0 \subset t\text{-butylPy}(H^+)$, and $ZnPgC_0 \subset$1-methylimidazole(1-MeIMD)(H^+), and the effect of neutral versus protonated guests on the capsular metric dimensions and host-guest thermochemistry was investigated. The effect on these properties of the position of the alkyl substituent on Py and PyH^+ was also studied. Finally, the change upon encapsulation in guest proton affinity (PA) and gas-phase basicity (GB) and guest-guest hydrogen-bonding energy was analyzed.

We chose to start our investigation by examining $ZnPgC_0 \subset guest(H^+)$ dimers for the following reasons (Ch. 6). (1) The effects of guest encapsulation will be accentuated

by using the smaller $ZnPgC_0$ capsular framework. (2) Modifications in the properties of the host-guest assemblies upon addition of *exo* ligands can be determined. (3) The calculational cost increases considerably in the presence of *exo* ligands, making the further inclusion of more complex linker groups cost prohibitive.

7.2 Computational details

The Gaussian09 suite of programs[89] was used for all calculations performed in this study, and results were visualized with GaussView5.[144] All equilibrium structures were optimized at the PBE0/LANL2DZ level of theory, as prescribed by previous studies involving mononuclear zinc model complexes[43,44,201] of the zinc-seamed pyrogallol[4]arene capsular framework and of the capsular framework itself (Ch. 6). The keyword int = ultrafine and normal convergence criteria were used for all optimizations. To obtain thermal correction terms and identify the nature of stationary points, normal-mode vibrational frequencies were evaluated.

In order to obtain more reliable thermochemical data, single-point energies (SPEs) were evaluated with the M05-2X method in conjunction with the cc-pVDZ basis set on all atoms and the fully relativistic small-core MDF10 pseudopotential (PP) on zinc.[259] This calculational level will be denoted as M05-2X/VDZ-PP for the remainder of the text. The basis set[260] and PP for zinc were retrieved from the EMSL basis set library.[261,262] The M05-2X/VDZ-PP SPEs were used to determine if encapsulation of a guest is favorable, on the basis of the derived encapsulation enthalpies and free energies (eq. 7.1, $\Delta_{rx7.1}H_{298}$ and $\Delta_{rx7.1}G_{298}$, respectively). To determine the effect of the

encapsulation on PA and GB, these data were determined for both encapsulated and isolated guests. The PAs are given as $-\Delta_{rx7.2}H_{298}$ and $-\Delta_{rx7.3}H_{298}$.

$$ZnPgC_0 + guest \rightarrow ZnPgC_0 \subset guest \quad \textbf{(7.1)}$$

$$ZnPgC_0 \subset guest + H^+ \rightarrow ZnPgC_0 \subset guestH^+ \quad \textbf{(7.2)}$$

$$guest + H^+ \rightarrow guestH^+ \quad \textbf{(7.3)}$$

A complete screening of the orientations of the isolated guests was performed at the M05-2X/VDZ-PP//PBE0/LANL2DZ level of theory. Only the most stable orientation of the guest was initially optimized within the capsule unless the guest did not fit. In this case, the alkyl group was contorted in a way such that the guest would fit. Molecular dynamics (MD) simulations carried out by Brewer et al.[269] located multiple stable guest arrangements for these nanoassemblies. The arrangements identified in this way are in the process of being tested with respect to their relative stabilities.

The diameter of the capsule is measured by the distance between zinc atoms that are directly across from one another. The length of the capsule is defined to be the distance between the centroids of the four topmost, upper-rim aryl carbons and the four bottommost, lower rim aryl carbons and has been calculated using Mercury CSD 2.0.[263] The $\tau 5$ value is an index used to determine the amount of square pyramidal ($\tau 5 = 0$) or trigonal bipyramidal ($\tau 5 = 1$) character a five-coordinate species exhibits.[151] We recognize that the capsules investigated herein are only 4-coordinate, but, due to the robust nature of the framework, only slight deviations are found in the $\tau 5$ values upon adding a fifth ligand to the zinc centers (Ch. 6). For the capsules, $\tau 5$ is given by the expression $\tau 5 = |\angle(HO–Zn–OH) – \angle(O–Zn–O)|/60$ (Fig. 6.1). The MSRoll interface in

X-Seed[264,265] with a probe radius of 1.25 Å was used to calculate the internal volume of the capsular framework. All volumes were measured with the guest removed (V_{empty}).

7.3 Results and analysis of results

7.3.1 Geometric properties of $ZnPgC_0$⊂guest and $ZnPgC_0$⊂guestH^+

Both neutral and protonated guests have been encapsulated in the synthesis of zinc-seamed pyrogallol[4]arene nanocapsular assemblies.[31,32,37] The neutral guests observed to date have been solvent molecules (CH_3OH, CH_3CN, and H_2O), whereas the protonated guests observed to date have been a ligand from the original reactant zinc complex (PyH^+, $MePyH^+$, and $EtPyH^+$). (We note that because the latter guests do not enter the capsule from the solvent, the gas-phase calculations are particularly relevant for their encapsulation energetics.) That the guest is protonated in the experimentally observed $ZnPgC_3Py⊂PyH^+$ dimer is supported by our quantum calculations (Ch. 6), i.e. $ZnPgC_0NH_3⊂PyH^+$ has a capsule $diameter_{avg}$ that matches that found experimentally. These observations raise the question as to why guests from the reactant zinc complex are protonated. One possible explanation for the protonation is given by the following suggested step in the mechanism of formation of the zinc-seamed dimers. Presumably in the formation of these dimers, all but one zinc reactant complex loses all but one of its ligands. Also, the metal seaming of the capsule occurs essentially instantaneously when R = alkyl.[31,32] The loss of the ligands would be greatly facilitated by their protonation by the protons stripped from the phenol groups when a capsule is formed. Thus, we suggest that it is likely that any guest that was originally a ligand from the reactant zinc complex will

be protonated. Accordingly, we have studied both the neutral and protonated forms of a number of guests.

7.3.1.1 $ZnPgC_0$⊂guest: guest alignment, capsule diameters, and τ5 values

The $diameter_{avg}$ of the capsule tends to be underestimated compared with the experimentally observed $ZnPgC_3Py⊂PyH^+$ [31] and $ZnPgC_3DMSO⊂3\text{-}MePyH^+$ [32] dimers, whether the encapsulated guest is neutral or protonated (Table 7.1). (Recall that *exo* ligands are not present in these calculations.) Neutral guests tend to be oriented towards a zinc center (Fig 7.1), leading to pentacoordination of the zinc with distances of Zn···guest as short as 2.154 Å ($ZnPgC_0⊂CH_3OH$). The exceptions are *p*-EtPy and *o*-EtPy, for which the N atoms are oriented axially, not towards a zinc center. The resulting 5-coordinate zinc tends to shift *endo* towards the guest. This arrangement of neutral guests decreases the $diameter_{avg}$ 0.03 – 0.15 Å compared with $ZnPgC_0$ (Table 7.1). In contrast, as the alkyl group increases in size from Me to Et to Pr for the *para*-substituted Py, a total increase of about 0.05 Å is observed for the capsule $diameter_{avg}$. Even with a Me group, the 1-MeIMD has a capsule $diameter_{avg}$ within 0.015 Å of the unsubstituted Py guest (Table 7.1). Overall, there tends to be a pinching effect on the capsule; while the Zn–Zn distance calculated with the zinc coordinating to the guest can decrease by as much as 0.4 Å, the distance calculated with a zinc center adjacent to the coordination site can increase up to 0.14 Å compared to $ZnPgC_0$. We suspect that this pinching effect will be minimized or even eliminated upon addition of *exo* ligands, an addition that has been shown to increase the capsular diameter significantly (Ch. 6).

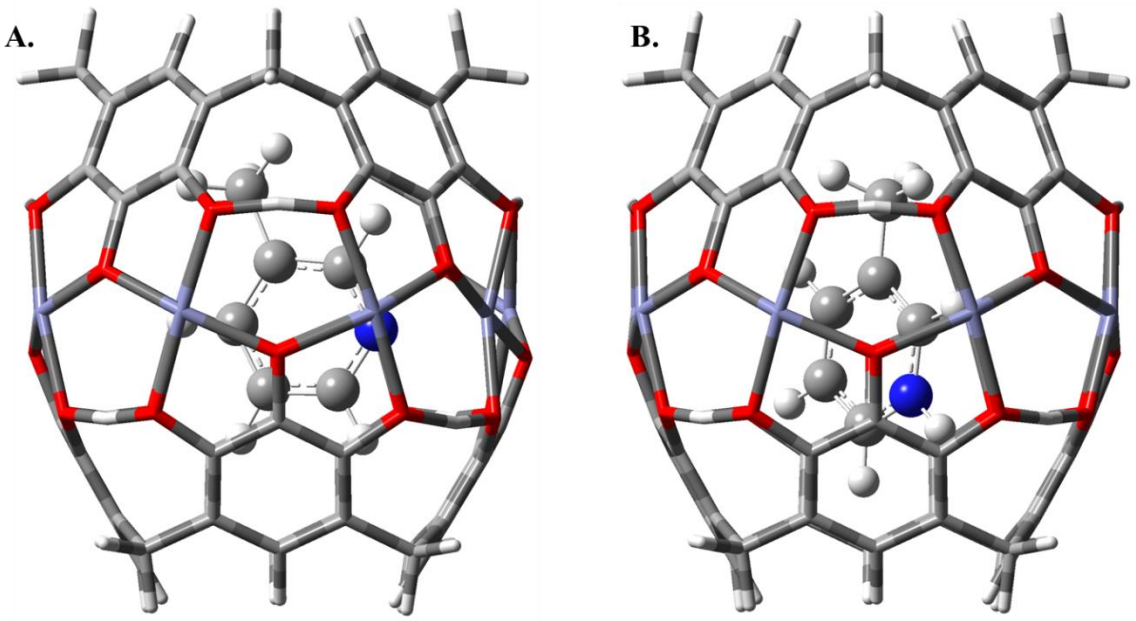

Figure 7.1 Representative orientations of $ZnPgC_0$⊂guest and $ZnPgC_0$⊂guestH^+ shown for $ZnPgC_0$⊂ *m*-MePy (A) and $ZnPgC_0$⊂ *m*-MePyH^+ (B).

Table 7.1 Geometric properties of $ZnPgC_0$⊂guest

guest	$diameter_{avg}$ (Å)	length (Å)	$\tau5_{avg}$		V_{empty} (Å^3)
Py[a]	9.984 ± 0.022	8.774	0.41	± 0.02	141
m-MePy[b]	9.893 ± 0.047	8.834	0.42	± 0.03	143
none[c]	9.582	8.962	0.39		165
Py	9.455 ± 0.257	8.989	0.38	± 0.04	168
PyH^+[c]	9.729 ± 0.095	8.922	0.39	± 0.01	163
o-MePy	9.497 ± 0.031	9.018	0.38	± 0.01	170
o-$MePyH^+$	9.679 ± 0.097	8.982	0.41	± 0.03	
m-MePy	9.447 ± 0.187	9.021	0.37	± 0.06	170
m-$MePyH^+$	9.678 ± 0.111	8.972	0.40	± 0.03	165
p-MePy	9.519 ± 0.141	8.967	0.31	± 0.05	172
p-$MePyH^+$	9.672 ± 0.117	8.972	0.40	± 0.03	165
o-EtPy	9.451 ± 0.124	9.054	0.35	± 0.09	173
o-$EtPyH^+$	9.656 ± 0.090	9.018	0.41	± 0.06	168
m-EtPy	9.419 ± 0.214	9.064	0.37	± 0.07	173
m$EtPyH^+$	9.654 ± 0.101	9.009	0.40	± 0.04	168
p-EtPy	9.534 ± 0.094	9.033	0.38	± 0.03	172
p-$EtPyH^+$	9.648 ± 0.100	9.011	0.40	± 0.04	168
p-PrPy	9.565 ± 0.141	8.961	0.28	± 0.11	175
p-$PrPyH^+$	9.714 ± 0.233	8.980	0.36	± 0.06	170
p-*t*-butylPy	9.554 ± 0.190	9.050	0.36	± 0.06	178
p-*t*-butylPyH^+	9.648 ± 0.204	9.049	0.37	± 0.07	175
1-MeIMD	9.471 ± 0.197	8.983	0.37	± 0.05	169
1-$MeIMDH^+$	9.701 ± 0.048	8.947	0.41	± 0.01	162
CH_3OH	9.471 ± 0.195	8.972	0.36	± 0.07	167
$CH_3OH_2^+$	9.668 ± 0.032	8.955	0.40	± 0.01	164
$(CH_3OH)_2$	9.471 ± 0.194	8.992	0.36	± 0.07	169
$(CH_3OH)_2H^+$	9.676 ± 0.013	8.962	0.41	± 0.01	163
CH_3CN	9.527 ± 0.161	8.968	0.34	± 0.14	167
CH_3CNH^+	9.701 ± 0.010	8.940	0.41	± 0.01	162
$(CH_3CN)_2$	9.433 ± 0.315	9.007	0.29	± 0.16	170

[a]Data of $ZnPgC_3Py$⊂Py.[31] [b]Data of $ZnPgC_3DMSO$⊂3-MePy.[32] [c]Data repeated for convenience.

Because the now 5-coordinate zinc shifts towards the guest, this zinc has a τ5 value in the range of 0.1 – 0.2, which affects the τ5 values of the two adjacent zinc centers. The remaining five zinc centers have τ5 values closer to the 0.40 value observed experimentally.[31,32] The exceptions are $ZnPgC_0$⊂ *p*-PrPy and $ZnPgC_0$⊂CH_3CN, for

which the guest-coordinated zinc centers are essentially square pyramidal ($\tau5$ = 0.03 and 0.00, respectively), although the remaining $\tau5$ values are within experimental limits.

7.3.1.2 $ZnPgC_0 \subset guestH^+$: guest alignment, capsule diameters, and $\tau5$ values

Unlike the neutral guests, protonated guests do not coordinate to the zinc but can form hydrogen bonds with the aryl rings (Fig. 7.1). That is, $guestH^+$ tends to be aligned perpendicular to the plane of the equatorial zincs. These interactions do not generally lead to a pinching effect as observed for $ZnPgC_0 \subset guest$, but rather an overall increase in Zn–Zn distances. In fact, the encapsulation of a protonated guest ($ZnPgC_0 \subset guestH^+$) leads to an increase in the capsule $diameter_{avg}$ by 0.09 – 0.15 Å compared to $ZnPgC_0$ (Table 7.1). The larger increases in $diameter_{avg}$ are due to steric interactions imposed by the orientation of the alkyl groups of $guestH^+$, although there is no systematic trend in the change as the alkyl group varies from Me up to Pr. Interestingly, due to the orientation of the protonated guest and possible contortion of the alkyl groups, only the capsules with PyH^+, *p*-$PrPyH^+$, CH_3CNH^+, and 1-$MeIMDH^+$ guests have average capsule diameters greater than 9.70 Å (Table 7.1). The explicit distortion caused by increasing the alkyl group size of the *para*-substituted Py is depicted in Fig. 7.2. Note the deviation from the "spherical" shape of $ZnPgC_0 \subset PyH^+$ as the larger guests cause the framework of the capsule to protrude, e.g. $ZnPgC_0 \subset$*p*-*t*-$butylPyH^+$.

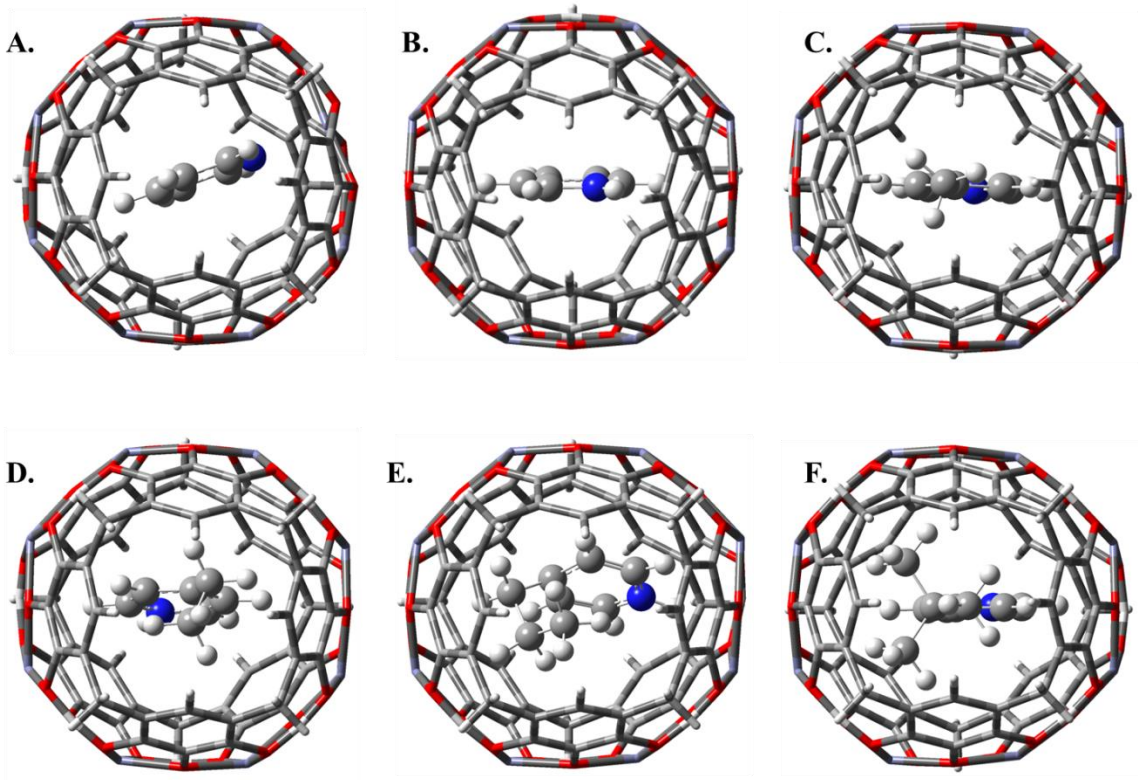

Figure 7.2 Exploring the flexibility and robustness of $ZnPgC_0$ with a variety of guests. Top views of $ZnPgC_0$⊂Py (A), $ZnPgC_0$⊂PyH^+ (B), $ZnPgC_0$⊂*p*-$MePyH^+$ (C), $ZnPgC_0$⊂*p*-$EtPyH^+$ (D), $ZnPgC_0$⊂*p*-$PrPyH^+$ (E), and $ZnPgC_0$⊂*p*-*t*-$butylPyH^+$ (F).

The individual τ5 values show less variation compared to the $ZnPgC_0$⊂guest systems and generally range from 0.35 – 0.45. This mixed square pyramidal and trigonal bipyramidal character of the $ZnPgC_0$⊂$guestH^+$ assemblies is not surprising given the lack of displacement of the zinc due to coordination to a guest.

In our previous studies of mononuclear zinc models of the zinc-seamed pyrogallol[4]arene nanocapsules,[43,44] it was found that one of the artifacts of the LANL2DZ basis set is an overemphasis of hydrogen bonding. In those studies, this overemphasis caused distortion of the zinc coordination sphere to the extent that the model geometric properties no longer lay within the experimentally observed ranges. With the exception of $ZnPgC_0$⊂$CH_3OH_2^+$, this artifact does not seem to affect the

capsular frameworks. Most of the guestH^+ do not disrupt the capsule, as evidenced by the $\tau 5$ values and capsule diameters of the $ZnPgC_0 \subset$guestH^+ assemblies, presumably because the hydrogen bond is a guest$H^+ \cdots$aryl interaction. As with the other protonated guests, the more stable form of $ZnPgC_0 \subset CH_3OH_2^+$ ($\approx$ 23 kJ/mol) exhibits little framework distortion; moreover, the aryl groups in one hemisphere stabilize the $CH_3OH_2^+$ by transferring electron density from $ZnPgC_0$ to the guest, reducing the Mulliken charge of $CH_3OH_2^+$ from +1.000 to +0.758. In contrast, for the less stable form of $ZnPgC_0 \subset CH_3OH_2^+$, there is actually a H^+ transfer from the $CH_3OH_2^+$ to one of the O$\cdots$H$\cdots$O capsule oxygens, leading to a collapse in the capsule wall but no fragmenting of the capsular framework. We recognize that $CH_3OH_2^+$ is an unlikely guest because CH_3OH is introduced only as a solvent, but this H^+ transfer is interesting because it does not occur for the other protonated systems. The energetics associated with this proton behavior will be discussed in the later sections.

One of the other properties to be investigated for guests with alkyl groups longer than Me is the orientation of the substituent alkyl chains. When considering isolated, gas-phase EtPy(H^+), for example, the ethyl group can be either planar or perpendicular with respect to Py(H^+). For *m*-EtPyH^+ both forms are essentially equivalent at the M05-2X/VDZ-PP//PBE0/LANL2DZ level of theory. However, upon encapsulation, the conformer with the Et group perpendicular to PyH^+ is some 20 kJ/mol more stable than the conformer with the Et group planar (Fig. 7. 3). In addition to exploring the planar versus perpendicular orientations, we are also investigating *trans* and *cis* orientations of the alkyl group with respect to the N atom.

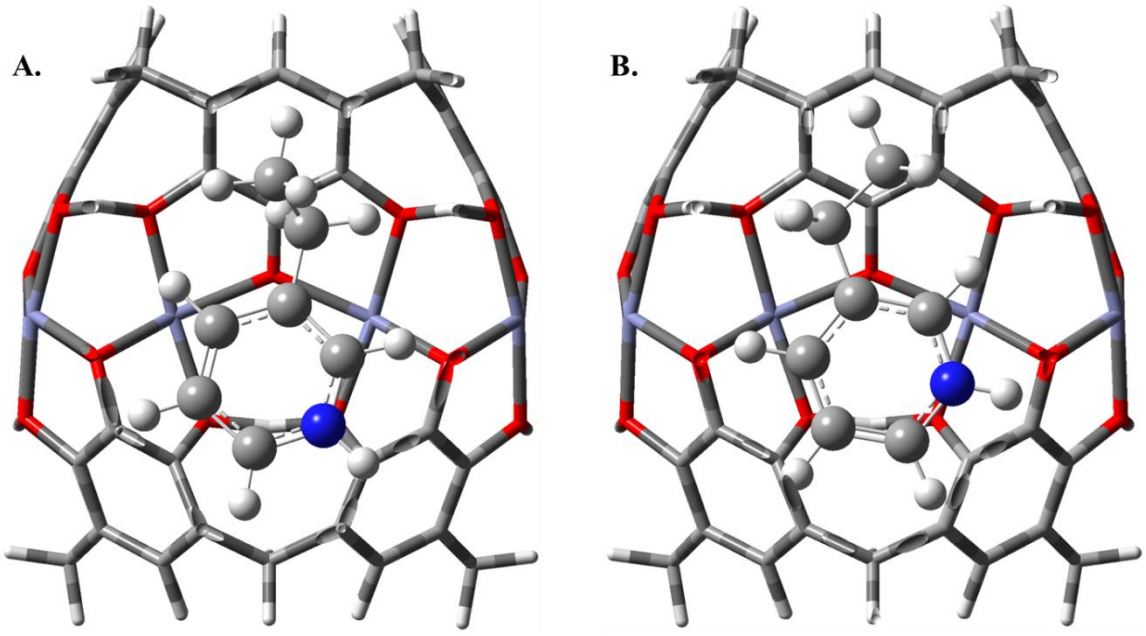

Figure 7.3 Side views of $ZnPgC_0 \subset m\text{-}EtPyH^+$ with the Et group perpendicular (A) and the Et group planar (B). The front side of the capsule has been hidden for clarity.

7.3.1.3 $ZnPgC_0 \subset (CH_3OH)_2$-based and $ZnPgC_0 \subset (CH_3CN)_2$-based assemblies: guest alignment, capsule diameters, and τ5 values

Adopting the same orientations as the lone encapsulated guests, the $ZnPgC_0 \subset (CH_3OH)_2$ and $ZnPgC_0 \subset (CH_3CN)_2$ guests are aligned so there is a Zn···guest interaction and the $ZnPgC_0 \subset (CH_3OH)_2H^+$ guest is aligned so there is a $(CH_3OH)_2H^+$···aryl interaction (Fig. 7.4). The changes in capsule $diameter_{avg}$ and τ_{avg} values fall within the ranges found for the previously examined guests (Table 7.1). As with $ZnPgC_0 \subset CH_3CN$, $ZnPgC_0 \subset (CH_3CN)_2$, which has C_2 symmetry, has a square pyramidal arrangement (τ5 = 0.03) of the ligands for both of the guest-coordinated zinc centers.

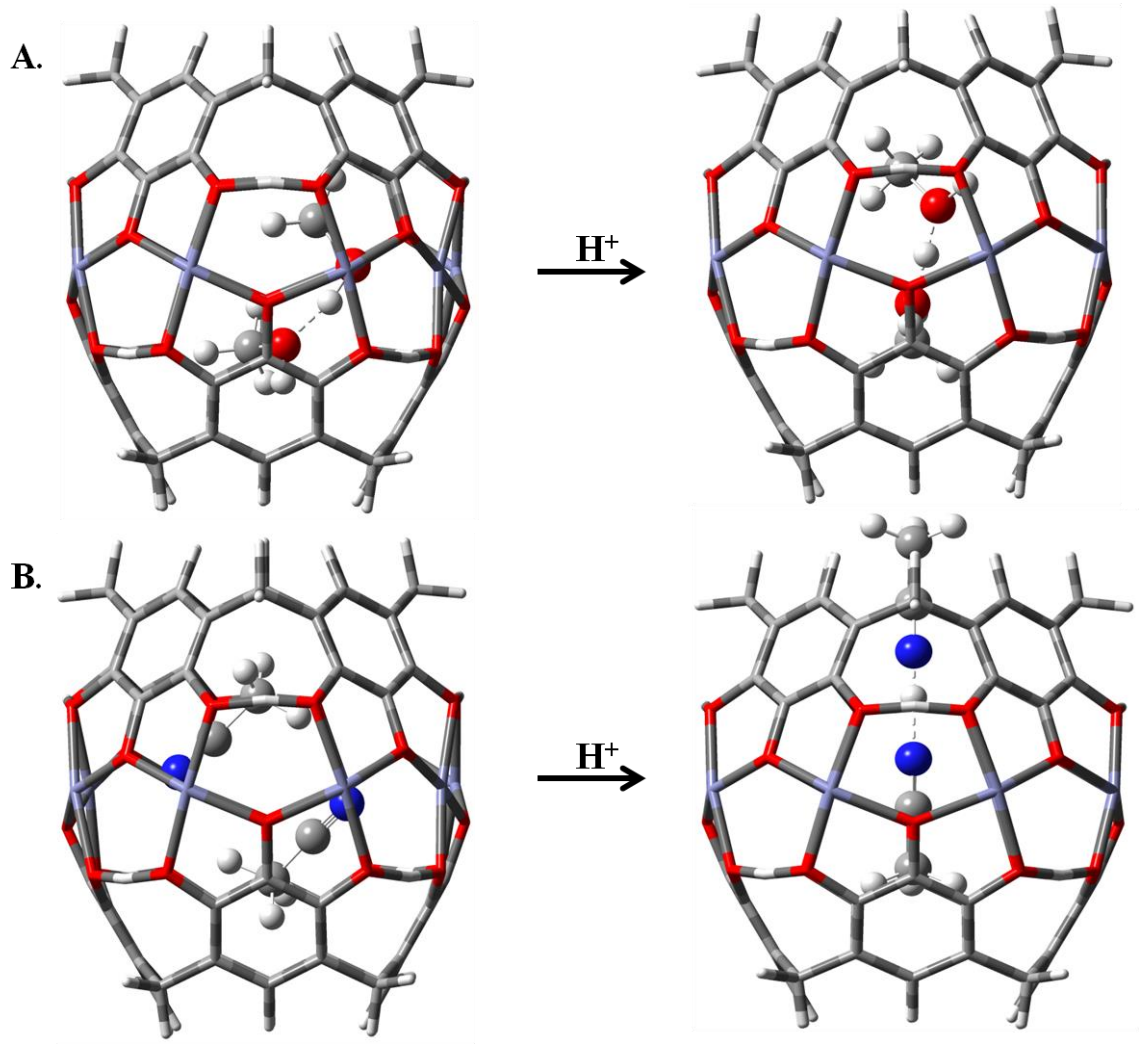

Figure 7.4 The protonation of $ZnPgC_0 \subset (CH_3OH)_2$ to form $ZnPgC_0 \subset (CH_3OH)_2H^+$ (A). Preliminary results for the protonation of $ZnPgC_0 \subset (CH_3CN)_2$ to form $ZnPgC_0 \subset (CH_3CN)_2H^+$ (B).

As with the larger substituted Py guests, the hydrogen bonded dimeric guests do contort, with respect to the isolated guests, upon encapsulation to minimize repulsive interactions with the capsule. The changes observed for the $(CH_3OH)_2$-based dimers are particularly noteworthy. The dihedral angle ∠C–O–O–C of the $(CH_3OH)_2$ backbone decreases considerably upon encapsulation for both $ZnPgC_0 \subset (CH_3OH)_2$ (94° to 61°) and $ZnPgC_0 \subset (CH_3OH)_2H^+$ (121° to 46°). There is actually a decrease in the H···O hydrogen

bond length from 1.718 Å to 1.496 Å for $(CH_3OH)_2$ upon encapsulation; this decrease can be rationalized by the donation of electron density from the proton-donating O atom to the coordinating Zn atom which in turn increases the positive charge on the hydrogen-bonded proton and strengthens the O–H⋯ O hydrogen bond. Less than a 3° change in the hydrogen bond angle ∠O–H⋯O for both $(CH_3OH)_2$-based dimers and no change in the hydrogen bond O⋯H for $(CH_3OH)_2H^+$ are observed.

The $(CH_3CN)_2$ and $(CH_3CN)_2H^+$ dimers have essentially the same orientations regardless of whether they are encapsulated or isolated. The CH_3CN molecules in $(CH_3CN)_2$ are anti-parallel with respect to each other and, when encapsulated, are aligned between the equatorial and axial planes of the capsule. Upon encapsulation, the distance between the N atoms and the adjacent Me group C atoms decreases by 0.06 Å (3.366 Å). Preliminary results show that the $(CH_3CN)_2H^+$ dimer is linear and that the Me group actually sticks out of the top of the capsule. This is the first example of a guest protruding from the capsule and showcases the importance of hydrogen bonding in stabilizing this guest. The experimentally determined gas-phase N–H⋯N hydrogen bond strength in $(CH_3CN)_2H^+$ is 126.4 kJ/mol.[270] Upon encapsulation, the H^+ moves slightly towards one N atom instead of being equidistant between the two N atoms, as it is in the isolated dimer, and the overall length of the dimer increases by 0.06 Å.

7.3.1.4 Capsule lengths and volumes for $ZnPgC_0$-based assemblies

Capsule lengths typically increase for both $ZnPgC_0$⊂(guest and guestH^+) compared with that of $ZnPgC_0$. The distortions in the capsular framework due to the Zn⋯guest interactions tend to lead to larger increases for the neutral guests than the

protonated guests. In fact, the length actually decreases or is unchanged compared with $ZnPgC_0$ for the PyH^+, 1-MeIMDH$^+$, $CH_3OH_2^+$, $(CH_3OH)_2H^+$, and CH_3CNH^+ guests (Table 7.1). The volumes of the equilibrium structures for these guestH^+ decrease (up to 3 Å^3) with respect to $ZnPgC_0$. All other $ZnPgC_0\subset$(guest and guestH^+) systems have increases in V_{empty} as great as 7 Å^3. For the smaller guests ranging in size from CH_3OH to MePy, the volumes of an isolated guest versus an encapsulated guest are within 1 Å^3. However, for the larger EtPy and *t*-butylPy guests, larger changes in the volume of the guest are observed. For $ZnPgC_0\subset$ *p*-*t*-butylPy and $ZnPgC_0\subset$ *p*-*t*-butylPyH^+, V_{empty} increases 13 and 10 Å^3, respectively, relative to that of $ZnPgC_0$.

The alkyl groups of these guests contort to adapt to the capsular environment; typical contortions involve the decrease of bond angle $\angle C_{Py}–C_{alkyl}–C_{alkyl}$ (up to 5°) or bond length $C_{Py}–C_{alkyl}$ (up to 0.04 Å) upon encapsulation. The dihedral angle $\angle C_{Py}–C_{Py}–C_{Et}–C_{Et}$ in isolated EtPy(H^+) is nearly perpendicular and ranges from 76 – 109°, except for *p*-EtPyH^+ and *o*-EtPyH^+ for which the Et group is planar. In order for EtPy(H^+) to fit within the capsule, the Et group, regardless of placement, is oriented so that it lies over the Py framework; the dihedral angle $\angle C_{Py}–C_{Py}–C_{Et}–C_{Et}$ ranges from 53 – 69°. For isolated *p*-PrPy(H^+), the propyl group is perpendicular to Py(H^+), resulting in a dihedral angle $\angle C_{Py}–C_{Pr}–C_{Pr}–C_{Pr}$ of 180°; however, upon encapsulation, the dihedral angle of *p*-PrPy and *p*-PrPyH^+ decreases significantly, resulting in $\angle C_{Py}–C_{Pr}–C_{Pr}–C_{Pr}$ values of 50 and 72°, respectively. Rebek observed similar guest contortions in his study of encapsulated alkanes and substituted alkanes: for example, longer alkanes, such as C_9H_{20} up to $C_{12}H_{26}$ have been found to fold within pyrogallolarenes.[271]

7.3.2 Energetic properties of $ZnPgC_0$⊂guest and $ZnPgC_0$⊂guestH^+

The trends in the current thermochemical data are described below, with the caveat that those trends may change if an as yet unexamined arrangement of the guest is determined to be significantly more stable.

7.3.2.1 Encapsulation thermochemistry

Our previous studies of encapsulation energies for $ZnPgC_0$⊂(Ph–H and PyH^+) showed that thermochemical values calculated at the M05-2X/VDZ-PP level of theory agree with those calculated at the M05-2X/B2-PP level and represent a lower threshold with respect to stability (Ch. 6). Nevertheless, all guests have negative free energies for the encapsulation reaction, indicating that the gas-phase reaction is spontaneous at 298 K, except for *p*-EtPy, *p*-PrPy(H^+), and *p*-*t*-butylPy(H^+) (Table 7.2). The previous calculations indicate that using the $ZnPgC_0NH_3$ capsular framework leads to more favorable encapsulation enthalpies and free energies (by up to 200 kJ/mol) than does using the $ZnPgC_0$ framework. Even if such a significant stabilization of the free energy occurs for $ZnPgC_0NH_3$⊂*p*-*t*-butylPy, encapsulation of *p*-*t*-butylPy would still be, at best, thermodynamically neutral. The thermodynamic data support the observed encapsulation of solvent molecules rather than *p*-*t*-butylPy(H^+), with its sterically demanding size, in experimental studies to date.[38] In addition, although the *p*-*t*-butylPy(H^+) guest rearranges to fit once it is inside the capsule, it is unlikely that the necessary flattening of the guest will occur and allow the capsule to seam around the guest. As the size of the alkyl group on the Py increases, the encapsulation energies indicate systematic destabilization; however, this destabilization is always smaller for the protonated guests than for the

neutral guests. For the Py, MePy, and EtPy guests, the encapsulation enthalpies for the protonated species are at least 30 kJ/mol more stable than those for the neutral species (Table 7.2). Because the encapsulated *p*-PrPy(H^+) orientations both have contorted Pr groups with respect to isolated *p*-PrPy(H^+), the encapsulation of the neutral species may be more favorable due to the Zn⋯*p*-PrPy interaction (Table 7.2). Given, however, that the protonated capsule-guest assembly is more stable than the neutral assembly for all of the other alkyl-substituted Py guests, including *p*-*t*-butylPy, it is likely that a more stable form of $ZnPgC_0$⊂*p*-$PrPyH^+$ will be located. The favorable encapsulation free energies for Py-based guests agree with experiment in that PyH^+, *m*-$MePyH^+$, and *m*-$EtPyH^+$ guests have been observed. The encapsulation enthalpy and free energy for $ZnPgC_0$⊂1-$MeIMDH^+$ are as favorable as those of $ZnPgC_0$⊂PyH^+, the most favorable of the experimentally observed Py-based guests.

Although the magnitudes of the encapsulation energies for $ZnPgC_0$⊂guest(H^+) may be underestimated with respect to $ZnPgC_0NH_3$⊂guest(H^+), the trends among related guests should hold upon *exo* ligation. The orientations resulting from unique host-guest interactions found for $ZnPgC_0$⊂guest(H^+) are directly applicable when configuring an initial geometry for $ZnPgC_0NH_3$⊂guest(H^+).

Table 7.2 Encapsulation energies.[a]

guest	ΔH	ΔG
Py	–164.2	–121.9
PyH^+	–179.6	–137.4
o-MePy	–108.8	–57.9
o-$MePyH^+$	–165.0	–112.5
m-MePy	–140.5	–88.1
m-$MePyH^+$	–171.4	–124.1
p-MePy	–137.8	–80.3
p-$MePyH^+$	–178.1	–128.3
o-EtPy	–68.4	–11.1
o-$EtPyH^+$	–95.4	–39.0
m-EtPy	–77.0	–16.0
m$EtPyH^+$	–132.9	–74.4
p-EtPy	–31.6	28.9
p-$EtPyH^+$	–138.2	–77.5
p-PrPy	–66.8	2.6
p-$PrPyH^+$	–38.1	28.3
p-*t*-butylPy	109.5	175.7
p-*t*-butylPyH^+	14.8	82.3
1-MeIMD	–186.9	–134.9
1-$MeIMDH^+$	–184.2	–141.0
CH_3OH	–113.6	–75.8
CH_3OH^+	–223.6	–177.3
$(CH_3OH)_2$	–172.0	–117.9
$(CH_3OH)_2H^+$	–191.0	–143.2
CH_3CN	–113.2	–76.3
CH_3CNH^+	–167.7	–127.6
$(CH_3CN)_2$	–217.4	–160.1

[a]M05-2X/VDZ-PP data in kJ/mol.

7.3.2.2 Relative isomer stabilities

The relative H_{298} and G_{298} values of the isolated isomers of MePy and EtPy have the same stability trends, with *ortho* substitution being most stable and *meta* substitution being least stable (≈ 15 kJ/mol), regardless of whether the isomer is protonated or not (Table 7.3). Upon encapsulation of a guest, the relative H_{298} and G_{298} values show that the *meta*-substituted Py assembly is most stable, whereas the *para*-substituted PyH^+ assembly is most stable. There is no clear trend in the relative stabilities of encapsulated

versus isolated isomers. The most noticeable differences in these trends occur for the encapsulated *o*-EtPyH$^+$, *o*-MePy, and *p*-EtPy guests. The general destabilization of the encapsulated *o*-substituted Py guests compared with their *m*-substituted and *p*-substituted counterparts can be attributed to the steric constraints imposed by placement of the alkyl group directly adjacent to the nitrogen. For encapsulated *o*-MePy, this steric restriction contributes to a weaker Zn···MePy interaction for *o*-MePy than for *m*-MePy and *p*-MePy (Table 7.2). Encapsulated *p*-EtPy is the least thermodynamically stable of the three isomers due to the absence of the Zn···EtPy interaction that is present for the other two isomers. Although we have not yet located a minimum for ZnPgC$_0$⊂*p*-EtPy with a Zn···*p*-EtPy interaction, we suspect such a minimum exists because the corresponding ZnPgC$_0$⊂*p*-PrPy minimum has been located. The trends and magnitudes for the relative encapsulation reaction thermochemistry (Table 7.2) agree with those for the relative stability of the encapsulated isomers (Table 7.3). That these thermochemical data agree within 8 kJ/mol (e.g. $\Delta_{rx7.1}H_{o\text{-MePy}} - \Delta_{rx7.1}H_{m\text{-MePy}}$ versus $H_{o\text{-MePy}} - H_{m\text{-MePy}}$) indicates that encapsulation has similar effects on all of the isomers with respect to their isolated forms.

Table 7.3 Relative isomer enthalpy and free energy for the neutral and protonated forms of encapsulated and isolated guests.[a]

	encapsulated				isolated			
guest	neutral		protonated		neutral		protonated	
MePy								
o-MePy	25	(23)	10	(10)	0	(0)	0	(0)
m-MePy	0	(0)	14	(14)	7	(7)	11	(15)
p-MePy	0	(1)	0	(0)	5	(0)	4	(5)
EtPy								
o-EtPy	0	(0)	36	(34)	0	(0)	0	(0)
m-EtPy	0	(3)	13	(11)	8	(8)	14	(13)
p-EtPy	43	(46)	0	(0)	6	(5)	7	(5)

[a] ΔH_{298} and ΔG_{298} (in parenthesis) M05-2X/VDZ-PP//PBE0/LANL2DZ data in kJ/mol.

7.3.2.3 Thermodynamic stability versus kinetic trapping

The first experimental studies on the zinc-seamed pyrogallol[4]arene dimers in which the dimers were synthesized from cone-shaped macrocycles (R = alkyl) yielded only guests that were originally ligands associated with the zinc reactant complex. Occupation of the capsule by these guests was unexpected for two reasons. First, due to the sheer ratio of solvent molecules to zinc reactant complex ligands, it was anticipated that the solvent would sweep out all of the zinc ligands that dissociated during capsule formation. Second, it was later determined that the guests are protonated. Because the CH_3OH solvent is smaller than the PyH^+ and *m*-$MePyH^+$ guests from these early studies, size constraints could not explain its absence and questions about the thermodynamic stability of encapsulated CH_3OH arose. However, our quantum chemical calculations showed that there is a strong, attractive interaction between $ZnPgC_0$ and CH_3OH and that encapsulation of CH_3OH should be thermodynamically favorable (Table 7.2). In fact, $\Delta_{rx7.1}G_{298}$ for all solvent molecules and dimers is at least –75 kJ/mol. Nevertheless,

encapsulation of solvent guests was not observed until the dimers were synthesized from chair-shaped macrocycles (R = aryl), from zinc reactant complexes with *t*-butylPy ligands and/or from large solvents such as *t*-butylPy, all of which led to non-instantaneous metal seaming of the capsules. A five-day NMR study by Kumari et al. showed the formation of both unoccupied capsules and capsules with $(CH_3OH)_2$.[38] Solid-state studies also showed the encapsulation of H_2O when the capsule was constructed in *t*-butylPy solvent from a *t*-butylPy zinc complex.[38] MALDI-TOF MS data from Maerz et al. indicates the presence of both CH_3CN and CH_3OH guests in $ZnPgC_{aryl}DMSO\subset(CH_3CN, CH_3OH)$.[37] Although the calculated thermochemical data (Table 7.2) suggest that zinc-seamed pyrogallol[4]arene dimers with PyH^+ and *m*-$MePyH^+$ are thermodynamically stable, an analysis of the results discussed above suggests that protonated guests originating from the reactant zinc complex are actually kinetically trapped.

7.3.3 Encapsulation effects on proton affinity and gas phase basicity

For this particular study, only the O or N electron-donating (Lewis base) sites were protonated for both the isolated and encapsulated guests. With the exception of 1-MeIMD and *p*-PrPy, the PA and GB are always larger for the encapsulated guest (Table 7.4). The significant decrease in PA and GB observed for *p*-PrPy is due to the stabilization of the zinc-coordinated *p*-PrPy and the destabilization of the current sterically hindered orientation of *p*-$PrPyH^+$ mentioned above. However, the observed increases in PA are most likely underemphasized because the $ZnPgC_0\subset$guest systems tend to have guests that are coordinated to a zinc center, thus enhancing Zn⋯guest interactions. Upon addition of *exo* ligands, the Zn becomes "6-"coordinate and the

weaker Zn···guest interaction will have less of an effect than for the non-ligated $ZnPgC_0$⊂guest systems.

Table 7.4 PAs and GBs of isolated and encapsulated guests.[a]

guest	$guest_{encapsulated}$		$guest_{isolated}$		ΔPA	(ΔGB)
Py	949.4	(917.4)	933.9	(901.9)	15.5	(15.5)
o-MePy	1008.0	978.1	951.8	(923.5)	56.2	(54.6)
m-MePy	978.9	(951.1)	947.9	(915.2)	31.0	(35.9)
p-MePy	993.4	(966.1)	953.0	(918.1)	40.4	(48.0)
o-EtPy	983.8	(951.0)	956.8	(923.1)	27.0	(27.9)
m-EtPy	1006.8	(976.7)	950.9	(918.4)	55.9	(58.3)
p-EtPy	1062.6	(1030.4)	956.0	(923.9)	106.6	(106.5)
p-PrPy	930.1	(900.8)	958.8	(926.5)	–28.7	(–25.7)
p-*t*-butylPy	1057.1	(1024.2)	962.4	(930.8)	94.7	(93.4)
1-MeIMD	969.4	(945.6)	972.1	(939.5)	–2.7	(6.1)
CH_3OH	872.5	(836.1)	762.6	(734.6)	109.9	(101.5)
$(CH_3OH)_2$	920.8	(889.8)	901.7	(864.4)	19.1	(25.4)
CH_3CN	832.0	(797.2)	777.5	(745.8)	54.4	(51.4)

[a]PA (ΔH_{298}) and GB (ΔG_{298}, in parenthesis) for M05-2X/VDZ-PP//PBE0/LANL2DZ data in kJ/mol.

Encapsulation of a guest has been found to increase its pKa by as much as 5 – 10 units,[272-274] which translates to a change in GB ($\Delta\Delta G_{298}$) of 28 – 57 kJ/mol. In our calculational studies the enhancement of PA and GB is dependent on three factors: (1) the length of the alkyl group, (2) the position of the alkyl group, and (3) orientation differences in the guest. The PA and GB tend to increase from the *ortho*- to *meta*- to *para*-substituted Py guests and as the alkyl group lengthens (Table 7.4). The former trend can be rationalized by the strength of the Zn···guest interaction for the three isomers. The latter trend can be rationalized by the significantly greater destabilization of the encapsulation energy of a neutral guest (base) than for the corresponding protonated guest (acid) with increasing alkyl chain length (Table 7.2). In general, ΔPA ($\Delta\Delta H_{298} = \Delta H_{298,encap} - \Delta H_{298,isolated}$) and ΔGB tend to be less than 50 kJ/mol. However, *p*-EtPy, *p*-*t*-

butylPy, and CH_3OH all have $\Delta\Delta H_{298}$ and $\Delta\Delta G_{298}$ values greater than 100 kJ/mol due to differences in the orientations of the guests. The more negative encapsulation enthalpies and free energies of $ZnPgC_0 \subset p\text{-}EtPyH^+$ lead to the greatest PA enhancement. The larger ΔPA for the former two guests is due to *p*-EtPy and *p*-*t*-butylPy not coordinating to the Zn, as opposed to the other neutral guests, whereas the larger ΔPA for the latter is due to the multiple $CH_3OH_2^+ \cdots$aryl interactions. The magnitude of the PAs and GBs of the solvents tend to be about 100 kJ/mol less than those of the other guests, with the exception of $(CH_3OH)_2$. The higher PA observed for $(CH_3OH)_2$ is primarily due to the presence of the strong hydrogen bond between the guest molecules in the protonated species and $Zn \cdots (CH_3OH)_2$ and $(CH_3OH)_2 \cdots$aryl interactions.

Although the more stable form of $ZnPgC_0 \subset CH_3OH_2^+$ maximizes $CH_3OH_2^+ \cdots$aryl interactions, as a proof of concept, we have chosen to use the slightly less stable form of $ZnPgC_0H^+ \subset CH_3OH$ (H^+ transferred to a hydrogen-bonded oxygen of $ZnPgC_0$) to qualitatively predict that the relative PAs of Py, $ZnPgC_0$, and CH_3OH are Py > $ZnPgC_0$ > CH_3OH. The H^+ transfer from $CH_3OH_2^+$ to the $ZnPgC_0$ explains why the enhancement in PA for CH_3OH is among the largest (85 kJ/mol). The PA for the less stable encapsulated CH_3OH (849 kJ/mol) is actually more representative of an enhanced PA for the respective oxygen site in $ZnPgC_0$, due to the $CH_3OH \cdots ZnPgC_0H^+$ interaction. In fact, Kumari et al. have shown that the *endo* protonation enthalpy (PA) of a hydrogen-bonded oxygen in $ZnPgC_0$ is $\approx$ 815 kJ/mol,[275] some 50 kJ/mol greater than the PA of isolated CH_3OH, a result which quantitatively describes the findings depicted in Fig 7.5.

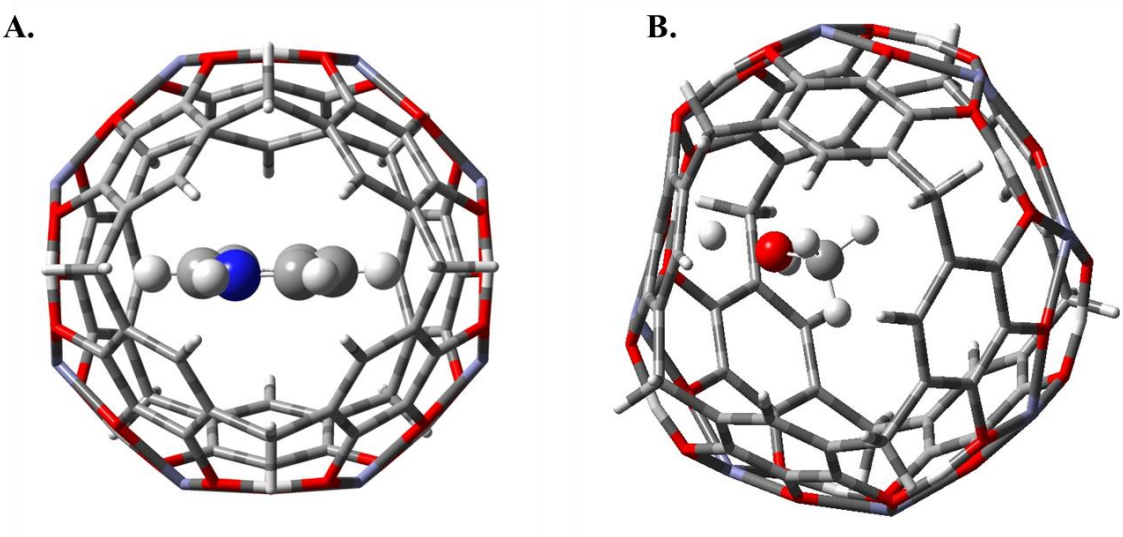

Figure 7.5 $ZnPgC_0 \subset PyH^+$ and $ZnPgC_0H^+ \subset CH_3OH$.

7.4 Summary

Quantum chemical calculations on zinc-seamed pyrogallol[4]arene nanocapsules have enabled us to probe the properties of guest encapsulation. The capsule geometry is dependent on the charge and, when applicable, the alkyl group substituent of the guest. Neutral guests shrink the framework, decreasing the capsule $diameter_{avg}$, and protonated guests cause an overall swelling of the capsule, increasing the capsule $diameter_{avg}$. No consistent trends are observed for the capsule lengths, $\tau 5$ values, and capsular volumes. Encapsulation of a guest is a spontaneous process unless steric effects from a larger alkyl substituent limit possible orientations of the guest. Early experimental results showed that only PyH^+-based molecules from the original zinc reactant complex were encapsulated despite the presence of CH_3OH. Entrapment of solvent was not observed until the formation of the capsule was slowed. Our encapsulation thermochemical data, which

shows that encapsulation of solvent guests is favorable, has led to the suggestion that the PyH^+-based guests are most likely kinetically trapped.

In addition to considering the encapsulation of guests, the relative stabilities and the PAs and GBs of the isolated and encapsulated guests were examined. The relative stabilities of the MePy and EtPy isomers agree with the relative encapsulation thermochemical data, thus suggesting that encapsulation has comparable effects on all of the guests. Encapsulation of a guest leads to typical PA and GB enhancements of nearly 50 kJ/mol. The atypical changes in PA and GB, enhancements nearing 100 kJ/mol or diminishments up to 30 kJ/mol, are believed to be a consequence of not yet having identified the global minimum for one of the assemblies.

Chapter 8: Future studies

A number of model complexes and capsular assemblies have been investigated to better understand the characteristics and properties of zinc-seamed pyrogallol[4]arene nanocapsules. Many of the results have led to additional insight into experimental results and to suggestions for additional experimental studies, including, but not limited, to the determination of *exo* ligand binding strength, which aided in the choice of solvent for crystallization and in the prediction of a metal-organic framework based on zinc-seamed pyrogallol[4]arene nanocapsules.[201] We also found that the capsule diameter$_{avg}$ of $ZnPgC_0NH_3{\subset}PyH^+$ matches that of the experimentally observed $ZnPgC_3Py{\subset}PyH^+$ (Ch. 6).

To further our understanding of guest behavior, the addition of *exo* ligands to the $ZnPgC_0{\subset}guest(H^+)$ assemblies reported previously will be investigated. The increase in capsule diameter will enable the relative stability of the axial versus equatorial orientation of a guest to be determined. Experimental NMR and MD simulation studies have shown the flipping of guests within the capsule.[266,269] Electronic structure calculations can be utilized to determine the barrier for the flipping of a guest within a $ZnPgC_0NH_3$-based capsule. Also, by evaluating the effect on the encapsulation enthalpies and free energies of examining $ZnPgC_0$-based versus $ZnPgC_0NH_3$-based assemblies, a general "stabilization factor" can be added to the encapsulation thermochemical data of $ZnPgC_0{\subset}guest(H^+)$ to determine if the encapsulation is spontaneous or not. More conformations of encapsulated guests such as *m*-EtPy(H^+) need to be identified and

compared to the isolated conformers (Fig. 7.3). Determining the relative stability of these conformers will provide additional insight into the effect of encapsulation.

The criteria set out to determine likely candidates for divergent tethering ligands are a contact distance between capsules ≥ 10.5 Å, a binding dissociation enthalpy (BDE) ≥ 80 kJ/mol, and a drop-off in BDE for the second binding site ≤ 5 kJ/mol.[201] By extending the tethering studies to more robust polynuclear zinc model complexes, which include *exo* ligands on zinc centers adjacent to the Y tethering ligand, the effect of steric constraints imposed by the *exo* ligands and a model curvature more representative of the capsule on the likelihood of capsule linking can be examined (Fig. 8.1). Considering these factors will enable us to refine our linking criteria. Energetics obtained from additional levels of theory, namely those with dispersion corrections such as the M05-2X-D3/VDZ-PP, which can be applied to the capsule, can also be investigated and compared to the MP2/B2-PP benchmark SPEs.

To date, only zinc-seamed models and assemblies have been investigated computationally. The next metal center suggested to be examined is Cu^{2+}. By implementing similar models and nanoassemblies in conjunction with a Cu^{2+} metal center, geometric and energetic differences between the Cu-seamed and Zn-seamed nanocapsules can be explored. The Cu-seamed capsules have been observed without a fifth coordinating *exo* ligand or with a weakly bound fifth coordinating ligand such as H_2O or CH_3OH.[39,126] These weakly bound ligands have not been observed for the Zn-seamed capsules, and the BDEs of these ligands can be compared between the two unique metal centers. Also, the electronic effects that the $CuPgC_0$-based framework has on a guest can be compared with those for an analogous $ZnPgC_0$-based assembly.

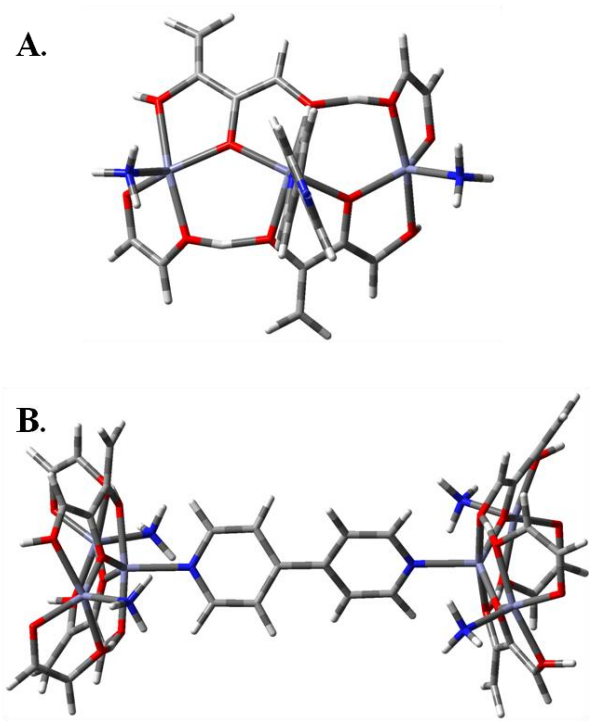

Figure 8.1 Top view of polynuclear zinc complex with 4,4'-bipyridyl divergent ligand and *exo* NH_3 ligands (A) and side view of linked polynuclear zinc complex.

Appendix

Chapter A1: Overview of the methods and basis sets implemented in the studies of zinc-seamed pyrogallol[4]arene dimeric nanocapsules-based systems

Please note that the reviews assessing these methods and basis sets hold true only for the systems studied in Chs. 2-7.

A1.1 Methods

B3LYP: The hybrid Becke, 3-parameter, Lee-Yang-Parr functional.[145,146] One of the most widely used functionals from density functional theory (DFT). B3LYP is among the most computationally efficient methods for geometric optimizations and vibrational frequency analyses. Reliable geometries can be obtained with this method. Energetics can be used to determine competitive systems, but should not be used to determine the magnitude of relative energies. Use this method on systems with > 20 heavy atoms. Equilibrium structures computed with this method agree well with experimental structures for the $ZnPgC_0$-based systems.

G4(MP2): Fourth generation composite method by Curtiss and coworkers.[42] Reliable geometries and energetics were obtained for the trihydroxybenzene building blocks.

M05-2X: Hybrid functional by Zhao and Truhlar.[86] Benchmark geometries and energetics were obtained with this functional. Excellent agreement with MP2 calculated energies was observed. Computational cost was prohibitive for performing M05-2X/B2-

PP geometric optimizations on the larger $ZnPgC_0$-based systems. However, out of the calculational levels explored in this work, preliminary results suggest that the M05-2X/B2-PP optimized structure for $ZnPgC_0$ differs the most with respect to experimental results.

M06-L: The pure functional by Zhao and Truhlar.[150] Reasonable geometries and energetics were obtained with this functional for model complexes. Capsular dimensions were slightly underestimated compared with experimental results.

MP2: Møller-Plesset 2nd order perturbation theory. MP2 accounts for 80 – 90% of the electron correlation energy. This method was used as a benchmark for the energetics of model complexes.

PBE0: This hybrid functional is also known as PBE1PBE.[147,148] Efficient geometric optimizations and reliable structures are obtained with this functional. In general, similar geometric parameters are found from B3LYP/LANL2DZ and PBE0/LANL2DZ optimizations, but the PBE0 results agree better with experimental results. Future minimizations on both models and capsules will be carried out at the PBE0/LANL2DZ level of theory.

ωB97X-D: This is a long-range corrected functional that includes empirical dispersion corrections.[149] Geometric optimizations carried out with this functional tend to be more computationally expensive and yield underestimated bond lengths with respect to those found experimentally. As with other dispersion-corrected methods examined, ωB97X-D encapsulation energies tend to be more favorable (negative) in comparison to M05-2X encapsulation energies, but may represent an upper limit for reaction energetics.

A1.2 Basis sets

cc-pVDZ: Correlation-consistent valence double-zeta basis set by Dunning and coworkers.[276] This basis set provides reasonable energetics for larger $ZnPgC_0$-based complexes. VDZ was regularly combined with the MDF10[259] small-core (10 e) pseudopotential (PP) on zinc and represented as VDZ-PP.

aug-cc-pVTZ: Correlation-consistent valence triple-zeta basis set augmented with diffuse functions by Dunning and coworkers.[277] This basis set was among the largest investigated and MP2/aVTZ was used as an energetic benchmark.

6-311+G(d,p): Pople-type valence triple-zeta basis set with diffuse and polarization functions. Similar geometric properties and energetic trends were obtained in comparison to the LANL2DZ basis set. More accurate energetic magnitudes are found for this basis set.

B2-PP: This basis set was developed by Amin and coworkers.[41] The B2 basis set designates a [10s7p4d3f] basis set and the MDF10 PP[259] on zinc atoms and the 6-311+G(2df,2p) basis set on all other atoms. Similar results were obtained for binding dissociation enthalpies at the M05-2X/B2-PP and MP2/aVTZ levels of theory, with the former being much more calculationally efficient.

LANL2DZ: Valence double-zeta basis set that uses the D95V[278] basis set on first row atoms and the large-core (18 e) Los Alamos effective core potential on the remaining atoms.[279-281] This basis set is among the most computationally efficient of those studied and reproduces experimental geometric properties for $ZnPgC_0$ligand⊂guest systems. Higher level single-point energies need to be performed on these equilibrium structures due to unreliable energetics.

SDD: Double-zeta basis set that uses the D95[278] basis set on atoms up to Ar and the MDF10 PP[259] on all remaining atoms. Capsular diameters are underestimated, but reasonable encapsulation thermochemistry is obtained.

REFERENCES

(1) Steed, J. W.; Atwood, J. L.; Editors *Supramolecular Chemistry, Second Edition*; John Wiley & Sons, Ltd., 2009.

(2) Phuengphai, P.; Youngme, S.; Gamez, P.; Reedijk, J. *Dalton Trans.* **2010**, *39*, 7936.

(3) Britt, D.; Furukawa, H.; Wang, B.; Glover, T. G.; Yaghi, O. M. *Proc. Natl. Acad. Sci. U.S.A.* **2009**, *106*, 20637.

(4) Bae, Y.-S.; Farha, O. K.; Hupp, J. T.; Snurr, R. Q. *J. Mater. Chem.* **2009**, *19*, 2131.

(5) Bae, Y.-S.; Farha, O. K.; Spokoyny, A. M.; Mirkin, C. A.; Hupp, J. T.; Snurr, R. Q. *Chem. Comm.* **2008**, 4135.

(6) Li, J.-R.; Kuppler, R. J.; Zhou, H.-C. *Chem. Soc. Rev.* **2009**, *38*, 1477.

(7) Gu, Z.-Y.; Yang, C.-X.; Chang, N.; Yan, X.-P. *Acc. Chem. Res.* **2012**, *45*, 734.

(8) Mittermueller, M.; Volmer, D. A. *Analyst (Cambridge, U. K.)* **2012**, *137*, 3195.

(9) Wang, J.-L.; Wang, C.; Lin, W. *ACS Catal.* **2012**, *2*, 2630.

(10) Khan, N. A.; Hasan, Z.; Jhung, S. H. *J. Hazard. Mater.* **2013**, *244–245*, 444.

(11) Murray, L. J.; Dinca, M.; Long, J. R. *Chem. Soc. Rev.* **2009**, *38*, 1294.

(12) Hu, Y. H.; Zhang, L. *Adv. Mat.* **2010**, *22*, E117.

(13) Kolotilov, S. V.; Pavlishchuk, V. V. *Theor. Exp. Chem.* **2009**, *45*, 277.

(14) Davis, M. E. *Nature (London, U. K.)* **2002**, *417*, 813.

(15) Horcajada, P.; Serre, C.; Vallet-Regi, M.; Sebban, M.; Taulelle, F.; Ferey, G. *Angew. Chem., Int. Ed.* **2006**, *45*, 5974.

(16) Taylor-Pashow, K. M. L.; Rocca, J. D.; Xie, Z.; Tran, S.; Lin, W. *J. Am. Chem. Soc.* **2009**, *131*, 14261.

(17) An, J.; Geib, S. J.; Rosi, N. L. *J. Am. Chem. Soc.* **2009**, *131*, 8376.

(18) Asfari, Z.; Bohmer, V.; Harrowfield, J.; Vicens, J.; Editors *Calixarenes*, 2001.

(19) Atwood, J. L.; Barbour, L. J.; Jerga, A.; Schottel, B. L. *Science (Washington, DC, U. S.)* **2002**, *298*, 1000.

(20) Kumari, H.; Erra, L.; Webb, A. C.; Bhatt, P. M.; Barnes, C. L.; Deakyne, C. A.; Adams, J. E.; Barbour, L. J.; Atwood, J. L. *J. Am. Chem. Soc.* **2013**.

(21) Atwood, J. L.; Barbour, L. J.; Thallapally, P. K.; Wirsig, T. B. *Chem. Commun. (Cambridge, U. K.)* **2005**, 51.

(22) Atwood, J. L.; Barbour, L. J.; Jerga, A. *Angew. Chem., Int. Ed.* **2004**, *43*, 2948.

(23) Dalgarno, S. J.; Thallapally, P. K.; Barbour, L. J.; Atwood, J. L. *Chem. Soc. Rev.* **2007**, *36*, 236.

(24) Dalgarno, S. J.; Thallapally, P. K.; Tian, J.; Atwood, J. L. *New J. Chem.* **2008**, *32*, 2095.

(25) Dalgarno, S. J.; Tian, J.; Warren, J. E.; Clark, T. E.; Makha, M.; Raston, C. L.; Atwood, J. L. *Chem. Commun. (Cambridge, U. K.)* **2007**, 4848.

(26) Thallapally, P. K.; Dalgarno, S. J.; Atwood, J. L. *J. Am. Chem. Soc.* **2006**, *128*, 15060.

(27) Adams, J. E.; Cox, J. R.; Christiano, A. J.; Deakyne, C. A. *J. Phys. Chem. A* **2008**, *112*, 6829.

(28) Thomas, H. M., Ph.D. Dissertation, University of Missouri, 2011.

(29) Drachnik, A. M.; Mayhan, C. M.; Atwood, J. L.; Deakyne, C. A. *(In Preparation).*

(30) Maerz, A. K.; Thomas, H. M.; Power, N. P.; Deakyne, C. A.; Atwood, J. L. *Chem. Commun. (Cambridge, U. K.)* **2010**, *46*, 1235.

(31) Power, N. P.; Dalgarno, S. J.; Atwood, J. L. *New J. Chem.* **2007**, *31*, 17.

(32) Power, N. P.; Dalgarno, S. J.; Atwood, J. L. *Angew. Chem., Int. Ed.* **2007**, *46*, 8601.

(33) Dalgarno, S. J.; Power, N. P.; Warren, J. E.; Atwood, J. L. *Chem. Commun. (Cambridge, U. K.)* **2008**, 1539.

(34) Atwood, J. L.; Brechin, E. K.; Dalgarno, S. J.; Inglis, R.; Jones, L. F.; Mossine, A.; Paterson, M. J.; Power, N. P.; Teat, S. J. *Chem. Commun. (Cambridge, U. K.)* **2010**, *46*, 3484.

(35) McKinlay, R. M.; Thallapally, P. K.; Atwood, J. L. *Chem. Commun. (Cambridge, U. K.)* **2006**, 2956.

(36) Kumari, H.; Kline, S. R.; Wycoff, W. G.; Paul, R. L.; Mossine, A. V.; Deakyne, C. A.; Atwood, J. L. *Angew. Chem., Int. Ed.* **2012**, *51*, 5086.

(37) Maerz, A. K., Ph.D. Dissertation, University of Missouri, 2011.

(38) Kumari, H.; Mayhan, C. M.; Brewer, K.; Wycoff, W. G.; Adams, J. E.; Atwood, J. L.; Deakyne, C. A. *(In Preparation)* **2014**.

(39) Fowler, D. A.; Mossine, A. V.; Beavers, C. M.; Teat, S. J.; Dalgarno, S. J.; Atwood, J. L. *J. Am. Chem. Soc.* **2011**, *133*, 11069.

(40) Mossine, A. V.; Mayhan, C. M.; Fowler, D. A.; Teat, S. J.; Deakyne, C. A.; Atwood, J. L. *Chem. Sci.* **2014**, 10.1039/C4SC00462K.

(41) Amin, E. A.; Truhlar, D. G. *J. Chem. Theory Comput.* **2008**, *4*, 75.

(42) Curtiss, L. A.; Redfern, P. C.; Raghavachari, K. *J. Chem. Phys.* **2007**, *127*.

(43) Mayhan, C. M.; Szabo, T. J.; Adams, J. E.; Deakyne, C. A. *Comput. Theor. Chem.* **2012**, *984*, 19.

(44) Mayhan, C. M.; Szabo, T. J.; Adams, J. E.; Deakyne, C. A. *Struct. Chem.* **2013**, *24*, 2089.

(45) Bouchoux, G.; Defaye, D.; McMahon, T.; Likholyot, A.; Mo, O.; Yanez, M. *Chem. - Eur. J.* **2002**, *8*, 2900.

(46) Olah, G. A.; Mo, Y. K. *J. Amer. Chem. Soc.* **1972**, *94*, 5341.

(47) Olah, G. A.; Mo, Y. K. *J. Org. Chem.* **1973**, *38*, 353.

(48) Mayhan, C. M.; Kumari, H.; McClure, E. M.; Liebman, J. F.; Deakyne, C. A. *J. Chem. Thermodyn.* **2014**, Ahead of Print.

(49) Kumari, H.; Mayhan, C. M.; Liebman, J. F.; Deakyne, C. A. *(In Preparation)* **2014**.

(50) Jin, P.; Dalgarno, S. J.; Atwood, J. L. *Coord. Chem. Rev.* **2010**, *254*, 1760.

(51) Rebek, J., Jr. *Angew. Chem., Int. Ed.* **2005**, *44*, 2068.

(52) Durola, F.; Dube, H.; Ajami, D.; Rebek, J., Jr. *Supramol. Chem.* **2011**, *23*, 37.

(53) Di Bella, S. *Chem. Soc. Rev.* **2001**, *30*, 355.

(54) Bernasconi, L.; Baerends, E. J.; Sprik, M. *J. Phys. Chem. B* **2006**, *110*, 11444.

(55) Frison, G.; Ohanessian, G. *J. Comput. Chem.* **2008**, *29*, 416.

(56) Smith, G. D.; Bell, R.; Borodin, O.; Jaffe, R. L. *J. Phys. Chem. A* **2001**, *105*, 6506.

(57) Tiraboschi, G.; Gresh, N.; Giessner-Prettre, C.; Pedersen, L. G.; Deerfield, D. W. *J. Comput. Chem.* **2000**, *21*, 1011.

(58) Zhu, M.; Pan, G. *J. Phys. Chem. A* **2005**, *109*, 7648.

(59) Cooper, T. E.; Armentrout, P. B. *J. Phys. Chem. A* **2009**, *113*, 13742.

(60) Deerfield, D. W., II; Carter, C. W., Jr.; Pedersen, L. G. *Int. J. Quantum Chem.* **2001**, *83*, 150.

(61) Fatmi, M. Q.; Hofer, T. S.; Randolf, B. R.; Rode, B. M. *J. Phys. Chem. B* **2007**, *111*, 151.

(62) Parkin, G. *Chem. Rev.* **2004**, *104*, 699.

(63) Wu, R.; Hu, P.; Wang, S.; Cao, Z.; Zhang, Y. *J. Chem. Theory Comput.* **2010**, *6*, 337.

(64) Vahrenkamp, H. *Acc. Chem. Res.* **1999**, *32*, 589.

(65) Bunn, S. E.; Liu, C. T.; Lu, Z.-L.; Neverov, A. A.; Brown, R. S. *J. Am. Chem. Soc.* **2007**, *129*, 16238.

(66) Jahn, B. O.; Eger, W. A.; Anders, E. *Z. Naturforsch., B: J. Chem. Sci.* **2010**, *65*, 425.

(67) Szeto, M. W. Y.; Mujika, J. I.; Zurek, J.; Mulholland, A. J.; Harvey, J. N. *J. Mol. Struct.: THEOCHEM* **2009**, *898*, 106.

(68) Chen, S.-L.; Fang, W.-H.; Himo, F. *J. Inorg. Biochem.* **2009**, *103*, 274.

(69) Liao, R.-Z.; Yu, J.-G.; Himo, F. *Inorg. Chem.* **2010**, *49*, 6883.

(70) Alzoubi, B. M.; Puchta, R.; van Eldik, R. *Chem.--Eur. J.* **2010**, *16*, 7300.

(71) Brandt, E. G.; Hellgren, M.; Brinck, T.; Bergman, T.; Edholm, O. *Phys. Chem. Chem. Phys.* **2009**, *11*, 975.

(72) Brown, D. A.; Cuffe, L. P.; Fitzpatrick, N. J.; Ryan, A. T. *Inorg. Chem.* **2004**, *43*, 297.

(73) Dudev, T.; Lim, C. *J. Am. Chem. Soc.* **2006**, *128*, 1553.

(74) Dudev, T.; Lim, C. *J. Am. Chem. Soc.* **2000**, *122*, 11146.

(75) Xiang, S.; Short, S. A.; Wolfenden, R.; Carter, C. W., Jr. *Biochemistry* **1996**, *35*, 1335.

(76) Sorkin, A.; Truhlar, D. G.; Amin, E. A. *J. Chem. Theory Comput.* **2009**, *5*, 1254.

(77) Rayón, V. M.; Valdés, H.; Diaz, N.; Suárez, D. *J. Chem. Theory Comput.* **2008**, *4*, 243.

(78) Blumberger, J.; Lamoureux, G.; Klein, M. L. *J. Chem. Theory Comput.* **2007**, *3*, 1837.

(79) Chen, S.-L.; Fang, W.-H.; Himo, F. *J. Phys. Chem. B* **2007**, *111*, 1253.

(80) Sivasankar, C.; Sadhukhan, N.; Bera, J. K.; Samuelson, A. G. *New J. Chem.* **2007**, *31*, 385.

(81) Starikov, A. G.; Minkin, V. I.; Minyaev, R. M.; Koval, V. V. *J. Phys. Chem. A* **2010**, *114*, 7780.

(82) Strenalyuk, T.; Samdal, S.; Volden, H. V. *J. Phys. Chem. A* **2007**, *111*, 12011.

(83) Wu, E. L.; Wong, K.-Y.; Zhang, X.; Han, K.; Gao, J. *J. Phys. Chem. B* **2009**, *113*, 2477.

(84) Cooper, T. E.; Carl, D. R.; Armentrout, P. B. *J. Phys. Chem. A* **2009**, *113*, 13727.

(85) Wachters, A. J. H. *J. Chem. Phys.* **1970**, *52*, 1033.

(86) Zhao, Y.; Schultz, N. E.; Truhlar, D. G. *J. Chem. Theory Comput.* **2006**, *2*, 364.

(87) Dolg, M.; Wedig, U.; Stoll, H.; Preuss, H. *J. Chem. Phys.* **1987**, *86*, 866.

(88) Lynch, B. J.; Zhao, Y.; Truhlar, D. G. *J. Phys. Chem. A* **2003**, *107*, 1384.

(89) Frisch, M. J.; Trucks, G. W.; Schlegel, H. B.; Scuseria, G. E.; Robb, M. A.; Cheeseman, J. R.; Scalmani, G.; Barone, V.; Mennucci, B.; Petersson, G. A.; Nakatsuji, H.; Caricato, M.; Li, X.; Hratchian, H. P.; Izmaylov, A. F.; Bloino, J.; Zheng, G.; Sonnenberg, J. L.; Hada, M.; Ehara, M.; Toyota, K.; Fukuda, R.; Hasegawa, J.; Ishida, M.; Nakajima, T.; Honda, Y.; Kitao, O.; Nakai, H.; Vreven, T.; Montgomery, J. A.; Peralta, J. E.; Ogliaro, F.; Bearpark, M.; Heyd, J. J.; Brothers, E.; Kudin, K. N.; Staroverov, V. N.; Kobayashi, R.; Normand, J.; Raghavachari, K.; Rendell, A.; Burant, J. C.; Iyengar, S. S.; Tomasi, J.; Cossi, M.; Rega, N.; Millam, J. M.; Klene, M.; Knox, J. E.; Cross, J. B.; Bakken, V.; Adamo, C.; Jaramillo, J.; Gomperts, R.; Stratmann, R. E.; Yazyev, O.; Austin, A. J.; Cammi, R.; Pomelli, C.; Ochterski, J. W.; Martin, R. L.; Morokuma, K.; Zakrzewski, V. G.; Voth, G. A.; Salvador, P.; Dannenberg, J. J.; Dapprich, S.; Daniels, A. D.; Farkas; Foresman, J. B.; Ortiz, J. V.; Cioslowski, J.; Fox, D. J. Wallingford CT, 2009.

(90) Boys, S. F.; Bernardi, F. *Mol. Phys.* **1970**, *19*, 553.

(91) Reed, A. E.; Curtiss, L. A.; Weinhold, F. *Chem. Rev.* **1988**, *88*, 899.

(92) Glendening, E. D.; Reed, A. E.; Carpenter, J. E.; Weinhold, F.; Version 3.1 ed. 1993

(93) Bader, R. F. W. *Atoms in Molecules: A Quantum Theory*; Oxford University Press: Oxford, UK, 1994.

(94) Alcami, M.; Mó, O.; Yáñez, M.; Abboud, J. L. M.; Elguero, J. *Chem. Phys. Lett.* **1990**, *172*, 471.

(95) Deakyne, C. A.; Thomas, H. M.; Liebman, J. F. *J. Fluorine Chem.* **2009**, *130*, 836.

(96) Mó, O.; Yáñez, M.; Eckert-Maksić, M.; Maksić, Z. B.; Alkorta, I.; Elguero, J. *J. Phys. Chem. A* **2005**, *109*, 4359.

(97) Sigel, H.; Martin, R. B. *Chem. Soc. Rev.* **1994**, *23*, 83.

(98) Alexiou, M.; Dendrinou-Samara, C.; Raptopoulou, C. P.; Terzis, A.; Kessissoglou, D. P. *Inorg. Chem.* **2002**, *41*, 4732.

(99) Li, Y.-H.; Ye, Q.; Tang, Y.-Z.; Xiong, R.-G. *Z. Anorg. Allg. Chem.* **2004**, *630*, 1553.

(100) Dordevic, T.; Stojanovic, J.; Karanovic, L. *Acta Crystallogr., Sect. E: Struct. Rep. Online* **2010**, *E66*, i79.

(101) Sham, S.; Wu, G. *Can. J. Chem.* **1999**, *77*, 1782.

(102) Sakai, K.-i.; Takahashi, S.; Kobayashi, A.; Akutagawa, T.; Nakamura, T.; Dosen, M.; Kato, M.; Nagashima, U. *Dalton Trans.* **2010**, *39*, 1989.

(103) Ghoshal, D.; Maji, T. K. *J. Chem. Sci.* **2010**, *122*, 801.

(104) Ayyappan, P.; Evans, O. R.; Lin, W. *Inorg. Chem.* **2002**, *41*, 3328.

(105) Cheng, M.; Moore, D. R.; Reczek, J. J.; Chamberlain, B. M.; Lobkovsky, E. B.; Coates, G. W. *J. Am. Chem. Soc.* **2001**, *123*, 8738.

(106) Chisholm, M. H.; Gallucci, J. C.; Zhen, H.; Huffman, J. C. *Inorg. Chem.* **2001**, *40*, 5051.

(107) Prust, J.; Hohmeister, H.; Stasch, A.; Roesky, H. W.; Magull, J.; Alexopoulos, E.; Uson, I.; Schmidt, H.-G.; Noltemeyer, M. *Eur. J. Inorg. Chem.* **2002**, 2156.

(108) Hlavinka, M. L.; Hagadorn, J. R. *Organometallics* **2005**, *24*, 5335.

(109) Jiang, T.; Zhang, X.-M. *Cryst. Growth Des.* **2008**, *8*, 3077.

(110) Sarazin, Y.; Wright, J. A.; Harding, D. A. J.; Martin, E.; Woodman, T. J.; Hughes, D. L.; Bochmann, M. *J. Organomet. Chem.* **2008**, *693*, 1494.

(111) Blake, A. J.; Gillibrand, N. L.; Moxey, G. J.; Kays, D. L. *Inorg. Chem.* **2009**, *48*, 10837.

(112) Spielmann, J.; Piesik, D.; Wittkamp, B.; Jansen, G.; Harder, S. *Chem. Commun. (Cambridge, U. K.)* **2009**, 3455.

(113) Cantalupo, S. A.; Lum, J. S.; Buzzeo, M. C.; Moore, C.; Di Pasquale, A. G.; Rheingold, A. L.; Doerrer, L. H. *Dalton Trans.* **2010**, *39*, 374.

(114) Pang, K.; Rong, Y.; Parkin, G. *Polyhedron* **2010**, *29*, 1881.

(115) Das, D.; Nag, S.; Datta, D. *Inorg. Chim. Acta* **2009**, *362*, 2890.

(116) Peschke, M.; Blades, A. T.; Kebarle, P. *J. Am. Chem. Soc.* **2000**, *122*, 10440.

(117) Pavlov, M.; Siegbahn, P. E. M.; Sandstroem, M. *J. Phys. Chem. A* **1998**, *102*, 219.

(118) Cooper, T. E.; O'Brien, J. T.; Williams, E. R.; Armentrout, P. B. *J. Phys. Chem. A* **2010**, *114*, 12646.

(119) Hannant, M. D.; Schormann, M.; Hughes, D. L.; Bochmann, M. *Inorg. Chim. Acta* **2005**, *358*, 1683.

(120) Afeefy, H. Y. L., J. F.; Stein, S. E., In: NIST Chemistry WebBook, NIST Standard Reference Database Number 69; Linstrom, P. J., Mallard, W.G., Eds.; National Institute of Standards and Technology: Gaithersburg MD, 20899, http://webbook.nist.gov (retrieved May, 2010)

(121) Conn, M. M.; Rebek, J., Jr. *Chem. Rev. (Washington, D. C.)* **1997**, *97*, 1647.

(122) Koblenz, T. S.; Wassenaar, J.; Reek, J. N. H. *Chem. Soc. Rev.* **2008**, *37*, 247.

(123) Stoyanov, S. R.; Titov, A. V.; Kral, P. *Coord. Chem. Rev.* **2009**, *253*, 2852.

(124) Deakyne, C. A.; Fowler, D. A.; Atwood, J. L. In *The Chemistry of Metal Phenolates*; Zabicky, J., Ed.; Wiley Chichester, 2013.

(125) Dalgarno, S. J.; Power, N. P.; Atwood, J. L. *Coord. Chem. Rev.* **2008**, *252*, 825.

(126) Kumari, H.; Mossine, A. V.; Kline, S. R.; Dennis, C. L.; Fowler, D. A.; Teat, S. J.; Barnes, C. L.; Deakyne, C. A.; Atwood, J. L. *Angew. Chem., Int. Ed.* **2012**, *51*, 1452.

(127) Mossine, A. V.; Kumari, H.; Fowler, D. A.; Shih, A.; Kline, S. R.; Barnes, C. L.; Atwood, J. L. *Chem. - Eur. J.* **2012**, *18*, 10258.

(128) Kumari, H.; Dennis, C. L.; Mossine, A. V.; Deakyne, C. A.; Atwood, J. L. *ACS Nano* **2012**, *6*, 272.

(129) Kumari, H.; Dennis, C. L.; Mossine, A. V.; Deakyne, C. A.; Atwood, J. L. *J. Am. Chem. Soc.* **2013**, *135*, 7110.

(130) Kumari, H.; Kline, S. R.; Dennis, C. L.; Mossine, A. V.; Paul, R. L.; Deakyne, C. A.; Atwood, J. L. *Angew. Chem., Int. Ed.* **2012**, *51*, 9263.

(131) Dvorakova, H.; Stursa, J.; Cajan, M.; Moravcova, J. *Eur. J. Org. Chem.* **2006**, 4519.

(132) Kimura, E. *Acc. Chem. Res.* **2001**, *34*, 171.

(133) Makowska-Grzyska, M. M.; Jeppson, P. C.; Allred, R. A.; Arif, A. M.; Berreau, L. M. *Inorg. Chem.* **2002**, *41*, 4872.

(134) Salter, M. H., Jr.; Reibenspies, J. H.; Jones, S. B.; Hancock, R. D. *Inorg. Chem.* **2005**, *44*, 2791.

(135) Hou, X.-J.; He, P.; Li, H.; Wang, X. *J. Phys. Chem. C* **2013**, *117*, 2824.

(136) Canepa, P.; Arter, C. A.; Conwill, E. M.; Johnson, D. H.; Shoemaker, B. A.; Soliman, K. Z.; Thonhauser, T. *Condens. Matter* **2013**, 1.

(137) Liao, R.-Z.; Yu, J.-G.; Himo, F. *J. Phys. Chem. B* **2010**, *114*, 2533.

(138) Rodriguez, O. M. P. G.; Montejo, M.; Lopez, G. J. J. *Struct. Chem.*, Ahead of Print.

(139) Mueller, U.; Schubert, M.; Teich, F.; Puetter, H.; Schierle-Arndt, K.; Pastre, J. *J. Mater. Chem.* **2006**, *16*, 626.

(140) Tanh, J. H. B.; Staudt, C.; Janiak, C. *Dalton Trans.* **2012**, *41*, 14003.

(141) Clausen, H. F.; Poulsen, R. D.; Bond, A. D.; Chevallier, M.-A. S.; Iversen, B. B. *J. Solid State Chem.* **2005**, *178*, 3342.

(142) Weston, J. *Chem. Rev. (Washington, DC, U. S.)* **2005**, *105*, 2151.

(143) Hernick, M.; Fierke, C. A. *Arch. Biochem. Biophys.* **2005**, *433*, 71.

(144) Dennington, R.; Keith, T.; Millam, J.; SemiChem Inc.: Shawnee Mission, KS, 2009.

(145) Becke, A. D. *J. Chem. Phys.* **1993**, *98*, 5648.

(146) Lee, C.; Yang, W.; Parr, R. G. *Phys. Rev. B: Condens. Matter* **1988**, *37*, 785.

(147) Perdew, J. P.; Burke, K.; Ernzerhof, M. *Phys. Rev. Lett.* **1996**, *77*, 3865.

(148) Adamo, C.; Barone, V. *J. Chem. Phys.* **1999**, *110*, 6158.

(149) Chai, J.-D.; Head-Gordon, M. *Phys. Chem. Chem. Phys.* **2008**, *10*, 6615.

(150) Zhao, Y.; Truhlar, D. G. *J. Chem. Phys.* **2006**, *125*, 194101/1.

(151) Addison, A. W.; Rao, T. N.; Reedijk, J.; Van, R. J.; Verschoor, G. C. *Dalton Trans.* **1984**, 1349.

(152) Deakyne, C. A. *Int. J. Mass Spectrom.* **2003**, *227*, 601.

(153) Gal, J.-F.; Maria, P.-C.; Raczynska, E. D. *J. Mass Spectrom.* **2001**, *36*, 699.

(154) Meot-Ner, M. *Chem. Rev. (Washington, DC, U. S.)* **2005**, *105*, 213.

(155) Meot-Ner, M. *Int. J. Mass Spectrom.* **2003**, *227*, 525.

(156) Bleiholder, C.; Suhai, S.; Paizs, B. *J. Am. Soc. Mass Spectrom.* **2006**, *17*, 1275.

(157) Bouchoux, G. *J. Mass Spectrom.* **2006**, *41*, 1006.

(158) Bouchoux, G. *Mass Spectrom. Rev.* **2007**, *26*, 775.

(159) Bouchoux, G.; Salpin, J.-Y. *Mass Spectrom. Rev.* **2012**, *31*, 353.

(160) Bouchoux, G. *Mass Spectrom. Rev.* **2012**, *31*, 391.

(161) Maksic, Z. B.; Kovacevic, B.; Vianello, R. *Chem. Rev. (Washington, DC, U. S.)* **2012**, *112*, 5240.

(162) Hunter, E. P. L.; Lias, S. G. *J. Phys. Chem. Ref. Data* **1998**, *27*, 413.

(163) Meot-Ner, M.; Karpas, Z.; Deakyne, C. A. *J. Am. Chem. Soc.* **1986**, *108*, 3913.

(164) Deakyne, C. A.; Meot-Ner, M.; Buckley, T. J.; Metz, R. *J. Chem. Phys.* **1987**, *86*, 2334.

(165) Viggiano, A. A.; Henchman, M. J.; Dale, F.; Deakyne, C. A.; Paulson, J. F. *J. Am. Chem. Soc.* **1992**, *114*, 4299.

(166) Bartmess, J. E.; Pittman, J. L.; Aeschleman, J. A.; Deakyne, C. A. *Int. J. Mass Spectrom.* **2000**, *195/196*, 215.

(167) Deakyne, C. A.; Corum, A. K.; Thomas, H. M.; Liebman, J. F. *J. Fluorine Chem.* **2006**, *127*, 1355.

(168) Buckley, T. J.; Sieck, L. W.; Metz, R.; Lias, S. G.; Liebman, J. F. *Int. J. Mass Spectrom. Ion Processes* **1985**, *65*, 181.

(169) Greenberg, A.; Liebman, J. F. *J. Org. Chem.* **1982**, *47*, 2084.

(170) Greenberg, A.; Winkler, R.; Smith, B. L.; Liebman, J. F. *J. Chem. Educ.* **1982**, *59*, 367.

(171) Lias, S. G.; Jackson, J. A. A.; Argentar, H.; Liebman, J. F. *J. Org. Chem.* **1985**, *50*, 333.

(172) Lias, S. G.; Karpas, Z.; Liebman, J. F. *J. Am. Chem. Soc.* **1985**, *107*, 6089.

(173) Deakyne, C. A.; Liebman, J. F.; Vlasov, E. A.; Zevatsky, Y. E. *Struct. Chem.* **2008**, *19*, 609.

(174) Kresge, A. J.; Chiang, Y.; Hakka, L. E. *J. Amer. Chem. Soc.* **1971**, *93*, 6167.

(175) Catalan, J.; Yanez, M. *J. Chem. Soc., Perkin Trans. 2* **1979**, 1627.

(176) Eckert-Maksic, M.; Klessinger, M.; Maksic, Z. B. *Chem. - Eur. J.* **1996**, *2*, 1251.

(177) Maksic, Z. B.; Eckert-Maksic, M.; Knezevic, A. *J. Phys. Chem. A* **1998**, *102*, 2981.

(178) Maksic, Z. B.; Kovacevic, B.; Kovacek, D. *J. Phys. Chem. A* **1997**, *101*, 7446.

(179) Aue, D. H.; Guidoni, M.; Betowski, L. D. *Int. J. Mass Spectrom.* **2000**, *201*, 283.

(180) DeFrees, D. J.; McIver, R. T., Jr.; Hehre, W. J. *J. Am. Chem. Soc.* **1977**, *99*, 3853.

(181) Olasz, A.; Mignon, P.; De, P. F.; Veszpremi, T.; Geerlings, P. *Chem. Phys. Lett.* **2005**, *407*, 504.

(182) Kuck, D. In *PATAI'S Chemistry of Functional Groups*; John Wiley & Sons, Ltd: 2009.

(183) Travkin, V. M.; Solyanikova, I. P.; Golovleva, L. A. *J. Environ. Sci. Health, Part B* **2006**, *41*, 1361.

(184) Perez-Pantoja, D.; De, l. I. R.; Pieper, D. H.; Gonzalez, B. *FEMS Microbiol. Rev.* **2008**, *32*, 736.

(185) Mammino, L.; Kabanda, M. M. *J.Mol. Struct.: THEOCHEM* **2008**, *852*, 36.

(186) Kabanda, M. M.; Mammino, L. *Int. J. Quantum Chem.* **2012**, *112*, 519.

(187) Mammino, L.; Kabanda, M. M. *Int. J. Quantum Chem.* **2011**, *111*, 3701.

(188) Brune, A.; Schink, B. *J. Bacteriol.* **1990**, *172*, 1070.

(189) Ribeiro, d. S. M. D. M. C.; Ribeiro, d. S. M. A. V.; Pilcher, G. *J. Chem. Thermodyn.* **1986**, *18*, 295.

(190) Moser, A.; Range, K.; York, D. M. *J. Phys. Chem. B* **2010**, *114*, 13911.

(191) Rao, J. S.; Sastry, G. N. *Int. J. Quantum Chem.* **2006**, *106*, 1217.

(192) Liu, H.; Bara, J. E.; Turner, C. H. *Chem. Phys.* **2013**, *416*, 21.

(193) Bera, N. C.; Maeda, S.; Morokuma, K.; Viggiano, A. A. *J. Phys. Chem. A* **2010**, *114*, 13189.

(194) Burk, P.; Koppel, I. A.; Koppel, I.; Leito, I.; Travnikova, O. *Chem. Phys. Lett.* **2000**, *323*, 482.

(195) Weinelt, F.; Schneider, H. J. *J. Org. Chem.* **1991**, *56*, 5527.

(196) Ebmeyer, F.; Voegtle, F. *Angew. Chem., Int. Ed.* **1989**, *101*, 95.

(197) Fowler, D. A.; Rathnayake, A. S.; Kennedy, S.; Kumari, H.; Beavers, C. M.; Teat, S. J.; Atwood, J. L. *J. Am. Chem. Soc.* **2013**, *135*, 12184.

(198) McDonald, I. K.; Thornton, J. M. *J. Mol. Biol.* **1994**, *238*, 777.

(199) Torshin, I. Y.; Weber, I. T.; Harrison, R. W. *Protein Eng.* **2002**, *15*, 359.

(200) Desiraju, G.; Steiner, T. *The Weak Hydrogen Bond: Applications to Structural Chemistry and Biology*; Oxford Univ Press, 1999.

(201) Mayhan, C. M.; Drachnik, A. M.; Mossine, A. V.; Kumari, H.; Adams, J. E.; Deakyne, C. A. *Chem.– Eur. J.* **2014**, (submitted).

(202) Farha, O. K.; Hupp, J. T. *Acc. Chem. Res.* **2010**, *43*, 1166.

(203) Li, F.; Xu, L. *Dalton Trans.* **2011**, *40*, 4024.

(204) Pan, Z.; Xu, J.; Zheng, H.; Huang, K.; Li, Y.; Guo, Z.; Batten, S. R. *Inorg. Chem.* **2009**, *48*, 5772.

(205) Bai, Y.-L.; Tao, J.; Huang, R.-B.; Zheng, L.-S. *Angew. Chem., Int. Ed.* **2008**, *47*, 5344.

(206) Chorazy, S.; Podgajny, R.; Nitek, W.; Rams, M.; Ohkoshi, S.-i.; Sieklucka, B. *Cryst. Growth Des.* **2013**, *13*, 3036.

(207) Li, H.; Eddaoudi, M.; O'Keeffe, M.; Yaghi, M. *Nature (London, U.K.)* **1999**, *402*, 276.

(208) Chapin, J. C.; Kvasnica, M.; Purse, B. W. *J. Am. Chem. Soc.* **2012**, *134*, 15000.

(209) Mossine, A. V.; Kumari, H.; Fowler, D. A.; Maerz, A. K.; Kline, S. R.; Barnes, C. L.; Atwood, J. L. *Isr. J.Chem.* **2011**, *51*, 840.

(210) Kline, K. K.; Fowler, D. A.; Tucker, S. A.; Atwood, J. L. *Chem. - Eur. J.* **2011**, *17*, 10848.

(211) Avram, L.; Cohen, Y.; Rebek, J., Jr. *Chem. Commun. (Cambridge, U. K.)* **2011**, *47*, 5368.

(212) Dalgarno, S. J.; Cave, G. W. V.; Atwood, J. L. *Angew. Chem., Int. Ed.* **2006**, *45*, 570.

(213) Kulikov, O. V.; Daschbach, M. M.; Yamnitz, C. R.; Rath, N.; Gokel, G. W. *Chem. Commun. (Cambridge, U. K.)* **2009**, 7497.

(214) Dalgarno Scott, J.; Tucker Sheryl, A.; Bassil Daniel, B.; Atwood Jerry, L. *Science (New York, N.Y.)* **2005**, *309*, 2037.

(215) Fujisawa, I.; Kitamura, Y.; Kato, R.; Murayama, K.; Aoki, K. *J. Mol. Struct.* **2014**, *1056-1057*, 292.

(216) Fujisawa, I.; Kitamura, Y.; Okamoto, R.; Murayama, K.; Kato, R.; Aoki, K. *J. Mol. Struct.* **2013**, *1038*, 188.

(217) Fujisawa, I.; Aoki, K. *Crystals* **2013**, *3*, 306.

(218) Fowler, D. A.; Atwood, J. L.; Baker, G. A. *Chem. Commun. (Cambridge, U. K.)* **2013**, *49*, 1802.

(219) Fujisawa, I.; Takeuchi, D.; Kitamura, Y.; Okamoto, R.; Aoki, K. *J. Phys. Conf. Ser.* **2012**, *352*, 012043/1.

(220) Fowler, D. A.; Tian, J.; Barnes, C.; Teat, S. J.; Atwood, J. L. *CrystEngComm* **2011**, *13*, 1446.

(221) Jin, P.; Dalgarno, S. J.; Warren, J. E.; Teat, S. J.; Atwood, J. L. *Chem. Commun. (Cambridge, U. K.)* **2009**, 3348.

(222) Dalgarno, S. J.; Power, N. P.; Atwood, J. L. *Chem. Commun. (Cambridge, U. K.)* **2007**, 3447.

(223) Ahman, A.; Nissinen, M. *Chem. Commun. (Cambridge, U. K.)* **2006**, 1209.

(224) Kumari, H.; Kline, S. R.; Fowler, D. A.; Mossine, A. V.; Deakyne, C. A.; Atwood, J. L. *Chem. Commun. (Cambridge, U. K.)* **2014**, *50*, 109.

(225) McKinlay, R. M.; Cave, G. W. V.; Atwood, J. L. *Proc. Acad. Sci. U.S.A.* **2005**, *102*, 5944.

(226) Li, H.; Eddaoudi, M.; Groy, T. L.; Yaghi, O. M. *J. Am. Chem. Soc.* **1998**, *120*, 8571.

(227) Tanh Jeazet, H. B.; Staudt, C.; Janiak, C. *Dalton Trans.* **2012**, *41*, 14003.

(228) Hou, X.-J.; He, P.; Li, H.; Wang, X. *J. Phys. Chem. C* **2013**, *117*, 2824.

(229) Lipscomb, W. N.; Sträter, N. *Chem. Rev. (Washington, D. C.)* **1996**, *96*, 2375.

(230) Zheng, Z.; Tu, X. *CrystEngComm* **2009**, *11*, 707.

(231) Su, Z.; Fan, J.; Okamura, T.-a.; Chen, M.-S.; Chen, S.-S.; Sun, W.-Y.; Ueyama, N. *Cryst. Growth Des.* **2010**, *10*, 1911.

(232) Andruh, M. *Chem. Commun. (Cambridge, U. K.)* **2007**, 2565.

(233) Su, Y.; Zhao, Y.; Gao, J.; Dong, Q.; Wu, B.; Yang, X.-J. *Inorg. Chem.* **2012**, *51*, 5889.

(234) Willans, C. E.; French, S.; Anderson, K. M.; Barbour, L. J.; Gertenbach, J.-A.; Lloyd, G. O.; Dyer, R. J.; Junk, P. C.; Steed, J. W. *Dalton Trans.* **2011**, *40*, 573.

(235) Roland, B. K.; Selby, H. D.; Cole, J. R.; Zheng, Z. *Dalton Trans.* **2003**, 4307.

(236) Zhang, Z. *J. Mater. Sci. Technol.* **2007**, *23*, 1.

(237) Ajami, D.; Schramm, M. P.; Volonterio, A.; Rebek, J., Jr. *Angew. Chem., Int. Ed.* **2007**, *46*, 242.

(238) Barrett, E. S.; Dale, T. J.; Rebek, J., Jr. *J. Am. Chem. Soc.* **2007**, *129*, 3818.

(239) Meissner, R. S.; Rebek, J., Jr.; de Mendoza, J. *Science (Washington, D. C.)* **1995**, *270*, 1485.

(240) Rebek, J. *Acc. Chem. Res.* **2009**, *42*, 1660.

(241) Shimizu, K. D.; Rebek, J., Jr. *Proc. Acad. Sci. U.S.A.* **1995**, *92*, 12403.

(242) Shivanyuk, A.; Rebek, J., Jr. *Proc. Acad. Sci. U.S.A.* **2001**, *98*, 7662.

(243) Wyler, R.; de Mendoza, J.; Rebek, J. *Angew. Chem., Int. Ed.* **1993**, *32*, 1699.

(244) Dillon, A. C.; Jones, K. M.; Bekkedahl, T. A.; Kiang, C. H.; Bethune, D. S.; Heben, M. J. *Nature (London, U. K.)* **1997**, *386*, 377.

(245) Dresselhaus, M. S.; Dresselhaus, G.; Eklund, P. C.; Editors *Science of Fullerenes and Carbon Nanotubes*, 1996.

(246) Ghadiri, M. R.; Granja, J. R.; Milligan, R. A.; McRee, D. E.; Khazanovich, N. *Nature (London, United Kingdom)* **1993**, *366*, 324.

(247) Kennedy, S.; Karotsis, G.; Beavers, C. M.; Teat, S. J.; Brechin, E. K.; Dalgarno, S. J. *Angew. Chem., Int. Ed.* **2010**, *49*, 4205.

(248) Dalgarno, S. J.; Hardie, M. J.; Atwood, J. L.; Raston, C. L. *Inorg. Chem.* **2004**, *43*, 6351.

(249) Fowler, D. A.; Teat, S. J.; Baker, G. A.; Atwood, J. L. *Chem. Commun. (Cambridge, U. K.)* **2012**, *48*, 5262.

(250) Scherer, M.; Caulder, D. L.; Johnson, D. W.; Raymond, K. N. *Angew. Chem., Int. Ed.* **1999**, *38*, 1588.

(251) Bordoli, R. J.; Goldup, S. M. *J. Am. Chem. Soc.* **2014**, *136*, 4817.

(252) Pang, M.; Cairns, A. J.; Liu, Y.; Belmabkhout, Y.; Zeng, H. C.; Eddaoudi, M. *J. Am. Chem. Soc.* **2012**, *134*, 13176.

(253) Warmuth, R. **2012**.

(254) Hahn, U.; Cardinali, F.; Nierengarten, J.-F. *New J. Chem.* **2007**, *31*, 1128.

(255) Kumari, H.; Kline, S. R.; Atwood, J. L. *Chem. Commun. (Cambridge, U. K.)* **2012**, *48*, 3599.

(256) Drachnik, A. M.; Kumari, H.; Barnes, C.; Deakyne, C. A.; Atwood, J. L. *CrystEngComm* **2014**, Submitted.

(257) MacGillivray, L. R.; Atwood, J. L. *Nature (London, United Kingdom)* **1997**, *389*, 469.

(258) Munakata, M.; Wu, L. P.; Kuroda-Sowa, T.; Maekawa, M.; Suenaga, Y.; Sugimoto, K.; Ino, I. *Dalton Trans.* **1999**, 373.

(259) Figgen, D.; Rauhut, G.; Dolg, M.; Stoll, H. *Chem. Phys.* **2005**, *311*, 227.

(260) Peterson, K. A.; Puzzarini, C. *Theor. Chem. Acc.* **2005**, *114*, 283.

(261) Feller, D. *J. Comput. Chem.* **1996**, *17*, 1571.

(262) Schuchardt, K. L.; Didier, B. T.; Elsethagen, T.; Sun, L.; Gurumoorthi, V.; Chase, J.; Li, J.; Windus, T. L. *J. Chem. Inf. Model.* **2007**, *47*, 1045.

(263) Macrae, C. F.; Bruno, I. J.; Chisholm, J. A.; Edgington, P. R.; McCabe, P.; Pidcock, E.; Rodriguez-Monge, L.; Taylor, R.; van de Streek, J.; Wood, P. A. *J. Appl. Crystallogr.* **2008**, *41*, 466.

(264) Connolly, M. L. *J. Mol. Graphics* **1993**, *11*, 139.

(265) Barbour, L. J. *J. Supramol. Chem.* **2003**, *1*, 189.

(266) Kumari, H.; Mayhan, C. M.; Adams, J. E.; Deakyne, C. A.; Atwood Jerry, L. **2014**, (In preparation).

(267) Kumari, H.; Erra, L.; Webb, A. C.; Bhatt, P.; Barnes, C. L.; Deakyne, C. A.; Adams, J. E.; Barbour, L. J.; Atwood, J. L. *J. Am. Chem. Soc.* **2013**, *135*, 16963.

(268) Power, N. P., University of Missouri, Columbia, MO. Personal communication, 2008.

(269) Brewer, K. E.; Adams, J. E., University of Missouri, Columbia, MO. Unpublished work, 2013.

(270) Meot-Ner, M.; Sieck, L. W.; Koretke, K. K.; Deakyne, C. A. *J. Am. Chem. Soc.* **1997**, *119*, 10430.

(271) Rebek, J., Jr. *Chem. Commun.* **2007**, 2777.

(272) Pluth, M. D.; Bergman, R. G.; Raymond, K. N. *Science (New York, N.Y.)* **2007**, *316*, 85.

(273) Koner, A. L.; Schatz, J.; Nau, W. M.; Pischel, U. *J. Org. Chem.* **2007**, *72*, 3889.

(274) Wang, R.; Yuan, L.; Macartney, D. H. *Chem. Commun. (Cambridge, U. K.)* **2005**, 5867.

(275) Kumari, H.; Mayhan, C. M.; Deakyne, C. A., University of Missouri, Columbia, MO. Unpublished work, 2013.

(276) Dunning, T. H., Jr. *J. Chem. Phys*. **1989**, *90*, 1007.

(277) Kendall, R. A.; Dunning, T. H., Jr.; Harrison, R. J. *J. Chem. Phys*. **1992**, *96*, 6796.

(278) Dunning, T.H., Jr.; Hay, P.J. In *Modern Theoretical Chemistry vol. 3*; Schaefer III, H.F., Ed., Plenum Press, New York, 1977; 1.

(279) Hay, P. J.; Wadt, W. R. *J. Chem. Phys.* **1985**, *82*, 270.

(280) Hay, P. J.; Wadt, W. R. *J. Chem. Phys*. **1985**, *82*, 299.

(281) Wadt, W. R.; Hay, P. J. *J. Chem. Phys*. **1985**, *82*, 284.

VITA

Collin M. Mayhan was born in Jefferson City, Missouri on March 23, 1987. He began his undergraduate studies at the University of Missouri in 2005, where his majors changed from Music Education to Biology to Chemistry, before graduating with an ACS certified BS in Chemistry in 2009. During the last year of his undergraduate studies, Collin joined the Deakyne group where his undergraduate research began with the investigation of zinc-seamed capsules. This project was of such interest that Collin decided to continue his education and pursue a Ph.D. in chemistry. Collin defended his dissertation entitled “Computational studies of zinc-seamed pyrogallol[4]arene nanocapsules and model systems” and graduated with his Ph.D. in May 2014.